COUPLED THERMO - HYDRO - MECHANICAL
EXPERIMENT AT KAMAISHI MINE

TECHNICAL NOTE 15-99-02

EXPERIMENTAL RESULTS

M. Chijimatsu, Y. Sugita and T. Fujita
Japan Nuclear Cycle Development Institute (JNC)

K. Amemiya
HAZAMA Corporation

〒319-1194　茨城県那珂郡東海村大字村松4-33
核燃料サイクル開発機構　東海事業所
運営管理部　技術情報室

Technical Information Section,
Administration Division,
Tokai Works,
Japan Nuclear Cycle Development Institute
4-33 Muramatsu, Tokai-mura, Naka-gun, Ibaraki-ken, 319-1194,
Japan

JNC TN8400 99-034
1999年7月

釜石原位置試験場における粘土充填・熱負荷試験
テクニカルノート 15-99-02
試験結果
(研究報告)

千々松正和*1・杉田裕*1・藤田朝雄*1・雨宮清*2

要 旨

地層処分における技術開発の観点からは，工学規模での試験によるニアフィールド環境である周辺岩盤の挙動が人工バリアに与える影響の把握および周辺岩盤を含むニアフィールド性能の定量的評価と室内および原位置における大型試験による人工バリアの品質性能の確認を行い，地層処分技術の信頼性向上を図ることが重要となっている。そのため，核燃料サイクル開発機構東海事業所の地層処分基盤研究施設等における工学規模の試験と並行して，原位置試験場において，人工バリアの品質性能の確認およびその実岩盤条件下でのニアフィールド連成挙動を評価することが必要となっている。

そこで，実条件でのニアフィールド環境を把握するため釜石原位置試験場において粘土充填・熱負荷試験を実施した。1995年には14本のボーリング孔の試錐を行い，種々のセンサーの設置を行なった。透水試験を実施した後，岩盤の力学物性を取得するために孔内載荷試験を実施した。その後，直径1.7m，深さ5.0mのテストピットの掘削を行なった。ピット掘削中は，試錐孔内に設置した計測機器により，間隙水圧，変位，温度の測定を行なった。その後，1996年にピット内に緩衝材および発熱体を設置し，連成試験を開始した。連成試験としては，ヒーターの加熱を行なう加熱試験を約260日間，ヒーター停止後の減熱試験を約180日間実施した。本論では，加熱試験および減熱試験期間中に岩盤内および緩衝材に設置した計測機器により観測された結果について報告する。また，加熱試験終了時，減熱試験終了時および緩衝材解体時に実施した緩衝材のサンプリング結果についても報告する。

---

*1 東海事業所 環境保全・研究開発センター 処分研究部 処分バリア性能研究グループ

*2 株式会社 間組

COUPLED THERMO-HYDRO-MECHANICAL EXPERIMENT AT KAMAISHI MINE
TECHNICAL NOTE 15-99-02
EXPERIMENTAL RESULTS

ABSTRACT

It is an important part of the near field performance assessment of nuclear waste disposal to evaluate coupled thermo-hydro-mechanical (T-H-M) phenomena, e.g., thermal effects on groundwater flow through rock matrix and water seepage into the buffer material, the generation of swelling pressure of the buffer material, and thermal stresses potentially affecting porosity and fracture apertures of the rock. An in-situ T-H-M experiment named 'Engineered Barrier Experiment' has been conducted at the Kamaishi Mine, of which host rock is granodiorite, in order to establish conceptual models of the coupled T-H-M processes and to build confidence in mathematical models and computer codes.

In 1995, fourteen boreholes were excavated in order to install the various sensors. After the hydraulic tests, mechanical tests were carried out to obtain the rock properties. After that, a test pit, 1.7m in diameter and 5.0m in depth, was excavated. During the excavation, the change of pore pressure, displacement and temperature of rock mass were measured. In 1996, the buffer material and heater were set up in the test pit, and then coupled thermo-hydro-mechanical test was started. The duration of heating phase was 250 days and that of cooling phase was 180 days. The heater surface was controlled to be 100 °C during heating phase. Measurement was carried out by a number of sensors installed in both buffer and rock mass during the test. The field experiment leads to a better understanding of the behavior of the coupled thermo-hydro-mechanical phenomena in the near field.

Contents

Contents

List of figures

Page

Chapter 1

Chapter 2

Chapter 3

List of figures (Continued)

List of figures (Continued)

Page

Chapter 4

List of figures (Continued)

Page

Chapter 5

List of figures (Continued)

List of figures (Continued)

Page

Chapter 6

List of figures (Continued)

List of figures (Continued)

Page

APPENDIX A

APPENDIX B

List of tables

page

Chapter 1

Chapter 2

Chapter 3

Chapter 5

List of tables (Continued)

page

Chapter 6

Chapter 7

APPENDIX A

List of tables (Continued)

page

APPENDIX B

1. Introduction

It is an important part of the near field performance assessment of nuclear waste disposal to evaluate the coupled T-H-M phenomena, e.g., thermal effects on ground water flow through rock matrix and water seepage into the buffer material, and generation of the swelling pressure of the buffer material and thermal stresses potentially affecting the change in the porosity and fracture aperture of the rock. In order to observe near field coupled T-H-M phenomena in situ, many in-situ experiment have been carried out in the world, e.g., the Buffer Mass Test in Stripa project (Sweden) [Pusch and Börgesson, 1985] and the Bacchus Backfill Experiment at the Hades Under-ground Research Facility at Mol (Belgium) [Neerdael et al., 1992] those are small-scale test, and the Buffer/Container Experiment in URL (Canada) [Kjartanson et al., 1993] and the FEBEX (Full-scale engineered barriers experiment in crystalline host rock) in Grimsel (Switzerland) [ENRESA, 1998] those are full-scale experiment. On the other hand, in Japan, only the mock-up test using the artificial rock (BIG-BEN) [Sato et al., 1991 ; Fujita et al., 1993] was conducted in the laboratory. Therefore, a full-scale in-situ experiment was planed at Kamaishi mine of which host rock is granodiorite. The main objects of the full-scale in-situ experiment at Kamaishi mine were to evaluate applicability of the engineered barrier technology, to observe near field coupled T-H-M phenomena in situ and to increase a confidence of coupled T-H-M models. Based on the current design of a repository considered by Power Reactor and Nuclear Fuel Development Corporation [PNC, 1993], the experiment was planned. The physical processes involved in this experiment covers almost spectrum of the T-H-M issues [Stephansson, 1993][Stephansson et al., 1995] related to near field performance of waste repositories as follows.

- •Groundwater flow through rock matrix, fractures, buffer and their interfaces under both saturated and unsaturated conditions
- •Heat transfer through rock matrix, fractures, buffer and their interfaces under both saturated and unsaturated conditions
- •Swelling pressure, possible phase change and multi-phase flow in buffer under both saturated and unsaturated conditions
- •Stress, deformation and failure of rock matrix, fractures, buffer and their interfaces.
- •Coupled T-H-M responses of rock matrix, fractures and buffer over the whole time period of the experiment
- •Interaction between the deformability and permeability of rock matrix, rock fractures, buffer and their interfaces

The Kamaishi mine is located approximately 600km north of Tokyo in Japan as shown in Figure 1-1 [Takeda and Osawa, 1993]. The bedrock in this area consists of Paleozoic sedimentary rock, Cretaceous sedimentary rock, and igneous complexes. The facilities of T-H-M experiment were located at the drift 550m above sea level in the Cretaceous-age Kurihashi granodiorite [Fujita et al., 1994]. The overburden thickness at this location in the mine is about 260m [Chijimatsu et al., 1996a]. Table 1-1 shows the time schedule of T-H-M experiment. New drift, which was 5.0 m in width and 7.0 m in height, for performance of coupled T-H-M experiment was excavated by the drill and blast method in 1994.

In 1995, fourteen boreholes were excavated in order to install the various sensors [Fujita et al., 1996a]. Then hydraulic tests and mechanical tests [Chijimatsu et al., 1996b, 1996c] were

carried out to obtain the rock properties. And then fracture survey was carried out [Fujita et al., 1996b, 1996c]. After that, a test pit, 1.7m in diameter and 5.0m in depth, was excavated. During the excavation, the change of pore pressure, displacement and temperature of rock were measured [Fujita et al., 1997a] and water inflow rate into the test pit was measured [Chijimatsu et al., 1997]. Mechanical and hydraulic phenomena related to the excavation of the test were simulated by various methods [Fujita et al., 1997b, 1998 ; Jing et al., 1998].

In 1996, the buffer was set up into the test pit [Sugita et al., 1999]. In this experiment, granulated bentonite, OT-9607, was used for the buffer material [Fujita et al., 1997c]. This is the granulated bentonite and mineral composition is the almost same with Kunigel V1. Bentonite was compacted directly with the tamper. Spreading depth of each layer was 10cm and initial water content of bentonite was 15 %, which were determined by the results of the laboratory compaction test and the mock-up test. The mean value of the water content is 14.99 % and standard deviation is 0.911. The mean value of dry density is 1.653 g/cm^3 and standard deviation is 0.0408. The heater and various sensors [Sugita. et al., 1997] were installed in the buffer.

After the emplacement of buffer and heater, T-H-M test was started. In order to establish the boundary condition for analysis and to accelerate the water flow through the rock mass, the dam for the pool was constructed on the floor of experiment area. Water head was kept 40 cm at the center of the test pit and temperature of water was constant at 12.3 °C. During heating phase, the heater frame was controlled to be 100 °C at the center of the bottom. Heating phase was started on Dec. 17 1996. The temperature of the controlled point went up quickly to be 100 °C and maintained its stability. Heating phase was stopped on Sept. 1 1997 and then cooling phase was started. The temperature of the controlled point went down gradually to be room temperature. Cooling phase was stopped on Mar. 10 1998. Therefore, the duration of heating phase was 260 days and that of cooling phase was 180 days. Before the end of heating and cooling phase, bentonite samplings were performed.

This note shows the measurement results of heating and cooling phase.

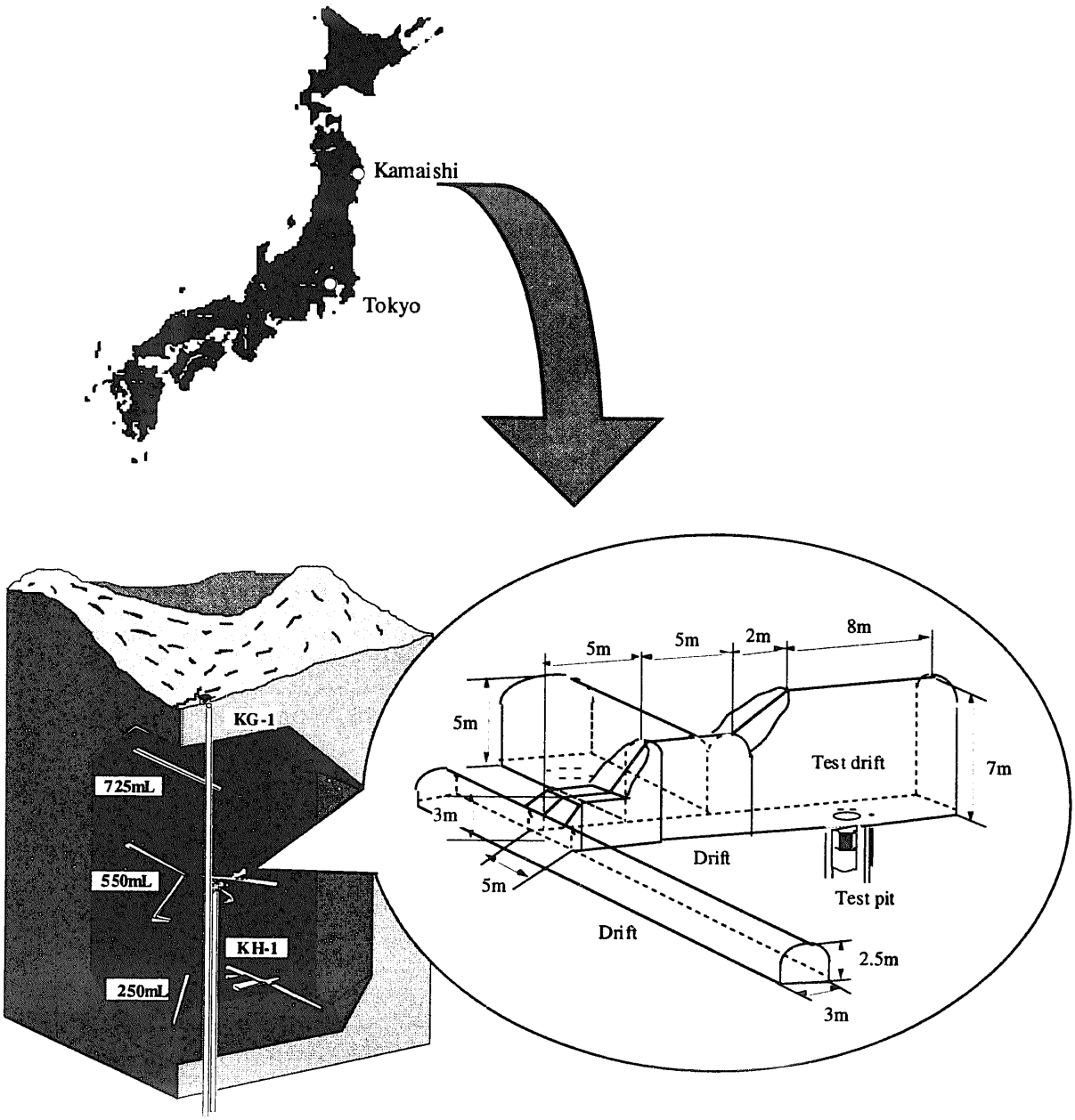

Figure 1-1 Layout of the experiment site

Table 1-1 Time schedule of the T-H-M experiment

		1994	1995	1996	1997	1998	99
Planning							
Excavation of Drifts							
Measurement of Rock Properties	Opening boreholes and borehole TV						
	Hydraulic tests						
	Borehole expansion tests						
	Install monitoring sensors						
	Monitoring						
	Laboratory tests						
Opening test pit	Opening test pit and Mapping joints						
	Measurement of water flow						
	Manufacture of heater						
Setting up Bentonite	Filling Bentonite (96. 8. 20 - 10. 23)						
	Install heater and monitoring sensors in bentonite						
	Plugging						
T-H-M test	Heating (96.12.17 - 97.9.1)						
	Cooling (97.9.1 - 98.3.10)						
	Monitoring						
	Sampling (97.8.20 - 8.29, 98.2.23 - 3.6)						
Decommision	Check of the sensor						
	Decomission						

2. Layout of the sensors

Various sensors were installed both in the buffer and rock to observe the T-H-M phenomena. Figure 2-1 shows the layout of the sensors in the rock and Table 2-1 shows the coordinates of sensor position. The origin (0.0, 0.0, 0.0) is set on the roof of NW drift and the X and Y coordinates correspond to the east and north directions, respectively [Fujita et al., 1996b]. The strain gauge was installed in the boreholes KBM1, KBM2 and KBM3. The thermocouples were also installed in the same boreholes to monitor the temperature. Figure 2-2 shows the location of the strain gauge. SD-1, SD-3, SD-5, SB-1 and SB-3 are the strain of radial direction. The others are the strain of tangential direction. KBM4 and KBM5 were the boreholes for TRIVEC to measure the rock displacement. In the boreholes KBM6 and KBM7, joint deformeters were installed to measure the fracture displacement. Figure 2-3 shows the location of the joint deformeter and displacement direction of fracture. From the entrance of borehole, longitudinal direction is the X-axis and positive value shows the upward movement of the front rock. From the entrance of borehole, transverse direction is the Y-axis and positive value shows the leftward movement of the front rock. Z-axis corresponds to the opening and closing of the fracture aperture, and positive value shows the closing of the fracture aperture. In the boreholes KBH1 to KBH6, pore pressure transducer with thermocouple was installed. Figure 2-4 shows the location of the pore pressure transducer.

Figure 2-5 shows the location of the sensors in the buffer. Sensors were installed at three sections as shown in Figure 2-5. These three sections were determined according to the measurement results of water inflow rate into the test pit [Chijimatsu et al., 1997]. The BBC section is characterized by having no major fracture and less water flux. The CD section is characterized by having major fracture and relatively much water flux. The DDA section is characterized by having major fractures and relatively much water flux. Figure 2-5 (a) shows the location of the sensors to measure the temperature, (b) shows the location of the sensors to measure the water content, (c) shows the location of the sensors to measure the pore pressure, (d) shows the location of the sensors to measure the total pressure, (e) shows the location of the sensors to measure the strain, (d) shows the location of the sensors to measure the heat flux and (g) shows the location of the sensors at the bottom of the test pit. In order to measure the water content in the buffer, the thermocouple psychrometer and the hygrometer were installed. These sensors do not measure the water content directly. The thermocouple psychrometer measures the chemical potential and the temperature, and the hygrometer measures the relative humidity and the temperature. Therefore, the equation is necessary to calculate the water content from the temperature and the chemical potential (or relative humidity). This equation was obtained by laboratory test in advance. This result is described in next section. In Table 2-2, sensor numbers, measurement numbers and coordinates of all sensors installed in the buffer in local cylindrical coordinate as shown in Figure 2-6 are listed. In the local coordinate, top of the test pit is $z=0$ and center of the test pit is $r=0$. In Table 2-3, sensor numbers, measurement numbers and coordinates of all sensors installed in the buffer mass in orthogonal coordinate are listed. The origin is the same with the coordinate of sensors in the rock.

All sensors, except for the thermocouple psychrometer, were connected to the data logger system, and to acquire the data automatically. The thermocouple psychrometer was used manually.

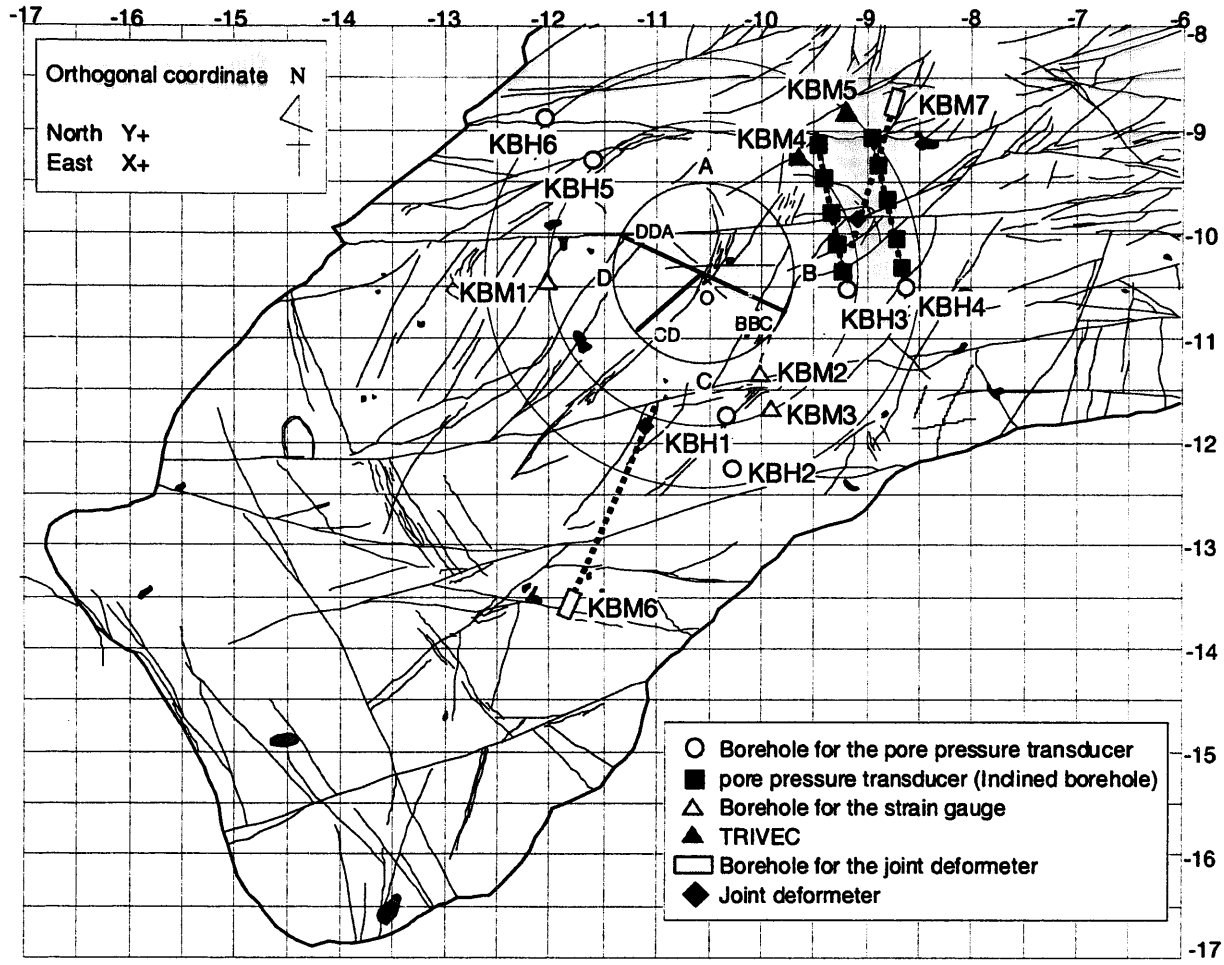

Figure 2-1 Location of the sensors in the rock

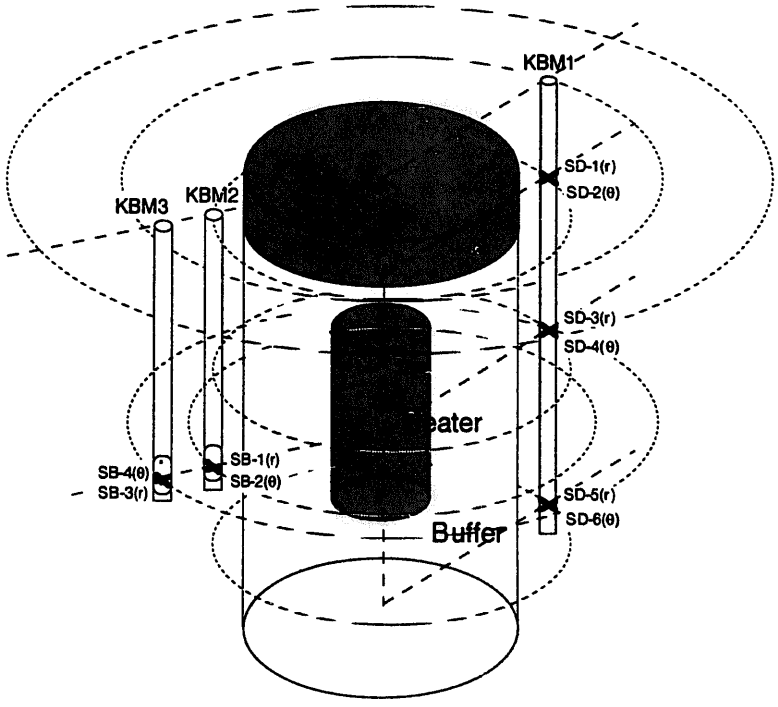

Figure 2-2 Location of the strain gauge in the rock

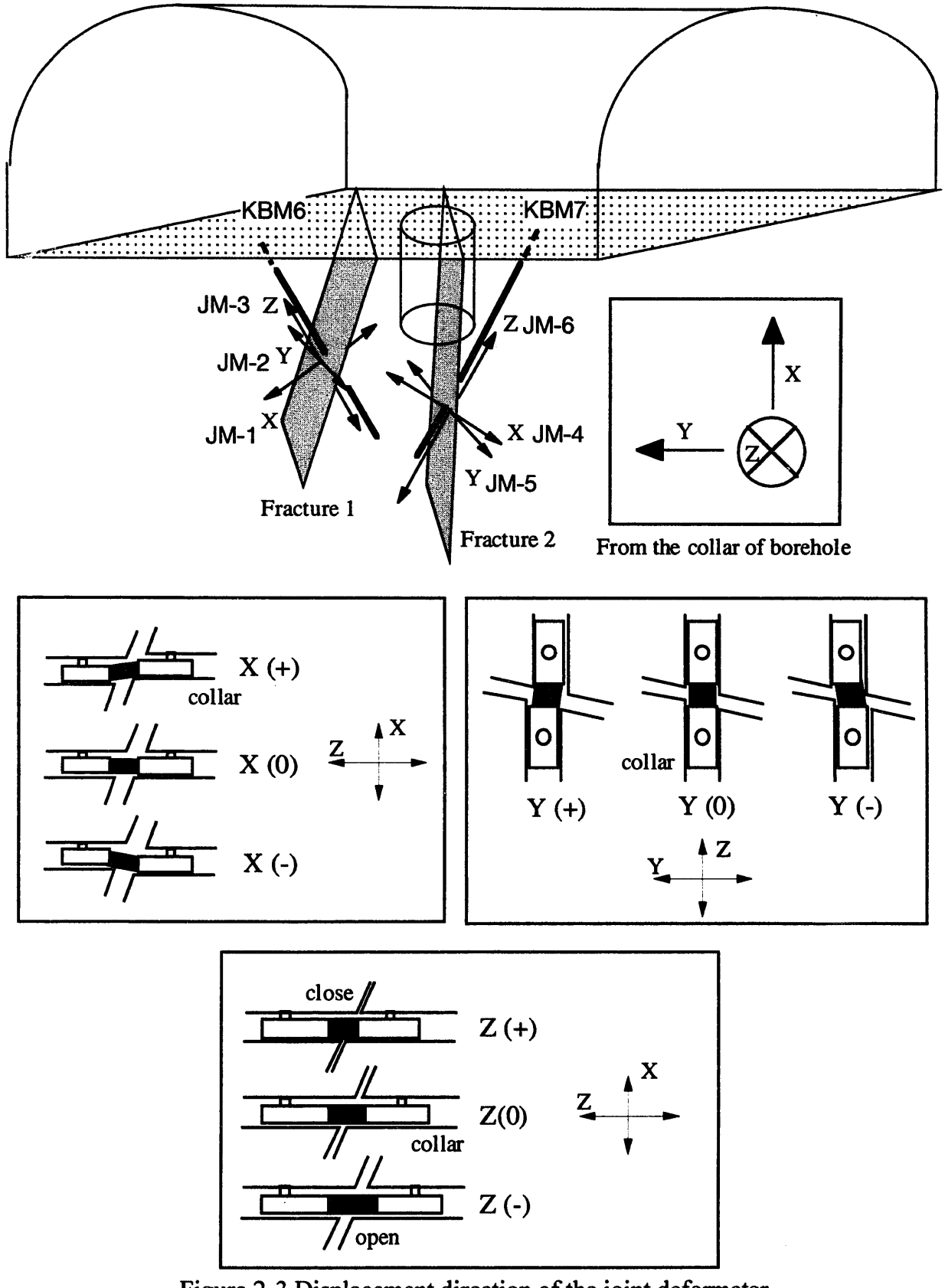

Figure 2-3 Displacement direction of the joint deformeter

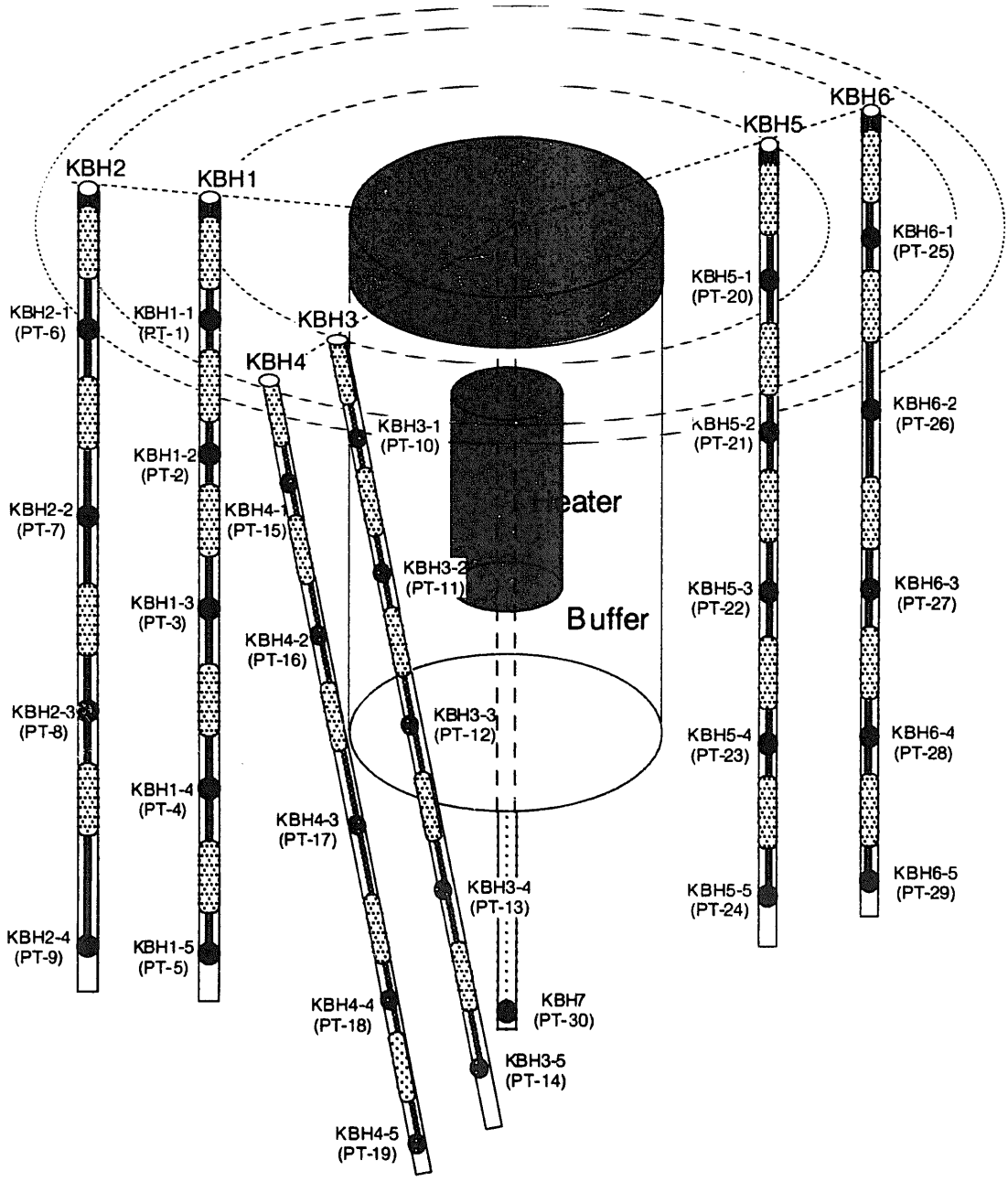

Figure 2-4 Location of the pore pressure transducer in the rock

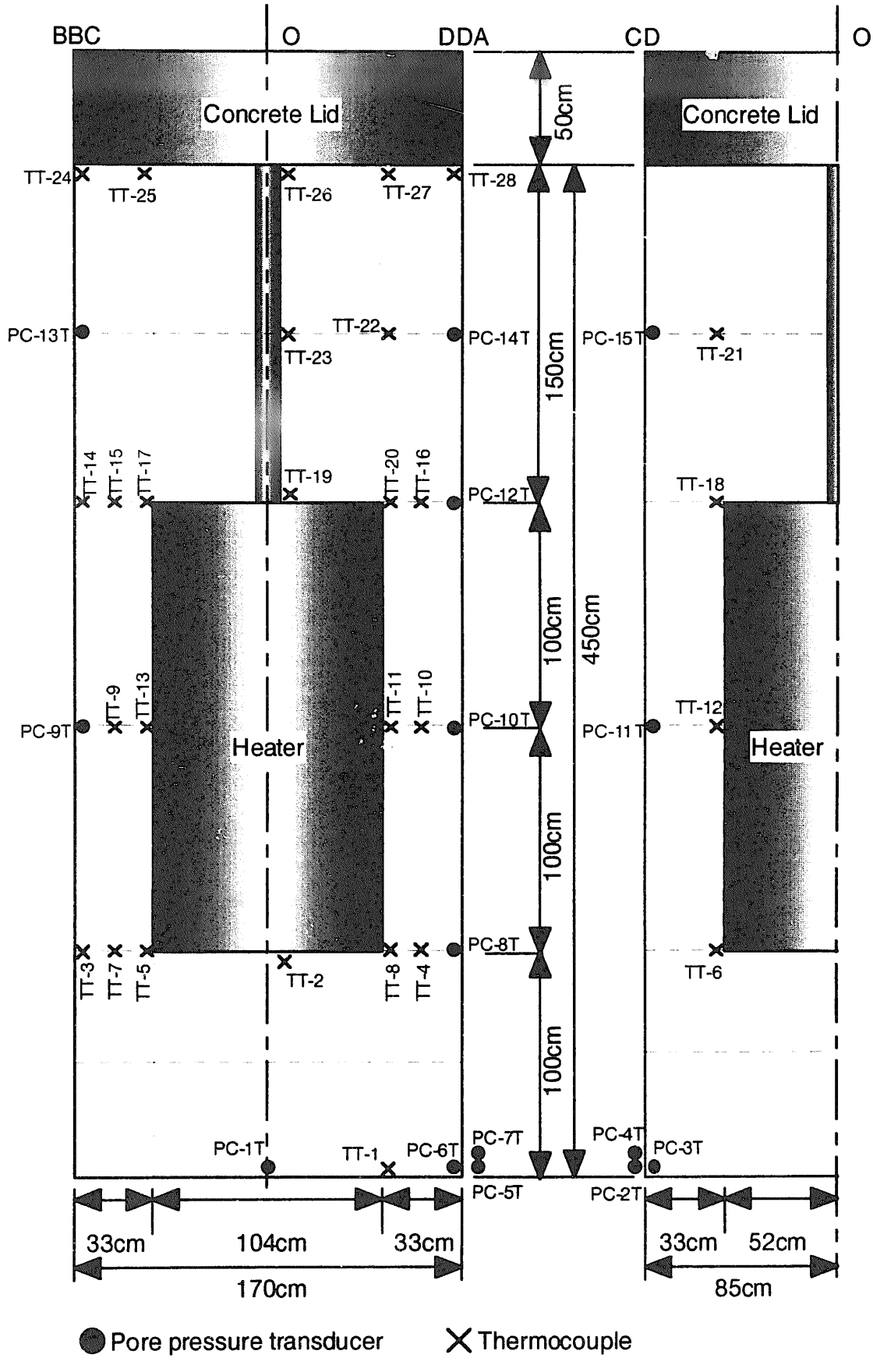

(a) Temperature

Figure 2-5 Location of the sensors in the buffer

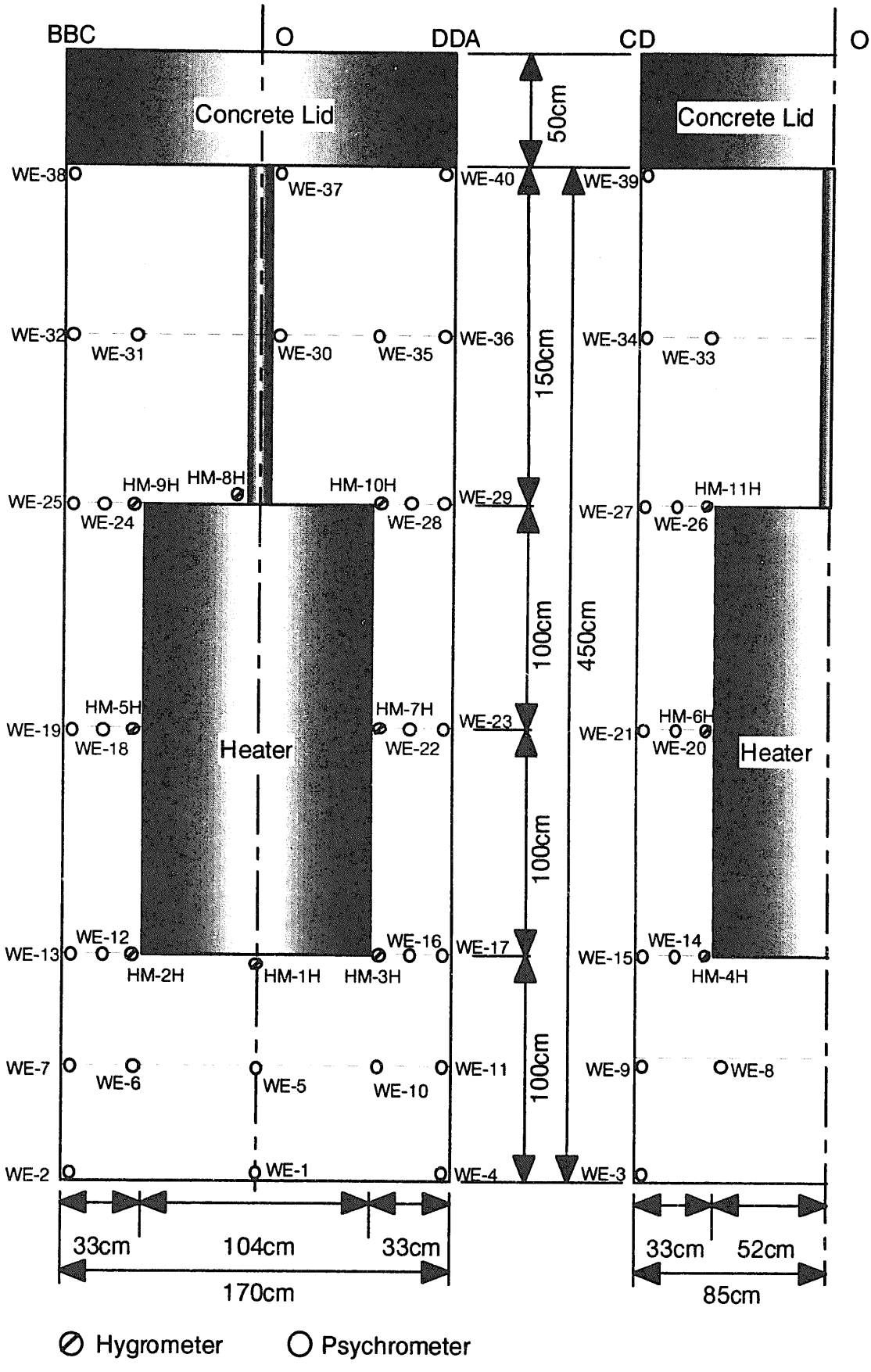

(b) Water content

Figure 2-5 Location of the sensors in the buffer (Contd.)

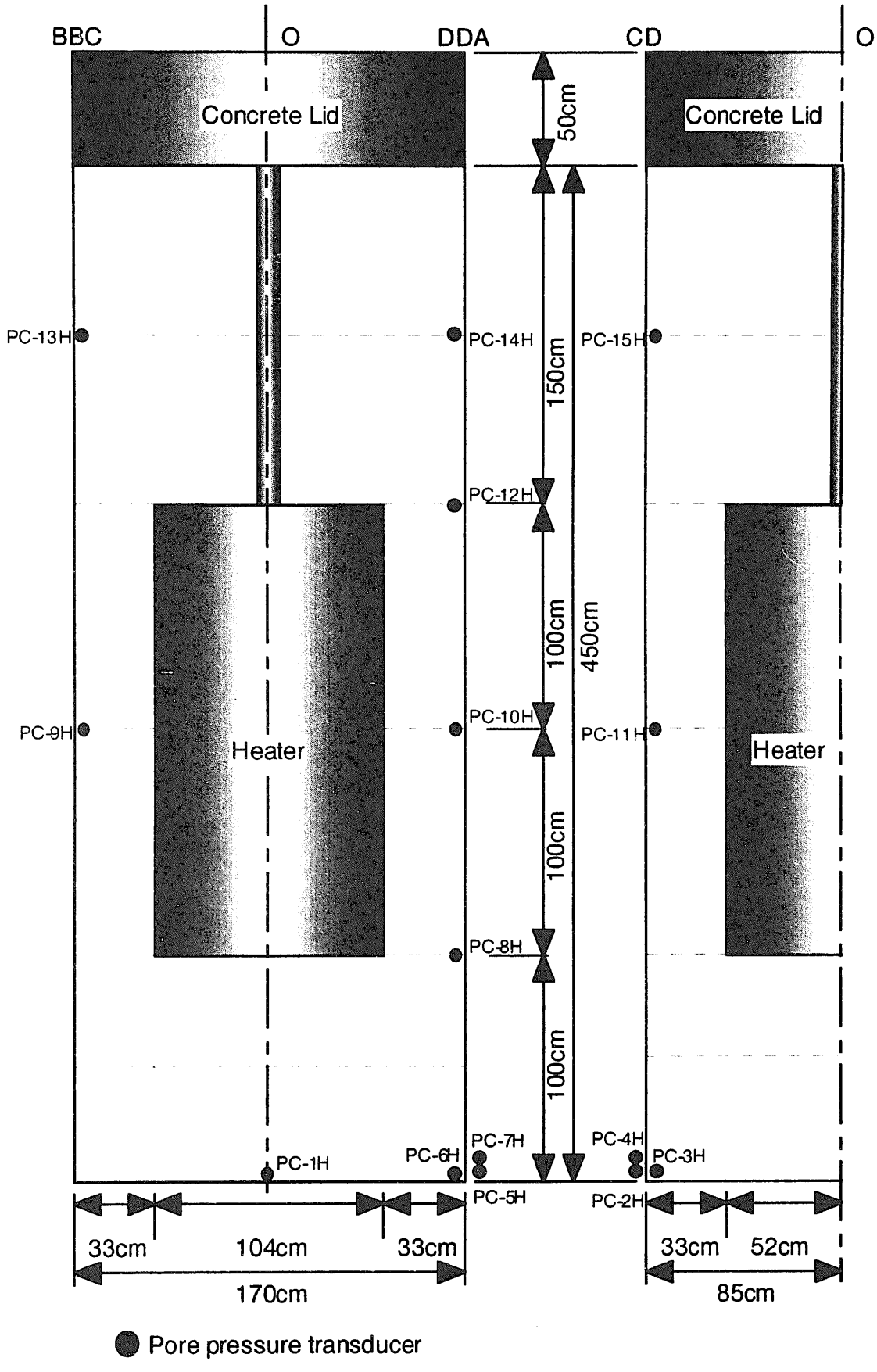

(c) Pore pressure

Figure 2-5 Location of the sensors in the buffer (Contd.)

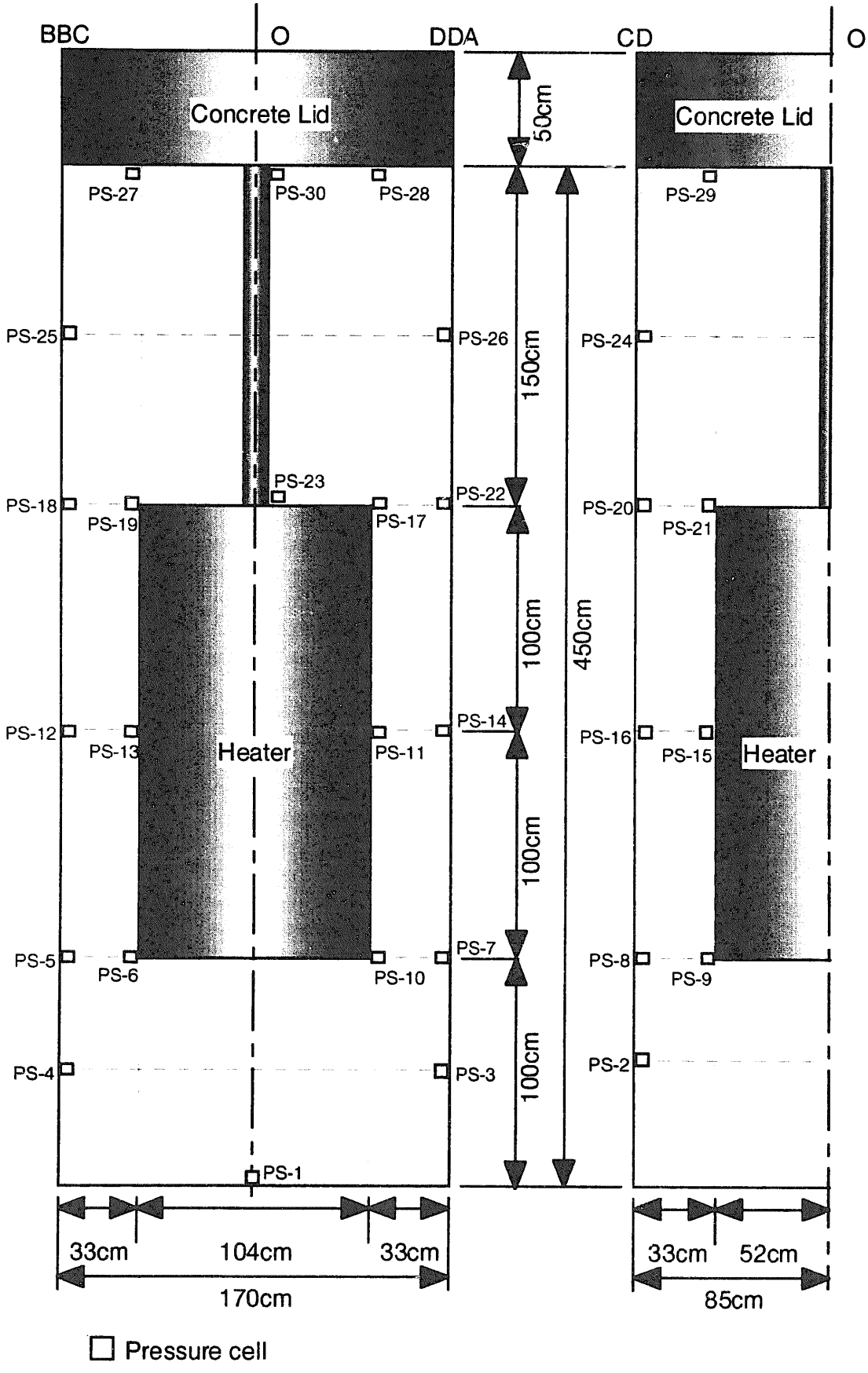

(d) Total pressure

Figure 2-5 Location of the sensors in the buffer (Contd.)

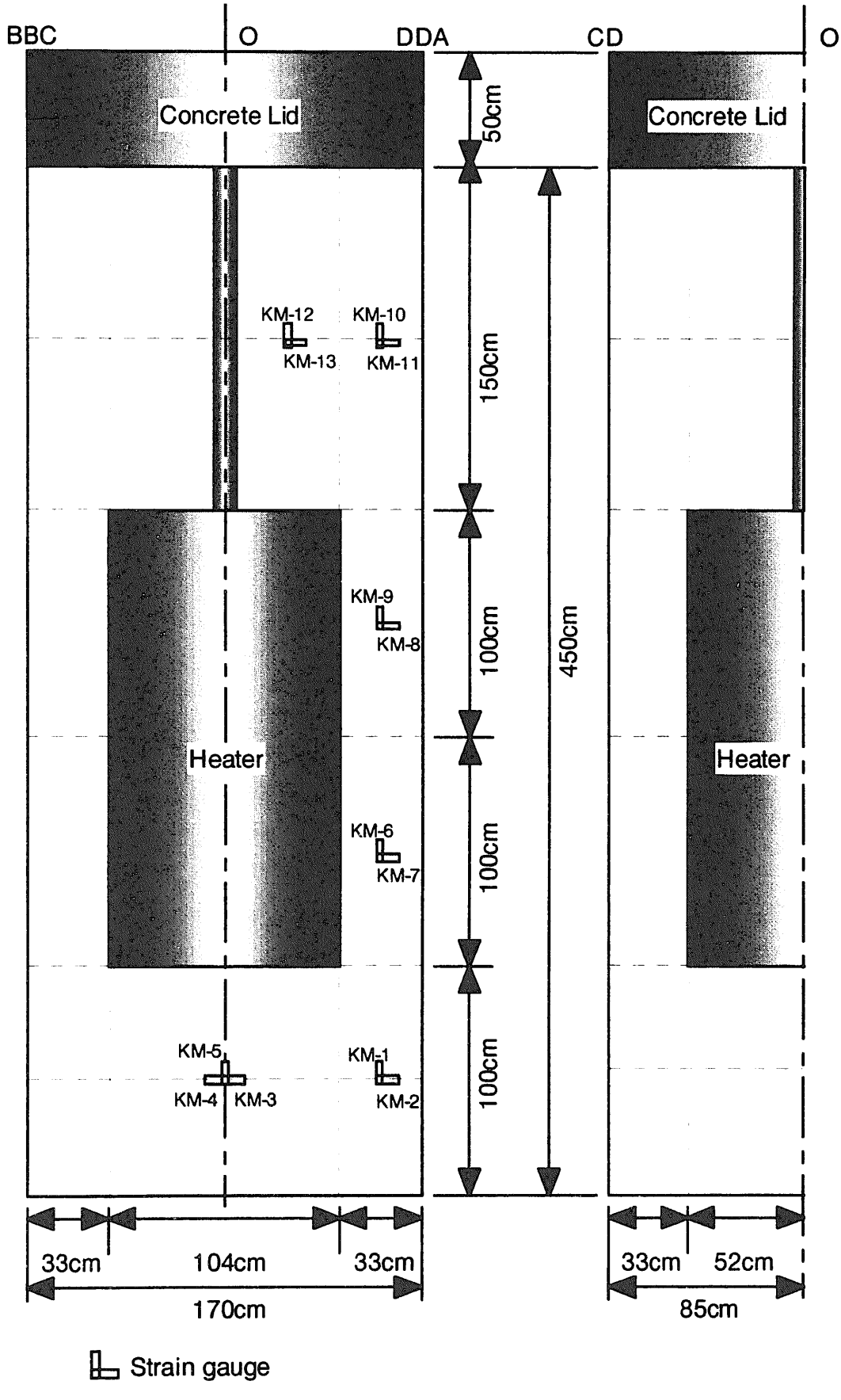

(e) Strain

Figure 2-5 Location of the sensors in the buffer (Contd.)

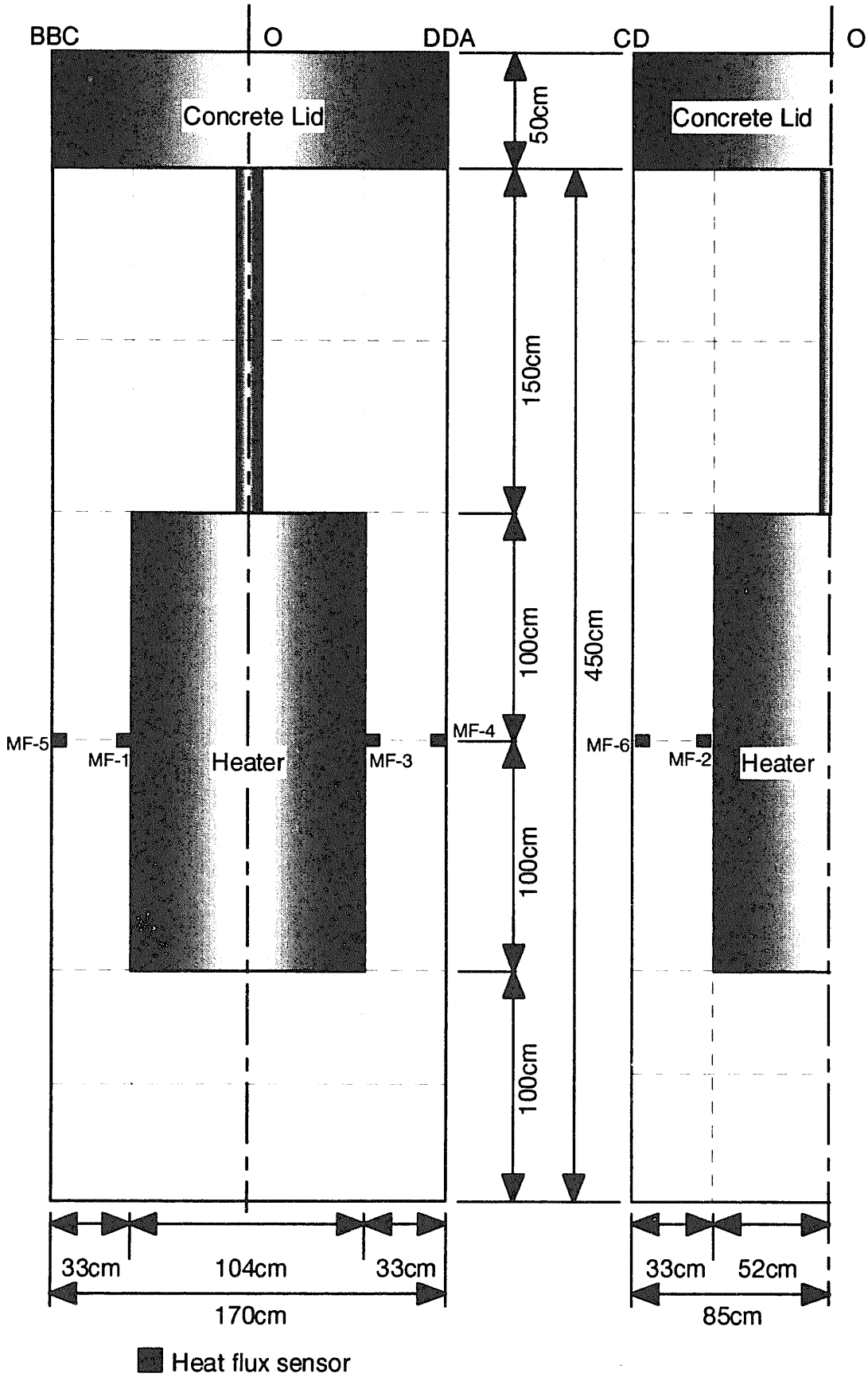

(f) Heat flux

Figure 2-5 Location of the sensors in the buffer (Contd.)

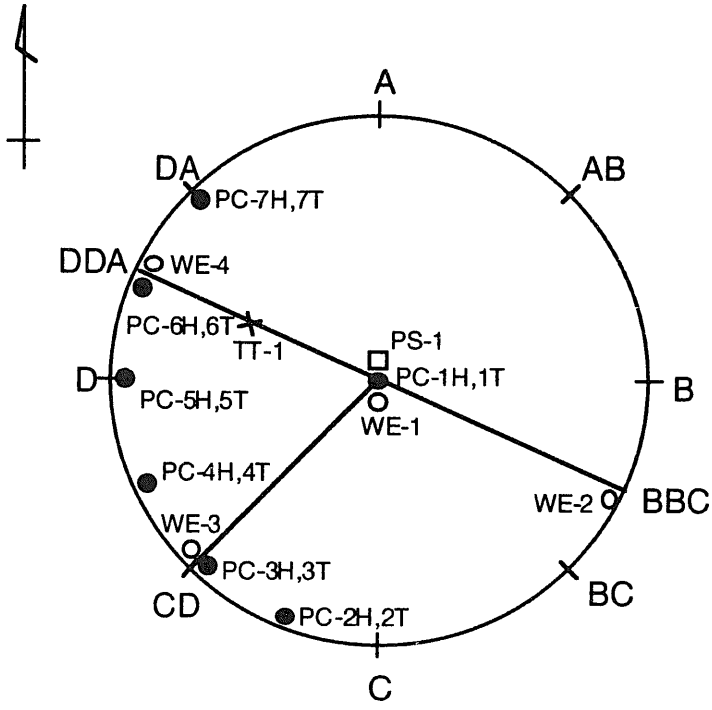

(g) Bottom of the test pit

Figure 2-5 Location of the sensors in the buffer (Contd.)

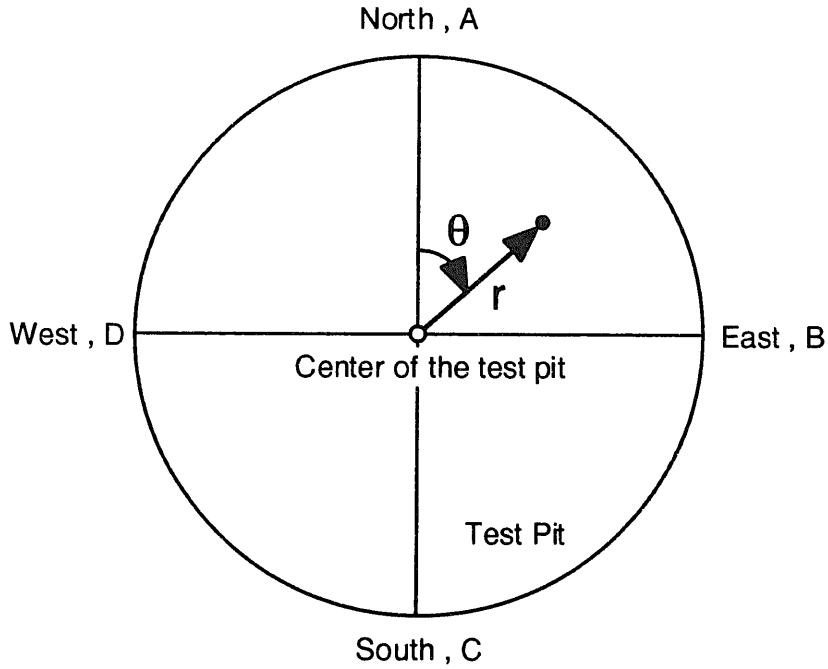

Figure 2-6 Local coordinate

Table 2-1(a) Sensors installed in the rock (Orthogonal coordinate)

Sensor	Sensor Number	Measurement	Measurement Number	Coordinate(m) x	y	z	Borehole or place	Section
Pore pressure transducer with thermometer	PT-1H	Pore pressure	H-1	-10.338	-11.764	-3.598	KBH1	KBH1-1
	2H	Pore pressure	H-2	-10.338	-11.764	-4.948	KBH1	KBH1-2
	3H	Pore pressure	H-3	-10.338	-11.764	-6.523	KBH1	KBH1-3
	4H	Pore pressure	H-4	-10.338	-11.764	-8.323	KBH1	KBH1-4
	5H	Pore pressure	H-5	-10.338	-11.764	-10.023	KBH1	KBH1-5
	6H	Pore pressure	H-6	-10.301	-12.237	-3.667	KBH2	KBH2-1
	7H	Pore pressure	H-7	-10.301	-12.237	-5.567	KBH2	KBH2-2
	8H	Pore pressure	H-8	-10.301	-12.237	-7.517	KBH2	KBH2-3
	9H	Pore pressure	H-9	-10.301	-12.237	-9.567	KBH2	KBH2-4
	10H	Pore pressure	H-10	-9.226	-10.342	-3.525	KBH3	KBH3-1
	11H	Pore pressure	H-11	-9.277	-10.080	-4.899	KBH3	KBH3-2
	12H	Pore pressure	H-12	-9.335	-9.785	-6.446	KBH3	KBH3-3
	13H	Pore pressure	H-13	-9.397	-9.466	-8.114	KBH3	KBH3-4
	14H	Pore pressure	H-14	-9.462	-9.129	-9.881	KBH3	KBH3-5
	15H	Pore pressure	H-15	-8.656	-10.314	-3.530	KBH4	KBH4-1
	16H	Pore pressure	H-16	-8.723	-10.026	-5.051	KBH4	KBH4-2
	17H	Pore pressure	H-17	-8.806	-9.663	-6.965	KBH4	KBH4-3
	18H	Pore pressure	H-18	-8.884	-9.328	-8.732	KBH4	KBH4-4
	19H	Pore pressure	H-19	-8.944	-9.068	-10.107	KBH4	KBH4-5
	20H	Pore pressure	H-20	-11.603	-9.306	-3.633	KBH5	KBH5-1
	21H	Pore pressure	H-21	-11.603	-9.306	-5.183	KBH5	KBH5-2
	22H	Pore pressure	H-22	-11.603	-9.306	-6.783	KBH5	KBH5-3
	23H	Pore pressure	H-23	-11.603	-9.306	-8.333	KBH5	KBH5-4
	24H	Pore pressure	H-24	-11.603	-9.306	-9.883	KBH5	KBH5-5
	25H	Pore pressure	H-25	-12.035	-8.896	-3.532	KBH6	KBH6-1
	26H	Pore pressure	H-26	-12.035	-8.896	-5.282	KBH6	KBH6-2
	27H	Pore pressure	H-27	-12.035	-8.896	-7.082	KBH6	KBH6-3
	28H	Pore pressure	H-28	-12.035	-8.896	-8.582	KBH6	KBH6-4
	29H	Pore pressure	H-29	-12.035	-8.896	-10.032	KBH6	KBH6-5

Table 2-1(b) Sensors installed in the rock (Orthogonal coordinate)

Sensor	Sensor Number	Measurement	Measurement Number	Coordinate(m) x	y	z	Borehole or place	Section
Pore pressure transducer with thermometer	PT-1T	Temperature	T-1	-10.338	-11.764	-3.598	KBH1	KBH1-1
	2T	Temperature	T-2	-10.338	-11.764	-4.948	KBH1	KBH1-2
	3T	Temperature	T-3	-10.338	-11.764	-6.523	KBH1	KBH1-3
	4T	Temperature	T-4	-10.338	-11.764	-8.323	KBH1	KBH1-4
	5T	Temperature	T-5	-10.338	-11.764	-10.023	KBH1	KBH1-5
	6T	Temperature	T-6	-10.301	-12.237	-3.667	KBH2	KBH2-1
	7T	Temperature	T-7	-10.301	-12.237	-5.567	KBH2	KBH2-2
	8T	Temperature	T-8	-10.301	-12.237	-7.517	KBH2	KBH2-3
	9T	Temperature	T-9	-10.301	-12.237	-9.567	KBH2	KBH2-4
	10T	Temperature	T-10	-9.226	-10.342	-3.525	KBH3	KBH3-1
	11T	Temperature	T-11	-9.277	-10.080	-4.899	KBH3	KBH3-2
	12T	Temperature	T-12	-9.335	-9.785	-6.446	KBH3	KBH3-3
	13T	Temperature	T-13	-9.397	-9.466	-8.114	KBH3	KBH3-4
	14T	Temperature	T-14	-9.462	-9.129	-9.881	KBH3	KBH3-5
	15T	Temperature	T-15	-8.656	-10.314	-3.530	KBH4	KBH4-1
	16T	Temperature	T-16	-8.723	-10.026	-5.051	KBH4	KBH4-2
	17T	Temperature	T-17	-8.806	-9.663	-6.965	KBH4	KBH4-3
	18T	Temperature	T-18	-8.884	-9.328	-8.732	KBH4	KBH4-4
	19T	Temperature	T-19	-8.944	-9.068	-10.107	KBH4	KBH4-5
	20T	Temperature	T-20	-11.603	-9.306	-3.633	KBH5	KBH5-1
	21T	Temperature	T-21	-11.603	-9.306	-5.183	KBH5	KBH5-2
	22T	Temperature	T-22	-11.603	-9.306	-6.783	KBH5	KBH5-3
	23T	Temperature	T-23	-11.603	-9.306	-8.333	KBH5	KBH5-4
	24T	Temperature	T-24	-11.603	-9.306	-9.883	KBH5	KBH5-5
	25T	Temperature	T-25	-12.035	-8.896	-3.532	KBH6	KBH6-1
	26T	Temperature	T-26	-12.035	-8.896	-5.282	KBH6	KBH6-2
	27T	Temperature	T-27	-12.035	-8.896	-7.082	KBH6	KBH6-3
	28T	Temperature	T-28	-12.035	-8.896	-8.582	KBH6	KBH6-4
	29T	Temperature	T-29	-12.035	-8.896	-10.032	KBH6	KBH6-5

Table 2-1(c) Sensors installed in the rock (Orthogonal coordinate)

Sensor	Sensor Number	Measurement	Measurement Number	Coordinate(m) x	y	z	Borehole or place
Strain gauge	SD-1	Strain(r)	M-1	-12.042	-10.453	-4.408	KBM1
	2	Strain(θ)	M-2	-12.042	-10.453	-4.408	KBM1
	3	Strain(r)	M-3	-12.042	-10.453	-7.408	KBM1
	4	Strain(θ)	M-4	-12.042	-10.453	-7.408	KBM1
	5	Strain(r)	M-5	-12.042	-10.453	-10.408	KBM1
	6	Strain(θ)	M-6	-12.042	-10.453	-10.408	KBM1
Borehole strain meter	SB-1	Strain(r)	M-7	-10.013	-11.342	-5.360	KBM2
	2	Strain(θ)	M-8	-10.013	-11.342	-5.360	KBM2
	3	Strain(r)	M-9	-9.913	-11.672	-5.480	KBM3
	4	Strain(θ)	M-10	-9.913	-11.672	-5.480	KBM3
Thermocouple	TC-1	Temperature	T-30	-12.042	-10.453	-4.408	KBM1
	2	Temperature	T-31	-12.042	-10.453	-7.408	KBM1
	3	Temperature	T-32	-12.042	-10.453	-10.408	KBM1
	4	Temperature	T-33	-10.013	-11.342	-5.360	KBM2
	5	Temperature	T-34	-9.913	-11.672	-5.480	KBM3
Joint deformeter	JM-1	Displacement	M-11	-11.107	-11.871	-6.359	KBM6
	2	Displacement	M-12	-11.107	-11.871	-6.359	KBM6
	3	Displacement	M-13	-11.107	-11.871	-6.359	KBM6
	4	Displacement	M-14	-9.087	-9.902	-4.821	KBM7
	5	Displacement	M-15	-9.087	-9.902	-4.821	KBM7
	6	Displacement	M-16	-9.087	-9.902	-4.821	KBM7
Joint transducer	T-1	Displacement	M-17	-7.699	-9.819	-2.542	PI3
	2	Displacement	M-18	-11.304	-8.995	-2.436	PI4
	3	Displacement	M-19	-12.570	-10.078	-2.196	PI2
	4	Displacement	M-20	-11.635	-11.869	-2.340	PI1
Surface displacement transducer	P-1	Displacement(90)	M-21	-7.699	-9.819	-2.542	PI3
	2	Displacement(45)	M-22	-7.699	-9.819	-2.542	PI3
	3	Displacement(90)	M-23	-11.304	-8.995	-2.436	PI4
	4	Displacement(45)	M-24	-11.304	-8.995	-2.436	PI4
	5	Displacement(90)	M-25	-12.570	-10.078	-2.196	PI2
	6	Displacement(45)	M-26	-12.570	-10.078	-2.196	PI2
	7	Displacement(90)	M-27	-11.635	-11.869	-2.340	PI1
	8	Displacement(45)	M-28	-11.635	-11.869	-2.340	PI1

Table 2-2 (a) Sensors installed in the Buffer (Local coordinate)

Sensor	Sensor Number	Measurement	Measurement Number	Unit	Coordinate			Observation line
					θ (°)	r (m)	z (m)	
Pore pressure transducer with thermometer	PC-1H	Pore pressure	H-31	kPa	258.50	0.150	-5.030	O
	2H	Pore pressure	H-32	kPa	217.00	0.840	-4.950	O-CCD
	3H	Pore pressure	H-33	kPa	225.00	0.840	-4.950	O-CD
	4H	Pore pressure	H-34	kPa	233.00	0.840	-4.950	O-CDD
	5H	Pore pressure	H-35	kPa	284.00	0.840	-4.950	O-D
	6H	Pore pressure	H-36	kPa	292.50	0.840	-4.950	O-DDA
	7H	Pore pressure	H-37	kPa	300.50	0.840	-4.950	O-DA
	8H	Pore pressure	H-38	kPa	287.50	0.840	-4.000	O-DDA
	9H	Pore pressure	H-39	kPa	102.50	0.840	-3.000	O-BBC
	10H	Pore pressure	H-40	kPa	287.50	0.840	-3.000	O-DDA
	11H	Pore pressure	H-41	kPa	235.00	0.840	-3.000	O-CD
	12H	Pore pressure	H-42	kPa	287.50	0.840	-2.050	O-DDA
	13H	Pore pressure	H-43	kPa	107.50	0.840	-1.250	O-BBC
	14H	Pore pressure	H-44	kPa	287.50	0.840	-1.250	O-DDA
	15H	Pore pressure	H-45	kPa	220.00	0.840	-1.250	O-CD
	PC-1T	Temperature	T-36	℃	258.50	0.150	-5.030	O
	2T	Temperature	T-37	℃	217.00	0.840	-4.950	O-CCD
	3T	Temperature	T-38	℃	225.00	0.840	-4.950	O-CD
	4T	Temperature	T-39	℃	233.00	0.840	-4.950	O-CDD
	5T	Temperature	T-40	℃	284.00	0.840	-4.950	O-D
	6T	Temperature	T-41	℃	292.50	0.840	-4.950	O-DDA
	7T	Temperature	T-42	℃	300.50	0.840	-4.950	O-DA
	8T	Temperature	T-43	℃	287.50	0.840	-4.000	O-DDA
	9T	Temperature	T-44	℃	102.50	0.840	-3.000	O-BBC
	10T	Temperature	T-45	℃	287.50	0.840	-3.000	O-DDA
	11T	Temperature	T-46	℃	235.00	0.840	-3.000	O-CD
	12T	Temperature	T-47	℃	287.50	0.840	-2.050	O-DDA
	13T	Temperature	T-48	℃	107.50	0.840	-1.250	O-BBC
	14T	Temperature	T-49	℃	287.50	0.840	-1.250	O-DDA
	15T	Temperature	T-50	℃	220.00	0.840	-1.250	O-CD
Hygrometer	HM-1H	Humidity	H-46	%	258.80	0.020	-4.030	O
	2H	Humidity	H-47	%	112.50	0.550	-4.000	O-BBC
	3H	Humidity	H-48	%	292.50	0.550	-4.000	O-DDA
	4H	Humidity	H-49	%	225.00	0.550	-4.000	O-CD
	5H	Humidity	H-50	%	112.50	0.550	-3.000	O-BBC
	6H	Humidity	H-51	%	225.00	0.550	-3.000	O-CD
	7H	Humidity	H-52	%	292.50	0.550	-3.000	O-DDA
	8H	Humidity	H-53	%	112.50	0.090	-2.020	O
	9H	Humidity	H-54	%	112.50	0.550	-2.050	O-BBC
	10H	Humidity	H-55	%	292.50	0.550	-2.050	O-DDA
	11H	Humidity	H-56	%	225.00	0.550	-2.050	O-CD
	HM-1T	Temperature	T-51	℃	258.80	0.020	-4.030	O
	2T	Temperature	T-52	℃	112.50	0.550	-4.000	O-BBC
	3T	Temperature	T-53	℃	292.50	0.550	-4.000	O-DDA
	4T	Temperature	T-54	℃	225.00	0.550	-4.000	O-CD
	5T	Temperature	T-55	℃	112.50	0.550	-3.000	O-BBC
	6T	Temperature	T-56	℃	225.00	0.550	-3.000	O-CD
	7T	Temperature	T-57	℃	292.50	0.550	-3.000	O-DDA
	8T	Temperature	T-58	℃	112.50	0.090	-2.020	O
	9T	Temperature	T-59	℃	112.50	0.550	-2.050	O-BBC
	10T	Temperature	T-60	℃	292.50	0.550	-2.050	O-DDA
	11T	Temperature	T-61	℃	225.00	0.550	-2.050	O-CD

Table 2-2 (b) Sensors installed in the Buffer (Local coordinate)

Sensor	Sensor Number	Measurement	Measurement Number	Unit	Coordinate			Observation line
					θ (°)	r (m)	z (m)	
Pcychrometer	WE-1	Water potential	W-1	MPa	0.00	0.150	-5.030	O
	2	Water potential	W-2	MPa	112.50	0.840	-5.030	O-BBC
	3	Water potential	W-3	MPa	230.00	0.840	-5.030	O-CD
	4	Water potential	W-4	MPa	287.50	0.840	-5.030	O-DDA
	5	Water potential	W-5	MPa	0.00	0.000	-4.500	O
	6	Water potential	W-6	MPa	112.50	0.520	-4.500	O-BBC
	7	Water potential	W-7	MPa	112.50	0.840	-4.500	O-BBC
	8	Water potential	W-8	MPa	225.00	0.520	-4.500	O-CD
	9	Water potential	W-9	MPa	221.00	0.840	-4.500	O-CD
	10	Water potential	W-10	MPa	292.50	0.520	-4.500	O-DDA
	11	Water potential	W-11	MPa	292.50	0.840	-4.500	O-DDA
	12	Water potential	W-12	MPa	112.50	0.690	-4.000	O-BBC
	13	Water potential	W-13	MPa	112.50	0.840	-4.000	O-BBC
	14	Water potential	W-14	MPa	225.00	0.690	-4.000	O-CD
	15	Water potential	W-15	MPa	225.00	0.840	-4.000	O-CD
	16	Water potential	W-16	MPa	292.50	0.690	-4.000	O-DDA
	17	Water potential	W-17	MPa	292.50	0.840	-4.000	O-DDA
	18	Water potential	W-18	MPa	112.50	0.690	-3.000	O-BBC
	19	Water potential	W-19	MPa	112.50	0.840	-3.000	O-BBC
	20	Water potential	W-20	MPa	225.00	0.690	-3.000	O-CD
	21	Water potential	W-21	MPa	225.00	0.840	-3.000	O-CD
	22	Water potential	W-22	MPa	292.50	0.690	-3.000	O-DDA
	23	Water potential	W-23	MPa	292.50	0.840	-3.000	O-DDA
	24	Water potential	W-24	MPa	112.50	0.690	-2.050	O-BBC
	25	Water potential	W-25	MPa	112.50	0.840	-2.050	O-BBC
	26	Water potential	W-26	MPa	225.00	0.690	-2.050	O-CD
	27	Water potential	W-27	MPa	225.00	0.840	-2.050	O-CD
	28	Water potential	W-28	MPa	292.50	0.690	-2.050	O-DDA
	29	Water potential	W-29	MPa	292.50	0.840	-2.050	O-DDA
	30	Water potential	W-30	MPa	292.50	0.060	-1.250	O
	31	Water potential	W-31	MPa	112.50	0.520	-1.250	O-BBC
	32	Water potential	W-32	MPa	112.50	0.840	-1.250	O-BBC
	33	Water potential	W-33	MPa	225.00	0.520	-1.250	O-CD
	34	Water potential	W-34	MPa	225.00	0.840	-1.250	O-CD
	35	Water potential	W-35	MPa	292.50	0.520	-1.250	O-DDA
	36	Water potential	W-36	MPa	292.50	0.840	-1.250	O-DDA
	37	Water potential	W-37	MPa	112.50	0.060	-0.550	O
	38	Water potential	W-38	MPa	112.50	0.840	-0.550	O-BBC
	39	Water potential	W-39	MPa	225.00	0.840	-0.550	O-CD
	40	Water potential	W-40	MPa	292.50	0.840	-0.550	O-DDA

Table 2-2 (c) Sensors installed in the Buffer (Local coordinate)

Sensor	Sensor Number	Measurement	Measurement Number	Unit	Coordinate			Observation line
					θ(°)	r (m)	z (m)	
Strain gauge	KM-1	Strain(V)	M-38	με	290.50	0.680	-4.500	O-DDA
	2	Strain(H)	M-39	με	296.50	0.620	-4.500	O-DDA
	3	Strain(H)	M-40	με	244.50	0.070	-4.500	O-DDA
	4	Strain(H)	M-41	με	112.00	0.070	-4.500	O-BBC
	5	Strain(V)	M-42	με	23.00	0.100	-4.500	O
	6	Strain(V)	M-43	με	290.50	0.680	-3.500	O-DDA
	7	Strain(H)	M-44	με	296.50	0.650	-3.500	O-DDA
	8	Strain(H)	M-45	με	296.50	0.650	-3.000	O-DDA
	9	Strain(V)	M-46	με	290.50	0.680	-3.000	O-DDA
	10	Strain(V)	M-47	με	290.50	0.700	-1.250	O-DDA
	11	Strain(H)	M-48	με	300.50	0.660	-1.250	O-DDA
	12	Strain(V)	M-49	με	297.50	0.270	-1.250	O-DDA
	13	Strain(H)	M-50	με	269.50	0.290	-1.250	O-DDA
Pressure cell	PS-1	Pressure	M-51	kPa	0.00	0.000	-5.030	O
	2	Pressure	M-52	kPa	229.50	0.850	-4.500	O-CD
	3	Pressure	M-53	kPa	287.50	0.850	-4.500	O-DDA
	4	Pressure	M-54	kPa	107.50	0.850	-4.500	O-BBC
	5	Pressure	M-55	kPa	117.50	0.850	-4.000	O-BBC
	6	Pressure	M-56	kPa	117.50	0.520	-4.000	O-BBC
	7	Pressure	M-57	kPa	297.50	0.850	-4.000	O-DDA
	8	Pressure	M-58	kPa	230.00	0.850	-4.000	O-CD
	9	Pressure	M-59	kPa	230.00	0.520	-4.000	O-CD
	10	Pressure	M-60	kPa	297.50	0.520	-4.000	O-DDA
	11	Pressure	M-61	kPa	297.50	0.520	-3.000	O-DDA
	12	Pressure	M-62	kPa	117.50	0.850	-3.000	O-BBC
	13	Pressure	M-63	kPa	117.50	0.520	-3.000	O-BBC
	14	Pressure	M-64	kPa	297.50	0.850	-3.000	O-DDA
	15	Pressure	M-65	kPa	220.00	0.520	-3.000	O-CD
	16	Pressure	M-66	kPa	220.00	0.850	-3.000	O-CD
	17	Pressure	M-67	kPa	297.50	0.520	-2.050	O-DDA
	18	Pressure	M-68	kPa	117.50	0.850	-2.050	O-BBC
	19	Pressure	M-69	kPa	117.50	0.520	-2.050	O-BBC
	20	Pressure	M-70	kPa	230.00	0.850	-2.050	O-CD
	21	Pressure	M-71	kPa	230.00	0.520	-2.050	O-CD
	22	Pressure	M-72	kPa	297.50	0.850	-2.050	O-DDA
	23	Pressure	M-73	kPa	225.00	0.080	-2.050	O
	24	Pressure	M-74	kPa	230.00	0.850	-1.250	O-CD
	25	Pressure	M-75	kPa	117.50	0.850	-1.250	O-BBC
	26	Pressure	M-76	kPa	297.50	0.850	-1.250	O-DDA
	27	Pressure	M-77	kPa	112.50	0.520	-0.500	O-BBC
	28	Pressure	M-78	kPa	292.50	0.520	-0.500	O-DDA
	29	Pressure	M-79	kPa	225.00	0.520	-0.500	O-CD
	30	Pressure	M-80	kPa	292.50	0.060	-0.500	O

Table 2-2 (d) Sensors installed in the Buffer (Local coordinate)

Sensor	Sensor Number	Measurement	Measurement Number	Unit	Coordinate(m)			Observation line
					θ (°)	r (m)	z (m)	
Thermocouple	TT-1	Temperature	T-62	℃	292.50	0.520	-5.030	O-DDA
	2	Temperature	T-63	℃	0.00	0.020	-4.000	O
	3	Temperature	T-64	℃	107.50	0.850	-4.000	O-BBC
	4	Temperature	T-65	℃	287.50	0.690	-4.000	O-DDA
	5	Temperature	T-66	℃	107.50	0.520	-3.950	O-BBC
	6	Temperature	T-67	℃	235.00	0.520	-3.950	O-CD
	7	Temperature	T-68	℃	107.50	0.690	-4.000	O-BBC
	8	Temperature	T-69	℃	287.50	0.520	-3.950	O-DDA
	9	Temperature	T-70	℃	102.50	0.690	-3.000	O-BBC
	10	Temperature	T-71	℃	287.50	0.690	-3.000	O-DDA
	11	Temperature	T-72	℃	287.50	0.520	-3.030	O-DDA
	12	Temperature	T-73	℃	238.00	0.520	-3.030	O-CD
	13	Temperature	T-74	℃	98.00	0.520	-3.030	O-BBC
	14	Temperature	T-75	℃	107.50	0.850	-2.050	O-BBC
	15	Temperature	T-76	℃	107.50	0.690	-2.050	O-BBC
	16	Temperature	T-77	℃	287.50	0.690	-2.050	O-DDA
	17	Temperature	T-78	℃	108.50	0.520	-2.080	O-BBC
	18	Temperature	T-79	℃	221.00	0.520	-2.080	O-CD
	19	Temperature	T-80	℃	288.50	0.520	-2.080	O-DDA
	20	Temperature	T-81	℃	10.00	0.070	-2.050	O
	21	Temperature	T-82	℃	231.00	0.520	-1.250	O-CD
	22	Temperature	T-83	℃	286.50	0.520	-1.250	O-DDA
	23	Temperature	T-84	℃	0.00	0.040	-1.250	O
	24	Temperature	T-85	℃	107.50	0.850	-0.500	O-BBC
	25	Temperature	T-86	℃	107.50	0.520	-0.500	O-BBC
	26	Temperature	T-87	℃	0.00	0.040	-0.500	O
	27	Temperature	T-88	℃	287.50	0.520	-0.500	O-DDA
	28	Temperature	T-89	℃	287.50	0.850	-0.500	O-DDA
Heat flux sensor	MF-1	Heat flux	T-90	W/m^2	107.50	0.520	-3.000	O-BBC
	2	Heat flux	T-91	W/m^2	230.00	0.520	-3.000	O-CD
	3	Heat flux	T-92	W/m^2	282.50	0.520	-3.000	O-DDA
	4	Heat flux	T-93	W/m^2	282.50	0.850	-3.000	O-DDA
	5	Heat flux	T-94	W/m^2	107.50	0.850	-3.000	O-BBC
	6	Heat flux	T-95	W/m^2	230.00	0.850	-3.000	O-CD

Table 2-3 (a) Sensors installed in the Buffer (Orthogonal coordinate)

Sensor	Sensor Number	Measurement	Measurement Number	Unit	Coordinate(m) X(m)	Y(m)	Z(m)	Observation line
Pore pressure transducer with thermometer	PC-1H	Pore pressure	H-31	kPa	-10.718	-10.386	-7.387	O
	2H	Pore pressure	H-32	kPa	-11.077	-11.027	-7.307	O-CCD
	3H	Pore pressure	H-33	kPa	-11.165	-10.950	-7.307	O-CD
	4H	Pore pressure	H-34	kPa	-11.242	-10.862	-7.307	O-CDD
	5H	Pore pressure	H-35	kPa	-11.386	-10.153	-7.307	O-D
	6H	Pore pressure	H-36	kPa	-11.347	-10.035	-7.307	O-DDA
	7H	Pore pressure	H-37	kPa	-11.295	-9.930	-7.307	O-DA
	8H	Pore pressure	H-38	kPa	-11.372	-10.103	-6.357	O-DDA
	9H	Pore pressure	H-39	kPa	-9.751	-10.538	-5.357	O-BBC
	10H	Pore pressure	H-40	kPa	-11.372	-10.103	-5.357	O-DDA
	11H	Pore pressure	H-41	kPa	-11.259	-10.838	-5.357	O-CD
	12H	Pore pressure	H-42	kPa	-11.372	-10.103	-4.407	O-DDA
	13H	Pore pressure	H-43	kPa	-9.770	-10.609	-3.607	O-BBC
	14H	Pore pressure	H-44	kPa	-11.372	-10.103	-3.607	O-DDA
	15H	Pore pressure	H-45	kPa	-11.111	-10.999	-3.607	O-CD
	PC-1T	Temperature	T-36	℃	-10.718	-10.386	-7.387	O
	2T	Temperature	T-37	℃	-11.077	-11.027	-7.307	O-CCD
	3T	Temperature	T-38	℃	-11.165	-10.950	-7.307	O-CD
	4T	Temperature	T-39	℃	-11.242	-10.862	-7.307	O-CDD
	5T	Temperature	T-40	℃	-11.386	-10.153	-7.307	O-D
	6T	Temperature	T-41	℃	-11.347	-10.035	-7.307	O-DDA
	7T	Temperature	T-42	℃	-11.295	-9.930	-7.307	O-DA
	8T	Temperature	T-43	℃	-11.372	-10.103	-6.357	O-DDA
	9T	Temperature	T-44	℃	-9.751	-10.538	-5.357	O-BBC
	10T	Temperature	T-45	℃	-11.372	-10.103	-5.357	O-DDA
	11T	Temperature	T-46	℃	-11.259	-10.838	-5.357	O-CD
	12T	Temperature	T-47	℃	-11.372	-10.103	-4.407	O-DDA
	13T	Temperature	T-48	℃	-9.770	-10.609	-3.607	O-BBC
	14T	Temperature	T-49	℃	-11.372	-10.103	-3.607	O-DDA
	15T	Temperature	T-50	℃	-11.111	-10.999	-3.607	O-CD
Hygrometer	HM-1H	Humidity	H-46	%	-10.591	-10.360	-6.387	O
	2H	Humidity	H-47	%	-10.063	-10.566	-6.357	O-BBC
	3H	Humidity	H-48	%	-11.079	-10.146	-6.357	O-DDA
	4H	Humidity	H-49	%	-10.960	-10.745	-6.357	O-CD
	5H	Humidity	H-50	%	-10.063	-10.566	-5.357	O-BBC
	6H	Humidity	H-51	%	-10.960	-10.745	-5.357	O-CD
	7H	Humidity	H-52	%	-11.079	-10.146	-5.357	O-DDA
	8H	Humidity	H-53	%	-10.488	-10.390	-4.377	O
	9H	Humidity	H-54	%	-10.063	-10.566	-4.407	O-BBC
	10H	Humidity	H-55	%	-11.079	-10.146	-4.407	O-DDA
	11H	Humidity	H-56	%	-10.960	-10.745	-4.407	O-CD
	HM-1T	Temperature	T-51	℃	-10.591	-10.360	-6.387	O
	2T	Temperature	T-52	℃	-10.063	-10.566	-6.357	O-BBC
	3T	Temperature	T-53	℃	-11.079	-10.146	-6.357	O-DDA
	4T	Temperature	T-54	℃	-10.960	-10.745	-6.357	O-CD
	5T	Temperature	T-55	℃	-10.063	-10.566	-5.357	O-BBC
	6T	Temperature	T-56	℃	-10.960	-10.745	-5.357	O-CD
	7T	Temperature	T-57	℃	-11.079	-10.146	-5.357	O-DDA
	8T	Temperature	T-58	℃	-10.488	-10.390	-4.377	O
	9T	Temperature	T-59	℃	-10.063	-10.566	-4.407	O-BBC
	10T	Temperature	T-60	℃	-11.079	-10.146	-4.407	O-DDA
	11T	Temperature	T-61	℃	-10.960	-10.745	-4.407	O-CD

Table 2-3 (b) Sensors installed in the Buffer (Orthogonal coordinate)

Sensor	Sensor Number	Measurement	Measurement Number	Unit	Coordinate(m)			Observation line
					X(m)	Y(m)	Z(m)	
Pcychrometer	WE-1	Water potential	W-1	MPa	-10.571	-10.206	-7.387	O
	2	Water potential	W-2	MPa	-9.795	-10.677	-7.387	O-BBC
	3	Water potential	W-3	MPa	-11.214	-10.896	-7.387	O-CD
	4	Water potential	W-4	MPa	-11.372	-10.103	-7.387	O-DDA
	5	Water potential	W-5	MPa	-10.571	-10.356	-6.857	O
	6	Water potential	W-6	MPa	-10.091	-10.555	-6.857	O-BBC
	7	Water potential	W-7	MPa	-9.795	-10.677	-6.857	O-BBC
	8	Water potential	W-8	MPa	-10.939	-10.724	-6.857	O-CD
	9	Water potential	W-9	MPa	-11.122	-10.990	-6.857	O-CD
	10	Water potential	W-10	MPa	-11.051	-10.157	-6.857	O-DDA
	11	Water potential	W-11	MPa	-11.347	-10.035	-6.857	O-DDA
	12	Water potential	W-12	MPa	-9.934	-10.620	-6.357	O-BBC
	13	Water potential	W-13	MPa	-9.795	-10.677	-6.357	O-BBC
	14	Water potential	W-14	MPa	-11.059	-10.844	-6.357	O-CD
	15	Water potential	W-15	MPa	-11.165	-10.950	-6.357	O-CD
	16	Water potential	W-16	MPa	-11.208	-10.092	-6.357	O-DDA
	17	Water potential	W-17	MPa	-11.347	-10.035	-6.357	O-DDA
	18	Water potential	W-18	MPa	-9.934	-10.620	-5.357	O-BBC
	19	Water potential	W-19	MPa	-9.795	-10.677	-5.357	O-BBC
	20	Water potential	W-20	MPa	-11.059	-10.844	-5.357	O-CD
	21	Water potential	W-21	MPa	-11.165	-10.950	-5.357	O-CD
	22	Water potential	W-22	MPa	-11.208	-10.092	-5.357	O-DDA
	23	Water potential	W-23	MPa	-11.347	-10.035	-5.357	O-DDA
	24	Water potential	W-24	MPa	-9.934	-10.620	-4.407	O-BBC
	25	Water potential	W-25	MPa	-9.795	-10.677	-4.407	O-BBC
	26	Water potential	W-26	MPa	-11.059	-10.844	-4.407	O-CD
	27	Water potential	W-27	MPa	-11.165	-10.950	-4.407	O-CD
	28	Water potential	W-28	MPa	-11.208	-10.092	-4.407	O-DDA
	29	Water potential	W-29	MPa	-11.347	-10.035	-4.407	O-DDA
	30	Water potential	W-30	MPa	-10.626	-10.333	-3.607	O
	31	Water potential	W-31	MPa	-10.091	-10.555	-3.607	O-BBC
	32	Water potential	W-32	MPa	-9.795	-10.677	-3.607	O-BBC
	33	Water potential	W-33	MPa	-10.939	-10.724	-3.607	O-CD
	34	Water potential	W-34	MPa	-11.165	-10.950	-3.607	O-CD
	35	Water potential	W-35	MPa	-11.051	-10.157	-3.607	O-DDA
	36	Water potential	W-36	MPa	-11.347	-10.035	-3.607	O-DDA
	37	Water potential	W-37	MPa	-10.516	-10.379	-2.907	O
	38	Water potential	W-38	MPa	-9.795	-10.677	-2.907	O-BBC
	39	Water potential	W-39	MPa	-11.165	-10.950	-2.907	O-CD
	40	Water potential	W-40	MPa	-11.347	-10.035	-2.907	O-DDA

Table 2-3 (c) Sensors installed in the Buffer (Orthogonal coordinate)

Sensor	Sensor Number	Measurement	Measurement Number	Unit	Coordinate(m) X(m)	Y(m)	Z(m)	Observation line
Strain gauge	KM-1	Strain(V)	M-38	$\mu\varepsilon$	-11.208	-10.118	-6.857	O-DDA
	2	Strain(H)	M-39	$\mu\varepsilon$	-11.126	-10.079	-6.857	O-DDA
	3	Strain(H)	M-40	$\mu\varepsilon$	-10.634	-10.386	-6.857	O-DDA
	4	Strain(H)	M-41	$\mu\varepsilon$	-10.506	-10.382	-6.857	O-BBC
	5	Strain(V)	M-42	$\mu\varepsilon$	-10.532	-10.264	-6.857	O
	6	Strain(V)	M-43	$\mu\varepsilon$	-11.208	-10.118	-5.857	O-DDA
	7	Strain(H)	M-44	$\mu\varepsilon$	-11.153	-10.066	-5.857	O-DDA
	8	Strain(H)	M-45	$\mu\varepsilon$	-11.153	-10.066	-5.357	O-DDA
	9	Strain(V)	M-46	$\mu\varepsilon$	-11.208	-10.118	-5.357	O-DDA
	10	Strain(V)	M-47	$\mu\varepsilon$	-11.227	-10.111	-3.607	O-DDA
	11	Strain(H)	M-48	$\mu\varepsilon$	-11.140	-10.021	-3.607	O-DDA
	12	Strain(V)	M-49	$\mu\varepsilon$	-10.810	-10.231	-3.607	O-DDA
	13	Strain(H)	M-50	$\mu\varepsilon$	-10.861	-10.359	-3.607	O-DDA
Pressure cell	PS-1	Pressure	M-51	kPa	-10.571	-10.356	-7.387	O
	2	Pressure	M-52	kPa	-11.217	-10.908	-6.857	O-CD
	3	Pressure	M-53	kPa	-11.382	-10.100	-6.857	O-DDA
	4	Pressure	M-54	kPa	-9.760	-10.612	-6.857	O-BBC
	5	Pressure	M-55	kPa	-9.817	-10.748	-6.357	O-BBC
	6	Pressure	M-56	kPa	-10.110	-10.596	-6.357	O-BBC
	7	Pressure	M-57	kPa	-11.325	-9.964	-6.357	O-DDA
	8	Pressure	M-58	kPa	-11.222	-10.902	-6.357	O-CD
	9	Pressure	M-59	kPa	-10.969	-10.690	-6.357	O-CD
	10	Pressure	M-60	kPa	-11.032	-10.116	-6.357	O-DDA
	11	Pressure	M-61	kPa	-11.032	-10.116	-5.357	O-DDA
	12	Pressure	M-62	kPa	-9.817	-10.748	-5.357	O-BBC
	13	Pressure	M-63	kPa	-10.110	-10.596	-5.357	O-BBC
	14	Pressure	M-64	kPa	-11.325	-9.964	-5.357	O-DDA
	15	Pressure	M-65	kPa	-10.905	-10.754	-5.357	O-CD
	16	Pressure	M-66	kPa	-11.117	-11.007	-5.357	O-CD
	17	Pressure	M-67	kPa	-11.032	-10.116	-4.407	O-DDA
	18	Pressure	M-68	kPa	-9.817	-10.748	-4.407	O-BBC
	19	Pressure	M-69	kPa	-10.110	-10.596	-4.407	O-BBC
	20	Pressure	M-70	kPa	-11.222	-10.902	-4.407	O-CD
	21	Pressure	M-71	kPa	-10.969	-10.690	-4.407	O-CD
	22	Pressure	M-72	kPa	-11.325	-9.964	-4.407	O-DDA
	23	Pressure	M-73	kPa	-10.628	-10.413	-4.407	O
	24	Pressure	M-74	kPa	-11.222	-10.902	-3.607	O-CD
	25	Pressure	M-75	kPa	-9.817	-10.748	-3.607	O-BBC
	26	Pressure	M-76	kPa	-11.325	-9.964	-3.607	O-DDA
	27	Pressure	M-77	kPa	-10.091	-10.555	-2.857	O-BBC
	28	Pressure	M-78	kPa	-11.051	-10.157	-2.857	O-DDA
	29	Pressure	M-79	kPa	-10.939	-10.724	-2.857	O-CD
	30	Pressure	M-80	kPa	-10.626	-10.333	-2.857	O

Table 2-3 (d) Sensors installed in the Buffer (Orthogonal coordinate)

Sensor	Sensor Number	Measurement	Measurement Number	Unit	Coordinate(m) X(m)	Y(m)	Z(m)	Observation line
Thermocouple	TT-1	Temperature	T-62	℃	-11.051	-10.157	-7.387	O-DDA
	2	Temperature	T-63	℃	-10.571	-10.336	-6.357	O
	3	Temperature	T-64	℃	-9.760	-10.612	-6.357	O-BBC
	4	Temperature	T-65	℃	-11.229	-10.149	-6.357	O-DDA
	5	Temperature	T-66	℃	-10.075	-10.512	-6.307	O-BBC
	6	Temperature	T-67	℃	-10.997	-10.654	-6.307	O-CD
	7	Temperature	T-68	℃	-9.913	-10.563	-6.357	O-BBC
	8	Temperature	T-69	℃	-11.067	-10.200	-6.307	O-DDA
	9	Temperature	T-70	℃	-9.897	-10.505	-5.357	O-BBC
	10	Temperature	T-71	℃	-11.229	-10.149	-5.357	O-DDA
	11	Temperature	T-72	℃	-11.067	-10.200	-5.387	O-DDA
	12	Temperature	T-73	℃	-11.012	-10.632	-5.387	O-CD
	13	Temperature	T-74	℃	-10.056	-10.428	-5.387	O-BBC
	14	Temperature	T-75	℃	-9.760	-10.612	-4.407	O-BBC
	15	Temperature	T-76	℃	-9.913	-10.563	-4.407	O-BBC
	16	Temperature	T-77	℃	-11.229	-10.149	-4.407	O-DDA
	17	Temperature	T-78	℃	-10.078	-10.521	-4.437	O-BBC
	18	Temperature	T-79	℃	-10.912	-10.748	-4.437	O-CD
	19	Temperature	T-80	℃	-11.064	-10.191	-4.437	O-DDA
	20	Temperature	T-81	℃	-10.559	-10.287	-4.407	O
	21	Temperature	T-82	℃	-10.975	-10.683	-3.607	O-CD
	22	Temperature	T-83	℃	-11.070	-10.208	-3.607	O-DDA
	23	Temperature	T-84	℃	-10.571	-10.316	-3.607	O
	24	Temperature	T-85	℃	-9.760	-10.612	-2.857	O-BBC
	25	Temperature	T-86	℃	-10.075	-10.512	-2.857	O-BBC
	26	Temperature	T-87	℃	-10.571	-10.316	-2.857	O
	27	Temperature	T-88	℃	-11.067	-10.200	-2.857	O-DDA
	28	Temperature	T-89	℃	-11.382	-10.100	-2.857	O-DDA
Heat flux sensor	MF-1	Heat flux	T-90	W/m^2	-10.075	-10.512	-5.357	O-BBC
	2	Heat flux	T-91	W/m^2	-10.969	-10.690	-5.357	O-CD
	3	Heat flux	T-92	W/m^2	-11.079	-10.243	-5.357	O-DDA
	4	Heat flux	T-93	W/m^2	-11.401	-10.172	-5.357	O-DDA
	5	Heat flux	T-94	W/m^2	-9.760	-10.612	-5.357	O-BBC
	6	Heat flux	T-95	W/m^2	-11.222	-10.902	-5.357	O-CD

3. Applicability test of sensors to obtain the water content

3.1 Introduction

In order to measure the water content in the buffer, the thermocouple psychrometer and the hygrometer are used. However, these sensors do not measure the water content directly. The thermocouple psychrometer measures the chemical potential and the temperature, and the hygrometer measures the relative humidity and the temperature. Therefore, the equation is necessary to calculate the water content from the temperature and the chemical potential (or relative humidity). This equation is obtained by laboratory test. This chapter shows the results of laboratory test.

3.2 Hygrometer

3.2.1 Test method

(1) Bentonite specimen

Applicability test for the hygrometer is carried out by using the five kinds of bentonite specimen with different gravimetric water content. The gravimetric water contents of specimens are 5%, 10%, 12%, 15% and 20%. The specimen is put in the sealed acrylic vessel with 7cm in inside diameter and 10cm in height. The dry density of specimen is 1.6g/cm^3. A hole is made at the center of the vessel lid and specimen. The hygrometer is installed to the center of the specimen from the hole of the vessel lid and the hole is sealed by the silicon rubber. Figure 3-1 shows the schematic of the test.

(2)Test apparatus and test method

Table 3-1 shows the specification of the test apparatus and Table 3-2 shows the test conditions. The parameters for the test are water content and temperature as shown in Table 3-2. Figure 3-2 shows the hygrometer. The diameter of sensor is 13.5mm and length is 70mm.

Test procedure is as follow;

①Water content of bentonite is adjusted to the required value and then the bentonite is cured
②Bentonite is compacted to the required dry density and the sensor is installed in the specimen.
③The vessel with specimen is set into the thermostat.
④Temperature in the thermostat is controlled at required value. Temperature control schedule is shown in Figure 3-3.
⑤Measurement program is started. Temperature and relative humidity are measured automatically during the test period.
⑥After the measurement by hygrometer, specimen is took out from the vessel and water content is measured by oven-dry method. As shown in Figure 3-4, water content of different part of specimen is measured.

In order to check the temperature distribution in the specimen, thermocouple is installed in the specimen. Figure 3-5 shows the location of the thermocouples.

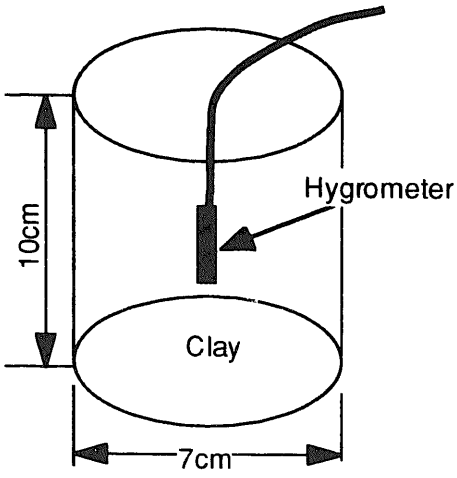

Figure 3-1 Schematic of the test

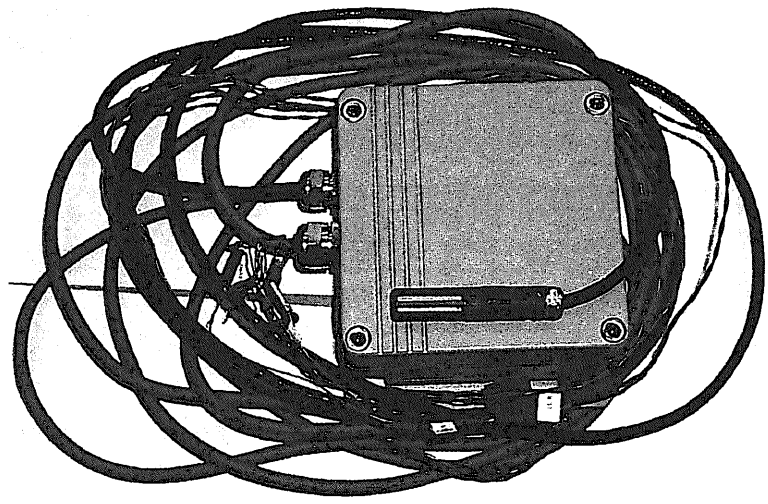

Figure 3-2 Hygrometer

Table 3-1 Specifications of the apparatus

Apparatus	Maker, Type	Remark
Hygrometer	VAISALA(Finland), HMP233	
Thermostat	Isuzu(Japan), ESF-115S	
Data Acquisition Controller	NEC San-ei(Japan), 7V14	Transform of analog data to digital
Personal Computer		Record of data

Table 3-2 Test conditions

Water content / Temperature	5%	10%	12%	15%	20%
Heating 25℃	○	○	○	○	○
Heating 45℃	○	○	○	○	○
Heating 65℃	○	○	○	○	○
Heating 80℃	○	○	○	○	○
Cooling 65℃	○	○	○	○	○
Cooling 45℃	○	○	○	○	○
Cooling 25℃	○	○	○	○	○

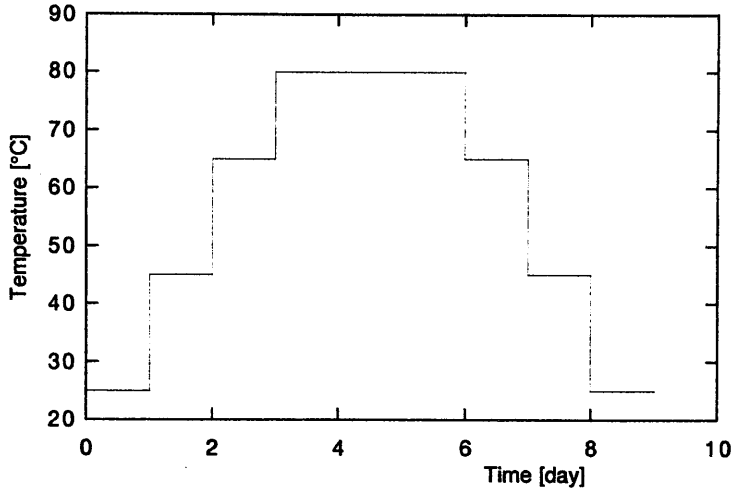

Figure 3-3 Controlled temperature in the thermostat

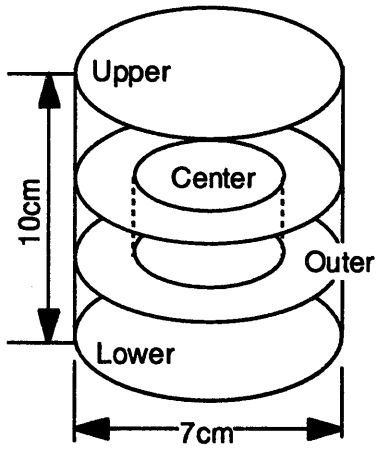

Figure 3-4 Measurement part of water content

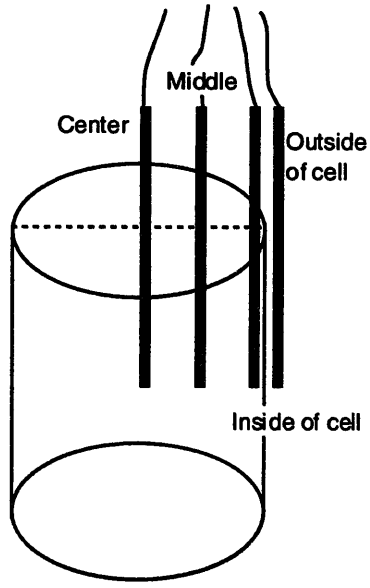

Figure 3-5 Location of the thermocouple

3.2.2 Test results

(1)Measurement of temperature distribution

Figure 3-6 shows the temperature distribution in the specimen. When the temperature in the thermostat is raised gradually, the temperature at the inside of cell is raised quickest, and that at the middle part of specimen, that at the center part following in that order. After 2 or 3 hours past, the temperature in the specimen becomes uniform. Therefore, it is indicated that temperature in the specimen becomes uniform after several hours past from the ascent of temperature of thermostat.

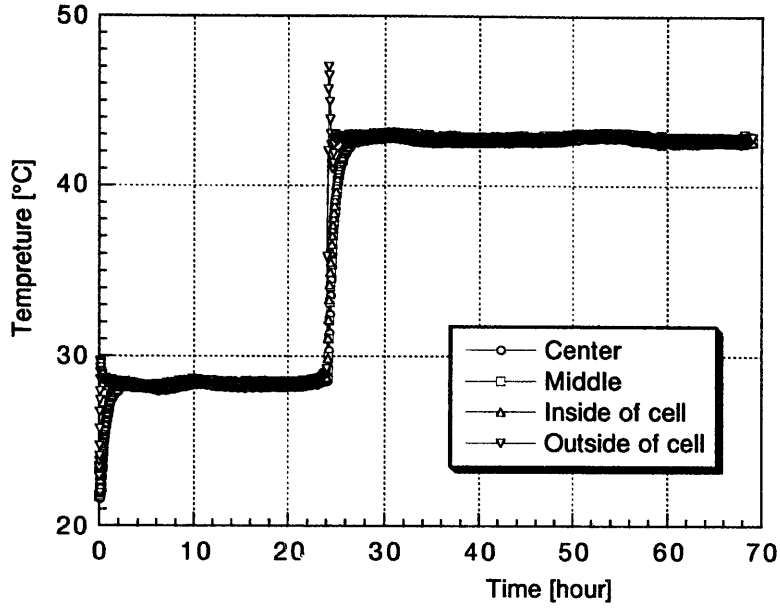

(a) Whole figure

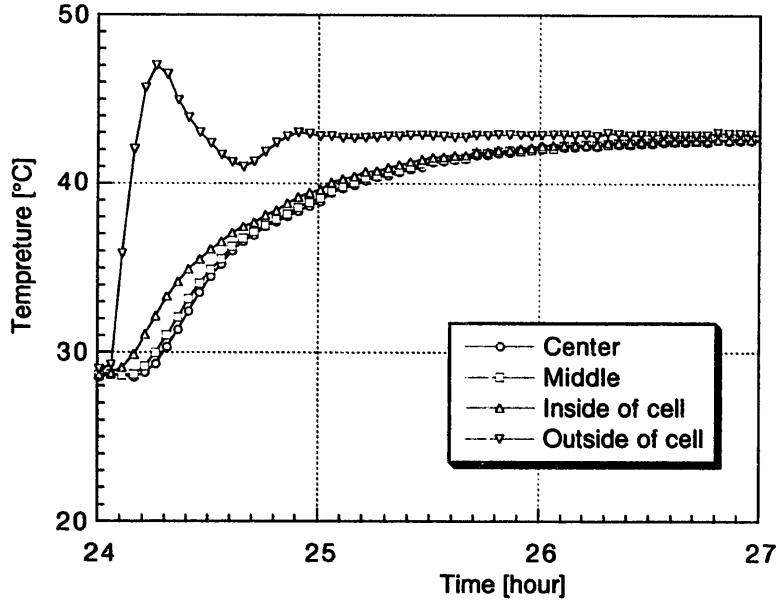

(b) Enlarged figure

Figure 3-6 Temperature distribution in the specimen

(2)Measurement results of water content by oven-dry method

After the end of experiment, test cell was demolished and water content in the specimen was measured by oven-dry method. Table 3-3 shows the measurement results. Water content was measured at the four parts of specimen as shown Figure 3-4. From this table, it is shown that water content in the specimen is uniform.

Table 3-3 Water content distribution in the specimen

Setting water content (%)			5%	10%	12%	15%	20%
Measured value(%)	Upper		6.40	10.6	11.1	15.9	18.9
	Middle	Center	6.39	10.3	10.9	15.8	19.0
		Outer	6.27	10.6	11.1	15.9	19.0
	Lower		6.33	11.0	11.1	15.9	19.0
Average			6.35	10.6	11.1	15.9	19.0

(3) Measurement results by hygrometer

Figures 3-7 to 3-11 show the measurement results by hygrometer with different water content. Relative humidity of the specimens with water content of 6.35%, 10.6% and 11.1% increases with temperature. Relative humidity of the specimens with water content of 15.9% and 19.0% is almost 100%RH at all time. Therefore, it is known from these figures that water content of 15.9% is above the upper limit water content that can be measured by hygrometer indirectly.

Relationship between water content, relative humidity and temperature is obtained by use of the measured relative humidity and temperature value after three hours past from the ascent of temperature at each setting temperature because temperature becomes uniform at that time as shown Figure 3-6. Table 3-4 shows the measured value of relative humidity and temperature.

Figure 3-12 shows the relationship between relative humidity and temperature at each water content. Relative humidity increases in direct proportion to the temperature except for the specimen with water content of 15.9% and 19.0%.

Figure 3-13 shows the relationship between relative humidity and water content at each temperature. From this figure, it is known that relative humidity increases with water content in the lower water content range down to 15.9%.

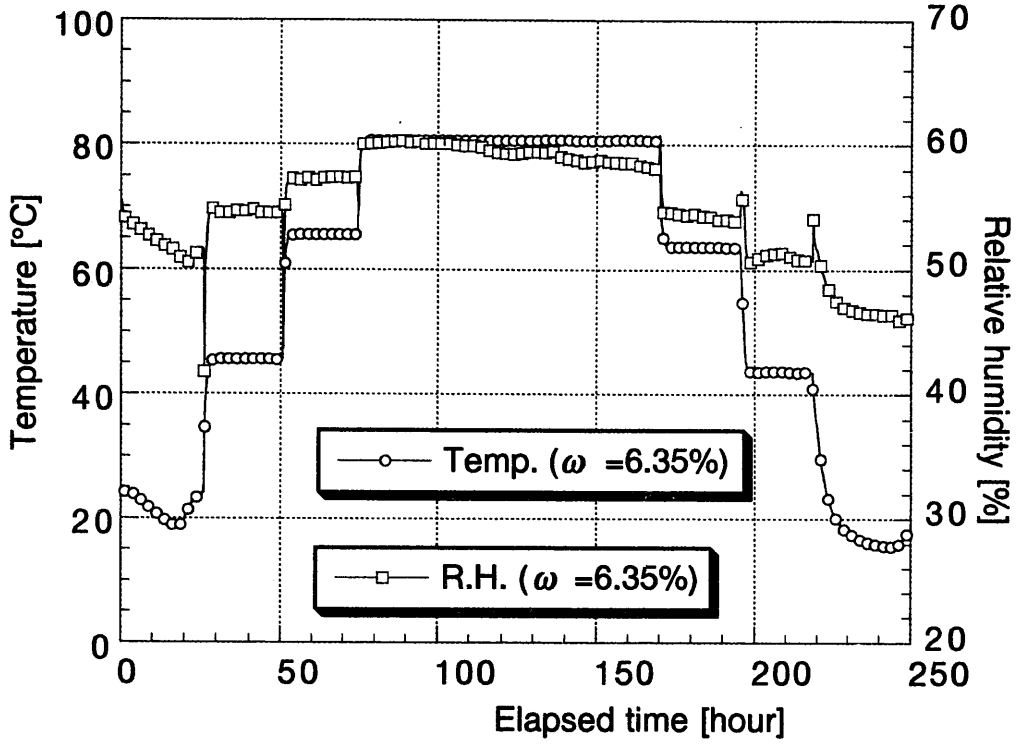

Figure 3-7 Measurement results by hygrometer with water content of 6.35%

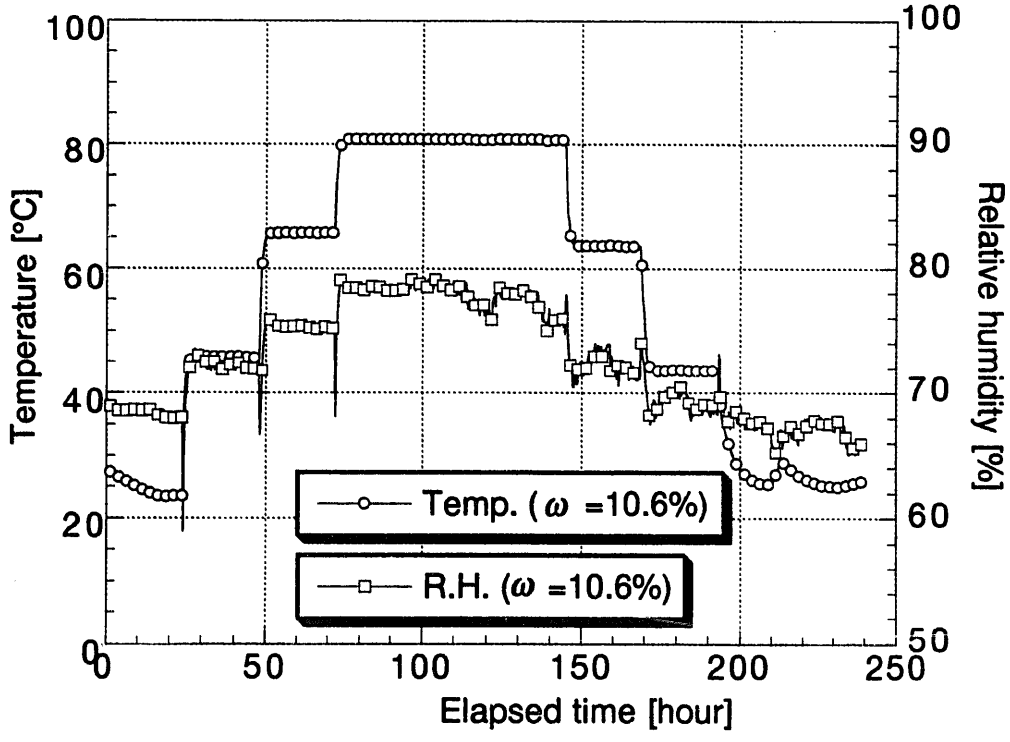

Figure 3-8 Measurement results by hygrometer with water content of 10.6%

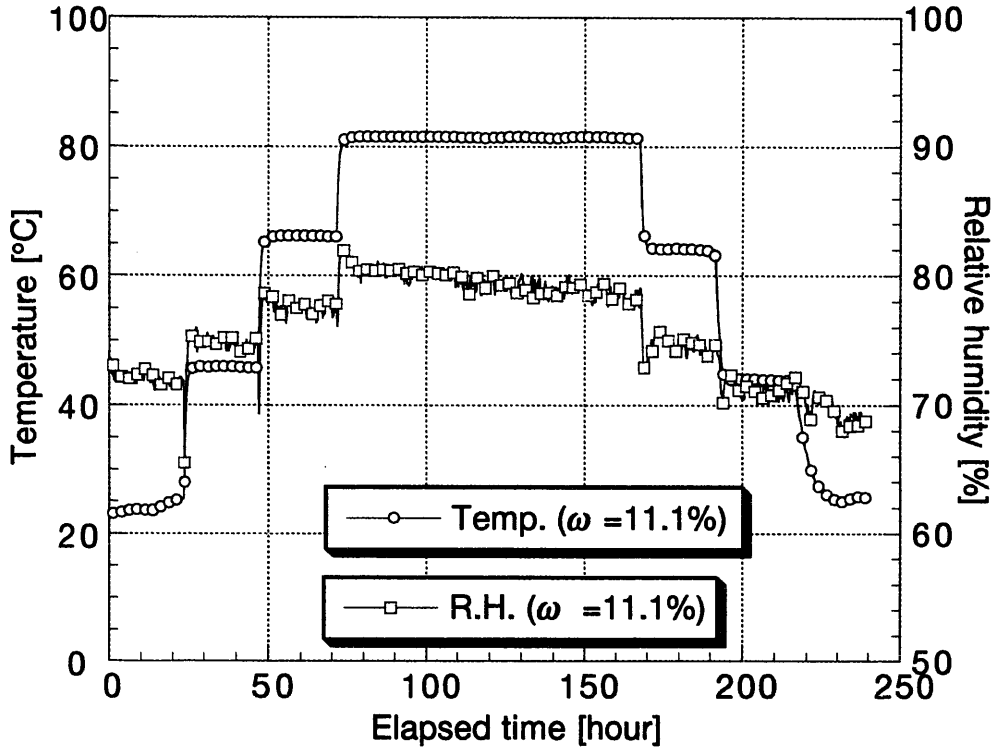

Figure 3-9 Measurement results by hygrometer with water content of 11.1%

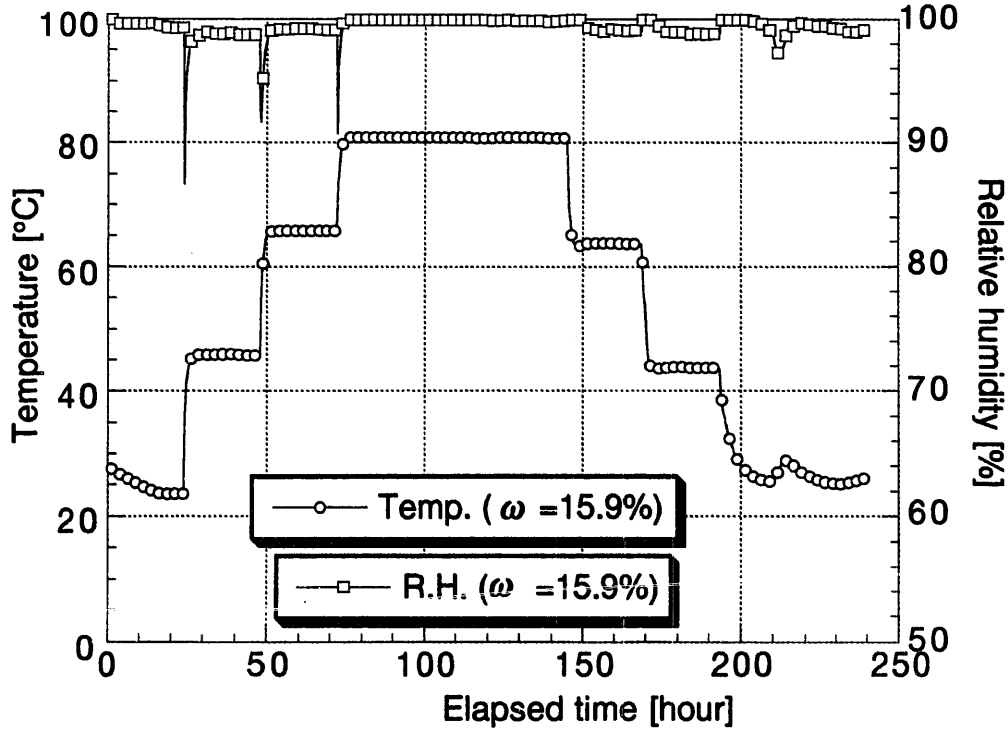

Figure 3-10 Measurement results by hygrometer with water content of 15.9%

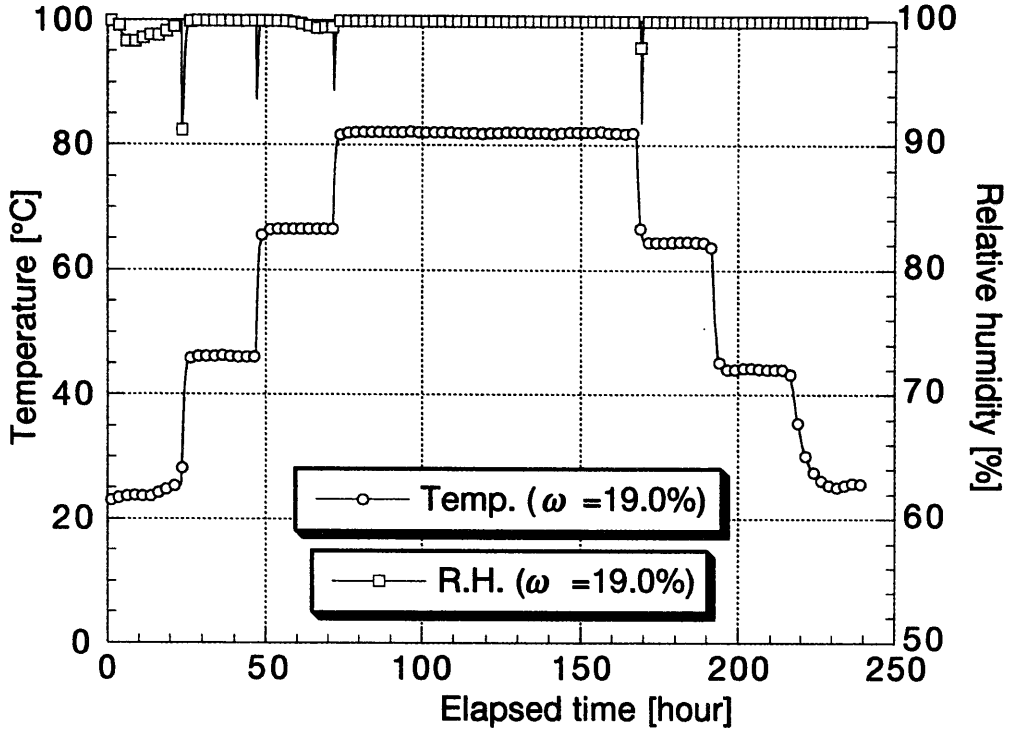

Figure 3-11 Measurement results by hygrometer with water content of 19.0%

Table 3-4 Measurement value by hygrometer at each temperature

Water content 6.35%		Water content 10.6%		Water content 11.1%		Water content 15.9%		Water content 19.0%	
Temp.	R.H.	Temp.	R.H.	Temp.	R.H.	Temp.	R.H.	Temp.	R.H.
℃	%RH	℃	% RH	℃	% RH	℃	% RH	℃	% RH
24.1	53.7	25.6	68.6	23.6	72.2	25.8	99.6	23.7	98.6
45.6	54.7	45.8	73.3	45.8	75.7	45.8	98.7	46.0	99.9
65.5	57.3	65.6	75.7	65.9	78.5	65.7	98.9	66.3	99.9
80.6	60.1	80.7	79.0	81.1	81.9	80.7	99.9	81.7	99.9

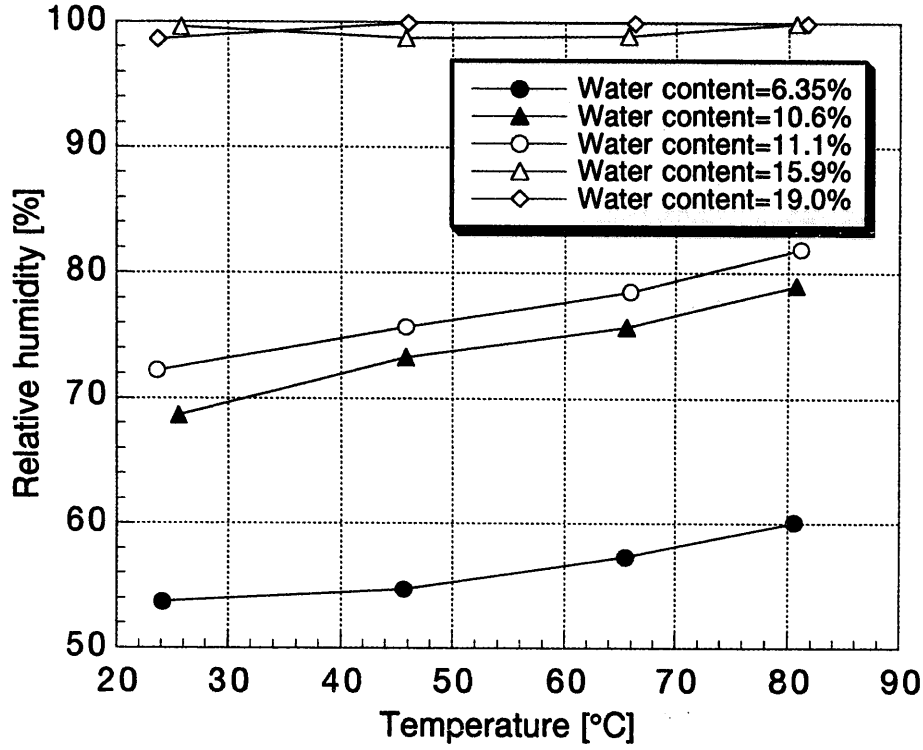

Figure 3-12 Relationship between temperature and relative humidity at each water content

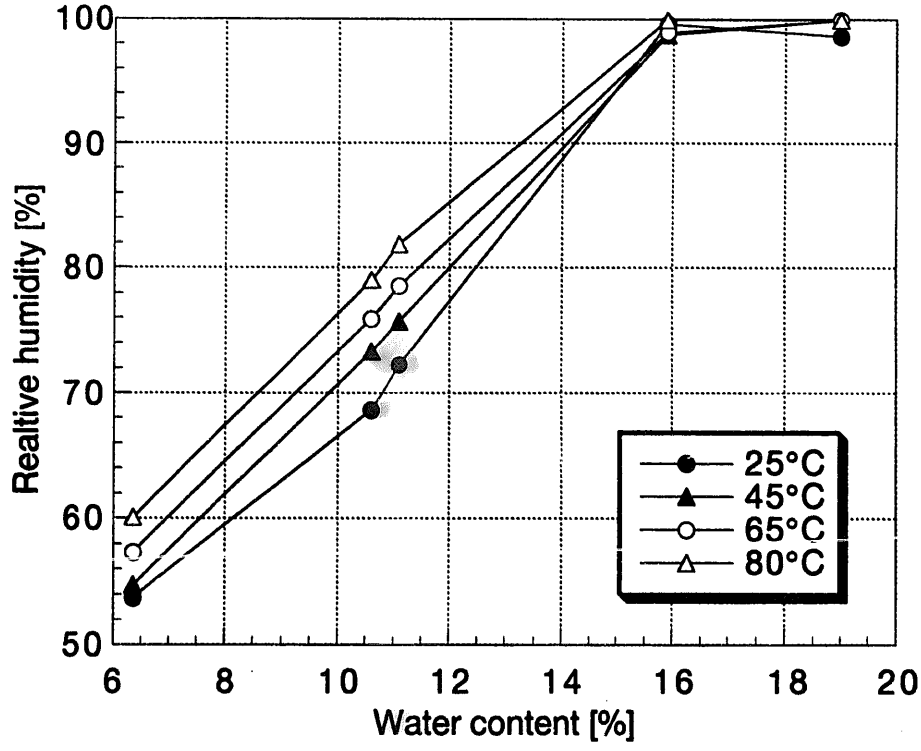

Figure 3-13 Relationship between water content and relative humidity at each temperature

(4)Multi-regression analysis

Multi-regression analysis is carried out by use of the measured relative humidity and temperature with water content of 6.35%, 10.6%, 11.1% and 15.9%. Linear multi-regression analysis which is expressed in [z=ax+by+c] is adopted as relative humidity and temperature for independent variables and as water content for dependent variable. The equation obtained by the analysis is as follow.

$$\omega = 0.220H\text{-}0.0257T\text{-}4.52 \qquad (3\text{-}1)$$

where, ω is the water content [%], H is the relative humidity [%RH] and T is the temperature [°C]. The upper limit of applicability of this equation is water content of 16.0%.

Figure 3-14 shows the comparison between measured water content and analytical water content by equation (3-1). Analytical values agree well with the measured values.

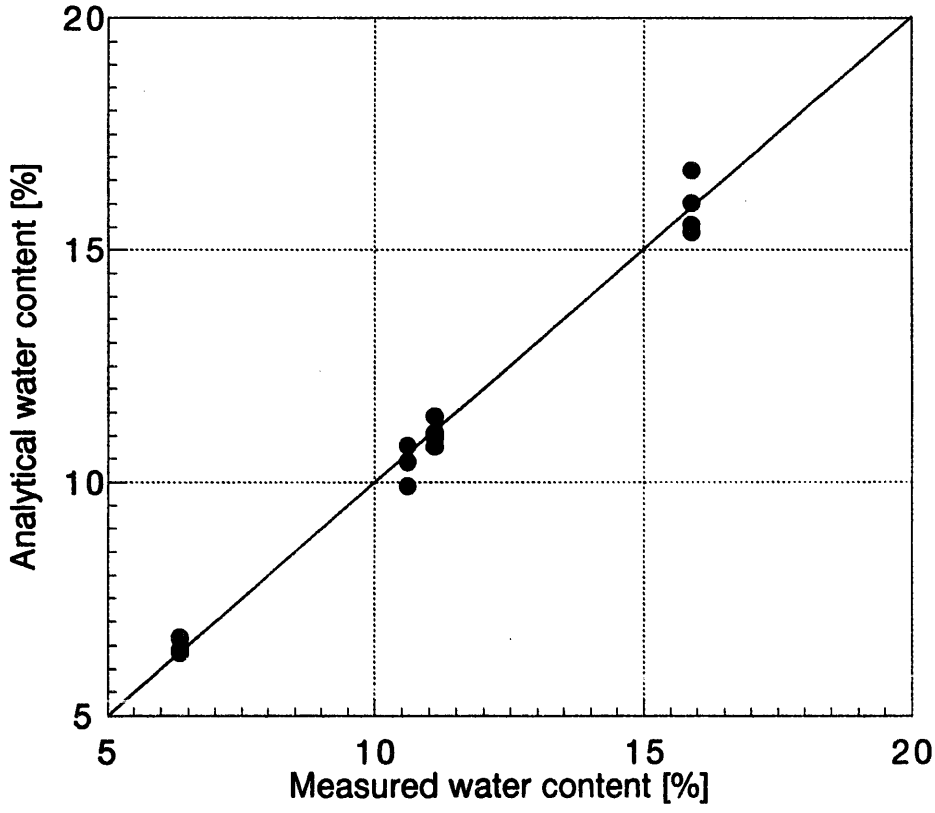

Figure 3-14 Comparison between measured and analytical water content

3.3 Thermocouple psychrometer

3.3.1 Test method

(1)Introduction

Following tests are carried out for the applicability test of thermocouple psychrometer.

- In order to examine the measuring range of thermocouple psychrometer for bentonite OT-9607, pre-test are carried out by use of bentonite OT-9607 with various gravimetric water contents under room temperature. (Pre-test)
- Chemical potential with various gravimetric water contents under controlled temperature (room temperature to 80°C) is measured. (Main test)
- Comparison of measured temperature between the thermocouple psychrometer and the other sensors are carried out. (Temperature test)

(2)Bentonite specimen

Pre-test is carried out by use of six kinds of bentonite specimen with different gravimetric water content The gravimetric water content of specimens are 10%, 15%, 20%, 25%, 30% and 35%. Main test is carried out by use of three kinds of bentonite specimen with different gravimetric water content. Temperature test is carried out by use of five kinds of bentonite specimen with different gravimetric water content. The test condition is seen in Table 3-5. Test conditions for main test are determined on the basis of the results of pre-test.

Table 3-5 Test conditions for the applicability test of thermocouple psychrometer

Water content	10%	15%	20%	25%	30%	35%	Controlled temperature
Pre-test	○	○	○	○	○	○	Room temperature
Main test	×	○	○	○	×	×	25, 45, 65, 80°C
Temperature test	×	○	○	○	○	○	25 – 80°C

(3)Test apparatus and test method

Table 3-6 shows the specifications of the test apparatus for the applicability test of thermocouple psychrometer. In order to measure the water potential, we use the Dew Point Microvoltmeter (HR-33T) made by WESCOR, USA. HR-33T is shown in Figure 3-15. This HR-33T can measure the water potential by use of several kinds of devise. In this time, we use two kinds of devise. First one is sample chamber made by WESCOR, USA (C-52 chamber, seen in Figure 3-16), and the other is in-situ sensor made by WESCOR, USA (PST-55, seen in Figure 3-17). In order to measure by in-situ sensor, bentonite specimen is put in the sealed acrylic vessel like applicability test of hygrometer (PST-55 chamber). This meter can measure the water potential by two methods. One is hygrometric method and the other is psychrometric method. In this test, we try to apply both methods.

Measuring procedure of thermocouple psychrometer is as follow.

①Microvoltmeter HR-33T is switched on and warmed up for ten minutes before the start of measurement

②"FUNCTION" switch is turned on to the "SHORT", and C-52 chamber and PST-55 chamber are connected to the Microvoltmeter.

③"RANGE" switch is changed to 100, 30 and 10, and the zero position of the pointer is checked by " ZERO OFFSET" control at every range.

④"RANGE" switch is changed to 100, "FUNCTION" switch is changed to the

"READ" and "°C/V" switch is changed to "°C". And after the temperature (T) is measured, "°C/V" switch is changed to "V".

⑤The value of "πV" is calculated by following equation

$$\text{"}\pi V\text{"} = \text{"Cooling coefficient"} + (T - 25) \times 0.7 \qquad (3\text{-}2)$$

While depressing the "πV" button, "πV" value is adjusted at the calculated value by the " πV set" control.

⑥" FUNCTION" switch is changed to the "READ", "RANGE" switch is changed to 100, 30 and 10, and the zero position is checked by " ZERO OFFSET" control at every range.

⑦Water potential is measured by hygrometric method.

"FUNCTION" switch is changed to the "COOL" and "RANGE" switch is changed to 100. When the pointer is stopped, "FUNCTION" switch is changed to "DP". When the pointer is stopped again, the value shown by the pointer is taken as $D1$ value. Water potential ($P1$) [bar] is calculated by equation (3-3)

$$P1 = -D1 / 0.75 \qquad (3\text{-}3)$$

⑧Water potential is measured by psychrometric method.

"FUNCTION' switch is changed to the "READ" from the "DP". When the pointer is stopped, the value shown by the pointer is taken as $A1$. Water potential ($P2$) [bar] is calculated equation (3-4)

$$P2 = -A1 / 0.47 \qquad (3\text{-}4)$$

In fact, when water potential is measured by psychrometeric method, compensation by the temperature is needed. However, there is no compensation in this stage because temperature is considered in the multi-regression equation as described in a later.

⑨"FUNCTION" switch is changed to the "SHORT"

⑩"FUNCTION" switch is changed to the "HEAT" and it keeps for ten seconds in order to avoid the condensation of water.

⑪"FUNCTION" switch is changed to the "SHORT" and water potential is measured at another channel.

⑫When all works are finished, "FUNCTION" switch is changed to the "SHORT" and Microvoltmeter is switched off.

The procedure of pre-test is as follow.

①Water content of bentonite is adjusted to the required value and then the bentonite is cured.

②Bentonite is put in the C-52 chamber and the PST-55 chamber

③Water potential is measured by hygrometric method

④Water potential is measured by psychrometric method

⑤After the measurement by thermocouple psychrometer, specimen is took out from the chamber and water content is measured by oven-dry method.

The procedure of main test is as follow.

①Water content of bentonite is adjusted to the required value and then the bentonite is cured.

②Bentonite is put in the C-52 chamber and the PST-55 chamber

③Chamber is set in the thermostat to control the temperature

④Measurement program is started Temperature in the thermostat is controlled at required value. Temperature control schedule is shown in Figure 3-3.

⑤Temperature and water potential are measured just before the temperature is step up to the next step. In other words, these are measured after 24 hours past from the set of temperature at required value. Water potential is measured by two methods.

⑥After the measurement by thermocouple psychrometer, specimen is took out from the chamber and water content is measured by oven-dry method.

According the manual of the thermocouple psychrometer, the thermocouple in the sensors has an error due to the non-linearity and calibration curve by temperature is shown under 60°C. Therefore, the temperature test is carried out to check those effects. During the temperature test, temperature in the PST-55 chamber is measured by resistance thermometer bulb and thermocouple.

Table 3-6 Specifications of apparatus for the applicability test of thermocouple psychrometer

Apparatus	Maker, Type	Remark
Microvoltmeter	HR-33T, WESCOR (USA)	
Sample chamber	C-52-SF, WESCOR (USA)	
Sample chamber	Acrylic vessel (Water potential is measured by PST-55 , WESCOR (USA))	
Thermostat	ESF-115S, Isuzu (Japan)	

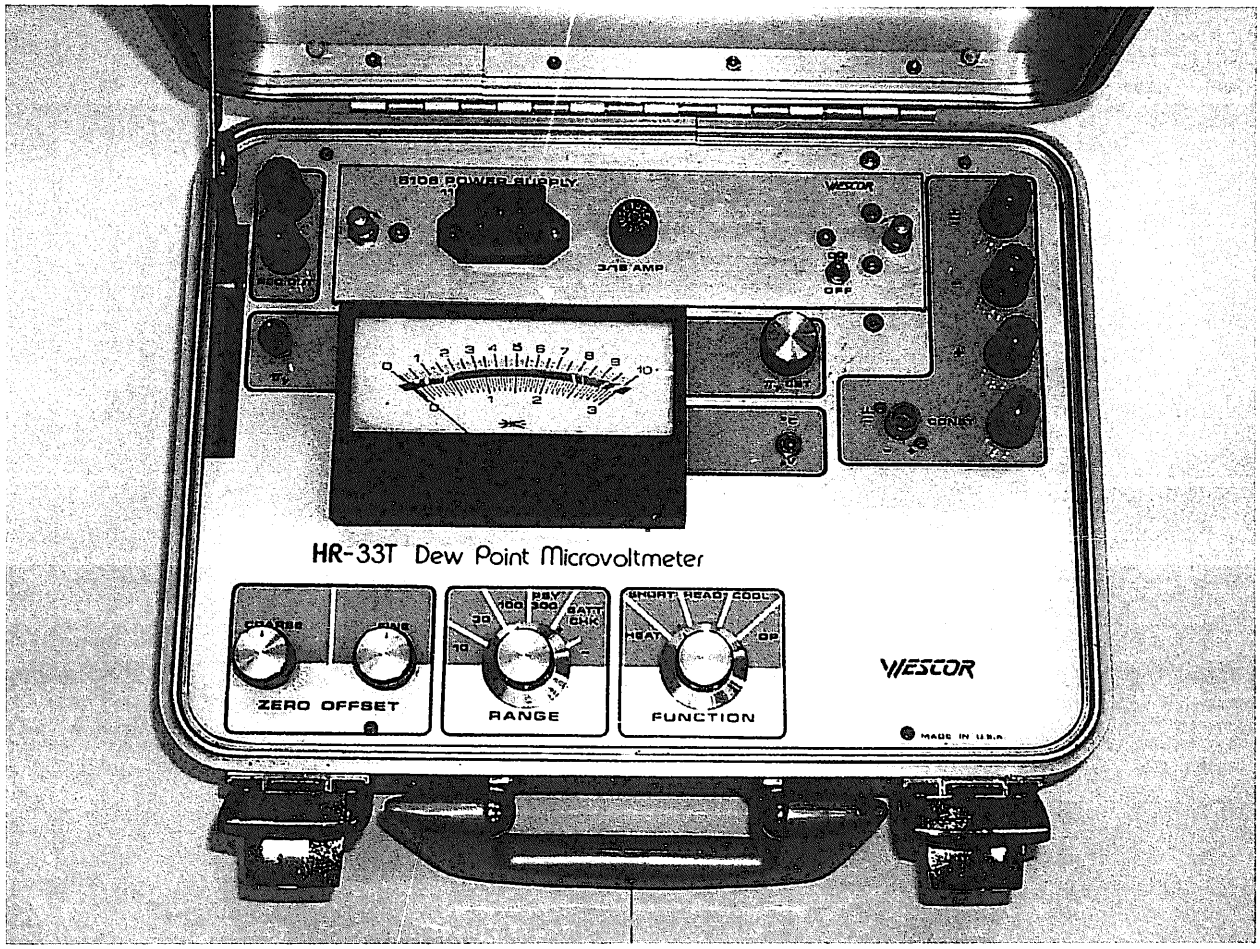

Figure 3-15 Microvoltmeter (HR-33T)

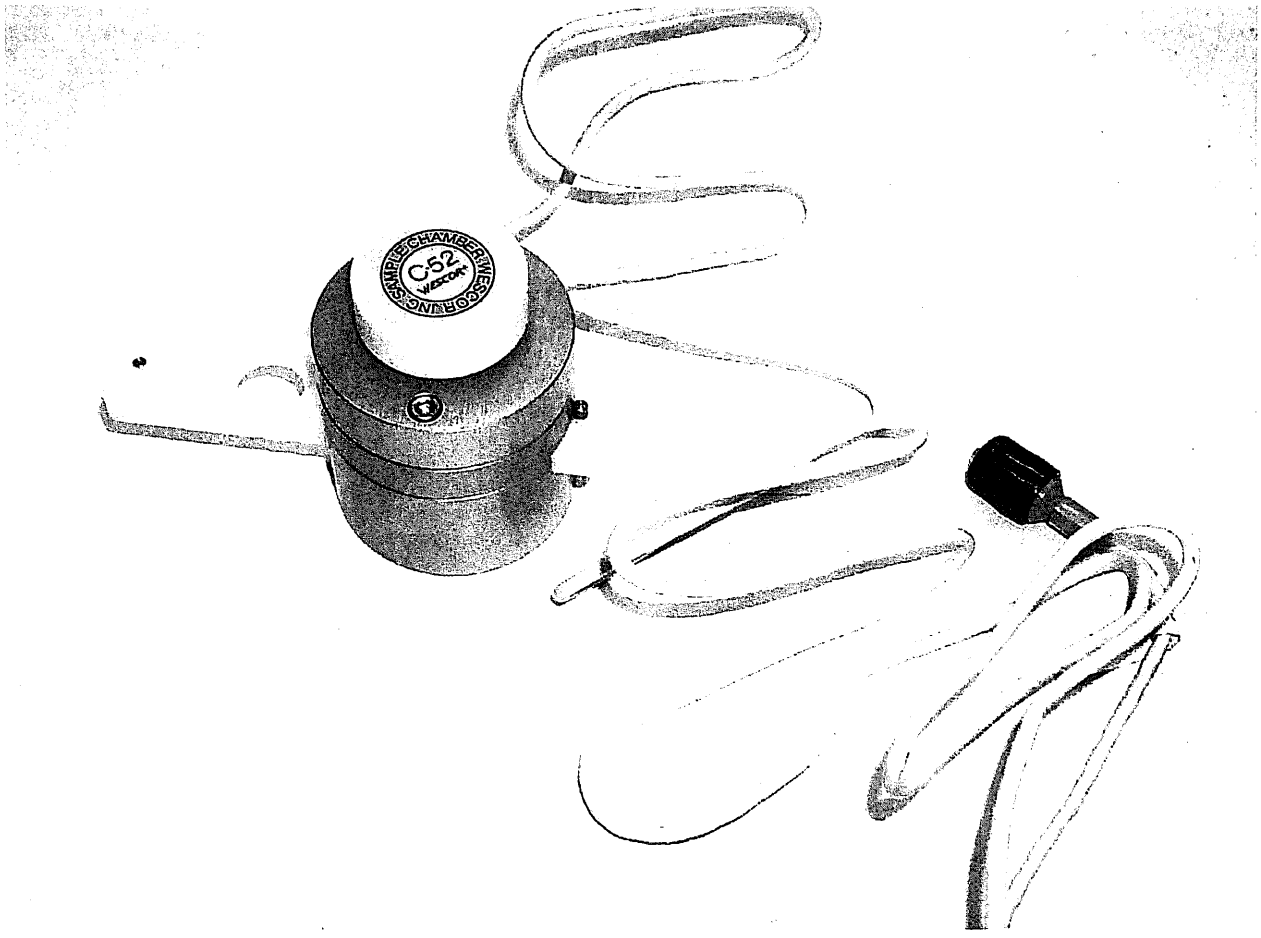

Figure 3-16 C-52 Sample chamber

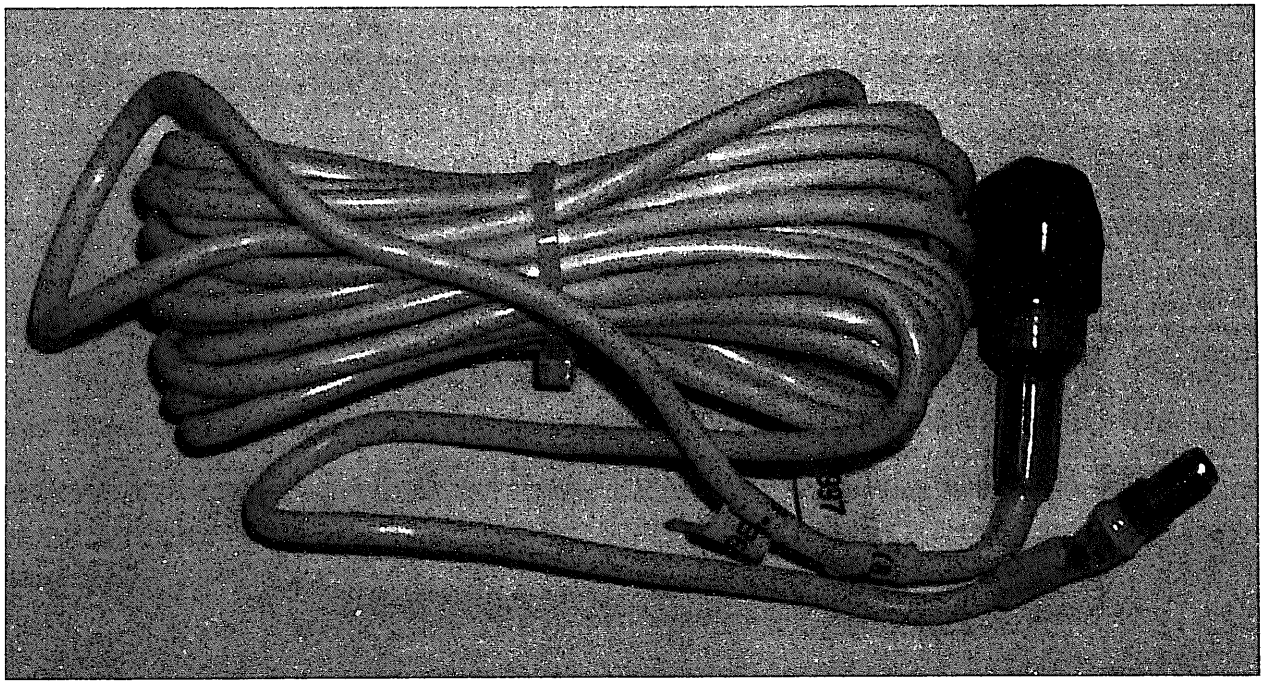

Figure 3-17 In-situ sensor (PST-55)

3.3.2 Test results

(1)Pre-test

Table 3-7 shows the results of pre-test regarding the measuring range of thermocouple psychrometer for bentonite OT-9607. Figures 3-18 and 3-19 show the measurement results by C-52 chamber and PST-55 chamber, respectively. Pre-test was carried out ubder the room temperature condition (22°C). From the results, it is shown that it is impossible to measure the water potential of the specimen with water content of 10%. Absolute value of water potential decrease with water content increase.

Table 3-7 Results of pre-test regarding the measuring range of thermocouple psychrometer

			C-52 sample chamber				PST-55sample chamber			
Water content (%)		Temp. *T*	Hygrometric Method		Psychrometric Method		Hygrometric Method		Psychrometric Method	
Each specimen	Average	(℃)	*D1*(μV)	*P1*(bar)	*A1*(μV)	*P2*(bar)	*D1*(μV)	*P1*(bar)	*A1*(μV)	*P2*(bar)
10.4										
10.6	10.6	22.0	Impossible							
10.8										
16.4										
16.6	16.6	22.0	40.8	-54.4	19.0	-40.0	32.3	-43.1	17.8	-37.9
16.7										
21.1										
20.9	20.9	22.0	21.0	-28.0	9.5	-20.2	19.8	-26.4	11.0	-23.4
20.8										
26.6										
26.2	26.4	22.0	14.5	-19.3	7.6	-16.2	17.5	-23.3	9.8	-20.9
26.4										
27.2										
29.2	28.2	22.0	14.2	-18.9	7.4	-15.7	11.8	-15.7	3.8	-8.1
28.1										
36.1										
35.9	36.3	22.0	8.4	-11.2	4.6	-9.8	8.8	-11.7	4.5	-9.6
37.0										

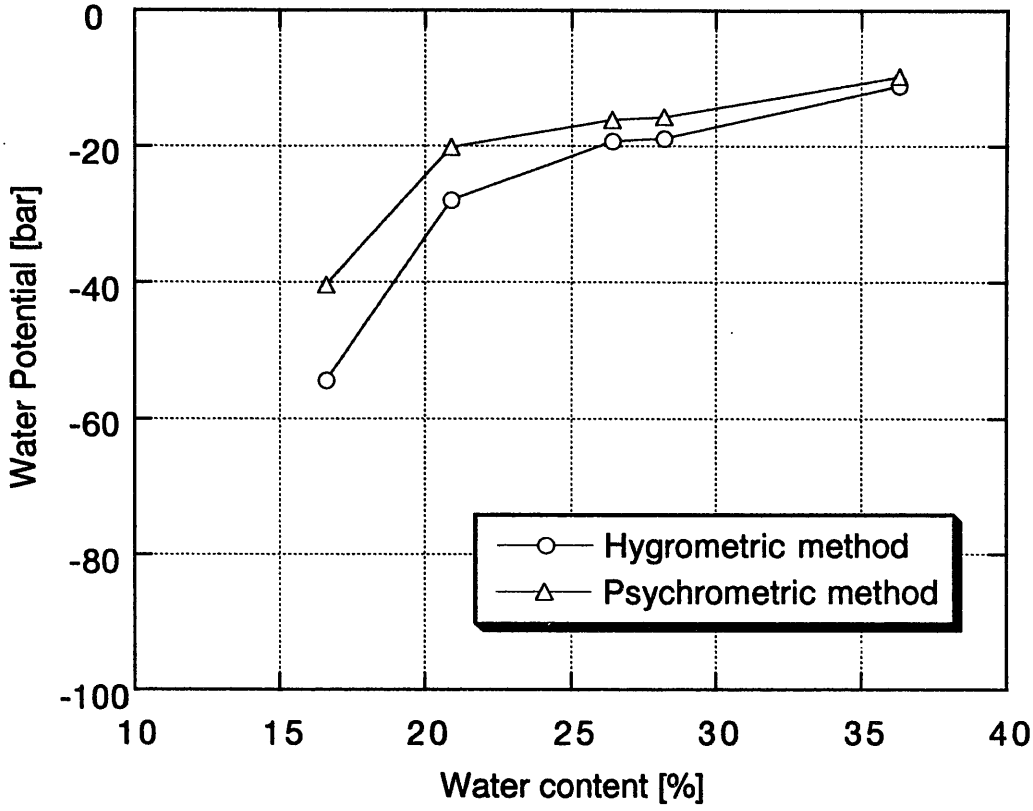

Figure 3-18 Pre-test result measured by C-52 chamber

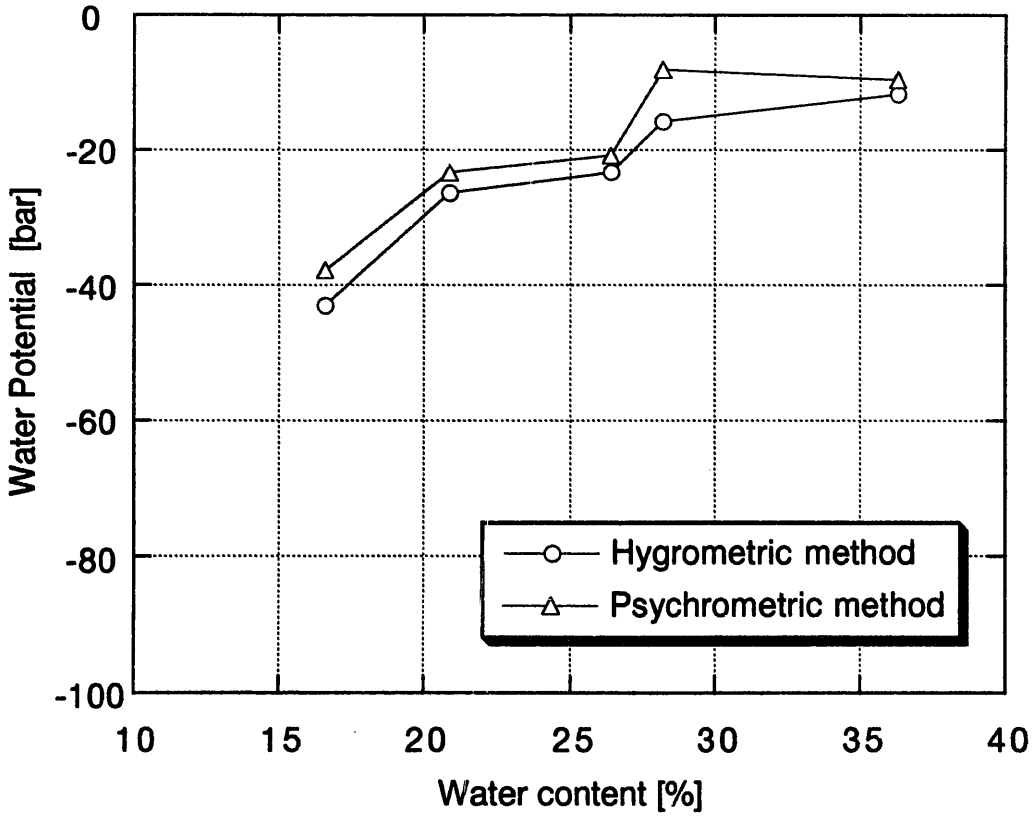

Figure 3-18 Pre-test result measured by PST-55 chamber

(2)Main test

Water content of the specimens used in the main test were 14.5%, 19.5% and 23.2%. Measurement results by thermocouple psychrometer are shown in Tables 3-8, 3-9 and 3-10. Figure 3-20 shows the relationship between temperature and water potential measured by C-52 chamber and Figure 3-21 shows that measured by PST-55 chamber. Figure 3-22 shows the relationship between water content and water potential measured by C-52 chamber and Figure 3-23 shows that measured by PST-55 chamber.

From these figures, following results are obtained.

- Four kinds of the relationship between temperature and water potential are obtained by use of two chambers and two methods. All results show that absolute value of water potential is increase with temperature. The relationship between temperature and water potential shows the linearity.
- Absolute value of water potential decrease with water content increase.
- As compared between two methods, the water potential value measured by hygrometric method is almost the same with the water potential value measured by psychrometric method under room temperature condition. However, absolute value measured by psychrometric method becomes bigger than that measured by hygrometric method when the temperature is high. This is because measurement value by psychrometric method is not compensated.
- As compared between two chambers, the water potential values measured under room temperature are almost the same. However, when temperature becomes high, absolute value measured by use of C-52 chamber becomes higher than that measured by use of PST-55 chamber. After the test, water content of each specimen was measured. As a result, the specimen in the C-52 chamber was dried as shown in Tables 3-8 to 3-10. The reason is considered that the amount of sample in the C-52 chamber is small as 0.3g and the C-52 chamber was not sealed enough.

Table 3-8 Results of main test with water content of 14.5%

C-52 chamber, Heating phase					C-52 chamber, Cooling phase				
Temp.	Hygrometric Method		Psychrometric Method		Temp.	Hygrometric Method		Psychrometric Method	
T (°C)	*D1* (μV)	*P1* (bar)	*A1* (μV)	*P2* (bar)	*T* (°C)	*D1* (μV)	*P1* (bar)	*A1* (μV)	*P2* (bar)
23.0	43.0	-57.3	21.5	-45.7	84.5	Impossible			
47.0	45.5	-60.7	33.5	-71.3	64.5	Impossible			
68.0	52.5	-70.0	44.5	-94.7	43.0	Impossible			
85.0	63.5	-84.7	57.5	-122.3	27.0	Impossible			

(Note)

Mass of chamber: 434.43g
Mass of sample: 0.27g
Before the test (chamber + sample): 434.70g
After the test (chamber + sample): 434.64g
Difference of mass: 0.06g (Specimen is dried from water content of 14.5%)

PST-55 chamber, Heating phase					PST-55 chamber, Cooling phase				
Temp.	Hygrometric Method		Psychrometric Method		Temp.	Hygrometric Method		Psychrometric Method	
T (°C)	*D1* (μV)	*P1* (bar)	*A1* (μV)	*P2* (bar)	*T* (°C)	*D1* (μV)	*P1* (bar)	*A1* (μV)	*P2* (bar)
23.5	39.5	-52.7	21.0	-44.7	83.5	45.0	-60.0	41.0	-87.2
47.0	41.0	-54.7	30.0	-63.8	66.5	43.0	-57.3	38.0	-80.9
68.0	43.5	-58.0	37.0	-78.7	43.0	43.0	-57.3	29.0	-61.7
85.5	44.5	-59.3	40.5	-86.2	28.0	38.5	-51.3	21.5	-45.7

(Note)

Mass of chamber: 946.03g
Mass of sample: 38.48g
Before the test (chamber + sample): 984.51g
After the test (chamber + sample): 984.47g
Difference of mass: 0.04g (Water content of sample decreased to 14.4% from 14.5%)

Table 3-9 Results of main test with water content of 19.5%

C-52 chamber, Heating phase					C-52 chamber, Cooling phase				
Temp.	Hygrometric Method		Psychrometric Method		Temp.	Hygrometric Method		Psychrometric Method	
T (°C)	*D1* (μV)	*P1* (bar)	*A1* (μV)	*P2* (bar)	*T* (°C)	*D1* (μV)	*P1* (bar)	*A1* (μV)	*P2* (bar)
25.0	17.5	-23.3	9.5	-20.2	84.5	43.5	-58.0	39.5	-84.0
46.0	21.0	-28.0	15.5	-33.0	65.0	43.0	-57.3	37.0	-78.7
68.0	25.5	-34.0	22.0	-46.8	44.0	39.0	-52.0	30.5	-64.9
85.5	31.0	-41.3	28.0	-59.6	25.5	35.0	-46.7	22.0	-46.8

(Note)

Mass of chamber: 434.40g
Mass of sample: 0.18g
Before the test (chamber + sample): 434.58g
After the test (chamber + sample): 434.56g
Difference of mass: 0.02g (Water content of sample decreased to 6.7% from 19.5%)

PST-55 chamber, Heating phase					PST-55 chamber, Cooling phase				
Temp.	Hygrometric Method		Psychrometric Method		Temp.	Hygrometric Method		Psychrometric Method	
T (°C)	*D1* (μV)	*P1* (bar)	*A1* (μV)	*P2* (bar)	*T* (°C)	*D1* (μV)	*P1* (bar)	*A1* (μV)	*P2* (bar)
25.5	19.0	-25.3	11.0	-23.4	85.0	27.0	-36.0	24.5	-52.1
46.0	20.5	-27.3	15.5	-33.0	65.0	25.0	-33.3	22.0	-46.8
68.0	24.0	-32.0	20.5	-43.6	42.0	22.0	-29.3	18.0	-38.3
84.5	25.0	-33.3	23.0	-48.9	25.5	19.5	-26.0	14.0	-29.8

(Note)

Mass of chamber: 945.96g
Mass of sample: 38.25g
Before the test (chamber + sample): 984.21g
After the test (chamber + sample): 984.12g
Difference of mass: 0.09g (Water content of sample decreased to 19.3% from 19.5%)

Table 3-10 Results of main test with water content of 23.2%

C-52 chamber, Heating phase					C-52 chamber, Cooling phase				
Temp.	Hygrometric Method		Psychrometric Method		Temp.	Hygrometric Method		Psychrometric Method	
T (°C)	*D1* (μV)	*P1* (bar)	*A1* (μV)	*P2* (bar)	*T* (°C)	*D1* (μV)	*P1* (bar)	*A1* (μV)	*P2* (bar)
23.5	12.5	-16.7	6.4	-13.6	83.0	24.5	-32.7	22.0	-46.8
46.0	16.0	-21.3	12.0	-25.5	65.0	22.5	-30.0	19.5	-41.5
67.0	19.0	-25.3	16.0	-34.0	44.0	19.0	-25.3	15.0	-31.9
83.0	22.5	-30.0	20.0	-42.6	24.0	15.5	-20.7	9.5	-20.2

(Note)

Mass of chamber: 433.58g
Mass of sample: 0.33g
Before the test (chamber + sample): 433.91g
After the test (chamber + sample): 433.89g
Difference of mass: 0.02g (Water content of sample decreased to 14.8% from 23.2%)

PST-55 chamber, Heating phase					PST-55 chamber, Cooling phase				
Temp.	Hygrometric Method		Psychrometric Method		Temp.	Hygrometric Method		Psychrometric Method	
T (°C)	*D1* (μV)	*P1* (bar)	*A1* (μV)	*P2* (bar)	*T* (°C)	*D1* (μV)	*P1* (bar)	*A1* (μV)	*P2* (bar)
24.0	9.5	-12.7	5.5	-11.7	84.0	17.5	-23.3	16.0	-34.0
46.0	15.0	-20.0	11.5	-24.5	66.0	17.5	-23.3	15.0	-31.9
67.0	17.0	-22.7	14.0	-29.8	45.0	17.5	-23.3	14.5	-30.9
83.0	17.0	-22.7	15.0	-31.9	24.0	15.0	-20.0	10.0	-21.3

(Note)

Mass of chamber: 945.92g
Mass of sample: 42.93g
Before the test (chamber + sample): 988.85g
After the test (chamber + sample): 988.82g
Difference of mass: 0.03g (Water content of sample decreased to 23.1% from 23.2%)

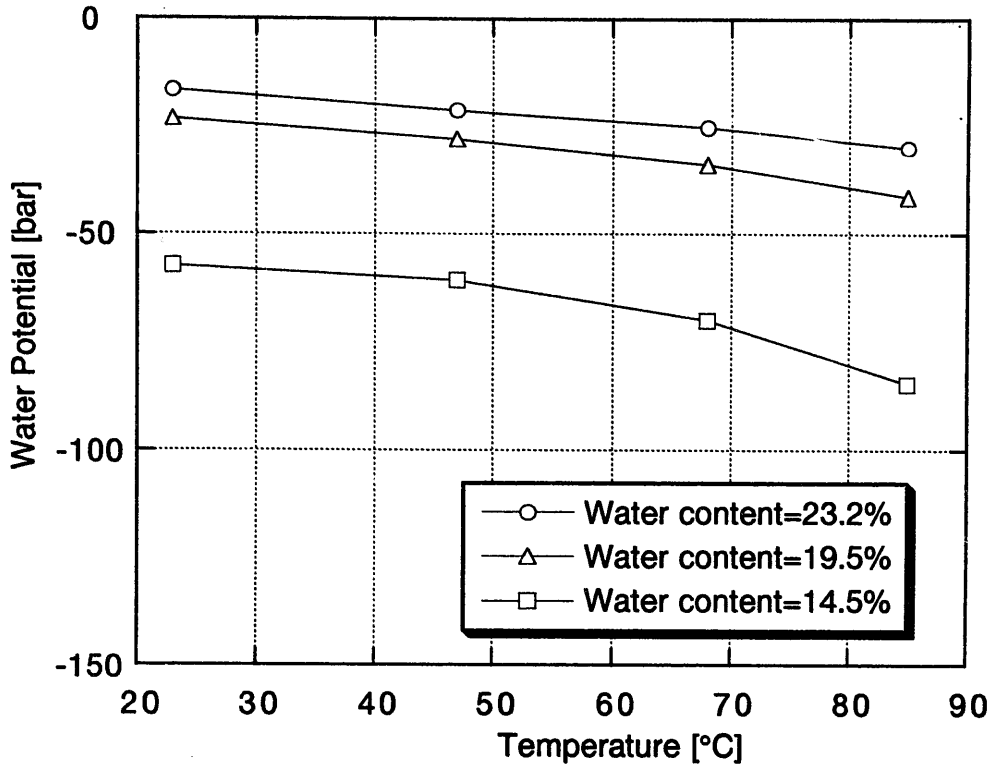

(a) Hygrometric method

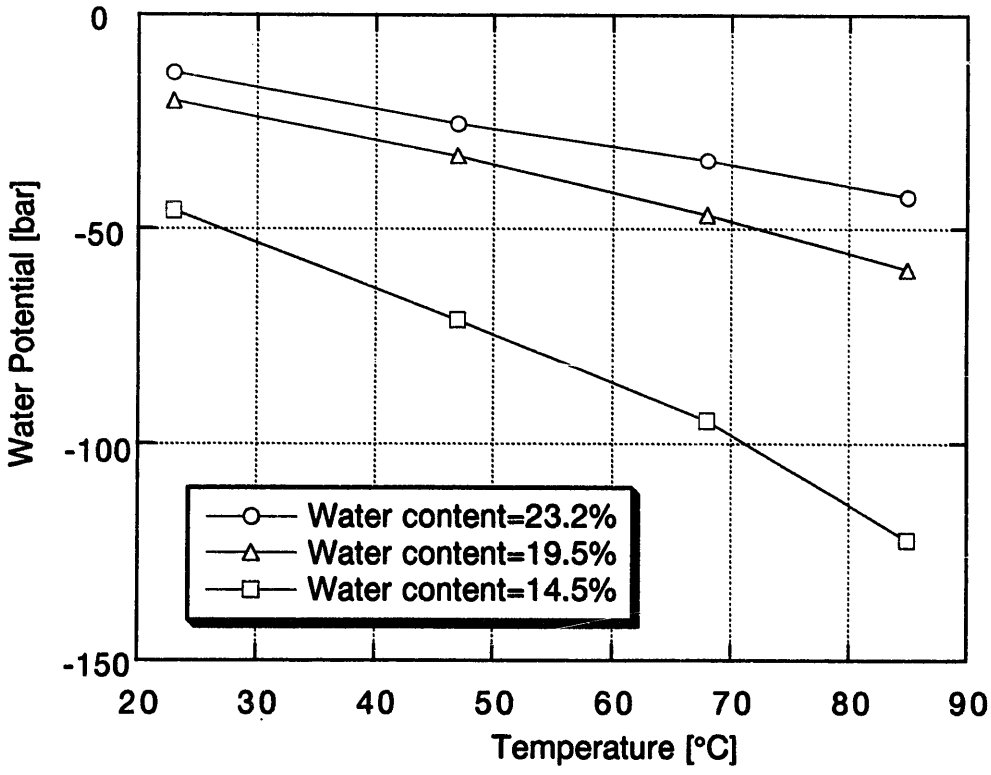

(b) Psychrometric method

Figure 3-20 Relationship between temperature and water potential (C-52 chamber)

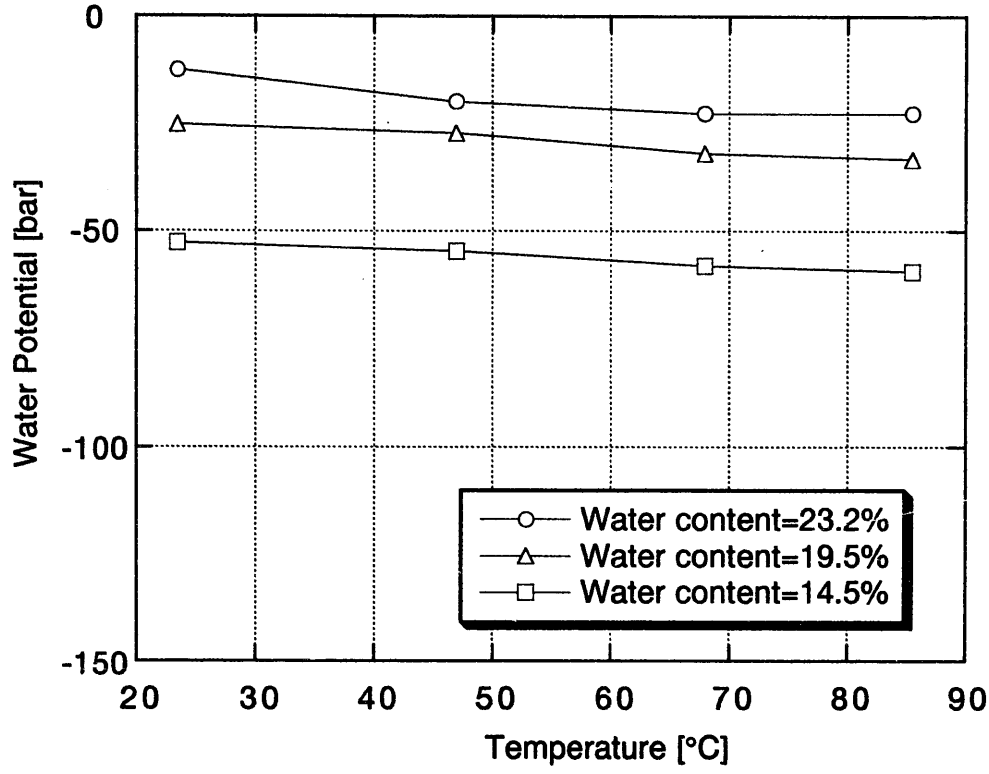

(a) Hygrometric method

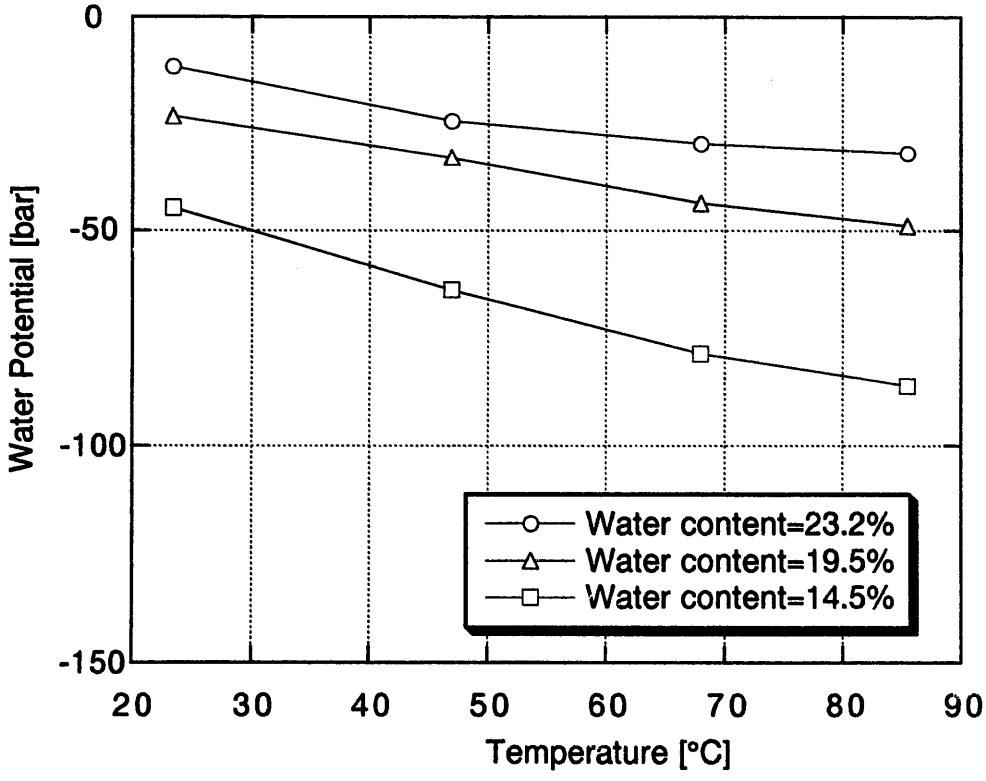

(b) Psychrometric method

Figure 3-21 Relationship between temperature and water potential (PST-55 chamber)

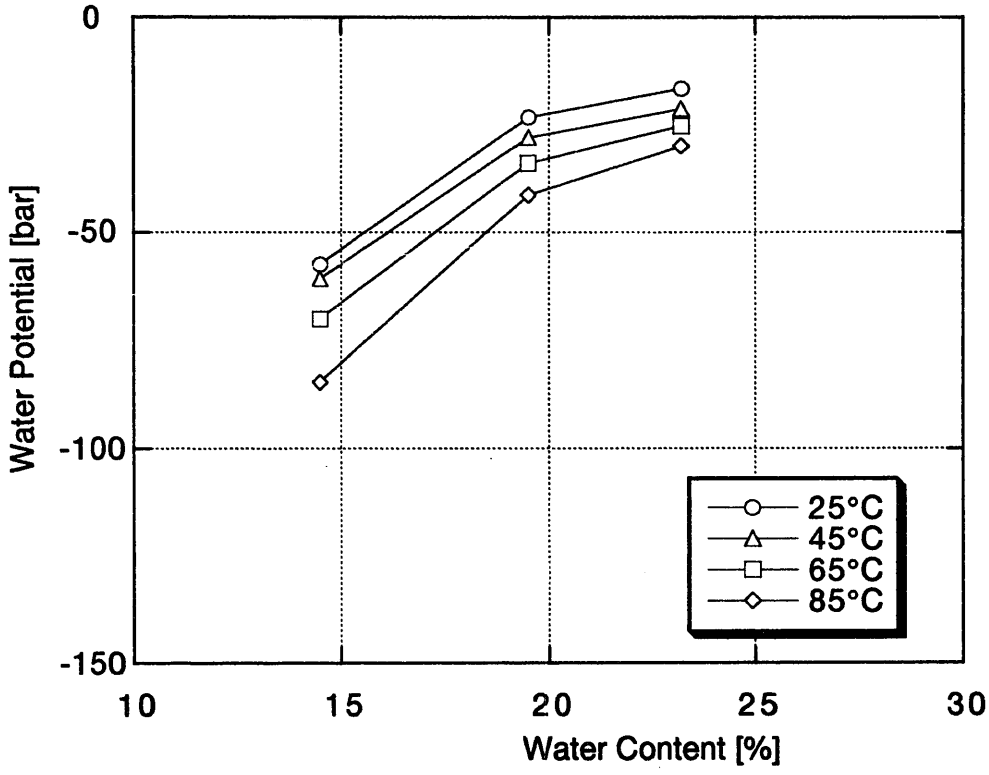

(a) Hygrometric method

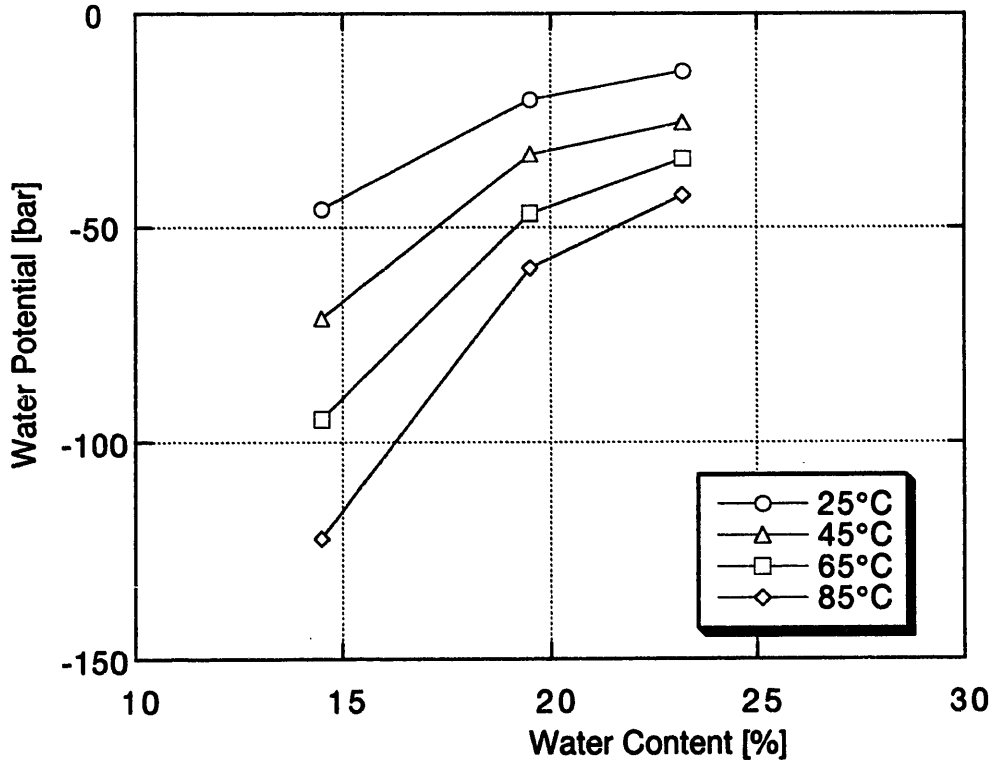

(b) Psychrometric method

Figure 3-22 Relationship between water content and water potential (C-52 chamber)

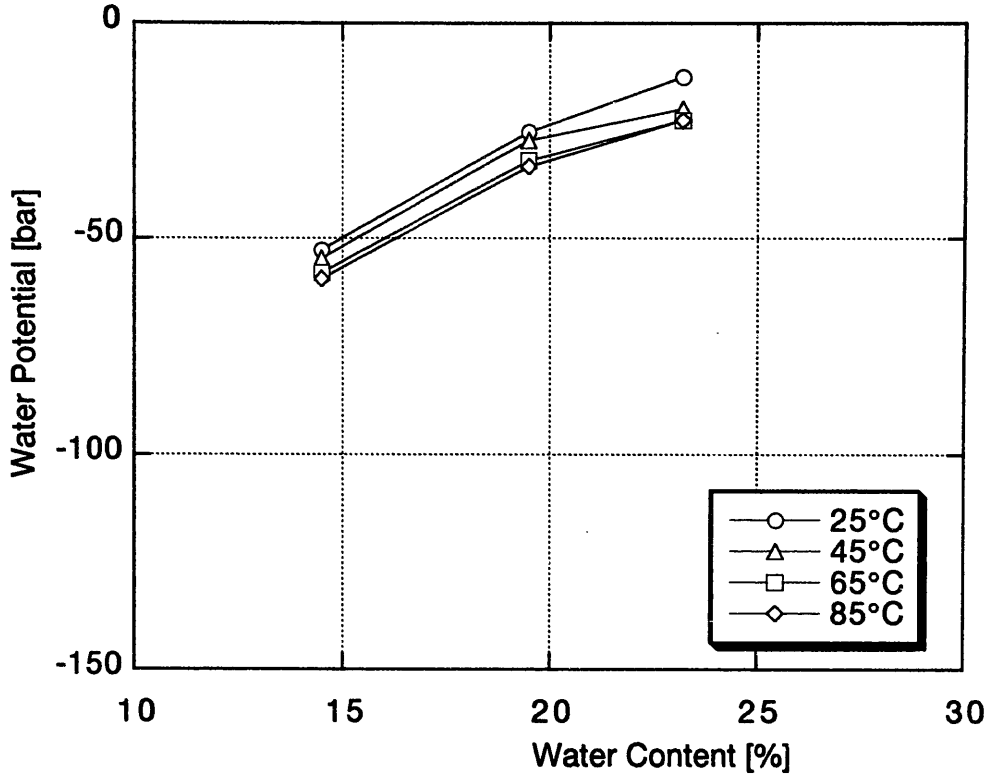

(a) Hygrometric method

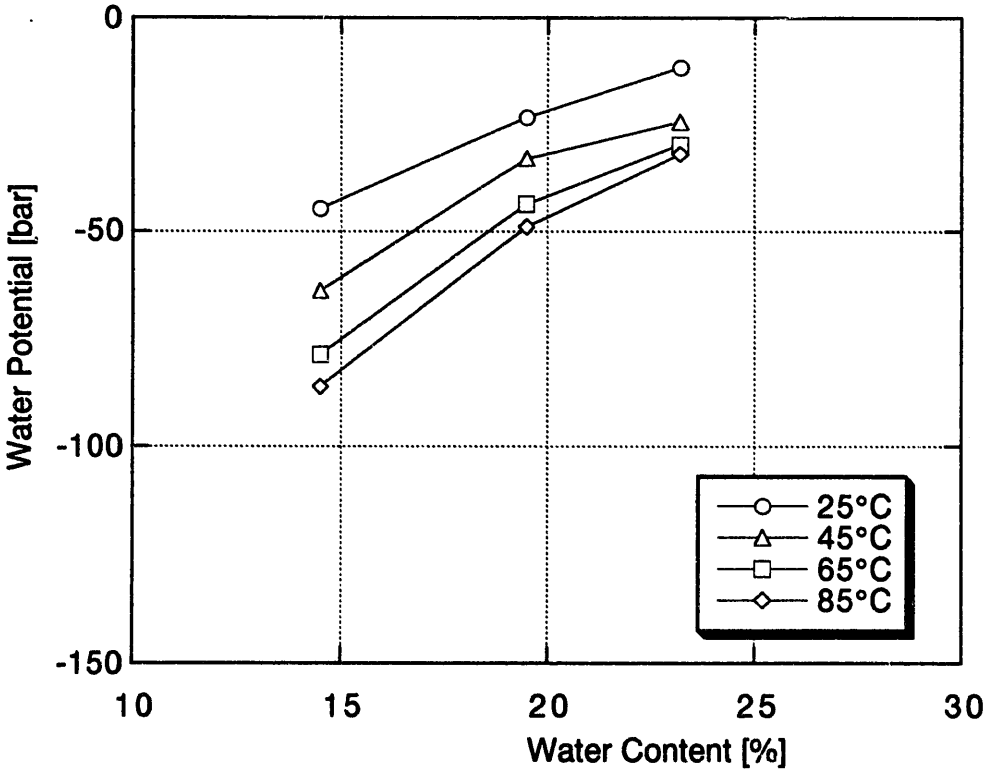

(b) Psychrometric method

Figure 3-23 Relationship between water content and water potential (PST-55 chamber)

(3)Multi-regression analysis

Multi-regression analysis is carried out by use of the measured water potential and temperature with water content of 14.5%, 19.5% and 23.2%. Linear multi-regression analysis which is expressed in [z=ax+by+c] is adopted as water potential and temperature for independent variables and as water content for dependent variable. Multi-regression analysis is carried out by use of four results; two sample chambers of C-55 chamber and PST-55 chamber, and two methods of hygrometric method and psychrometric method, respectively. The equations obtained by the analysis are as follows.

C-52 chamber, Hygrometric method;

$$\omega = 0.0606P + 0.219T + 7.52 \quad (3\text{-}5)$$

C-52 chamber, Psychrometric method method;

$$\omega = 0.114P + 0.284T + 7.28 \quad (3\text{-}6)$$

PST-55 chamber, Hygrometric method;

$$\omega = 0.0265P + 0.198T + 7.19 \quad (3\text{-}7)$$

PST-55 chamber, Psychrometric method method;

$$\omega = 0.102P + 0.254T + 7.50 \quad (3\text{-}8)$$

where, ω is the water content [%], P is the water potential [bar] and T is the temperature[°C]. The lower limit of applicability of these equations is water content of 15.0%.

Figures 3-24 to 3-27 show the comparisons between measured water content and analytical water content obtained by above equations. Analytical water content does not agree with the measured value because the relationship between water content and water potential is not linear. Maximum error is approximately 40%.

Therefore, non-linear multi-regression analysis which is expressed in [$\omega = a \ln(-P)+bT+c$] is adopted as logarithm of water potential and temperature for independent variables and as water content for dependent variable. The results are as follows.

C-52 chamber, Hygrometric method;

$$\omega = -7.66 \ln(-P) + 0.0636T + 43.03 \quad (3\text{-}9)$$

C-52 chamber, Psychrometric method method;

$$\omega = -7.71 \ln(-P) + 0.133T + 40.59 \quad (3\text{-}10)$$

PST-55 chamber, Hygrometric method;

$$\omega = -7.70 \ln(-P) + 0.0419T + 43.29 \quad (3\text{-}11)$$

PST-55 chamber, Psychrometric method method;

$$\omega = -7.74 \ln(-P) + 0.102T + 41.52 \quad (3\text{-}12)$$

where, ω is the water content [%], P is the water potential [bar] and T is the temperature[°C]. The lower limit of applicability of these equations is water content of 15.0%.

Figures 3-28 to 3-31 show the comparisons between measured water content and analytical water content obtained by above equations. Analytical values by equations (3-9) to (3-12) agree with the measured values better than analytical values by equations (3-5) to (3-8).

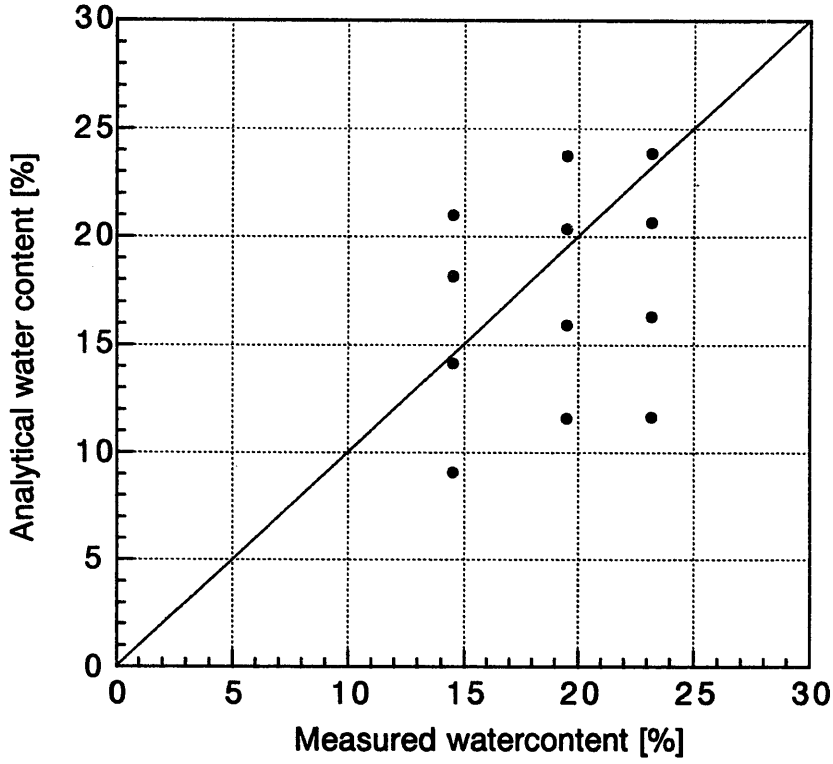

Figure 3-24 Comparison between measured and analytical water content
(Linear analysis, C-52 chamber, Hygrometric method)

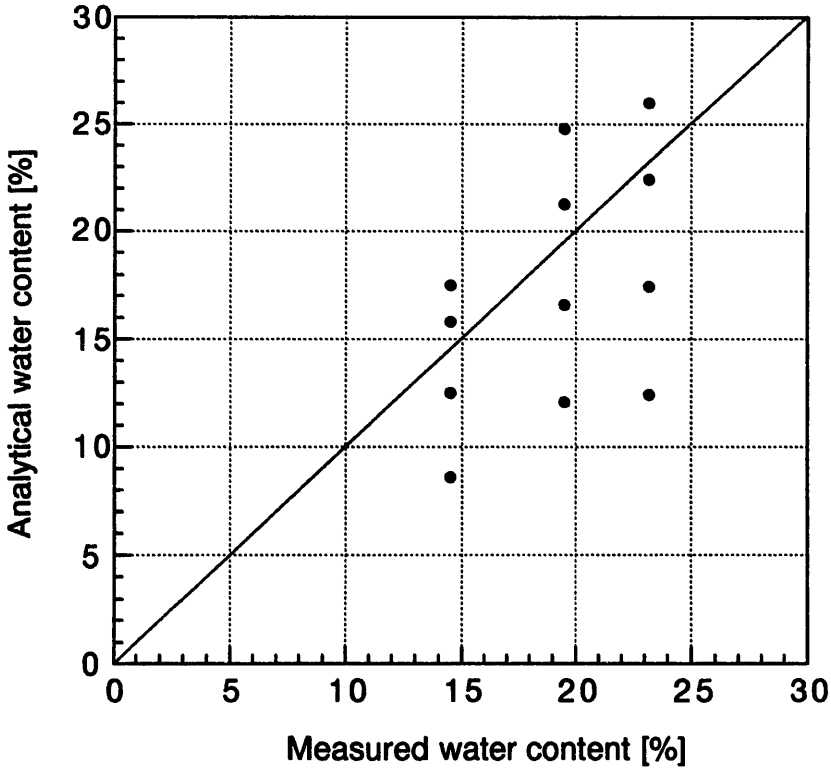

Figure 3-25 Comparison between measured and analytical water content
(Linear analysis, C-52 chamber, Psychrometric method)

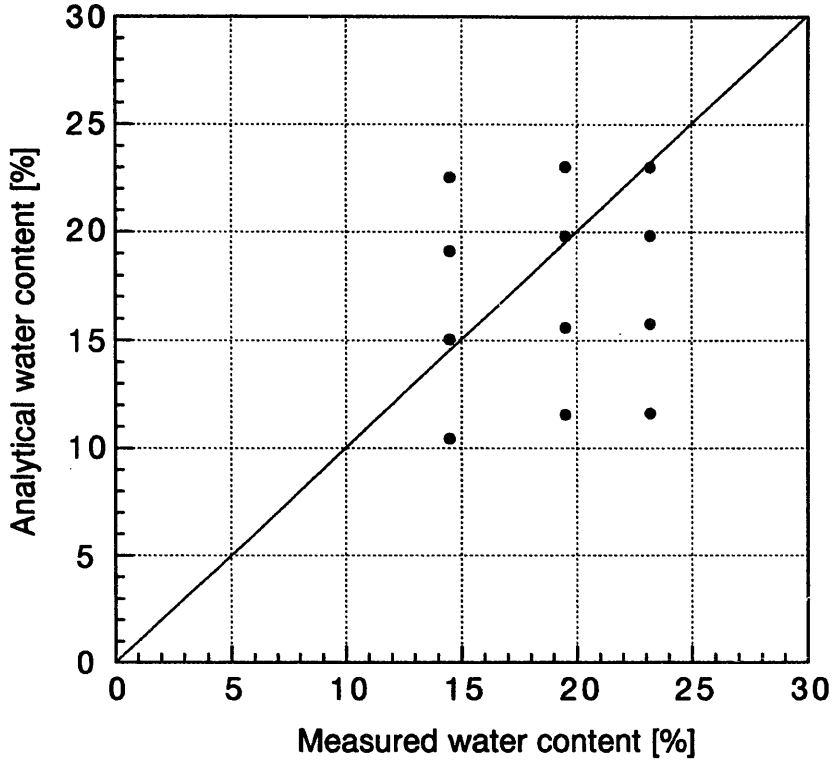

Figure 3-26 Comparison between measured and analytical water content
(Linear analysis, PST-55 chamber, Hygrometric method)

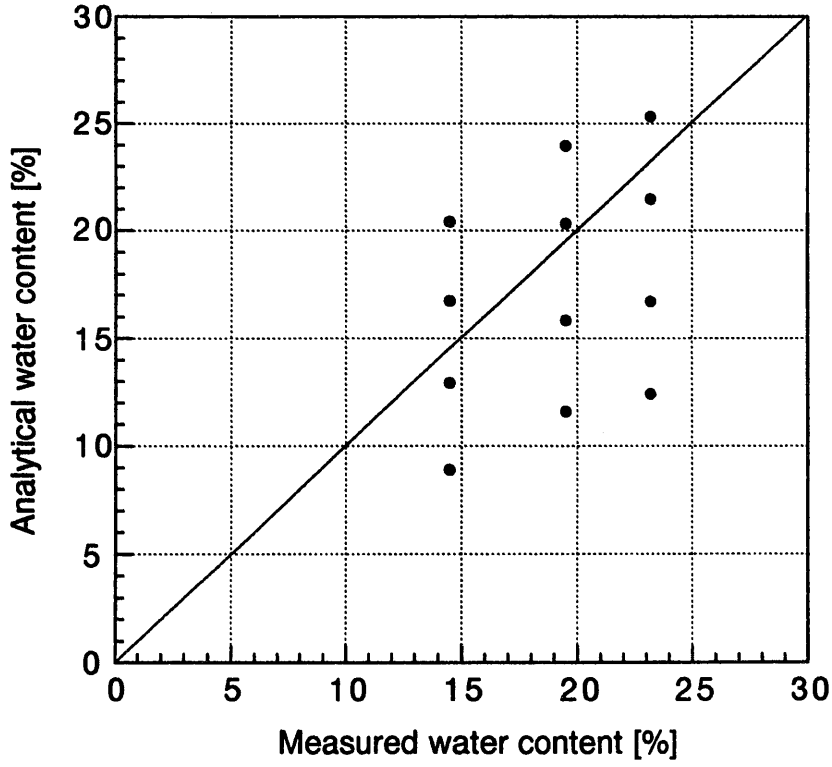

Figure 3-27 Comparison between measured and analytical water content
(Linear analysis, PST-55 chamber, Psychrometric method)

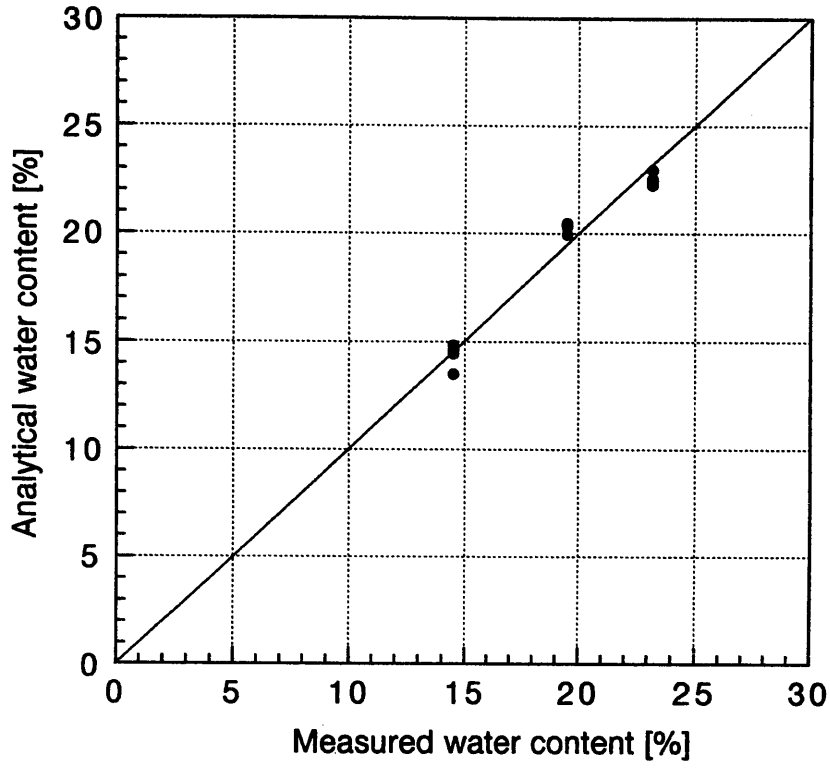

Figure 3-28 Comparison between measured and analytical water content
(Non-Linear analysis, C-52 chamber, Hygrometric method)

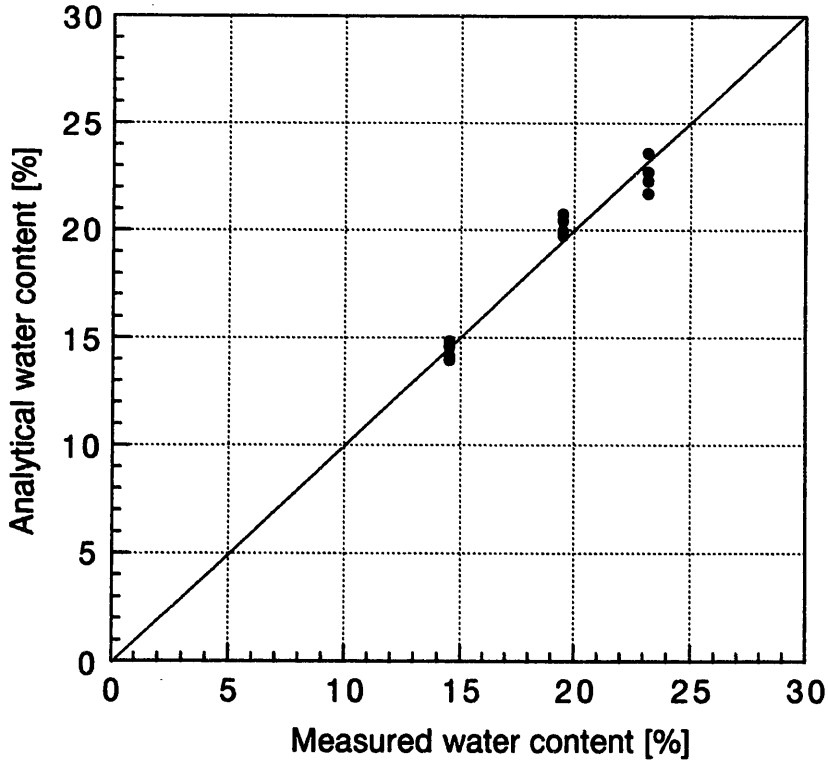

Figure 3-29 Comparison between measured and analytical water content
(Non-Linear analysis, C-52 chamber, Psychrometric method)

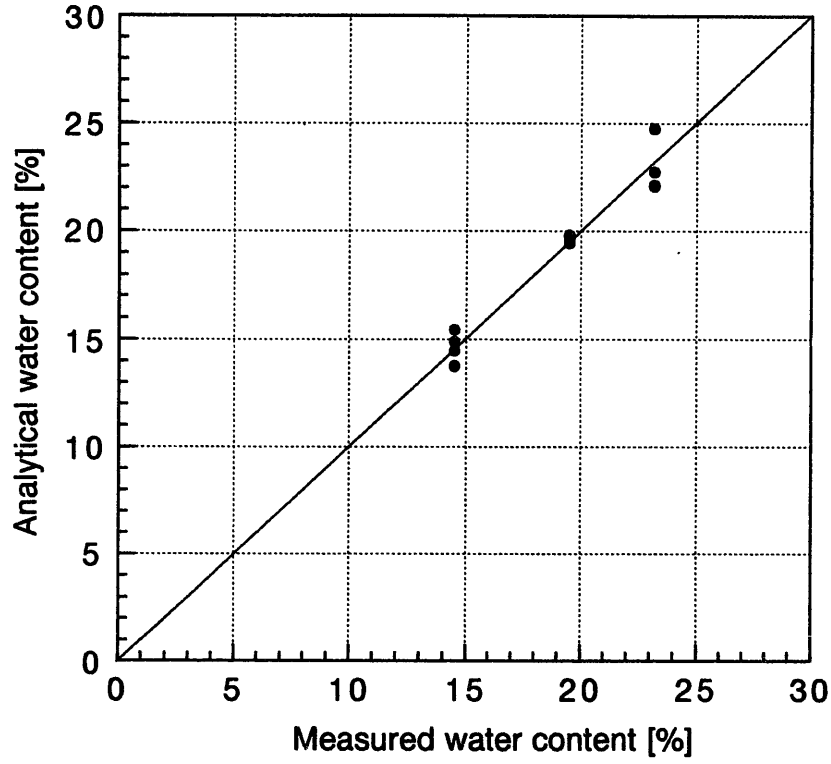

Figure 3-30 Comparison between measured and analytical water content (Non-Linear analysis, PST-55 chamber, Hygrometric method)

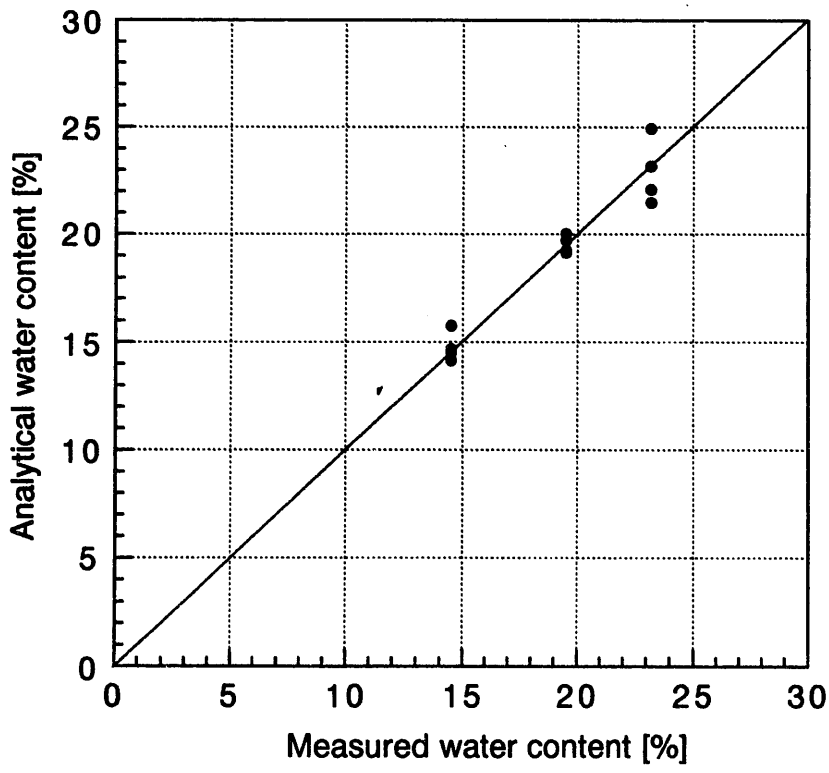

Figure 3-31 Comparison between measured and analytical water content (Non-Linear analysis, PST-55 chamber, Psychrometric method)

(4) Temperature test

Measurement value of temperature by thermocouple psychrometer has error when the temperature is high because of the non-linearity of thermocouple in the sensor. Then temperature test is carried out in order to confirm this error by use of PST-55 chamber. In order to compare the temperature, two resistance thermometer bulbs (Chino Corp. (Japan)) and one thermocouple (Chino Corp. (Japan)) is installed near the thermocouple psychrometer in the PST-55 chamber.

Figure 3-32 shows the time history of temperature measured by thermocouple psychrometer, resistance thermometer bulb and thermocouple. Figure 3-33 shows the comparison of temperature between thermocouple psychrometer and resistance thermometer bulb. The value of resistance thermometer bulb is average value of two sensors. From these figures, it is shown that the temperature measured by the thermocouple psychrometer is a little higher than that by the others. Figure 3-34 shows the temperature difference between resistance thermometer bulb and thermocouple psychrometer and Figure 3-35 shows the relationship between the temperature difference and temperature measured by resistance thermometer bulb. In the heating phase, temperature difference increses with temperature. And the temperature difference decreases with temperature decrease. However, hysteresis is seen during the heating and cooling. Becasuse the heating speed was not so fast, it is inconceivable that hysteresis is caused by the heat cinduction of material.

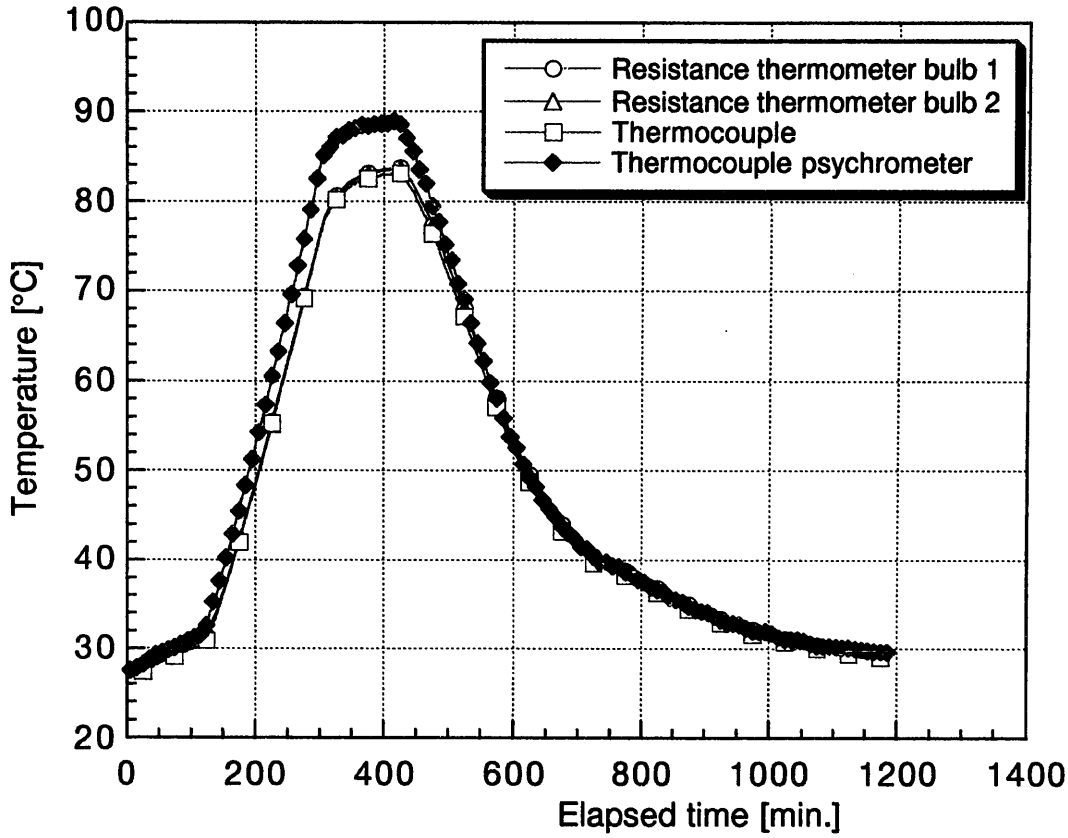

Figure 3-32 Measurement results of temperature by resistance thermometer bulb, thermocouple and thermocouple psychrometer

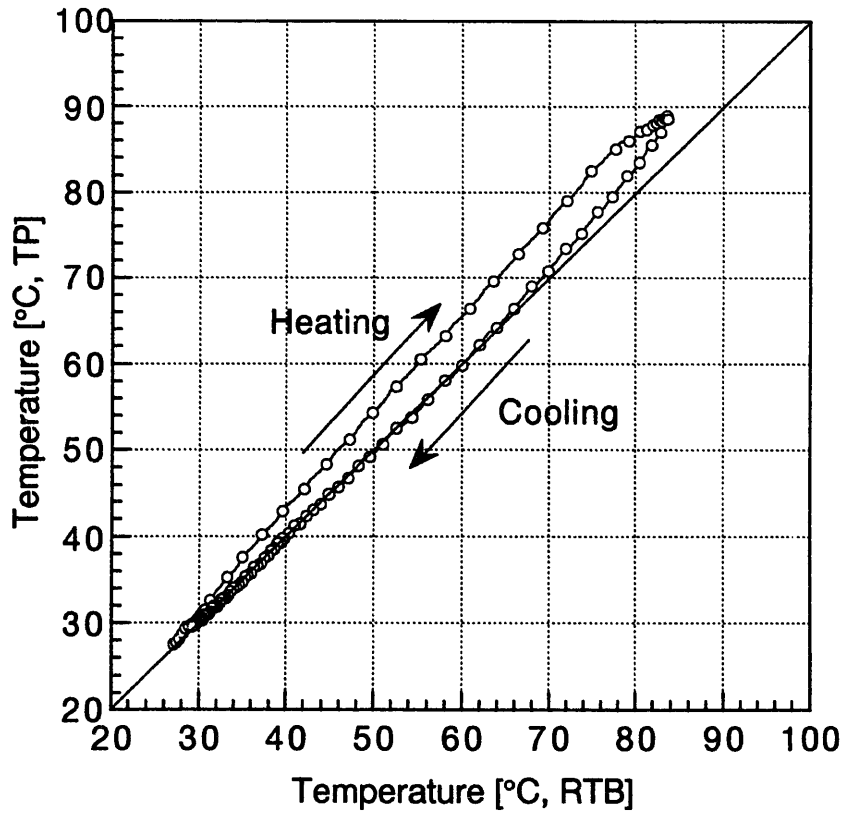

Figure 3-33 Comparison of temperature between thermocouple psychrometer [TP] and resistance thermometer bulb [RTB]

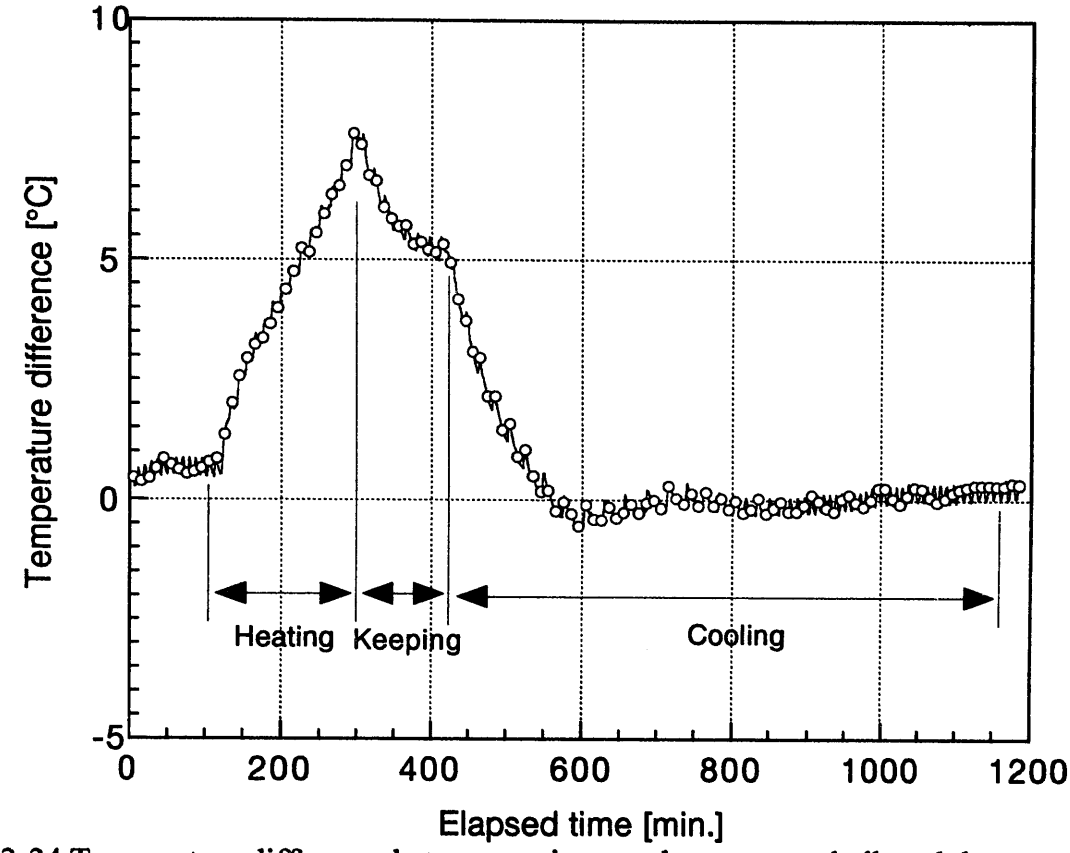

Figure 3-34 Temperature difference between resistance thermometer bulb and thermocouple psychrometer

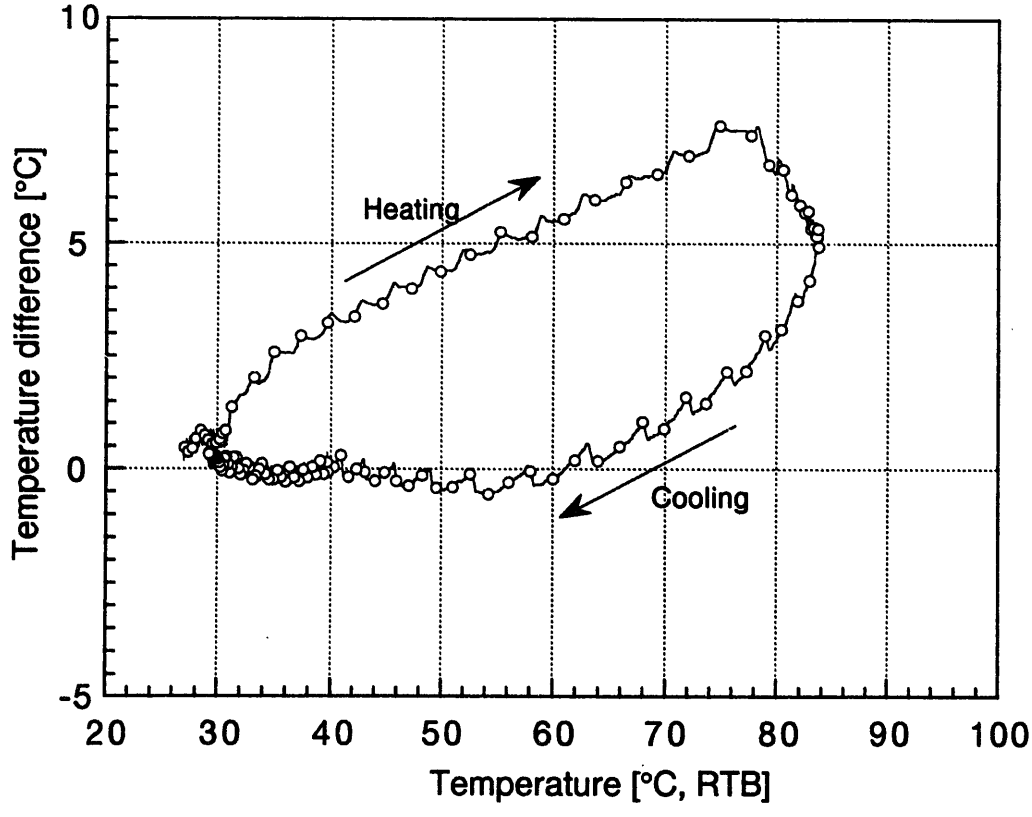

Figure 3-35 Relationship between the temperature difference and temperature by resistance thermometer bulb

3.4 Equation to calculate the water content

Applicability tests of hygrometer and thermocouple psychrometer were carried out and equations to calculate the water conetnt from the relative humidity and temperature measured by hygrometer, and from the water potential and temperature measured by thermocouple psychrometer are obtained.

In respect to the thermocouple psychrometer, two chambers were used and two measuring methods were adopted. As compared between two chambers, C-52 chamber was not sealed enough, that is, it is difficult to apply this chamber to measure the water potential at high temperature condition. As compared between two measuring methods, hygrometric method is unaffected by temperature and the sensitivity coefficient of hygrometric method is two times of psychrometric method. Therefore, we determine that in-situ measurement will be carried out by hygrometric method and water content will be calculated by the equation that was obtained by the result of PST-55 chamber and hygrometric method.

As mentioned above, we determine to use following equations to calculate the water content by the measurement results of hygrometer and thermocouple psychrometer.

Hygrometer:

$$\omega = 0.220H - 0.0257T - 4.52 \quad (\omega \leqq 16\%) \tag{3-1}$$

where, ω is the water content [%], H is the relative humidity [%RH] and T is the temperature[°C].

Thermocouple psychrometer:

$$\omega = -7.70 \ln(-P) + 0.0419T + 43.29 \quad (\omega \geqq 15\%) \tag{3-11}$$

where, ω is the water content [%], P is the water potential [bar] and T is the temperature[°C].

4. Outline of T-H-M test

4.1 Heater

A heater consists of ① carbon-steel heater annulus and oil circulation system, ② electric heater and ③ internal oil. The heater annulus is cylindrical vessel with a diameter of 1040 mm and a height of 1950 mm. The electric heater and oil are installed in the heater annulus and temperature on the heater surface is controlled at a constant value by circulating the internal oil. Specification of each component is mentioned below. Figure 4-1 shows the schematic of heater used in this test compared with the real concept of the waste package [Power Reactor and Nuclear Fuel Development Corporation, 1992].

①Carbon-steel heater annulus and oil circulation system

The carbon-steel heater annulus is made of SM400B, JIS G3106. Figure 4-2 is an external view of the heater annulus. The dimension of the heater is 1040 mm in diameter and 1950 in height. The thickness of side part and bottom part is 50 mm, and the thickness of the top is 55 mm. This heater annulus consists of 4 segments, each 500 mm thick and 1040 mm in diameter which was installed sequentially as the buffer was compacted around it [Sugita et al., 1999]. Figure 4-3 shows the inner part of the heater annulus.

As the oil circulation system, one screw stirrer and two air supply pipes to agitate the internal oil are installed in the heater annulus.

②Electric heater

The electric heater consists of six cartridges with 1600 mm in length. The capacity of each cartridge is 1667 W. Maximum capacity of the electric heater is approximately 10 kW and maximum temperature is 300°C.

③Internal oil

Oil is installed in the heater annulus in order to transfer heat from the electric heater to the heater annulus. Oil is THERMOL No. 32 (Nippon Sekiyu, Japan) and specific gravity is 0.909, the pour point is –25°C and the flashing point is 230°C. In order to monitor the oil level, a float is installed in the heater annulus.

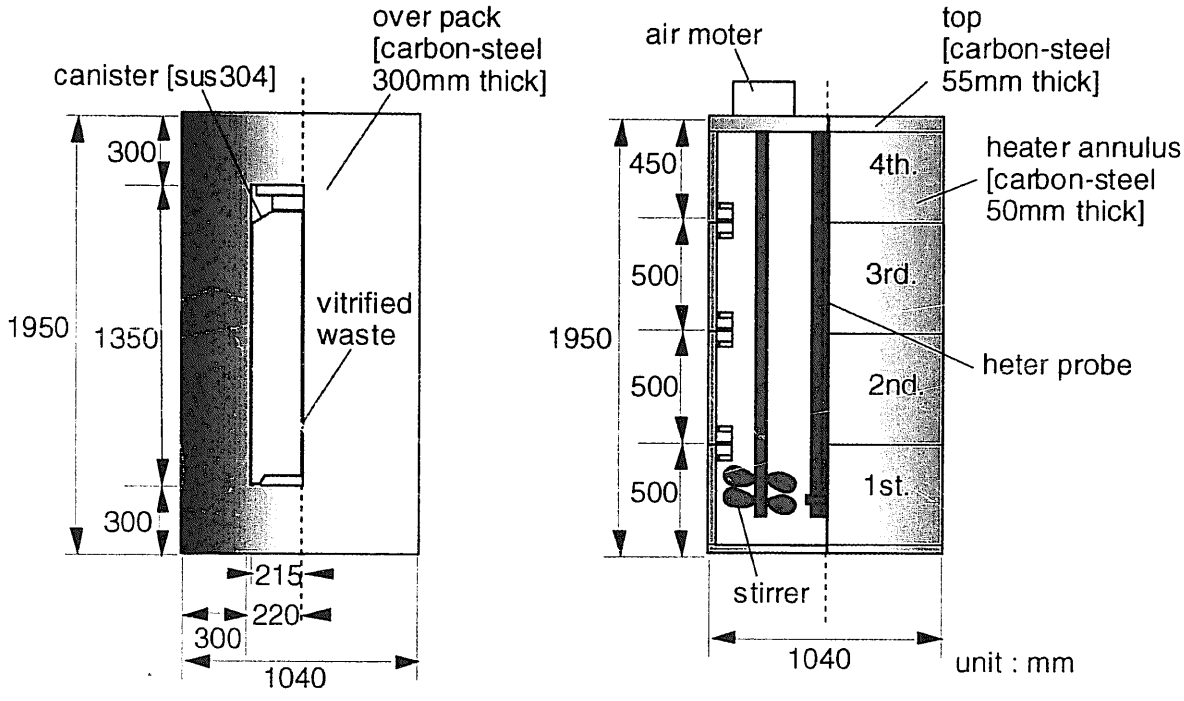

(a)Waste package (b)Heater used in this test

Figure 4-1 Schematic of heater

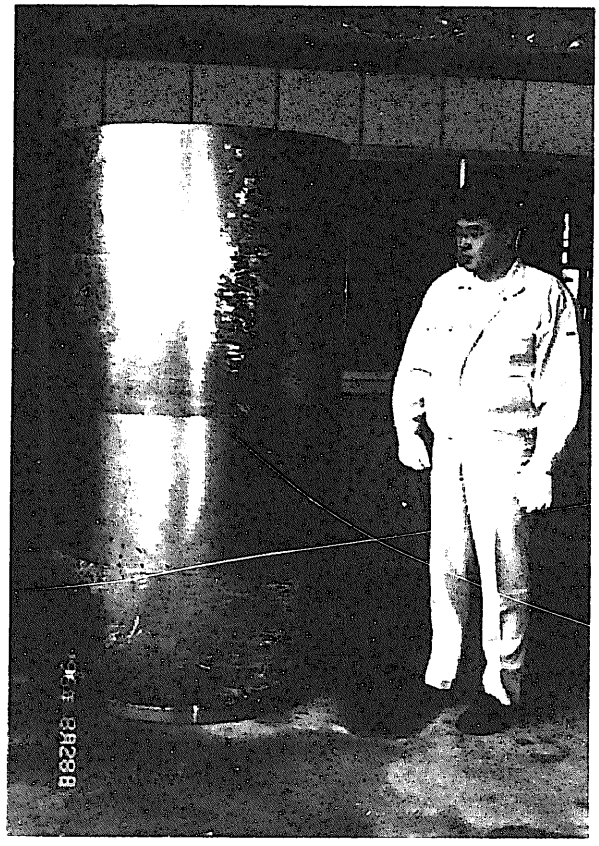

Figure 4-2 External view of the heater annulus

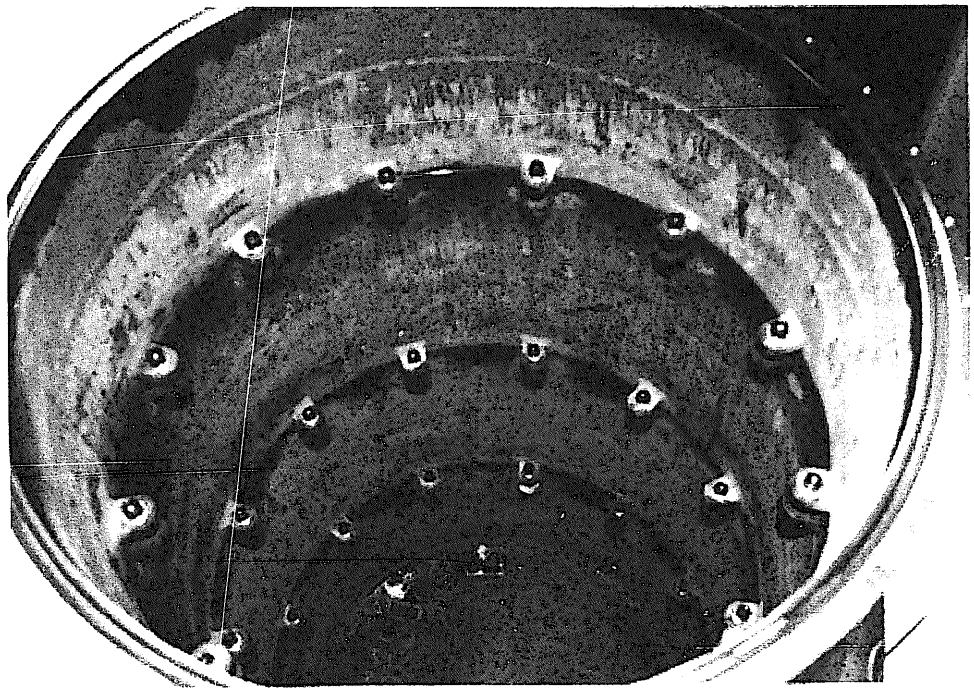

Figure 4-3 Inner part of the heater annulus

4.2 Concrete lid

Figure 4-4 shows the concrete lid that is settled in order to avoid the extrusion of the buffer. Figure 4-5 shows the horizontal projection of the concrete lid. The casing pipe that was used for the excavation of the test pit [Fujita, et al, 1997a] is installed upside down on the top of buffer and concrete is emplaced into the casing pipe. Sensor cables that were installed in the buffer are fixed in the tube by resin to avoid the extrusion of the buffer or inflow of the water from the flooding pool. Sensor cables are threaded through the flexible tube in the concrete lid not to contact the concrete directly. The flexible tube is filled with the urethane foam. As shown in Figure 4-5, steel pipe is installed in the concrete lid to perform the core boring for the sampling of the buffer.

Figure 4-6 shows the fixation method of the concrete lid. The concrete lid is fixed to the rock by the anchor and four steel H piles are established on the top of the concrete lid. The hydraulic jack is installed at the bottom part of each steel H pile and pressurized in the vertical direction to fix the steel H pile. Horizontal steel H piles are established to avoid the buckling of the vertical steel H pile.

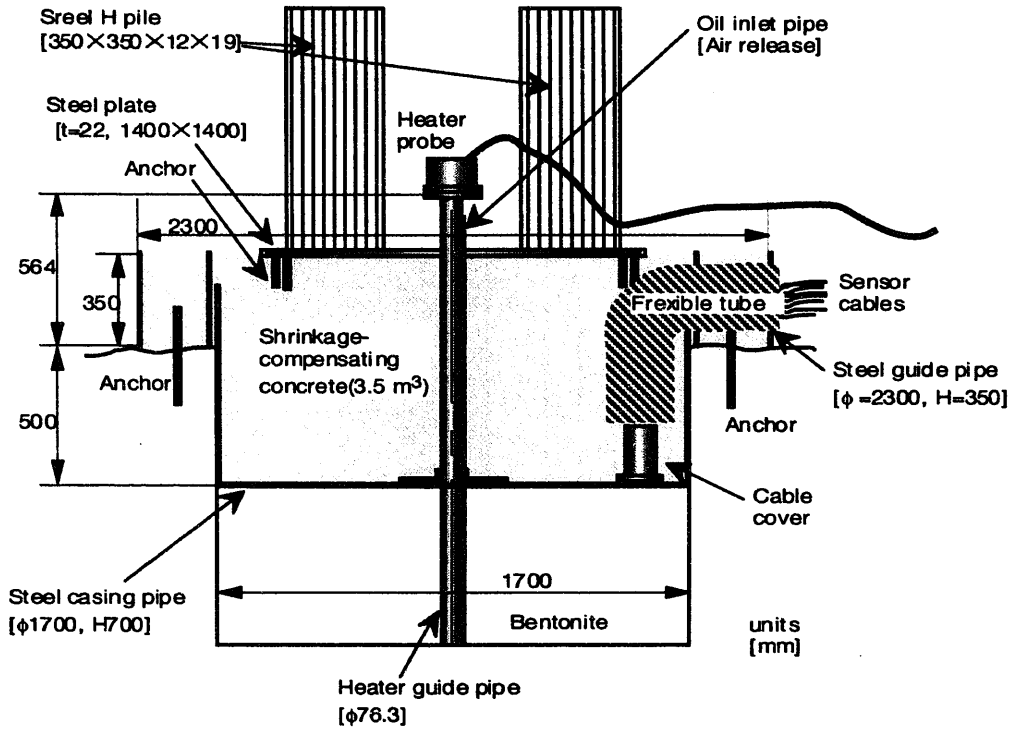

Figure 4-4 Concrete lid

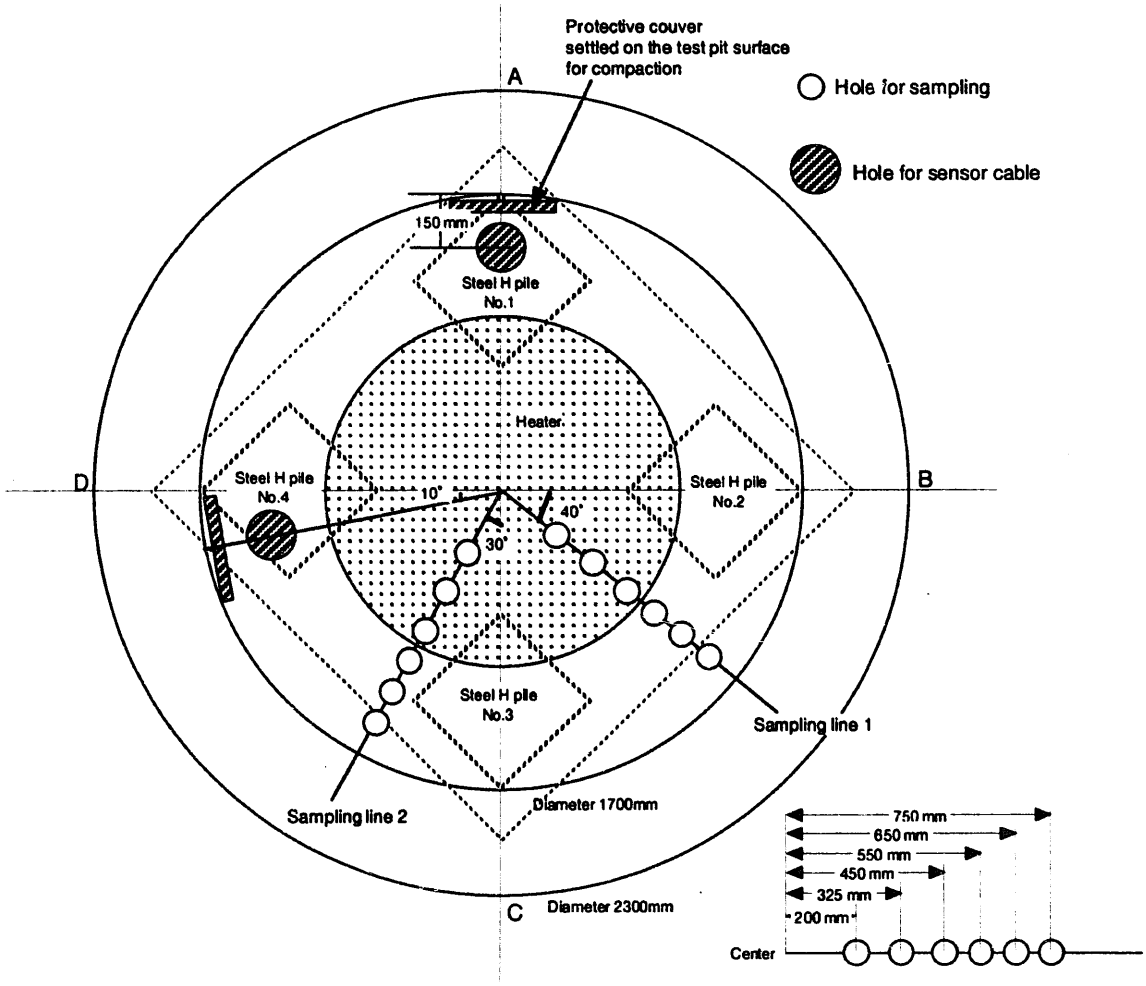

Figure 4-5 Horizontal projection of the concrete lid

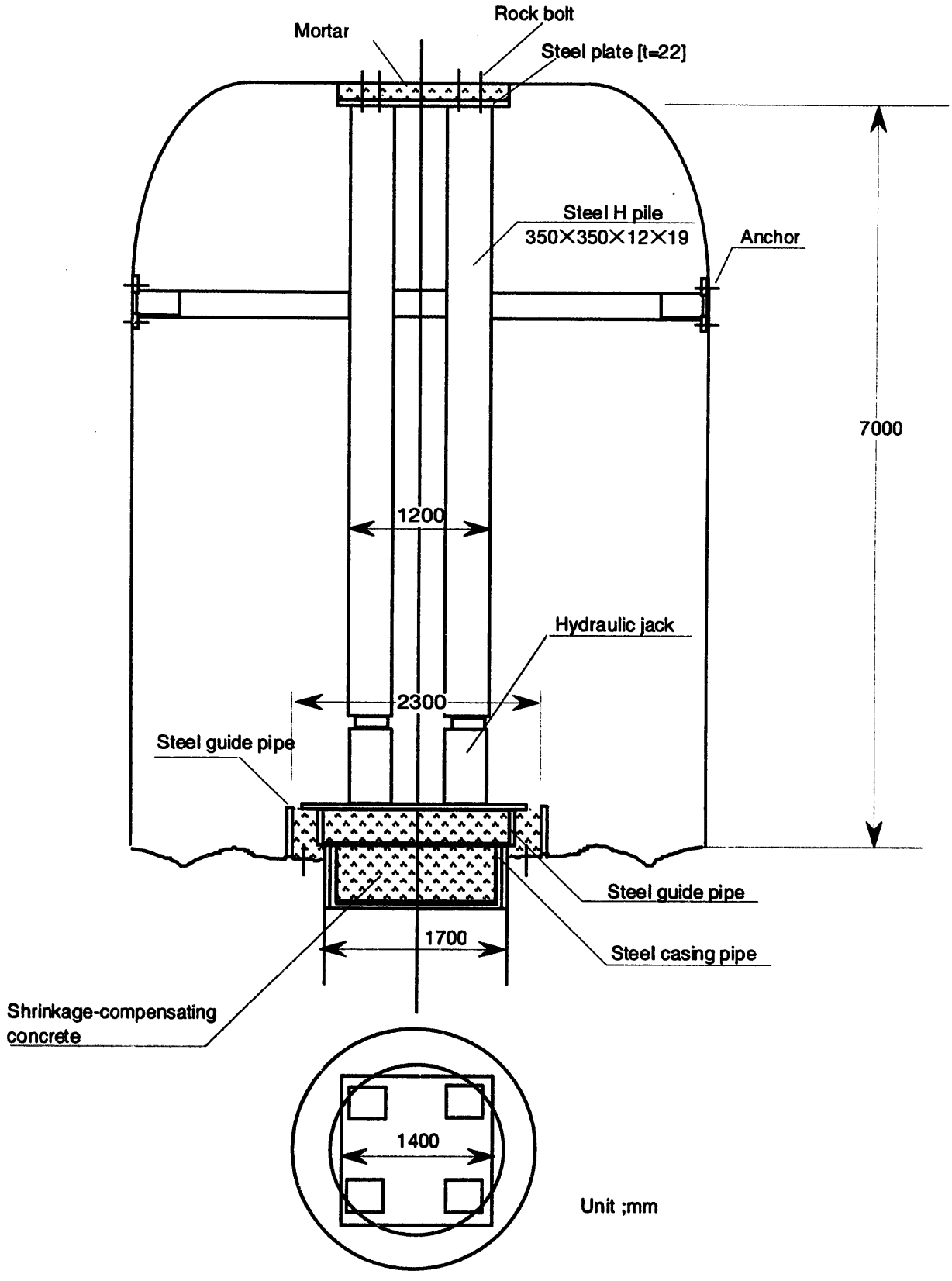

Figure 4-6 Fixation the concrete lid

4.3 Test area

Figure 4-7 shows the test area. In order to control the temperature and the humidity in the test drift, a bulkhead is established in the test drift and an air conditioner is installed in the test area. Figure 4-7 shows the location of the bulkhead and Figure 4-8 shows the schematic of the bulkhead. The air conditioner is installed to control the temperature and the humidity, and the bulkhead is established to maintain the temperature and the humidity.

A monitoring room is placed at the entrance of the test are as shown in Figure 4-7. Data loggers, scanners and microvoltmeter are settlement in the monitoring room.

In order to establish the boundary condition for analysis and to accelerate the water flow through the rock mass, the dam for the pool is constructed on the floor of the test area as shown in Figure 4-7. Water head is kept 40cm at the center of the test pit as shown in Figure 4-9.

4.4 Test condition

The heating test was started on December 17 1996. During the heating test, the heater annulus was controlled to be 100°C at the center of the bottom as shown in Figure 4-10. Heating test stopped on September 1 1997 and then cooling test started. The test period is as follows.

○Heating test (Approx. 260days)
December 17, 1996, 14:00 - September 1, 1997, 14:00

○Cooling test (Approx. 180days)
September 1, 1997, 14:00 - March 10, 1998, 15:00

Figure 4-11 shows the time history of the temperature at the control point. The temperature of the control point went up quickly to be 100°C and maintained its stability. From 8:30 of June 13, 1997 to 12:50 of June 16, the heater was stopped due to the electricity failure. When the heater was stopped, temperature went down gradually. However, it did not return to the initial value. On 12:50 of June 16, heater was started and then temperature returned back to be 100°C immediately. After about 200days past from the start of heating, heater trouble was occurred. Because of this effect, temperature of heater was raised. However, temperature became constant again after the repair of the heater. After the heater was stopped on September 1, temperature at the control point went down gradually.

Temperature of the water of the flooding pool was constant at 12.3°C and water head of the flooding pool was kept 40cm at the center of the test pit.

At the end of heating test, bentonite sampling was carried out by using the sampling holes along the sampling line 1 shown in Figure 4-5. At the end of cooling test, bentonite sampling was carried out by using the sampling holes along the sampling line 2 shown in Figure 4-5. After the cooling test, the buffer and the heater were demolished and water content and dry density of buffer were measured.

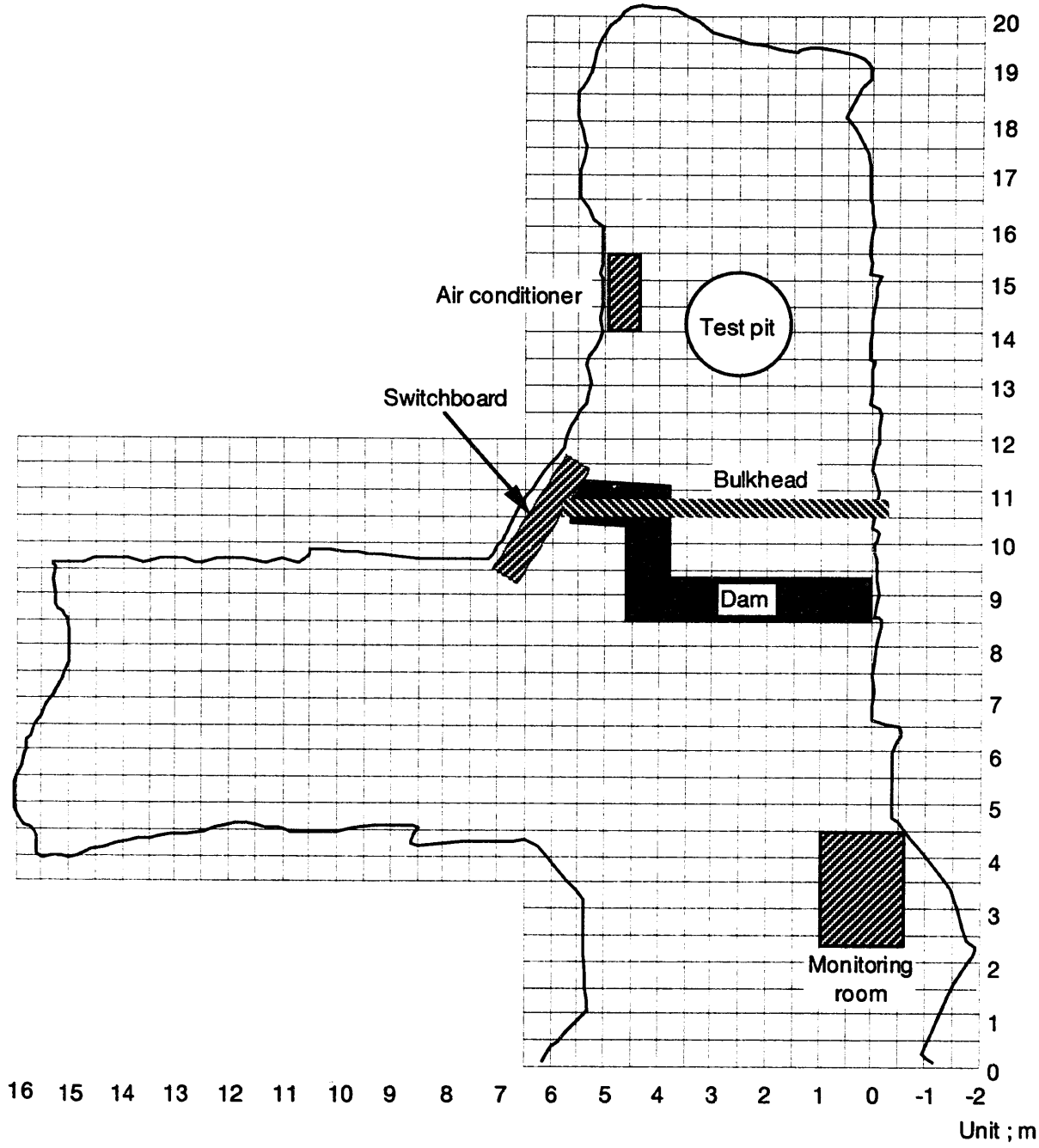

Figure 4-7 Test area

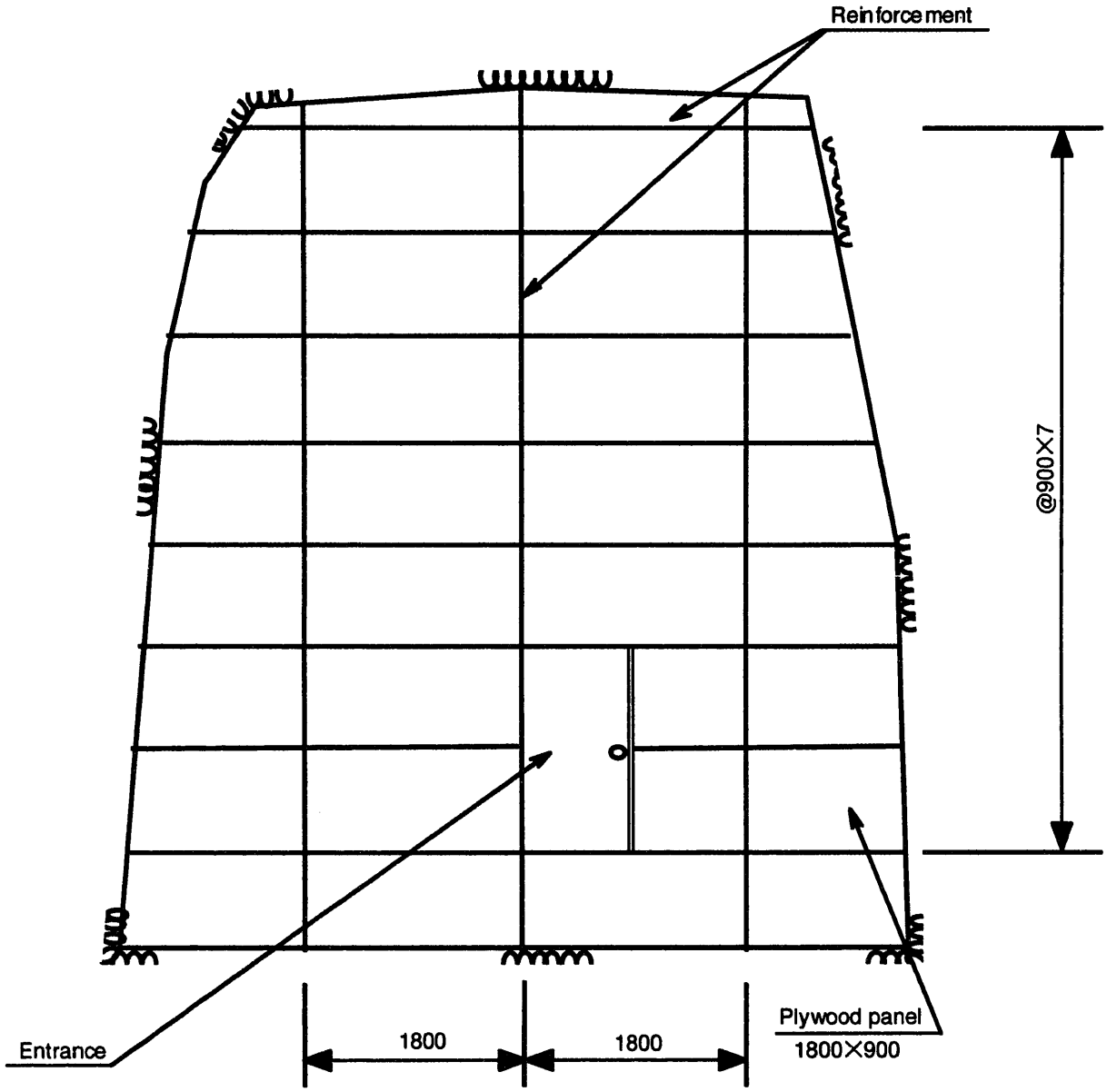

Figure 4-8 Schematic of bulkhead

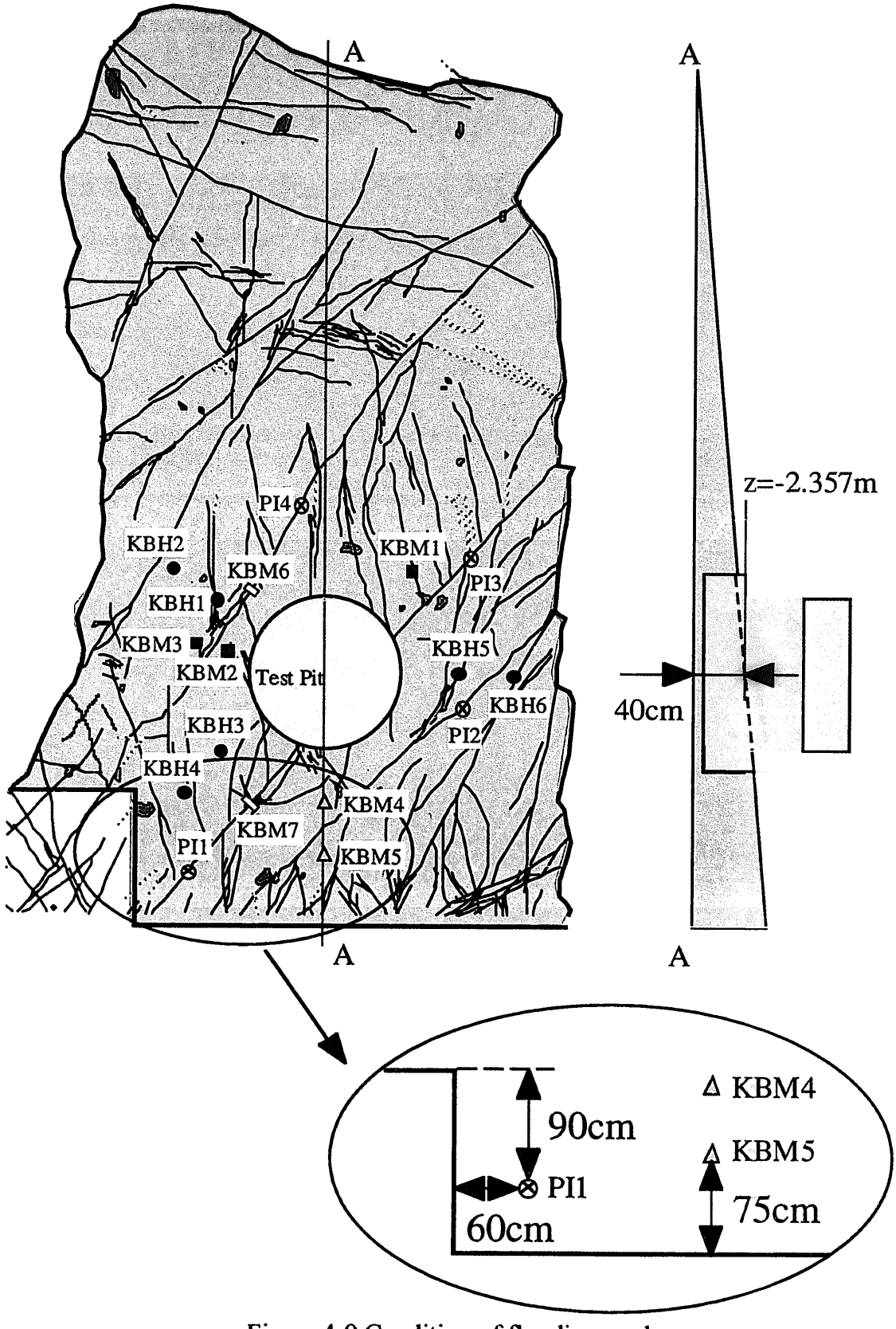

Figure 4-9 Condition of flooding pool

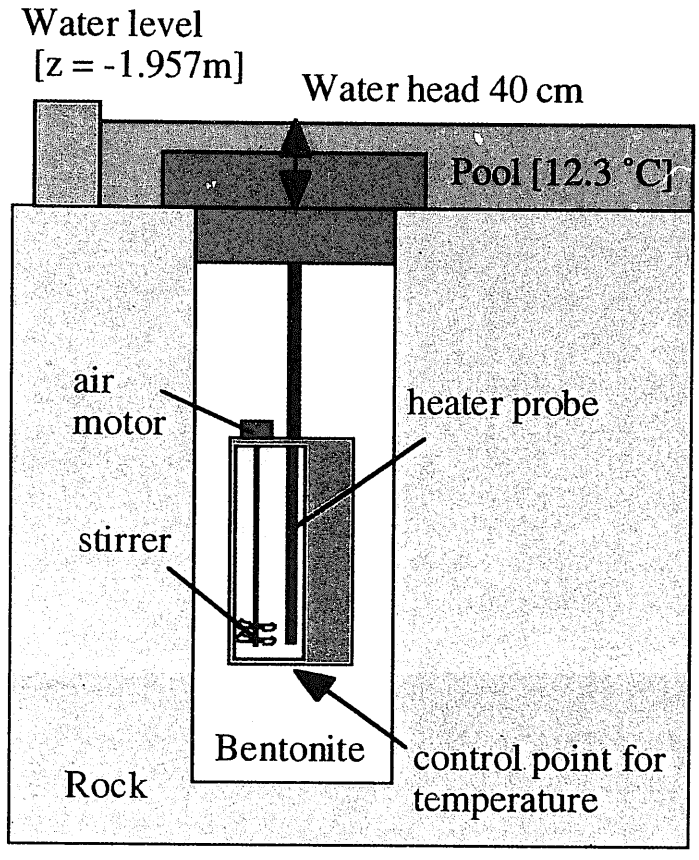

Figure 4-10 Test condition

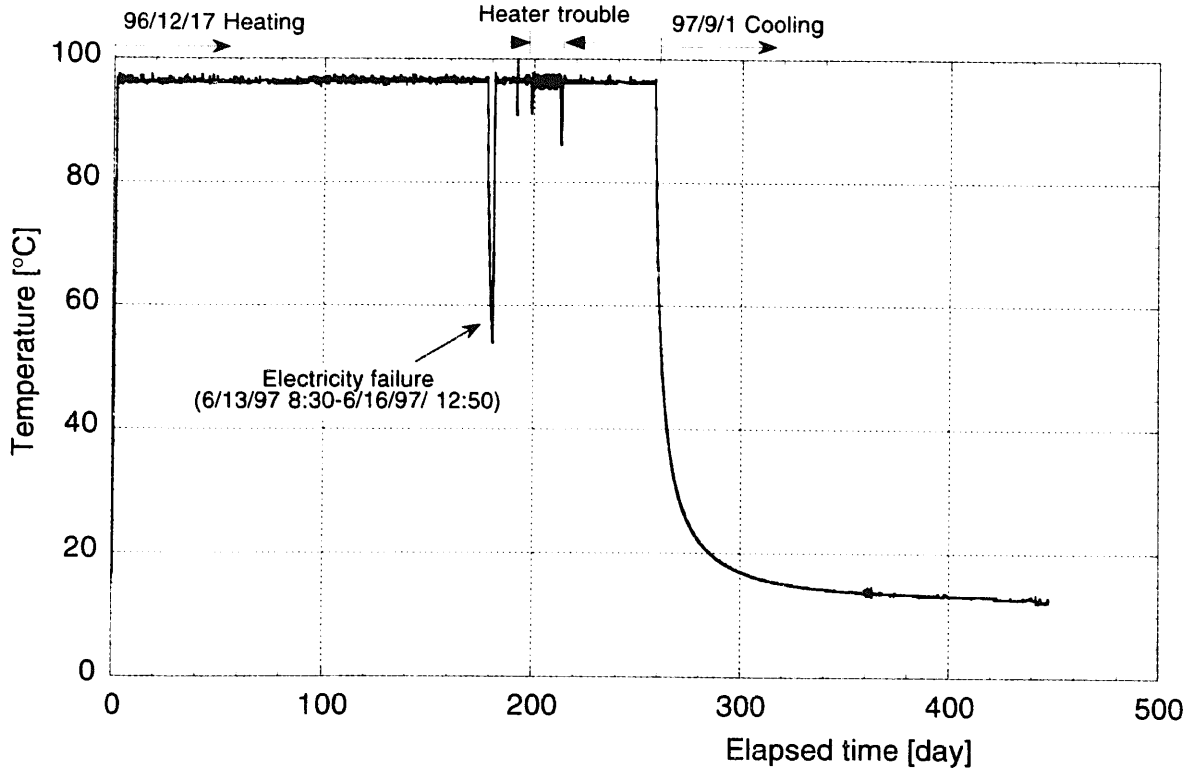

Figure 4-11 Time history of temperature at the control point

5. Measurement results

In this chapter, we discuss the measurement results monitored by sensors that were installed in the rock mass and the buffer. During the experiment, some sensors were broken. Then figures are drawn except for the data obtained by these sensors fundamentally. However, the data those were obtained before the trouble of sensor were plotted in figures. In following figures, the data by pore pressure transducer and pressure cell were compensated as mentioned in Appendix A.

5.1 Thermal effect

Figure 5-1 shows the time history of heat flux at the surface of heater and test pit wall. Just after the heating was started, the heat flux was very high, and it became low and constant as the temperature became constant. The value of heat flux is approximately 130 W/m^2 when it became constant, therefore, total heat flux is estimated to be approximately 1.27kW if heat flux was the same at all surface of heater. After 180 days from the start of heating, heat flux decreased due to the electricity failure and it continued about 3 days. After 200 days from the start of heating, heat flux increased due to the trouble of heater. The ratio of the heat flux at the surface of heater to that at the surface of test pit wall is in the range of 0.63 to 0.73 as shown in Table 5-1. The ratio of the heat flux will be proportional to the distance from the center of the heater if the heat flow is the ideal two-dimensional flow, because the heater is cylindrical. The diameter of the heater is 0.52m, that of test pit is 0.85m and that of the heat flux meter is 0.0017m. Then the ratio of the ideal heat flow is calculated to be 0.61 (heat flux at the surface of the test pit wall/ heat flux at the surface of the heater = 0.61). Therefore, it is known that heat flow at the center level of the heater is approximately two-dimensional flow.

Figures 5-2 to 5-7 show the time history of temperature in the buffer and Figures 5-8 to 5-14 show the time history of temperature in the rock mass. The temperature in the buffer is raised immediately and becomes constant at 20 days past, while that in the rock mass is raised slowly and becomes constant at 100 days past. At the end of heating test, the temperature at the buffer-rock interface is 55°C and then radial temperature gradient is approximately 1.3°C/cm. After the heater was turned off, temperature in both buffer and rock decreased slowly and they became constant at 150 days past from the start of cooling phase.

Figure 5-15 shows the time history of temperature at the center level of the heater. There is some difference of temperature between the directions at the middle part of buffer. However, there is no difference of temperature between the directions at the outside part of buffer. Figure 5-16 shows the relationship between the temperature and the distance from the center of the heater at the steady state during the heating test. There is no difference of temperature between the rock mass and the buffer if the distance from the center of the heater is the same. It is considered from this figure that temperature is the function of the distance from the center of the heater in this experiment because this experiment was performed under temperature control of the heater.

Table 5-1 Ratio of the heat flux at the surface of heater to that at the surface of test pit wall

After 50 days from the start of heating		
BBC section	MF-5(outside)/MF-1(inside)	94.2(w/m^2)/129.9(w/m^2) = 0.73
DDA section	MF-4(outside)/MF-3(inside)	89.1(w/m^2)/139.4(w/m^2) = 0.64
CD section	MF-6(outside)/MF-2(inside)	85.3(w/m^2)/132.7(w/m^2) = 0.64
After 100 days from the start of heating		
BBC section	MF-5(outside)/MF-1(inside)	92.0(w/m^2)/129.0(w/m^2) = 0.71
DDA section	MF-4(outside)/MF-3(inside)	87.4(w/m^2)/138.4(w/m^2) = 0.63
CD section	MF-6(outside)/MF-2(inside)	81.9(w/m^2)/129.0(w/m^2) = 0.64

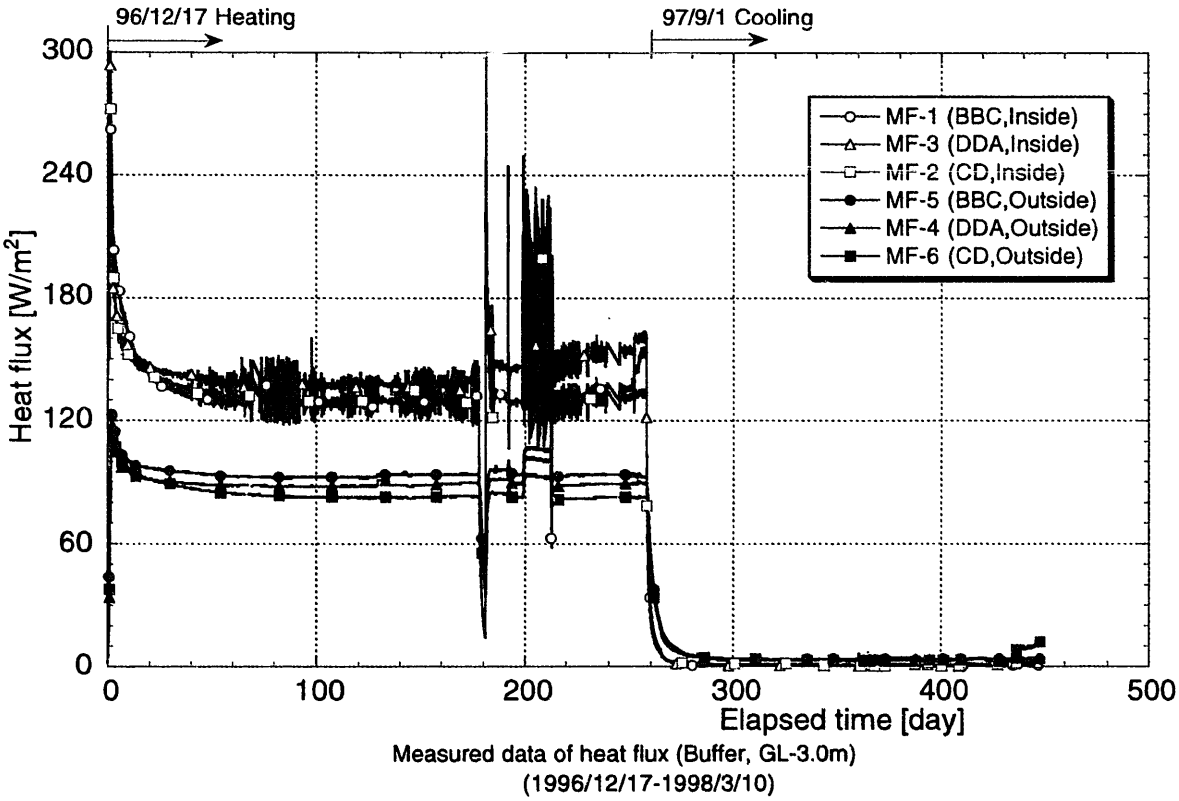

Figure 5-1 Time history of the heat flux (GL-3.0m)

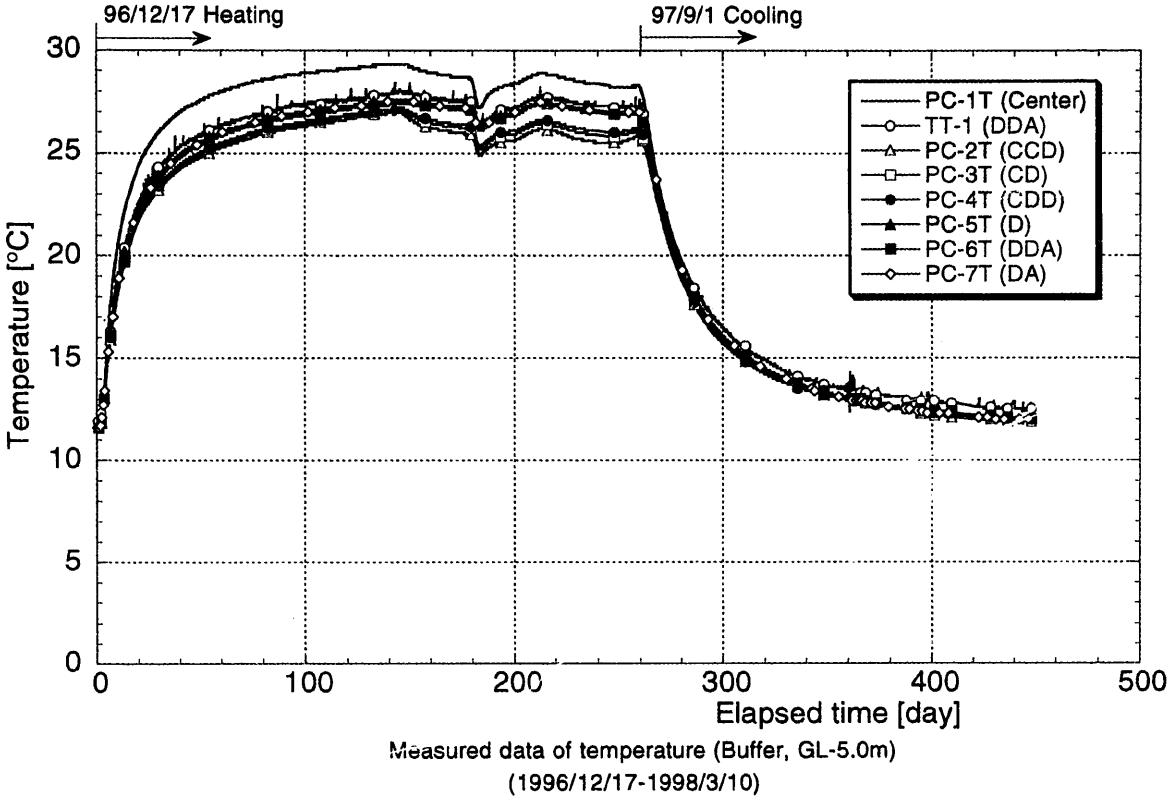

Measured data of temperature (Buffer, GL-5.0m)
(1996/12/17-1998/3/10)

Figure 5-2 Time history of the temperature in the buffer (GL-5.0m)

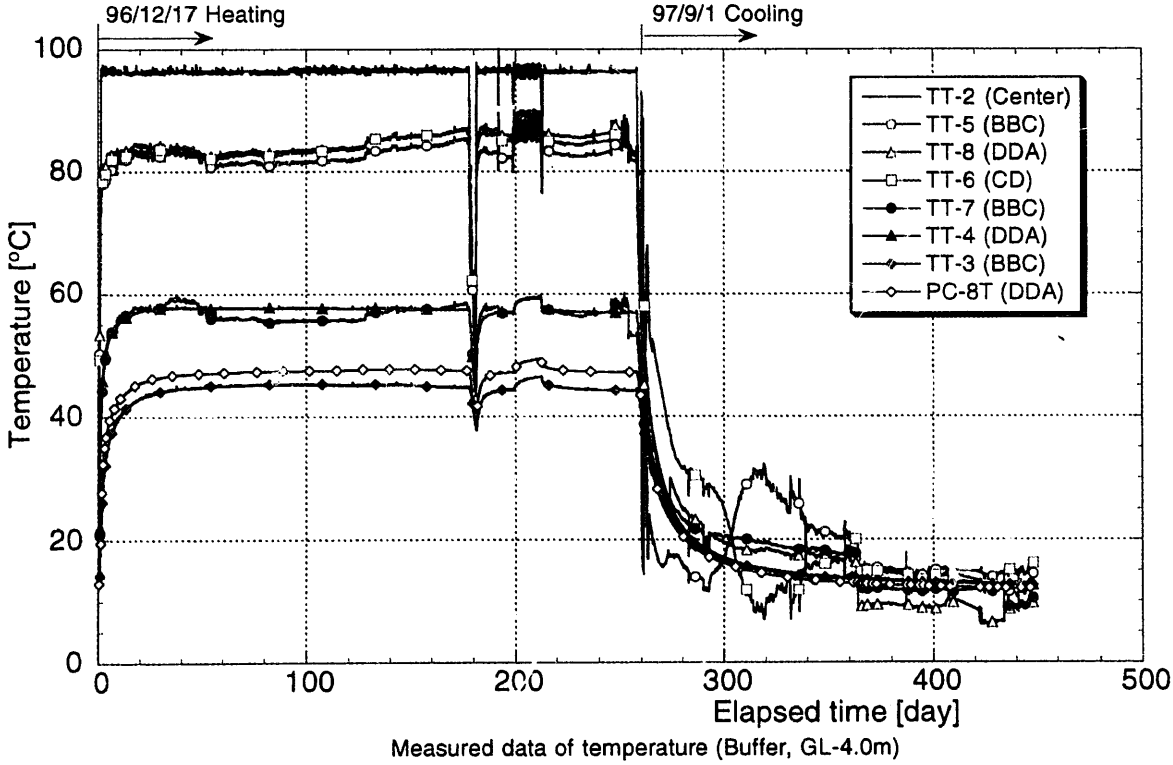

Measured data of temperature (Buffer, GL-4.0m)
(1996/12/17-1998/3/10)

Figure 5-3 Time history of the temperature in the buffer (GL-4.0m)

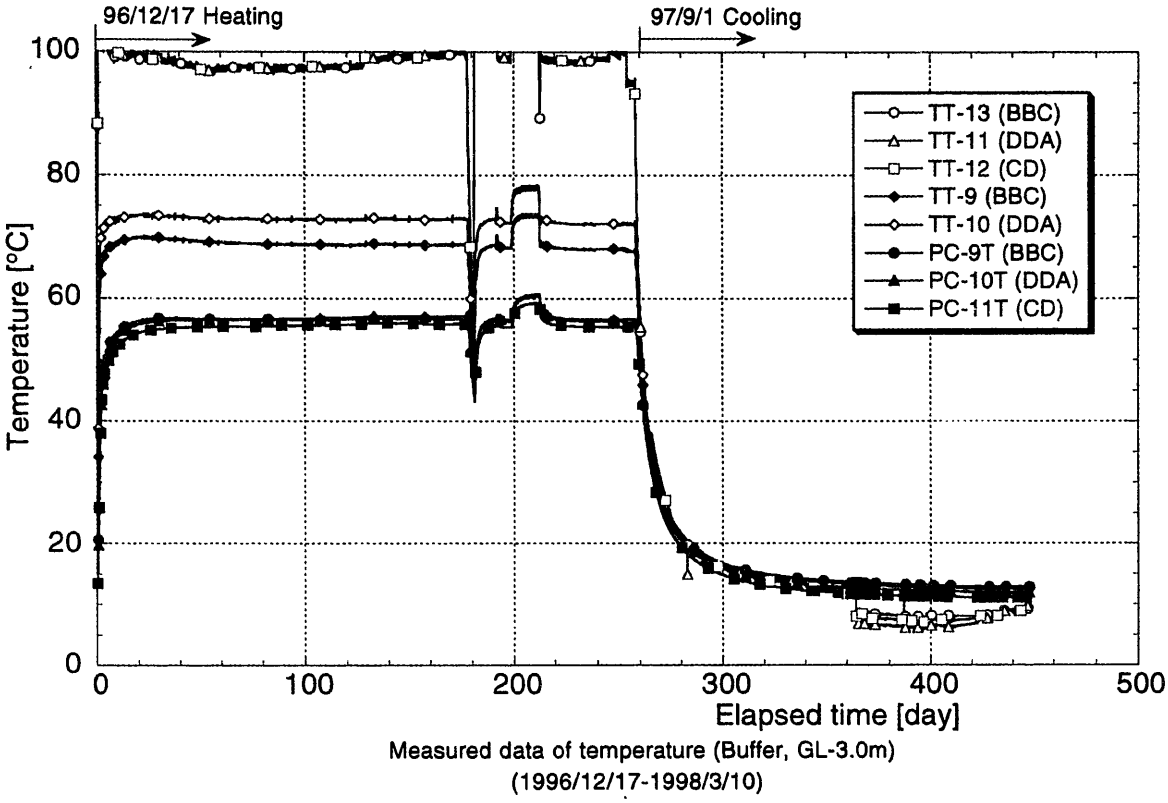

Figure 5-4 Time history of the temperature in the buffer (GL-3.0m)

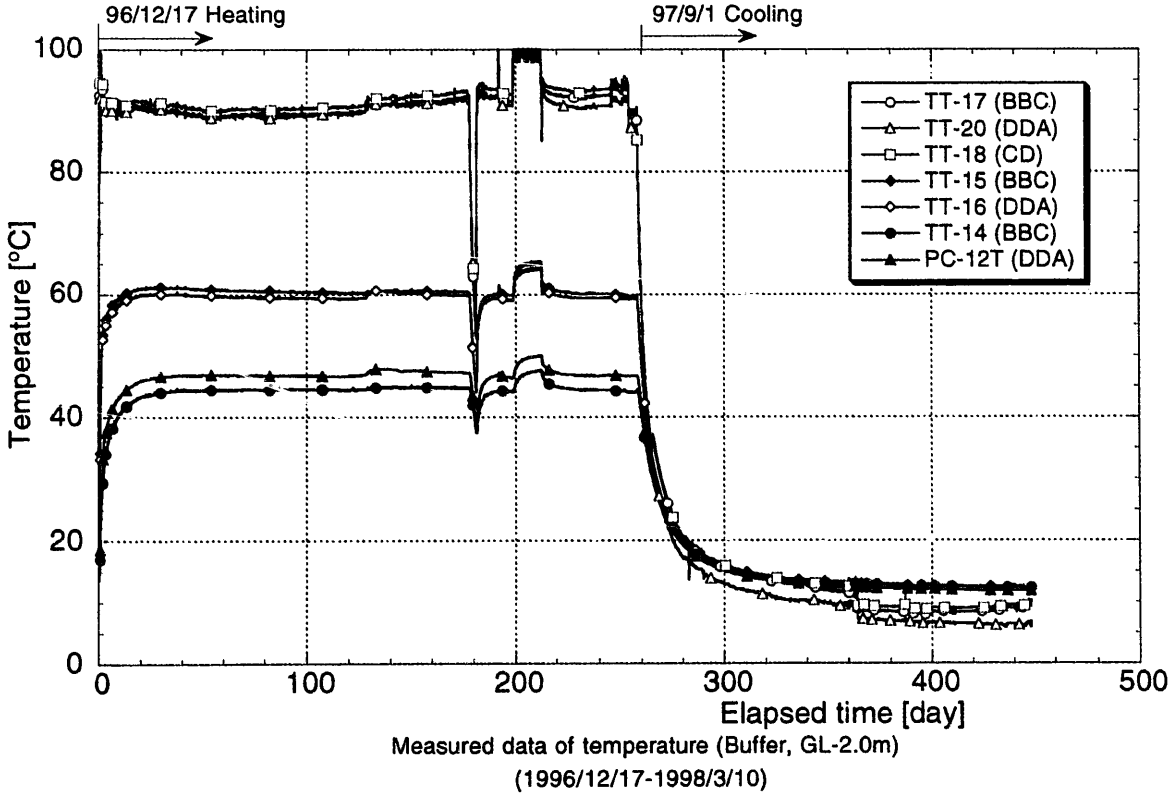

Figure 5-5 Time history of the temperature in the buffer (GL-2.0m)

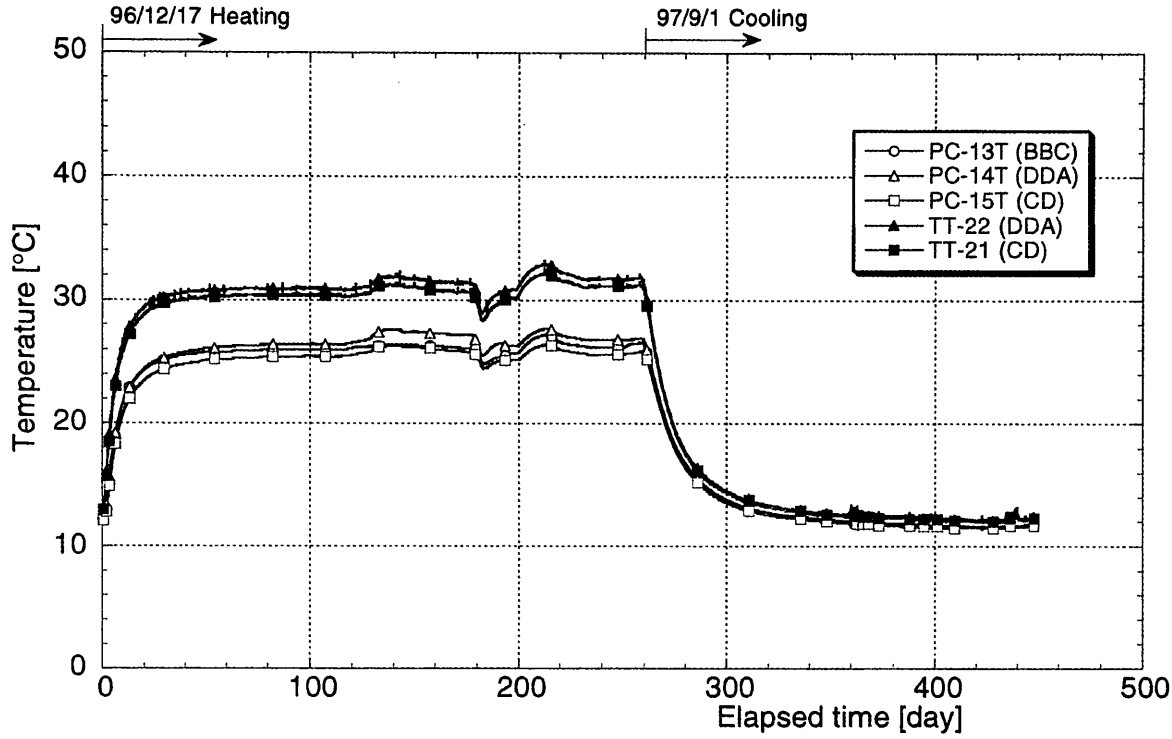

Measured data of temperature (Buffer, GL-1.25m)
(1996/12/17-1998/3/10)

Figure 5-6 Time history of the temperature in the buffer (GL-1.25m)

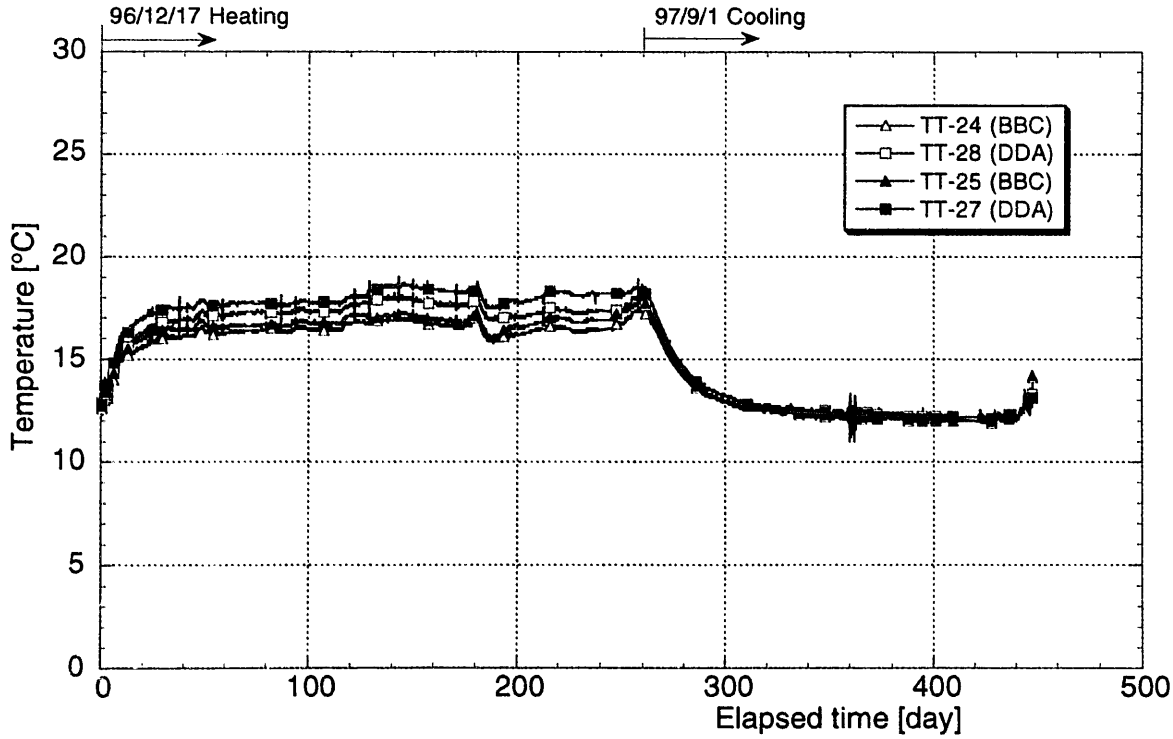

Measured data of temperature (Buffer, GL-0.5m)
(1996/12/17-1998/3/10)

Figure 5-7 Time history of the temperature in the buffer (GL-0.5m)

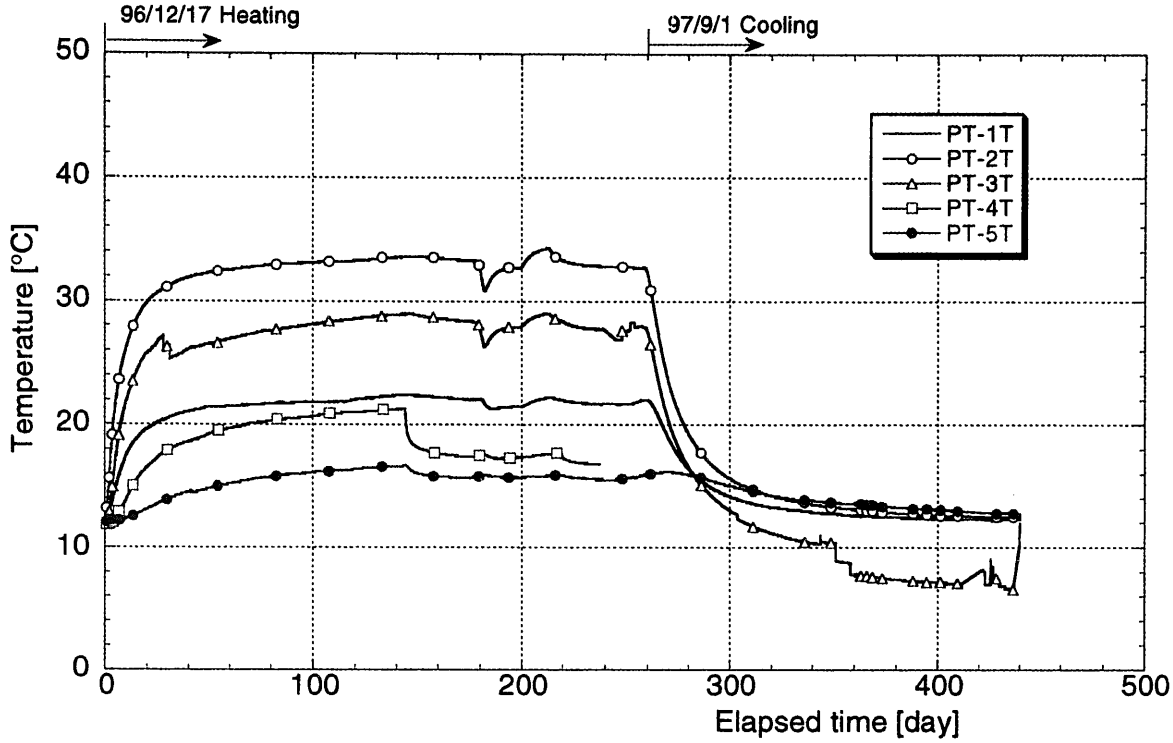

Measured data of temperature (Rock, KBH1)
(1996/12/17-1998/3/10)

Figure 5-8 Time history of the temperature in the rock (KBH1)

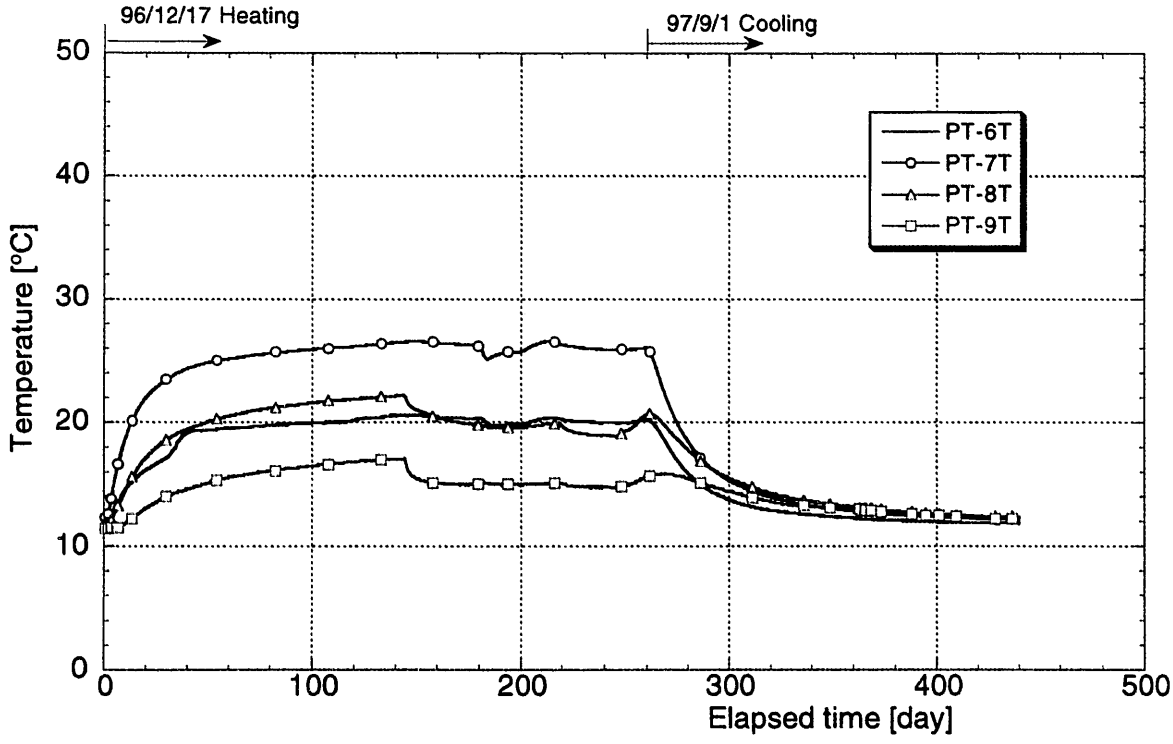

Measured data of temperature (Rock, KBH2)
(1996/12/17-1998/3/10)

Figure 5-9 Time history of the temperature in the rock (KBH2)

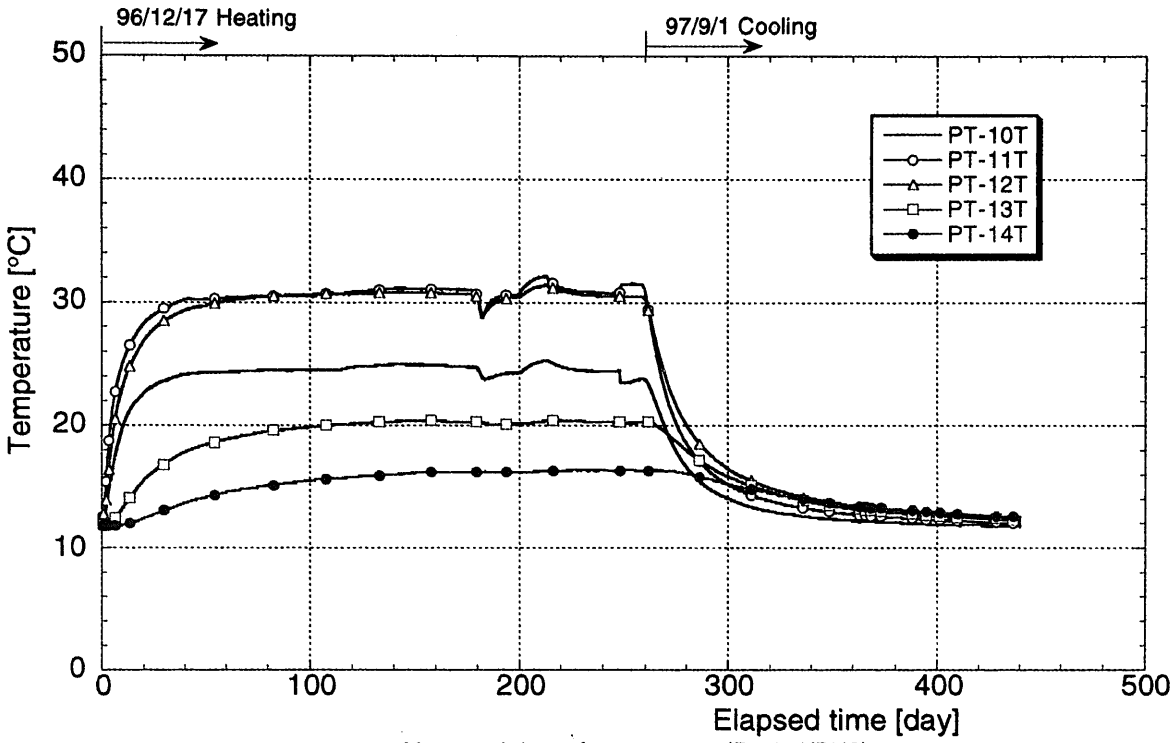

Figure 5-10 Time history of the temperature in the rock (KBH3)

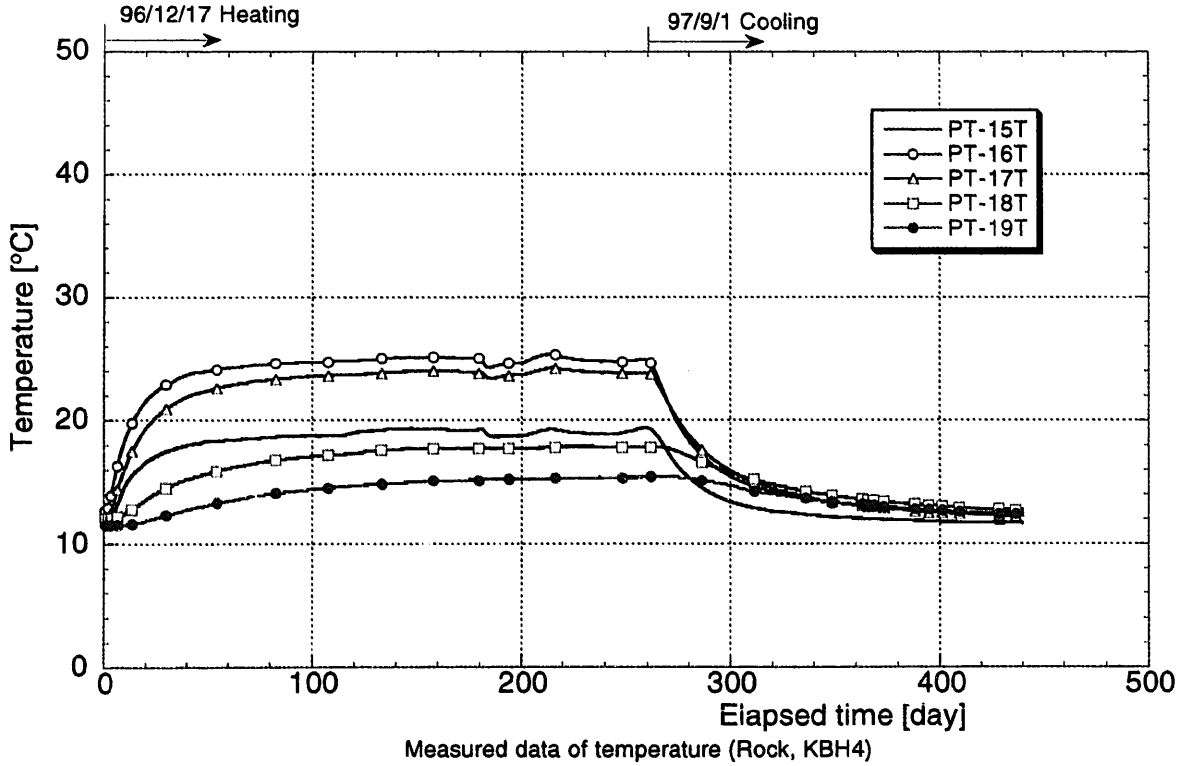

Figure 5-11 Time history of the temperature in the rock (KBH4)

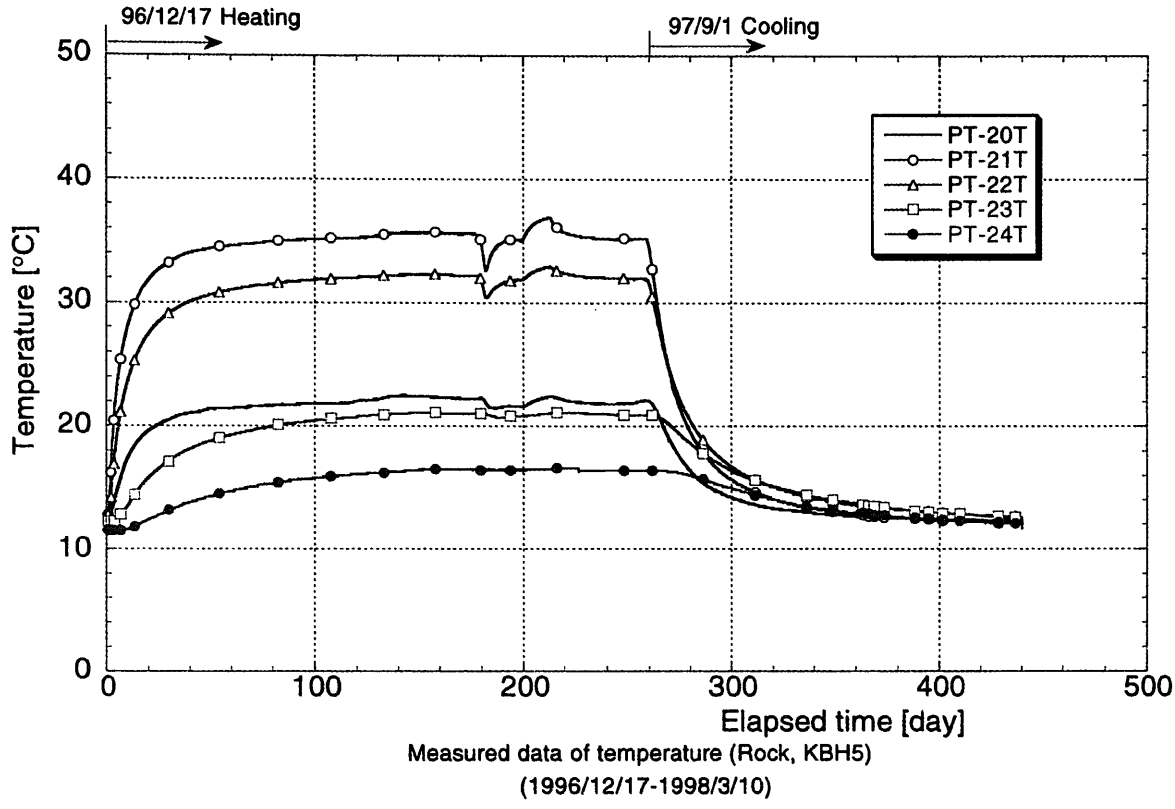

Figure 5-12 Time history of the temperature in the rock (KBH5)

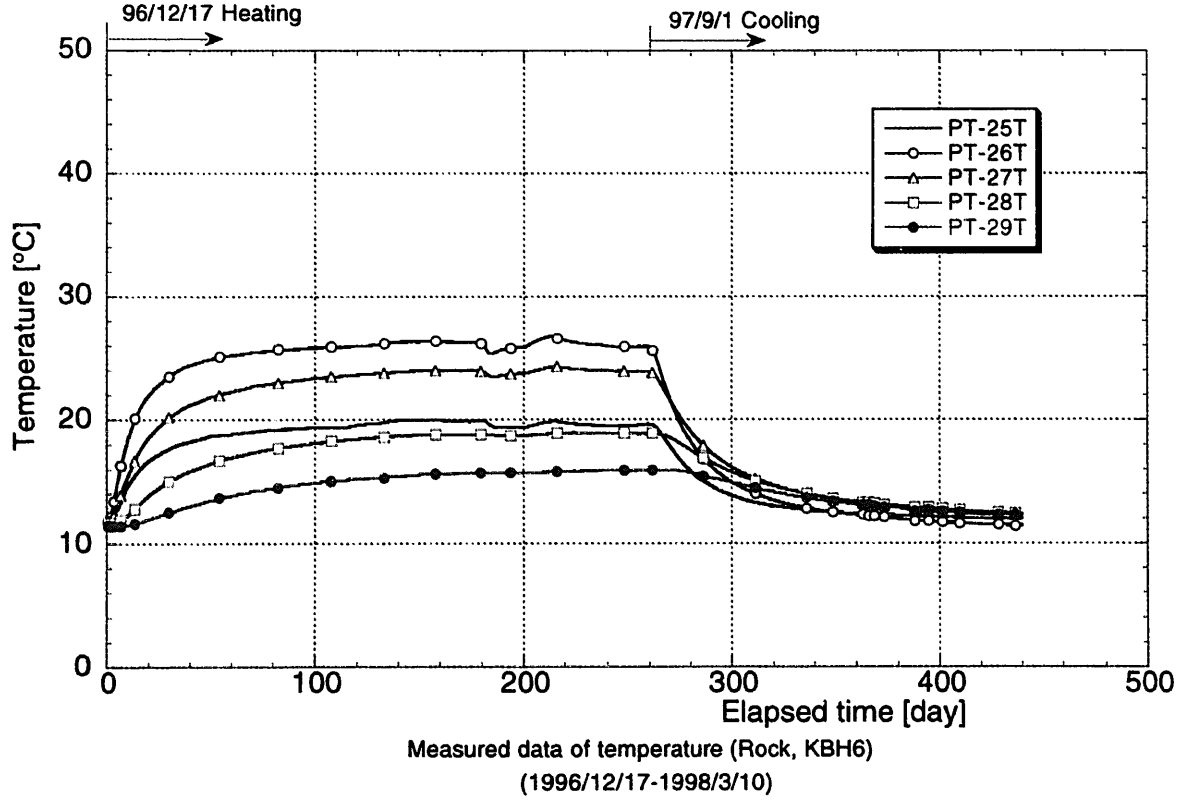

Figure 5-13 Time history of the temperature in the rock (KBH6)

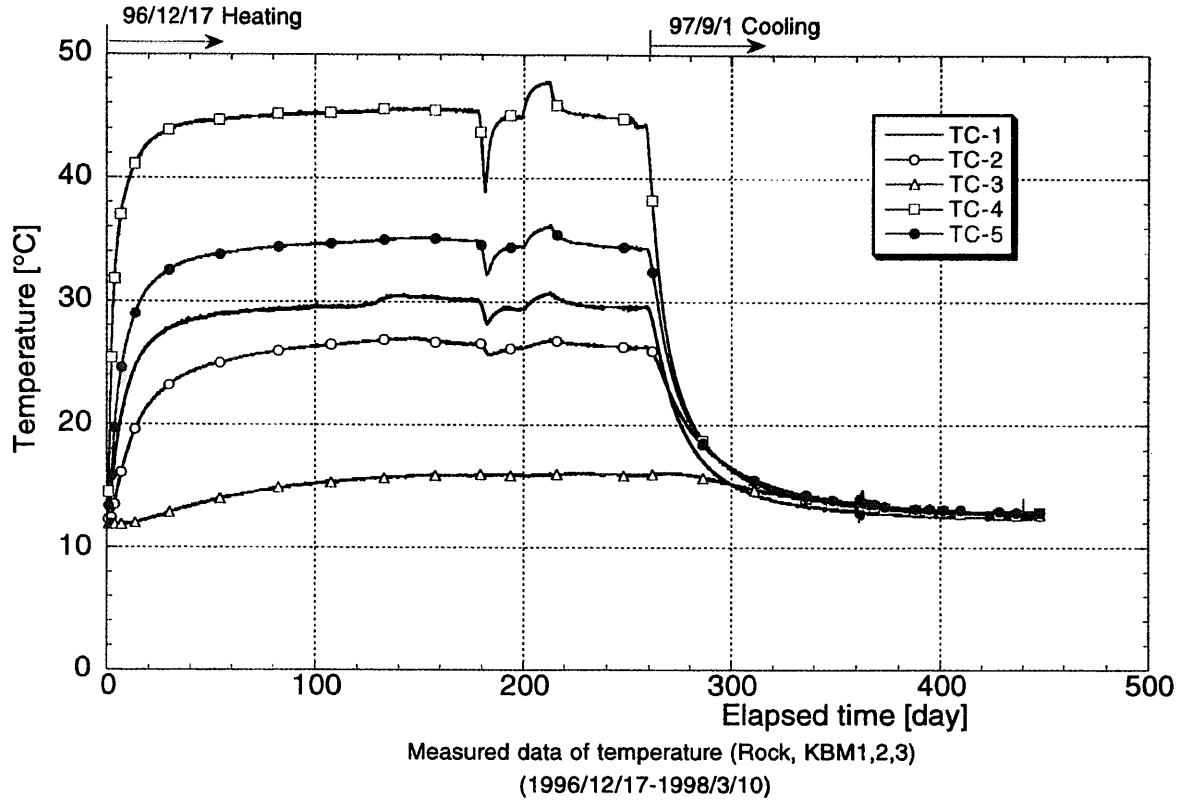

Figure 5-14 Time history of the temperature in the rock (KBM1,2,3)

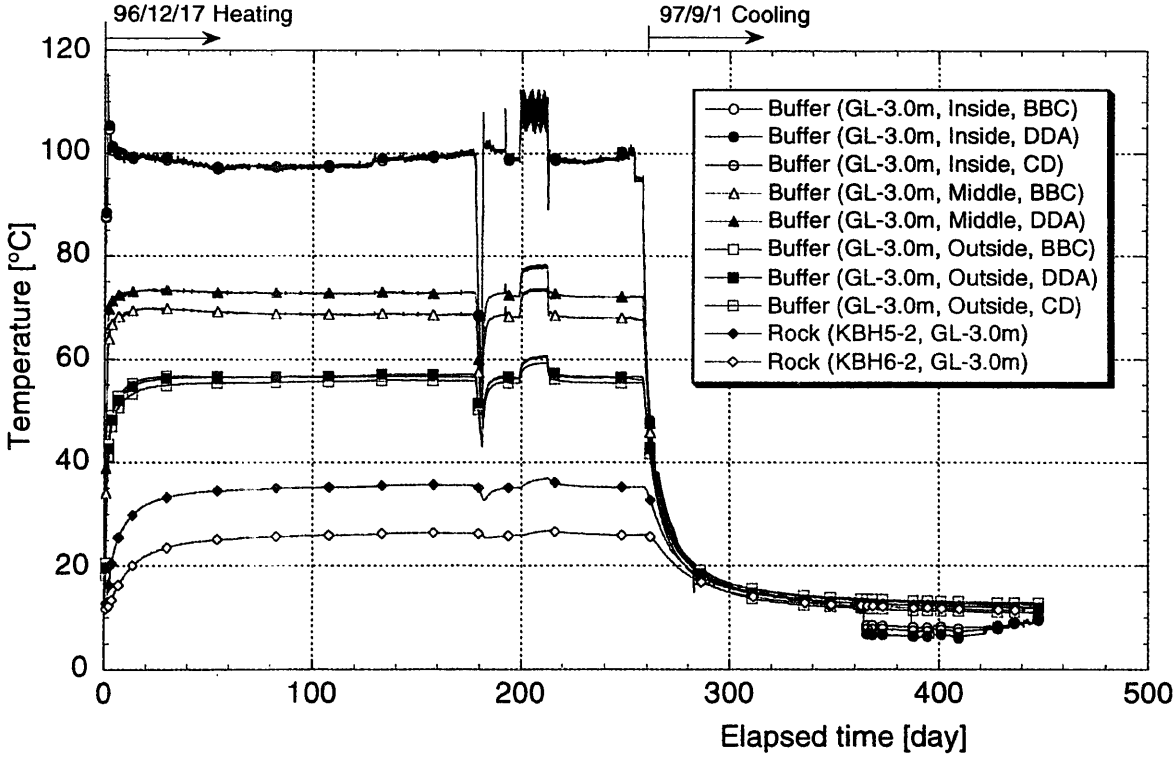

Figure 5-15 Time history of the temperature at the center level of the heater

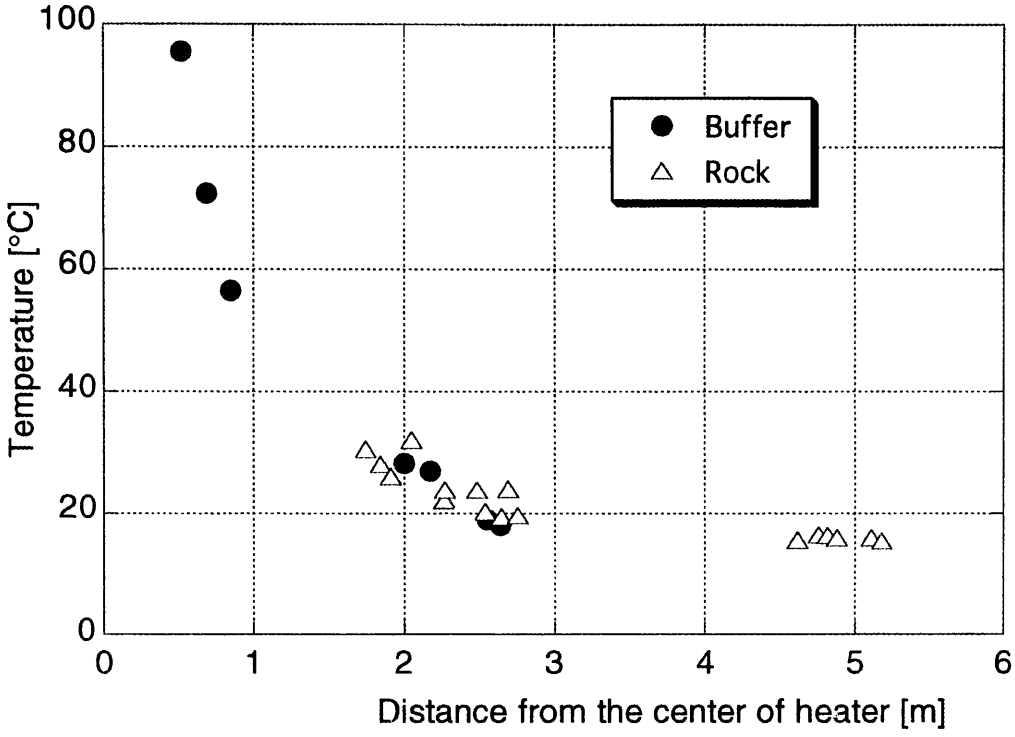

Figure 5-16 Relationship between the temperature and the distance from the center of the heater

5.2 Hydraulic effect

Figures 5-17 to 5-19 show the time history of the pore pressure measured by the pore pressure transducer that was installed at the interface between the rock mass and the buffer. Pore pressure transducer was settled in the sand that was emplaced at the interface. Because the sand was unsaturated, pore pressure was negative value at first. Then pore pressure was changed to the positive value due to inflow of the groundwater from the rock mass. In all figures, pore pressure is raised suddenly at 120days past from the start of heating. It is not because of inflow of the groundwater from the rock mass. It is due to the effect of measurement by thermocouple psychrometer. When measurement by thermocouple psychrometer was carried out, the value of pore pressure had been vibrated. Therefore, as a power source of the thermocouple psychrometer, the dry battery was used after 200days past from the start of heating.

The effect of power failure and heater trouble appeared clearly. As shown in Figures 5-2 to 5-7, the temperature in the buffer decreases immediately when electric power fails, and the temperature in the buffer increases when electric power recovers. The pore pressure at the interface between the rock mass and the buffer shows the same tendency. In the case of temperature, recovery near the heater is faster than that near rock, that is, the recovery speed of temperature near rock is slow. However, the recovery speed of the pore pressure at the interface between the rock mass and the buffer is very fast.

During the heater trouble, the temperature at the control point maintains at about 100°C somehow, but temperature at the other part around the heater increases temporarily. Pore pressure at all monitoring points at the interface between the rock mass and the buffer respond to this heater trouble clearly. However, the response shows the opposite tendency between the monitoring points at the heater center level and the other monitoring point. That is, pore pressure at the heater center level increases and that at the other point decreases. These phenomena mean that pore pressure changes by the effect of heat evolution, and tendency of pore pressure change does not depend on temperature at the monitoring point but temperature environment around the monitoring point.

Pore pressure at GL –3.0m increases after about 60 days from the start of test. This may be because of the water inflow from the rock mass and water movement from the heater-side of buffer to outside due to the temperature gradient.

Figures 5-20 to 5-25 show the time history of pore pressure in the rock mass. In contrast with temperature, it is known that pore pressure increases suddenly at the monitoring points PT-4, PT-5 and PT-9 after 140days from the start of test and at the same time temperature decreases. This phenomenon can be seen at other points with different time except for the boreholes KBH5 and KBH6, where there are few fractures. Furthermore, this phenomenon occurs during only the heating test. As a result of this phenomenon, pore pressure value has been close to the hydrostatic pressure. This may be because that the fracture aperture was changed due to the temperature and the groundwater infiltrated into the monitoring point in the boreholes from the rock mass.

Figures 5-26 and 5-27 show the time history of gravimetric water content. The water potential was measured by thermocouple psychrometer and the relative humidity was measured by hygrometer. The equation to calculate the water content from the temperature and the water potential (or relative humidity) was obtained by laboratory test in advance. The gravimetric water contents of these figures are obtained by calculating with these equations.

The buffer close to the heater is drying and that close to the test pit wall is wetting. It is due to thermal effect from the heater and water flow from the rock mass. The water content at the point of 15 cm apart from the heater (middle part) is raised at first and then goes down. It is considered that the water in the buffer close to the heater moves to middle part due to thermal gradient, and consequently the buffer at the middle part is wetting at first. As time passed, the buffer at the middle part is drying, because water moves to outside further. After the discontinuation of heating, the water content is raised throughout the buffer. Figure 5-28 shows the difference in the water content between the measurement direction. From this figure, it is not seen the difference between the direction. Therefore, there is no difference in the water content between the direction of the buffer, although there are large difference in the water inflow rate between the direction by the effect of fracture existence (Chijimatsu et al, 1997). This is considered that the permeability of buffer is much smaller than that of rock mass.

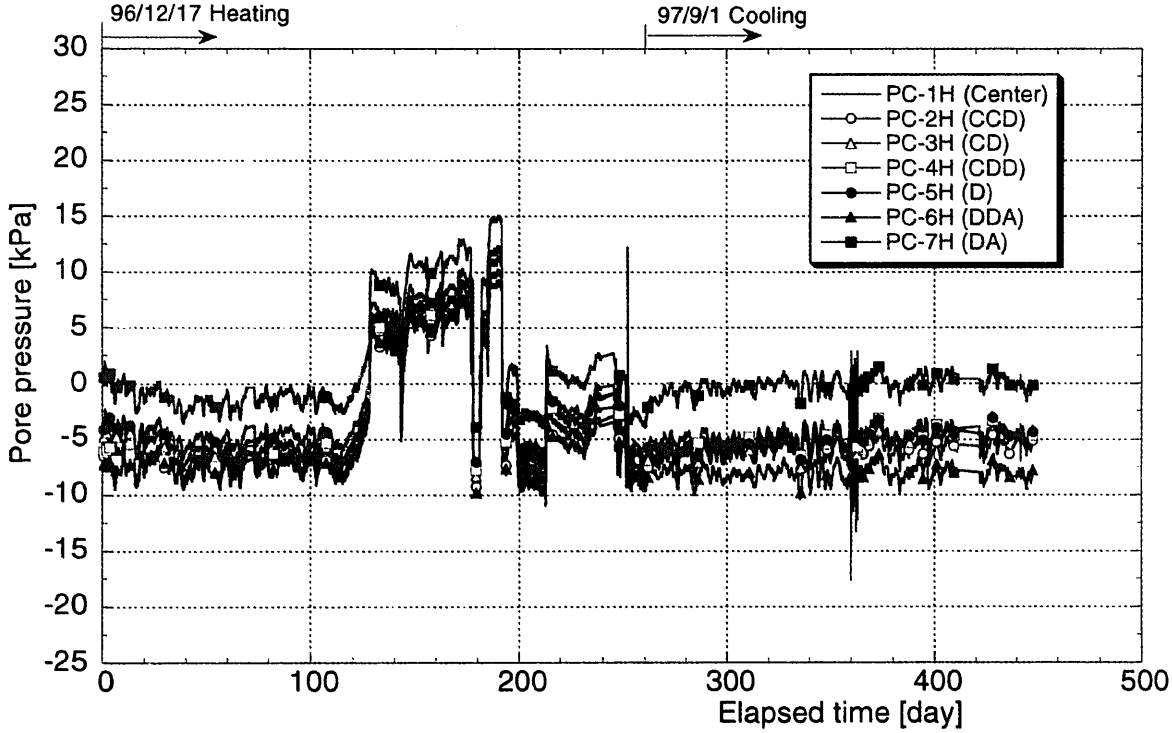

Figure 5-17 Time history of pore pressure in the buffer (GL-5.0m)

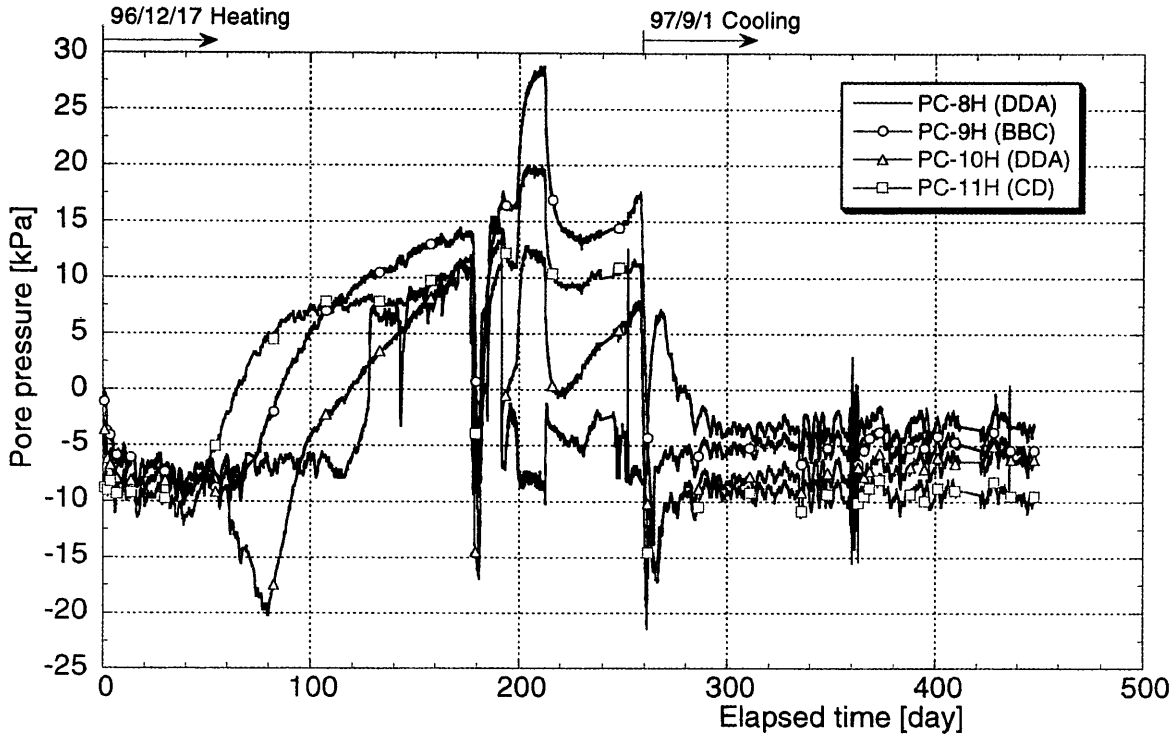

Measured data of pore pressure (Buffer, GL-3.0,-4.0m)
(1996/12/17-1998/3/10)

Figure 5-18 Time history of pore pressure in the buffer (GL-3.0m, -4.0m)

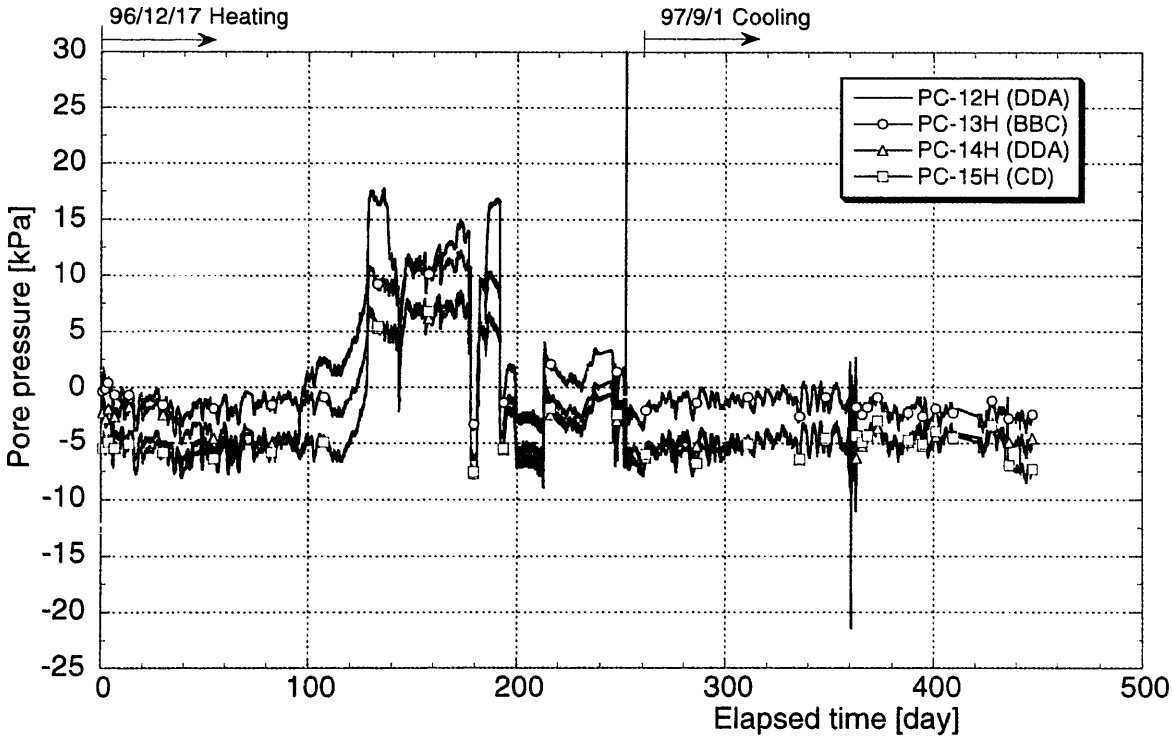

Measured data of pore pressure (Buffer, GL-1.25,-2.0m)
(1996/12/17-1998/3/10)

Figure 5-19 Time history of pore pressure in the buffer (GL-1.25m, -2.0m)

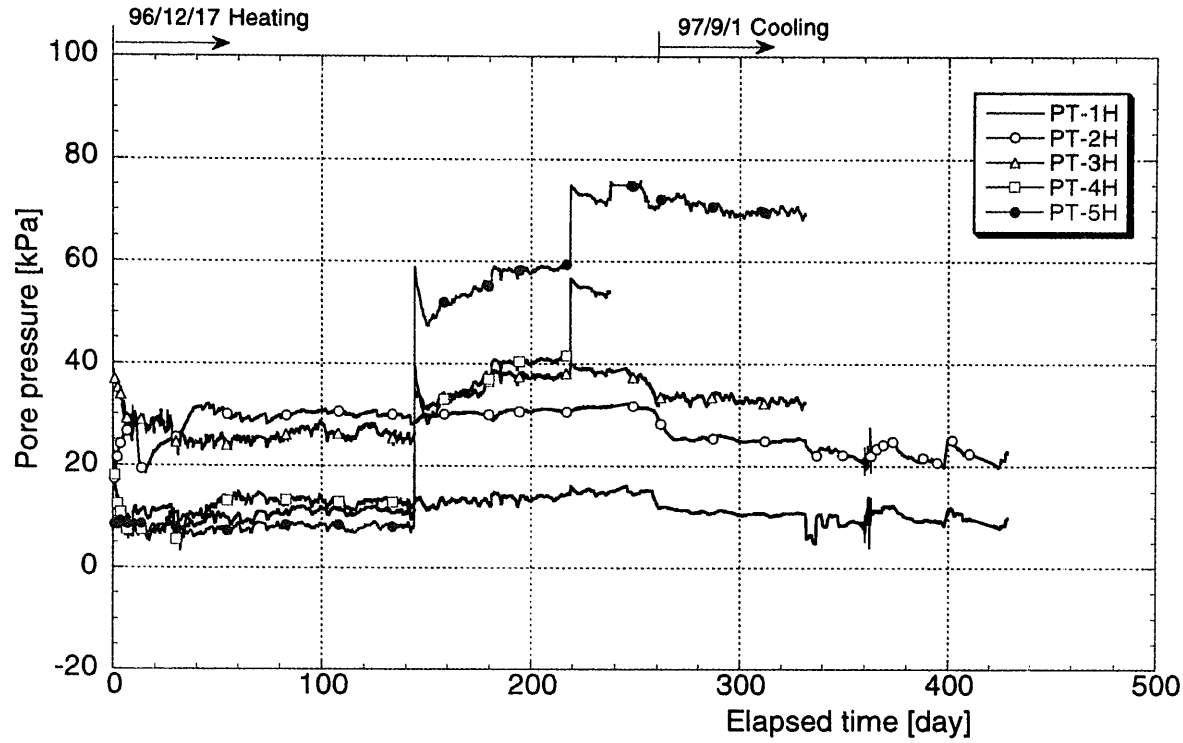

Measured data of pore pressure (Rock, KBH1)
(1996/12/17-1998/3/10)

Figure 5-20 Time history of pore pressure in the rock (KBH1)

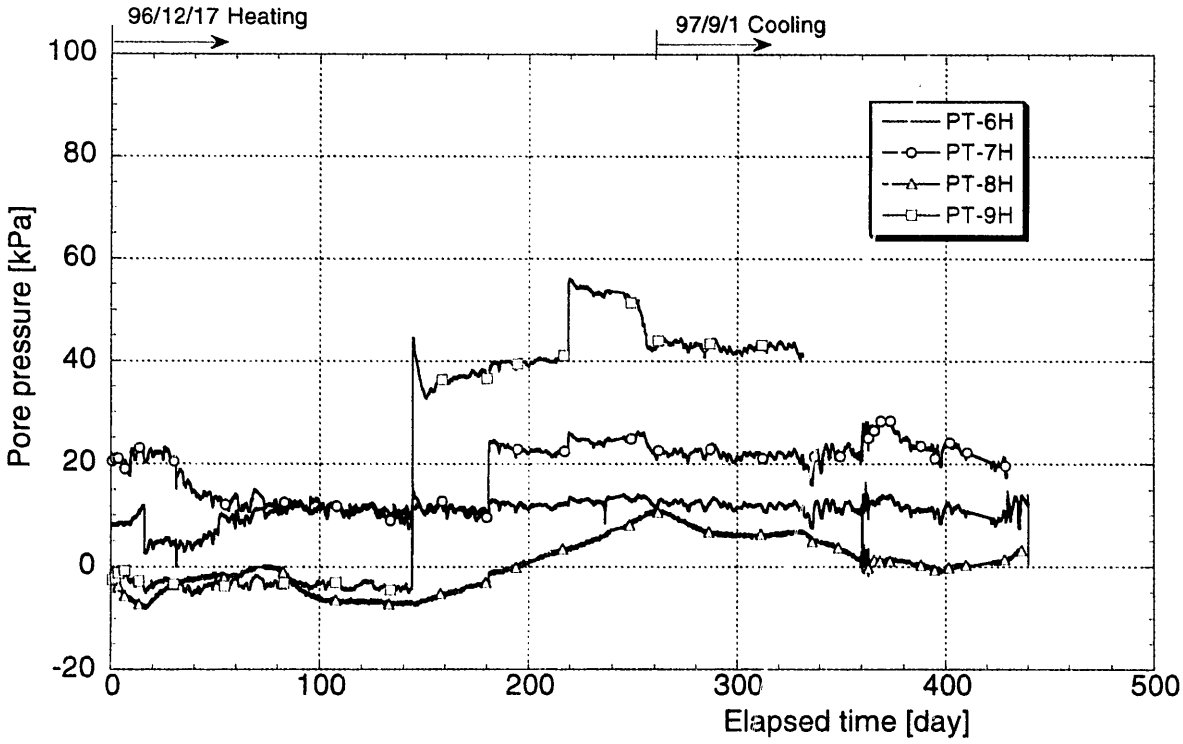

Measured data of pore pressure (Rock, KBH2)
(1996/12/17-1998/3/10)

Figure 5-21 Time history of pore pressure in the rock (KBH2)

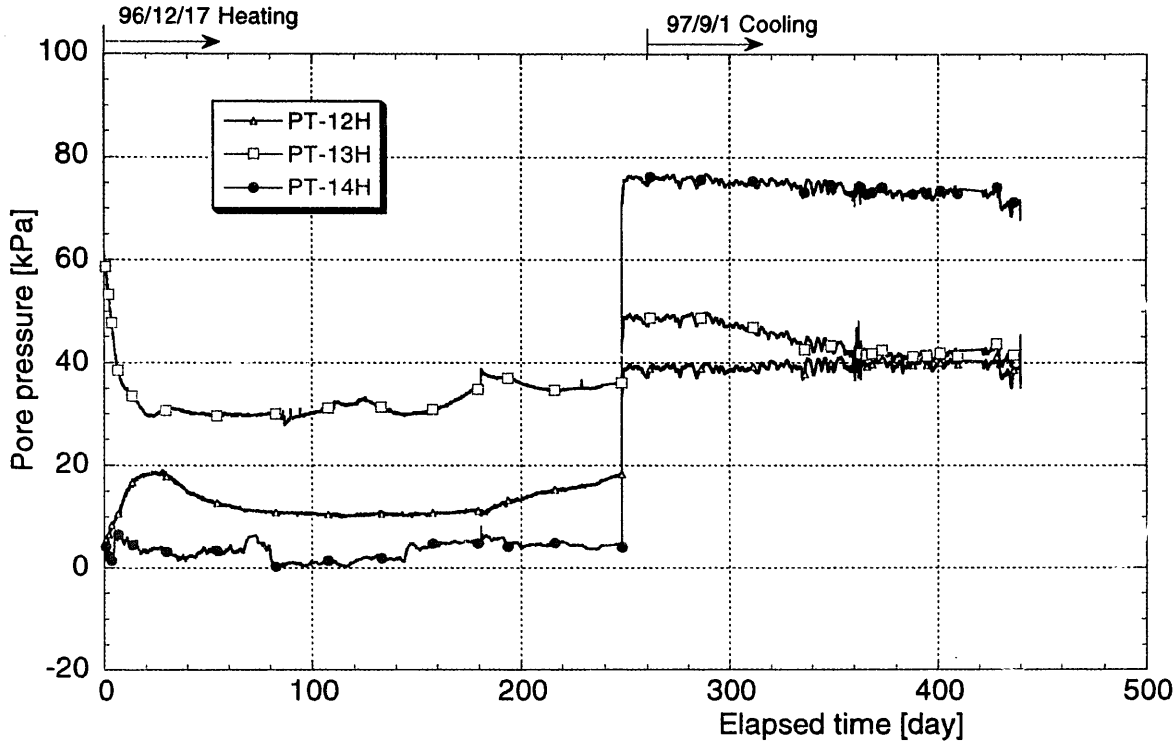

Measured data of pore pressure (Rock, KBH3)
(1996/12/17-1998/3/10)

Figure 5-22 Time history of pore pressure in the rock (KBH3)

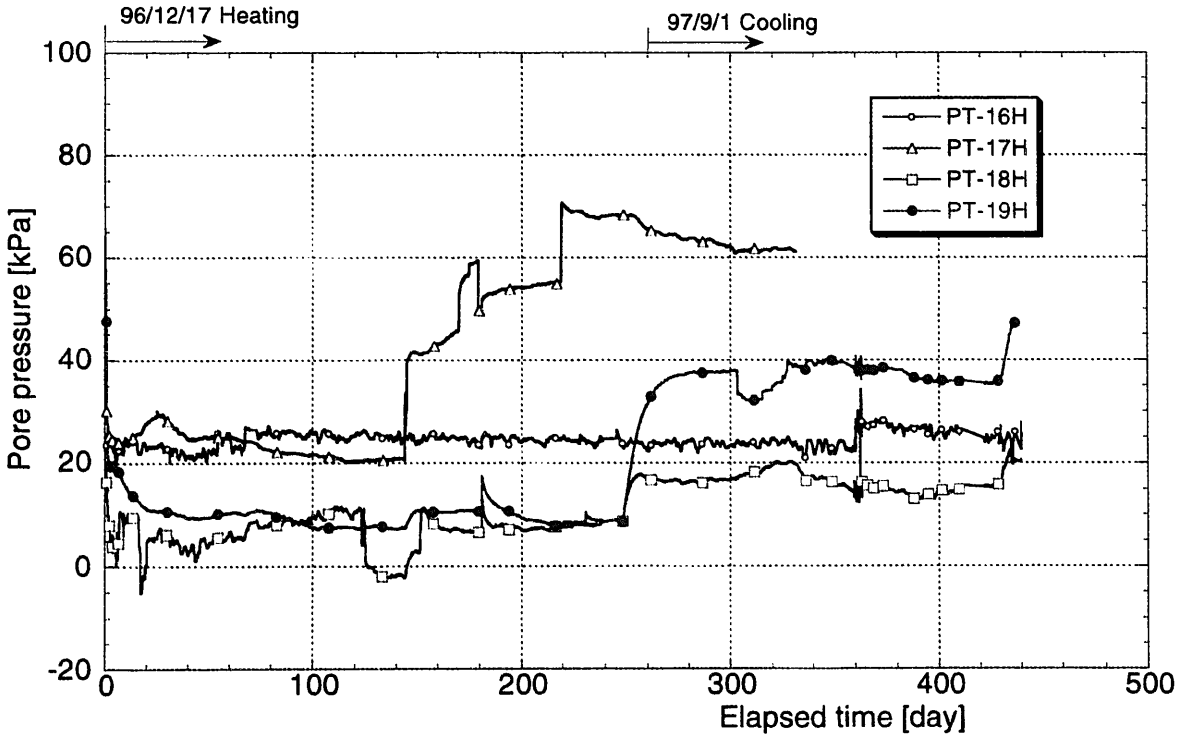

Measured data of pore pressure (Rock, KBH4)
(1996/12/17-1998/3/10)

Figure 5-23 Time history of pore pressure in the rock (KBH4)

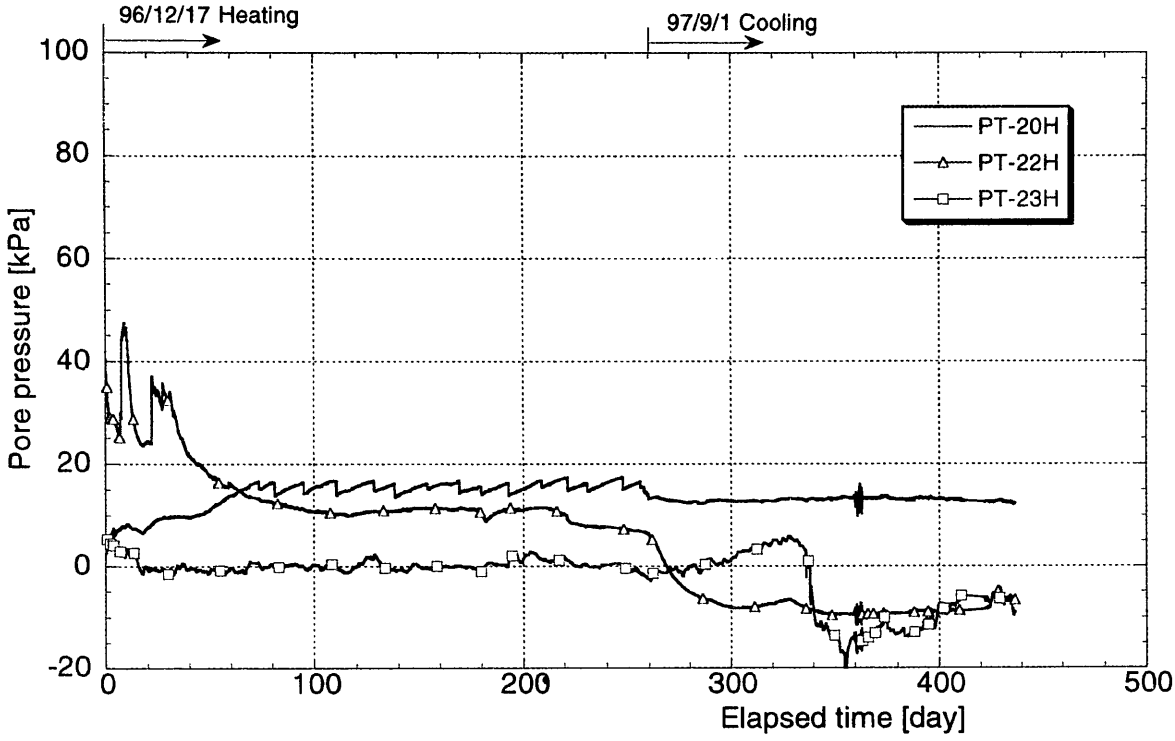

Measured data of pore pressure (Rock, KBH5)
(1996/12/17-1998/3/10)

Figure 5-24 Time history of pore pressure in the rock (KBH5)

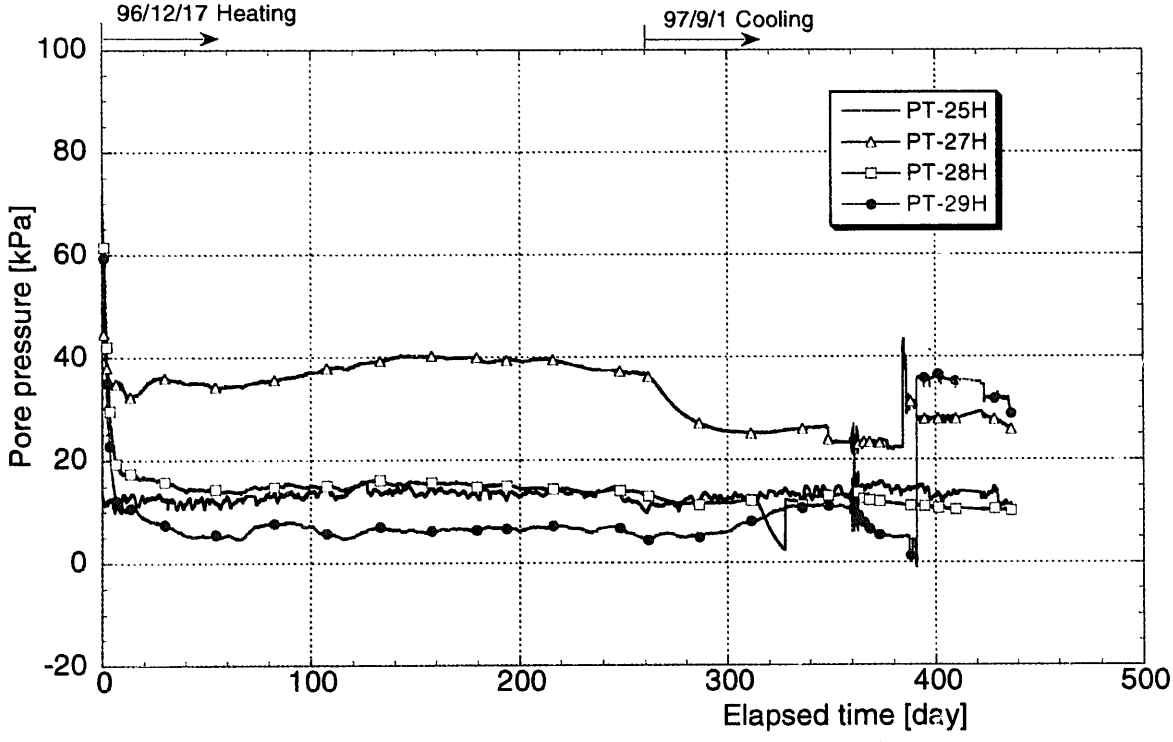

Measured data of pore pressure (Rock, KBH6)
(1996/12/17-1998/3/10)

Figure 5-25 Time history of pore pressure in the rock (KBH6)

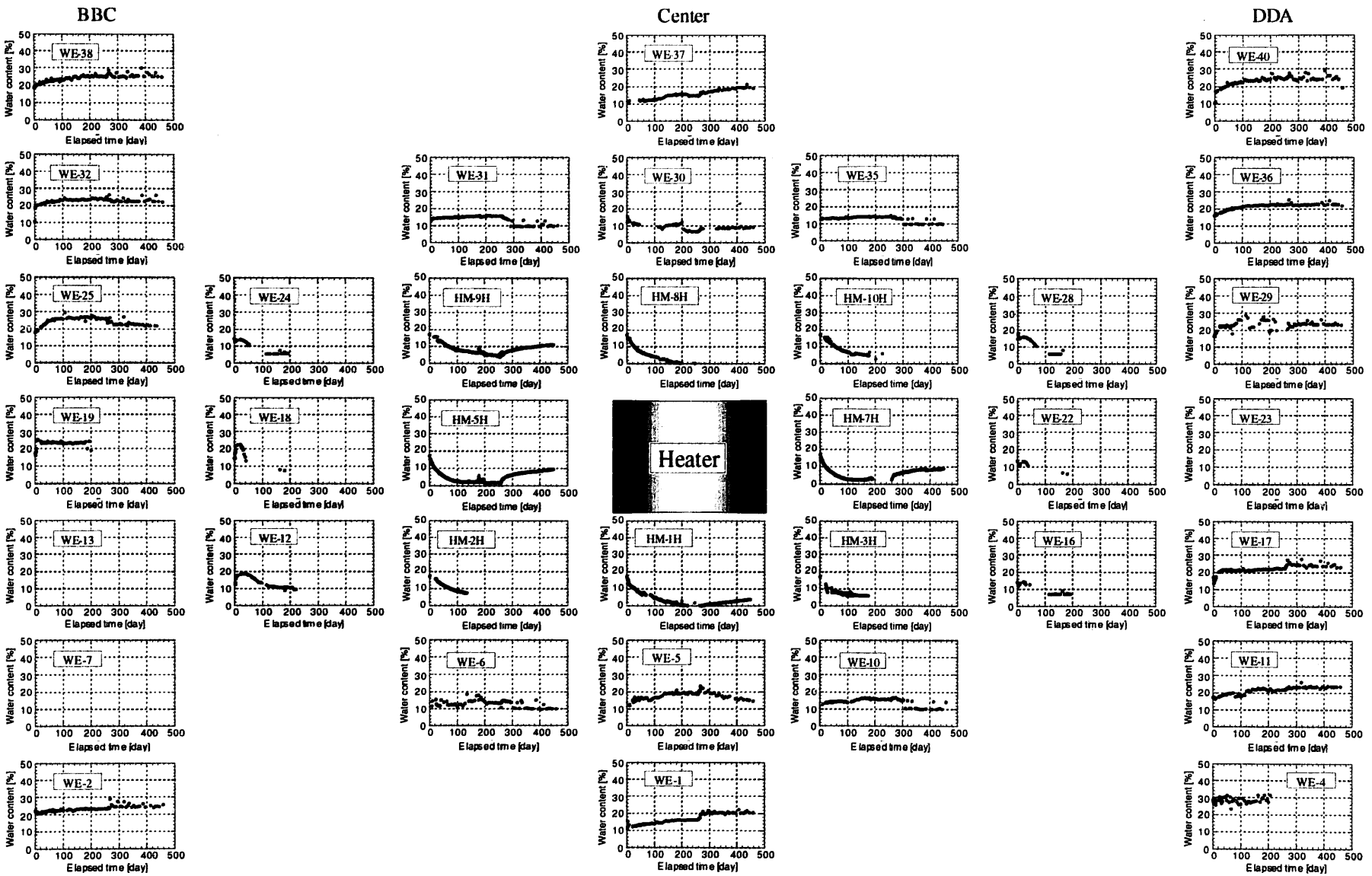

Figure 5-26 Time history of water content in the buffer (BBC-O-DDA Section)

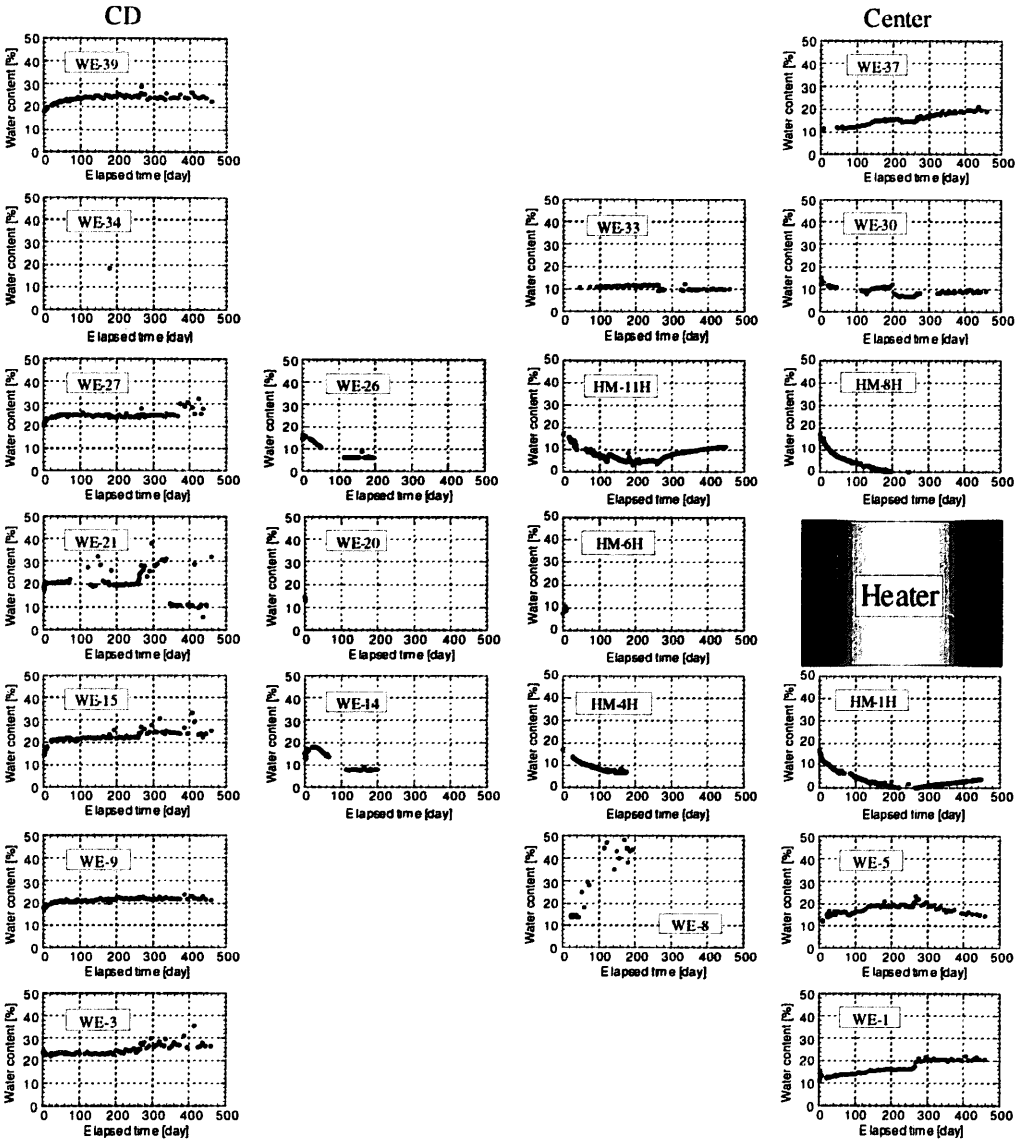

Figure 5-27 Time history of water content in the buffer (CD-O Section)

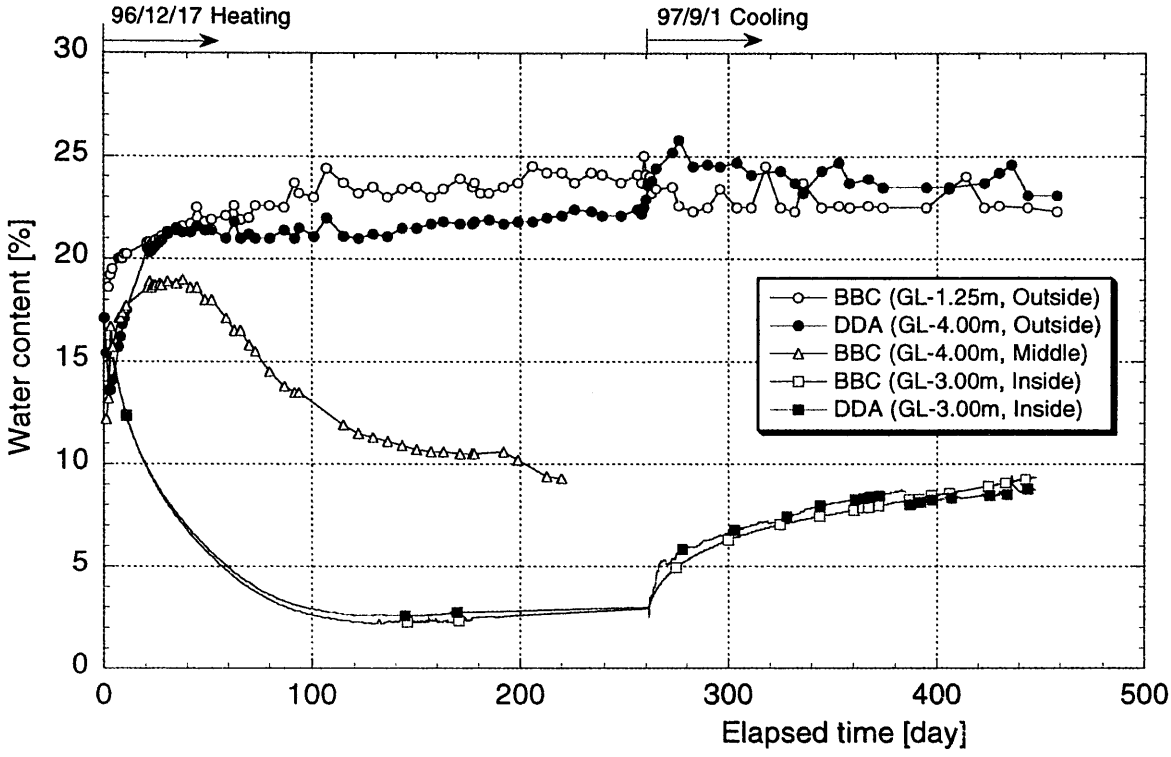

Figure 5-28 Difference in the water content between the measurement direction

5.3 Mechanical effect

Figures 5-29 to 5-37 show the measurement results of total pressure by pressure cell. Data in Figures 5-29, 5-30, 5-32, 5-34, 5-36 and 5-36 were measured by the sensors installed on the wall of test pit except for PS-30. The pressure cell installed on the wall of test pit did not work sufficiently. Because the size of pressure cell is small (diameter is 25mm), the cell did not function due to the adverse effect of roughness of rock surface. When the excavation of test pit was finished, we thought that the wall of test pit was smooth. However, it was not smooth enough for the pressure cell. On the other hand, the sensors installed on the heater surface show the same tendency. Total pressure goes up from the start of test and it becomes almost constant immediately. After the heater was turned off, it decreases. The value at the cooling phase is considered to be the swelling pressure. Therefore, it is considered that the value at the heating phase is governed by the expansion due to heating. After the heater was turned off, some data became to be negative value because of the drift of sensors, for instance PS-17. From this reason it is difficult to decide the swelling pressure value. However, it is considered to be under 0.5MPa.

Figures 5-38 to 5-40 show the time history of strain in the buffer. Positive value shows the tension and negative value shows the compression. At the side of heater, tensile strain occurs along the radial direction just after the start of heating, and it changes to the compression, as temperature becomes constant. Furthermore, value of compressive strain becomes little after the heater was turned off. It is seen from the Figure 5-28 that the middle part of buffer is wetting at first. Therefore, the middle part of buffer was expansive at first. After that middle part of buffer was drying, then the buffer was compressive due to the drying shrinkage. Furthermore, the buffer was compressive due to the expansion of heater. After the heater was turned off, the value of compressive strain becomes small due to the occurrence of swelling pressure and the shrinkage of the heater. The strain along the vertical direction shows the opposite phenomena. At the lower part of buffer under the heater, tensile strain occurs along the vertical direction and compressive strain occurs along the radial direction after the start of heating. After the temperature is constant, the change of strain is the same tendency with the strain at the side of heater.

Figures 5-41 and 5-42 show the time history of strain and displacement in the rock mass. Positive value of the strain shows the tension and negative value shows the compression. Figure 5-41 shows the strain at the borehole KBM1 measured by the strain gauge and Figure 5-42 shows the displacement at the boreholes KBM2 and KBM3 measured by the borehole strain meter. Tensile strain occurs in the rock mass along the radial direction just after the start of heating and value of strain decreases and becomes constant as temperature becomes constant. And strain of rock changes to compression after the heater was turned off.

Figure 5-43 shows the measurement results by the Joint deformeter. At both boreholes KBM6 and KBM7, the change along the Z-direction is occurred. During the heating test, JM-3 shows the positive value. It means that fracture aperture closed. Then, after the heater was turned off, the values of JM-3 and JM-6 becomes negative, that is, fracture aperture opened. Because there are no data at the JM-2 and JM-4, it is difficult to evaluate the three dimensional movement of fracture. However, it is considered that both fractures where the Joint deformeter was installed shows the same movement qualitatively.

Figures 5-44 and 5-45 show the measurement results by TRIVEC. Figure 5-44 is the result at the borehole KBM4 and Figure 5-45 is the result at the borehole KBM5. At both boreholes KBM4 and KBM5, the displacements along the X-direction and Y-direction are larger than

that along the Z-direction. However, because the measurement accuracy of X-direction and Y-direction is lower than that of Z-direction, it is considered that the displacements along the X-direction and Y-direction are not significant. Therefore, we can only discuss about the displacement along the Z-direction (vertical direction). The displacement along the Z-direction shows the positive value at the upper part during the heating test. This result shows that rock extended during the heating phase.

Figures 5-46, 5-47 and 5-48 show the strain distribution both in the rock and buffer at the heater center level after 161days and 255days past from the start of heating and after 180days past from the stop of heating. The strain in the rock along the radial and tangential directions were measured by the borehole strain meter, and the strain along the vertical direction was measured by the TRIVEC. The big compression that was measured by the borehole strain meter SB-3 was removed from the measurement data as the out of order of the sensor.

From the figures 5-46 and 5-47, it is shown that temperature was almost constant after 161days past from the start of heating. And strain also became almost constant, even though the tensile strain along the vertical direction and the compressive strain along the radial direction in the buffer were increasing gradually. On the other hand, in the rock mass, tensile strain along the vertical direction and along the radial direction were measured, and the value of strain along the tangential direction was small, for instance, $\pm 3\mu$. In Figure 5-48, the recovery of the strain and temperature due to the stop of the heater was seen except for the strain along the tangential direction in the rock mass.

These measurement data are caused by the thermal expansion of the heater, the rock mass and the buffer, and the drying shrinkage of the buffer due to the influence of the heating. Furthermore, swelling phenomena are compound in the buffer. Here, we assume the thermal expansion coefficient of the rock mass as 5×10^{-6}/°C, the strain of the rock mass due to the thermal effect is calculated to be 100×10^{-6} when the ascent of the temperature is 20°C. This temperature ascent corresponds to the measurement result at the point of 60cm apart from the test pit. Measurement result of the strain in the buffer along the vertical direction is the same order with the calculated result, and those along the radial and tangential directions are smaller than calculated one. This is because the thermal expansion is restrained along the radial and tangential directions, and then, it is supposed that thermal stress is occurred. Because the strain distribution in the buffer will be determined by the complex phenomena mentioned above, it is difficult to understand the phenomena completely by only the measurement results. However, the compressive strain in the buffer along the radial direction is considered to be the effect of the drying shrinkage of the buffer and the thermal expansion of the heater.

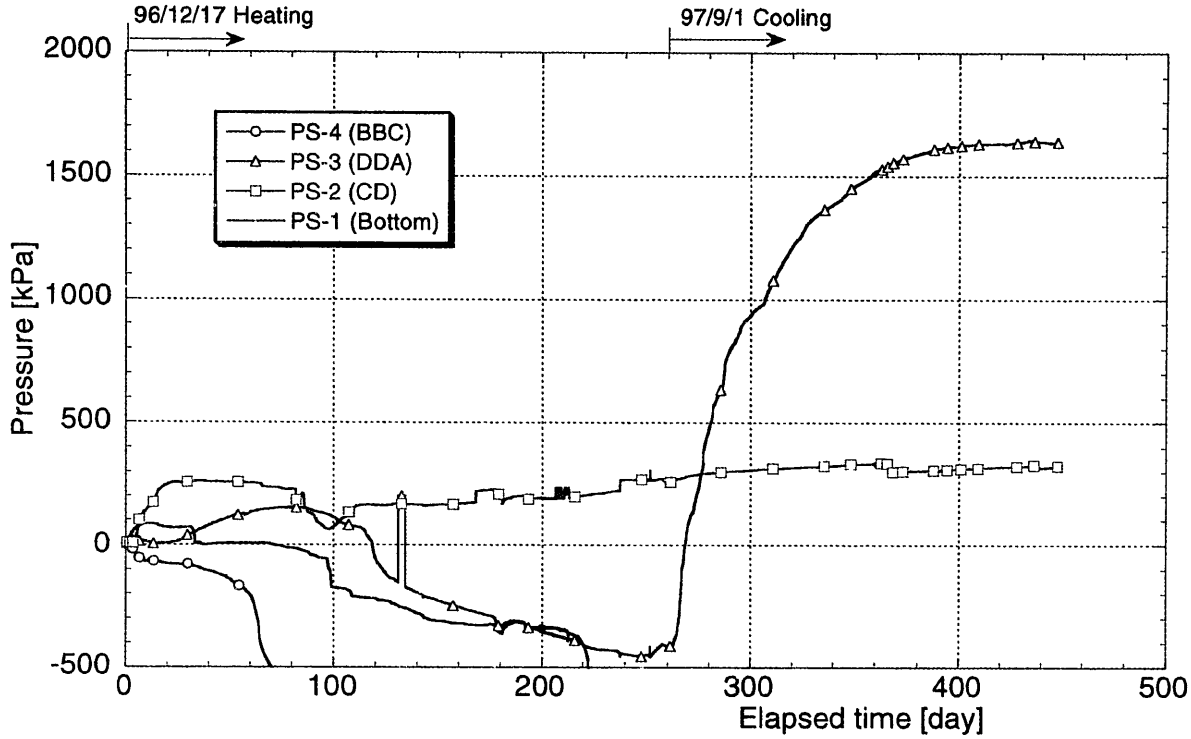

Measured data of pressure by pressure cell (Buffer, GL-4.5,-5.0m)
(1996/12/17-1998/3/10)

Figure 5-29 Time history of the total pressure (GL-4.5m; Outside, GL-5.0m; Bottom)

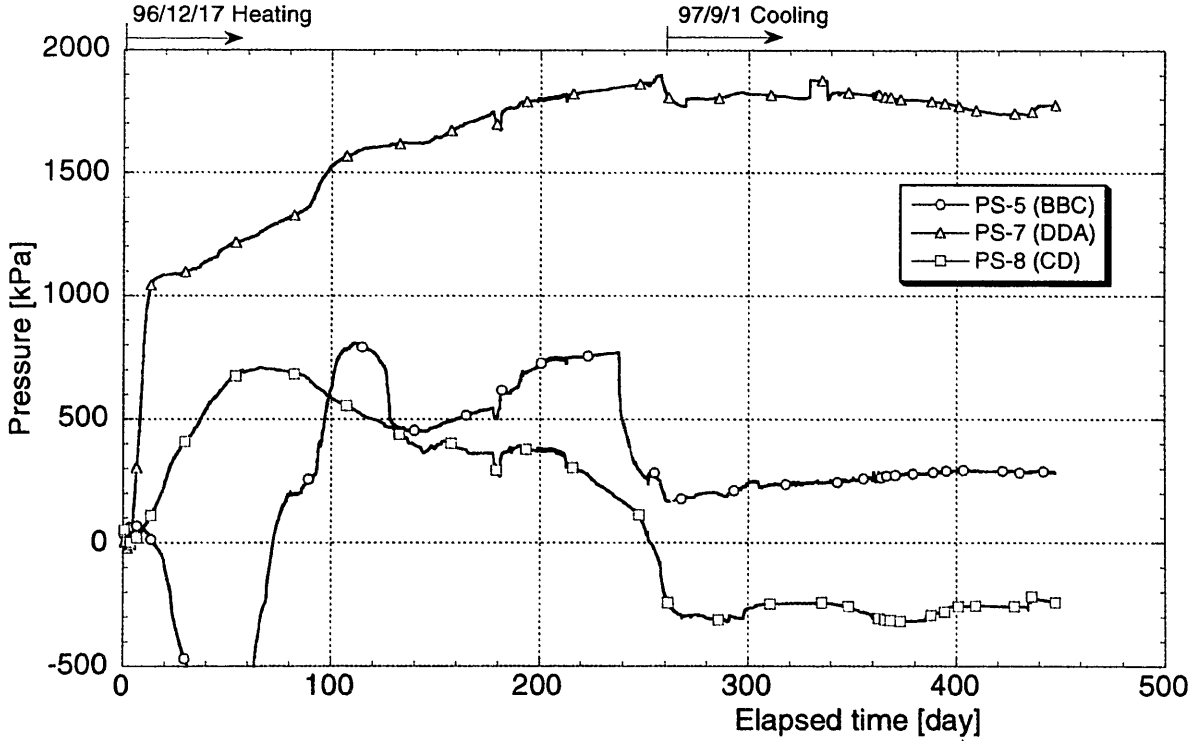

Measured data of pressure by pressure cell (Buffer, GL-4.0m, Outside)
(1996/12/17-1998/3/10)

Figure 5-30 Time history of the total pressure (GL-4.0m; Outside)

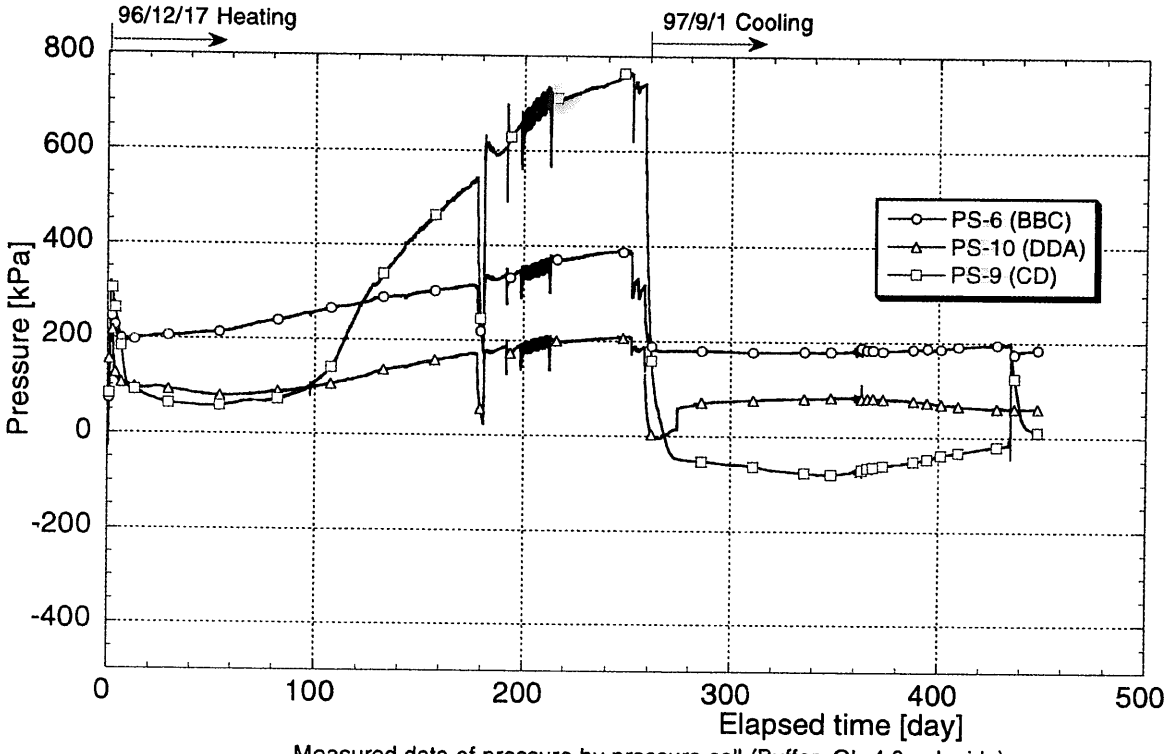

Measured data of pressure by pressure cell (Buffer, GL-4.0m, Inside)
(1996/12/17-1998/3/10)

Figure 5-31 Time history of the total pressure (GL-4.0m; Inside)

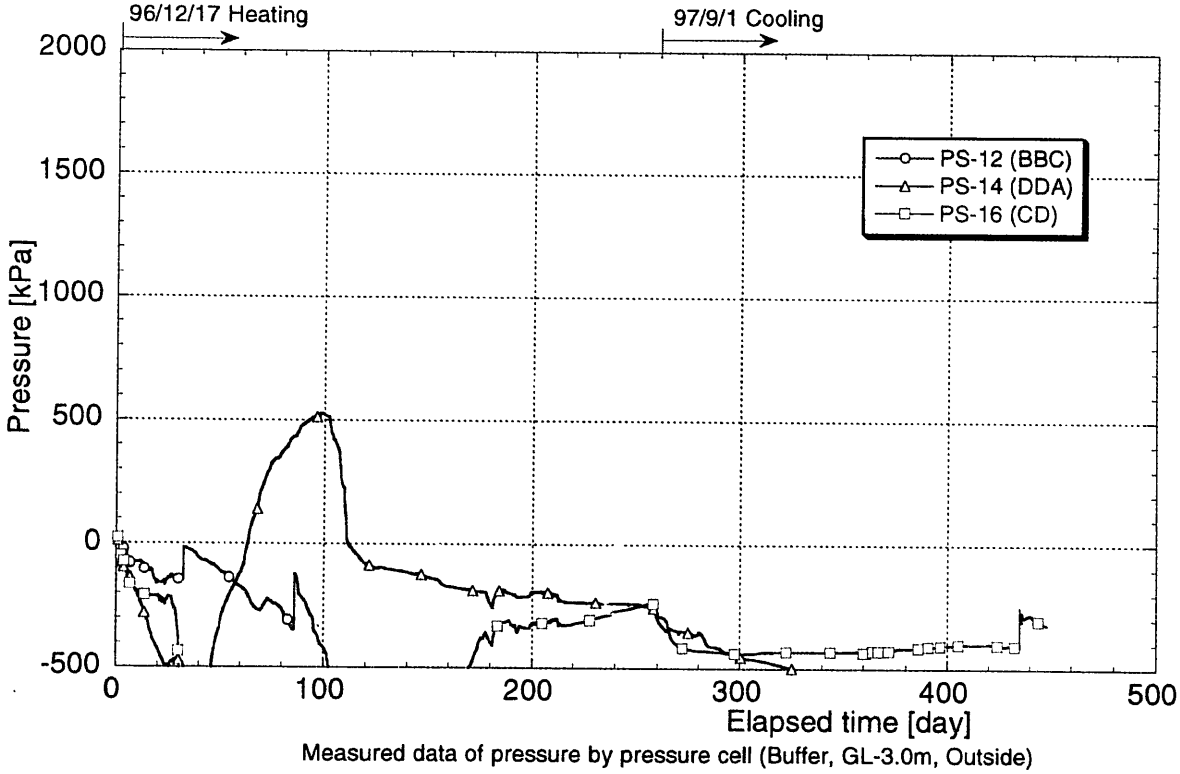

Measured data of pressure by pressure cell (Buffer, GL-3.0m, Outside)
(1996/12/17-1998/3/10)

Figure 5-32 Time history of the total pressure (GL-3.0m; Outside)

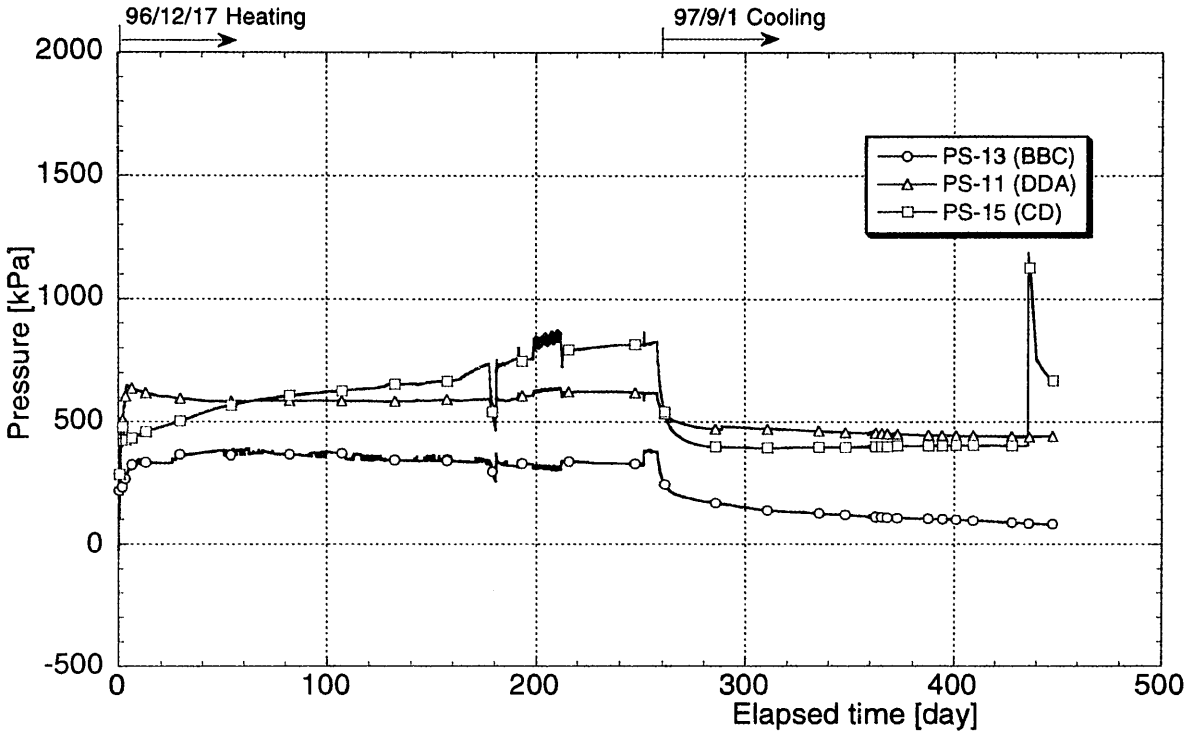

Measured data of pressure by pressure cell (Buffer, GL-3.0m, Inside)
(1996/12/17-1998/3/10)

Figure 5-33 Time history of the total pressure (GL-3.0m; Inside)

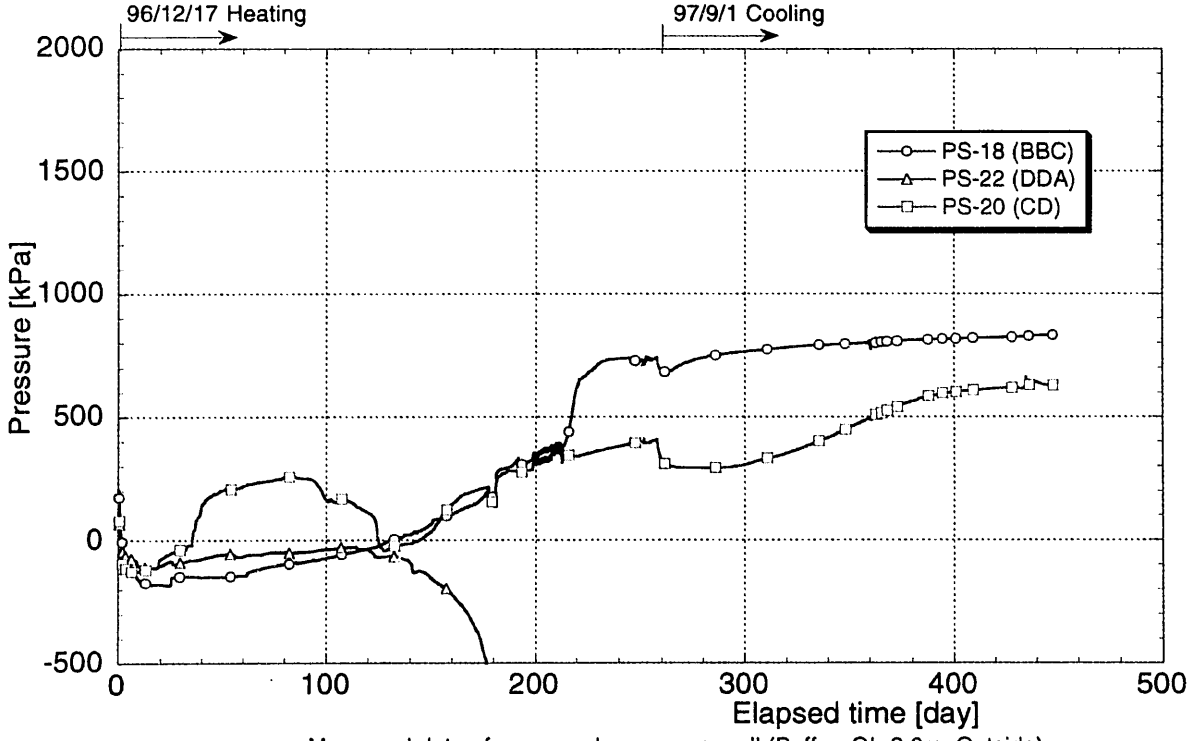

Measured data of pressure by pressure cell (Buffer, GL-2.0m, Outside)
(1996/12/17-1998/3/10)

Figure 5-34 Time history of the total pressure (GL-2.0m; Outside)

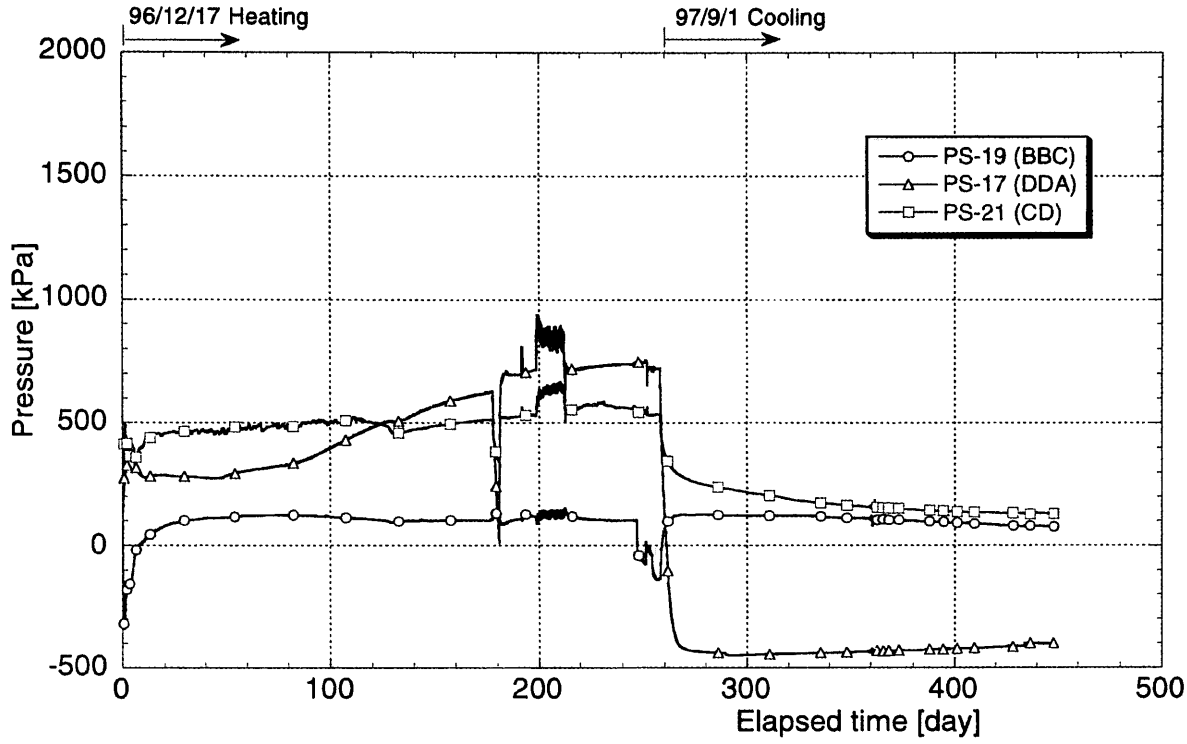

Measured data of pressure by pressure cell (Buffer, GL-2.0m, Inside)
(1996/12/17-1998/3/10)

Figure 5-35 Time history of the total pressure (GL-2.0m; Inside)

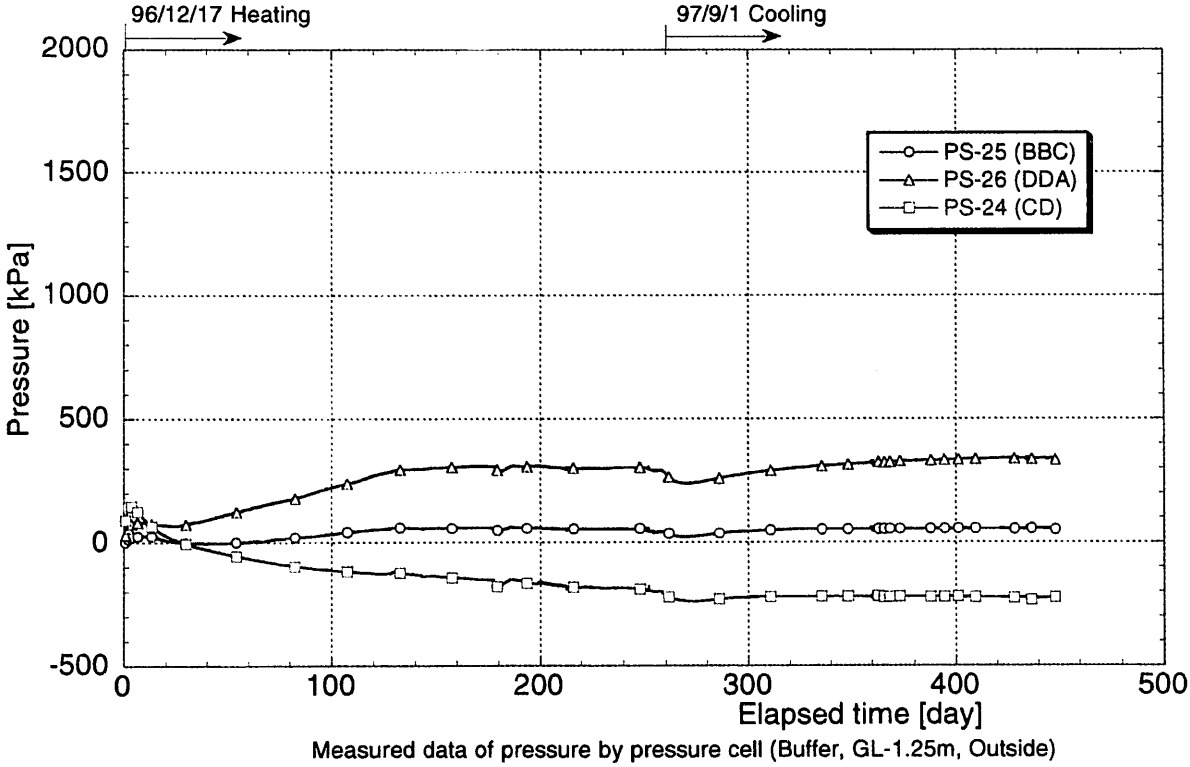

Measured data of pressure by pressure cell (Buffer, GL-1.25m, Outside)
(1996/12/17-1998/3/10)

Figure 5-36 Time history of the total pressure (GL-1.25m; Outside)

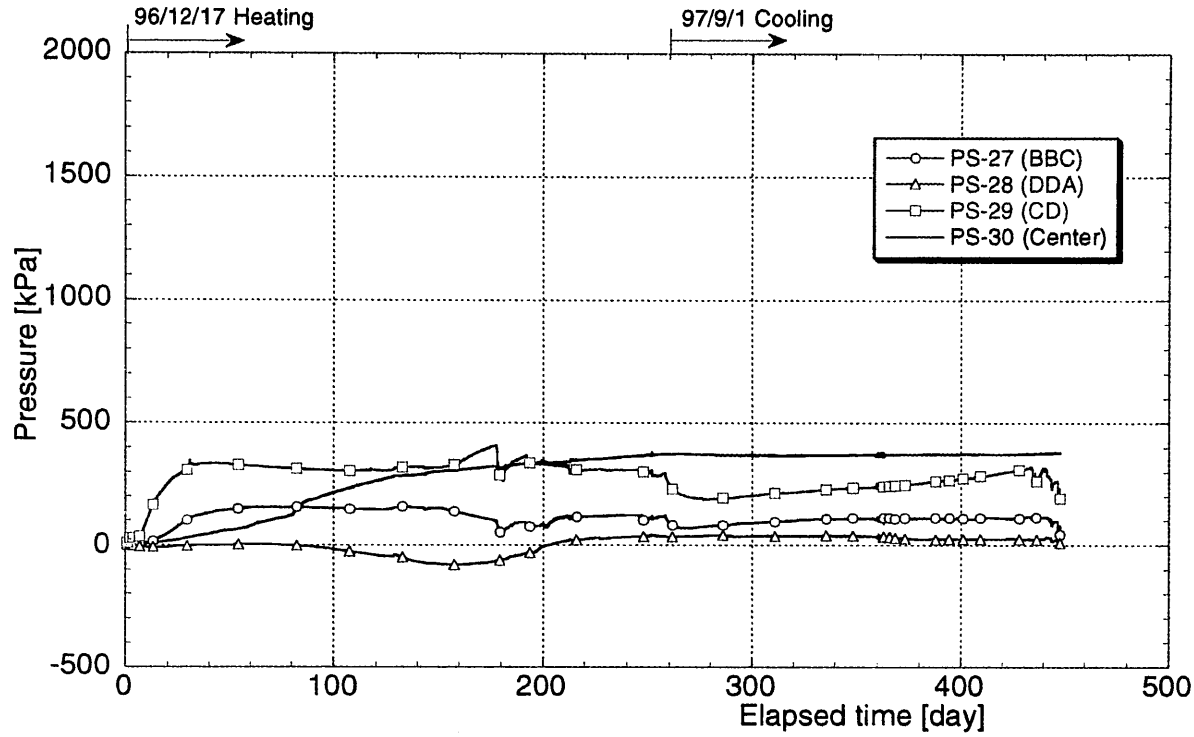

Measured data of pressure by pressure cell (Buffer, GL-0.5m, Top)
(1996/12/17-1998/3/10)

Figure 5-37 Time history of the total pressure (GL-0.5m; Upper)

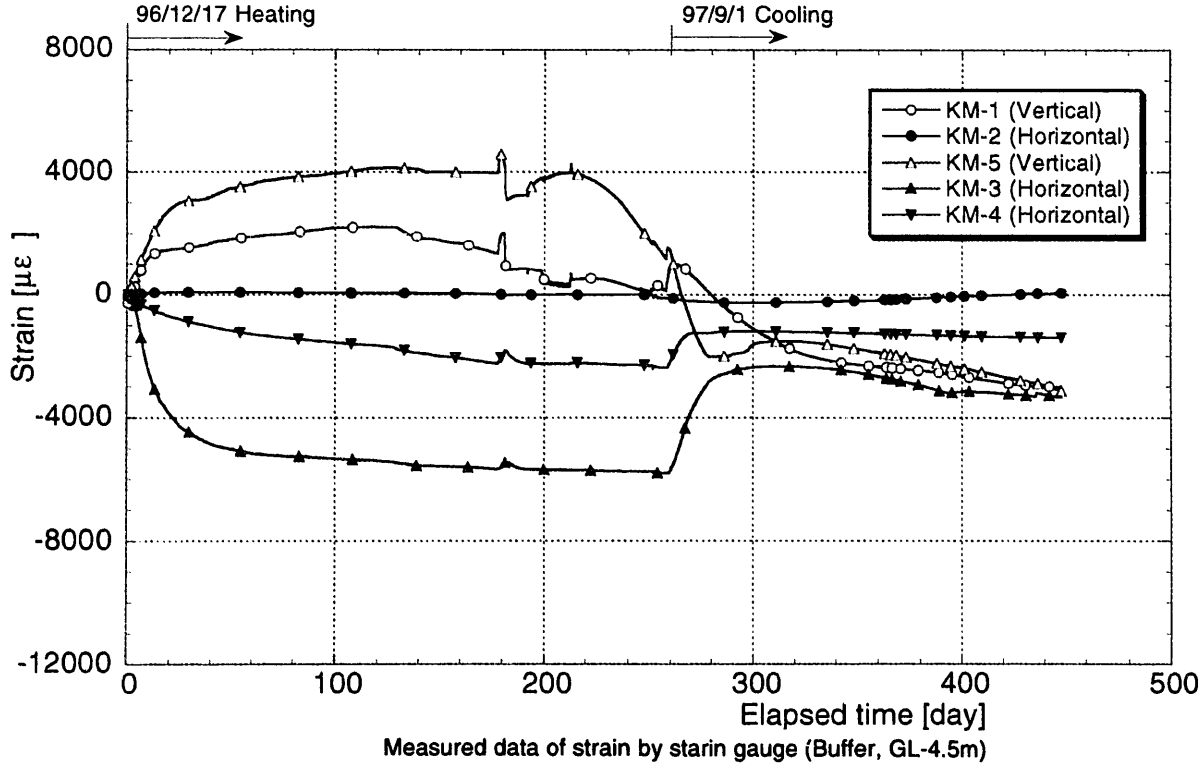

Measured data of strain by starin gauge (Buffer, GL-4.5m)
(1996/12/17-1998/3/10)

Figure 5-38 Time history of the strain in the buffer (GL-4.5m)

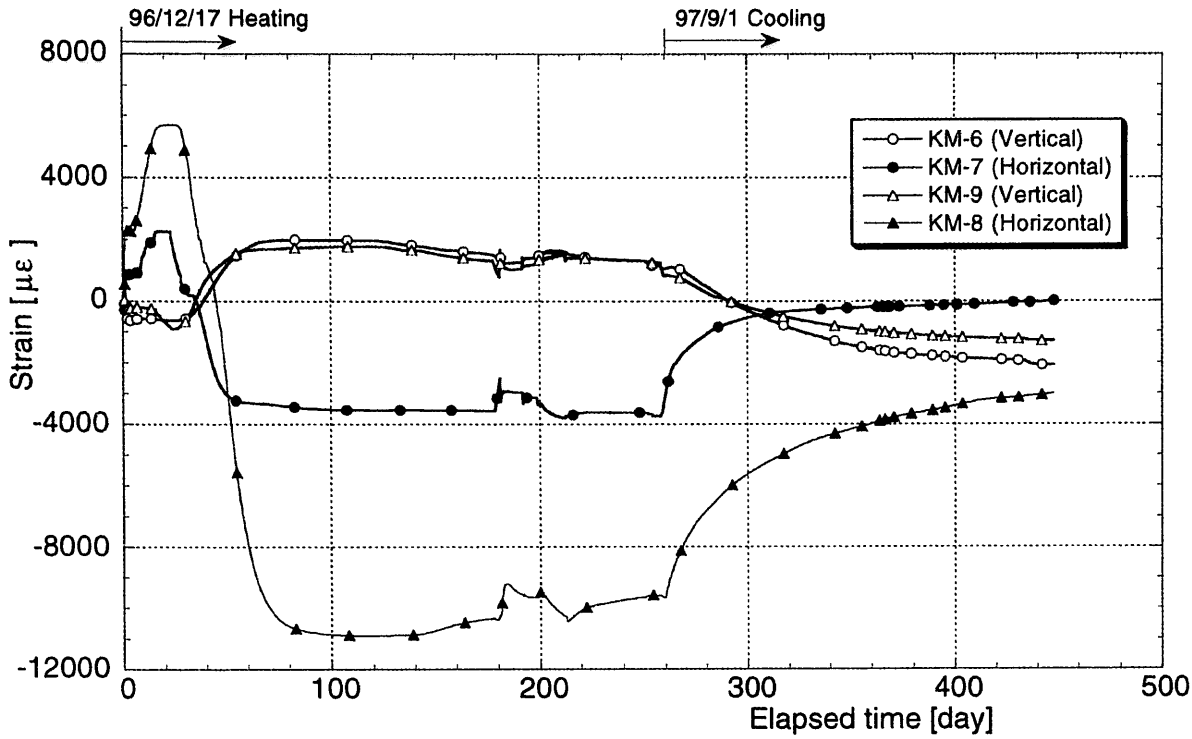

Measured data of strain by starin gauge (Buffer, GL-2.5,-3.5m)
(1996/12/17-1998/3/10)

Figure 5-39 Time history of the strain in the buffer (GL-2.5m, -3.5m)

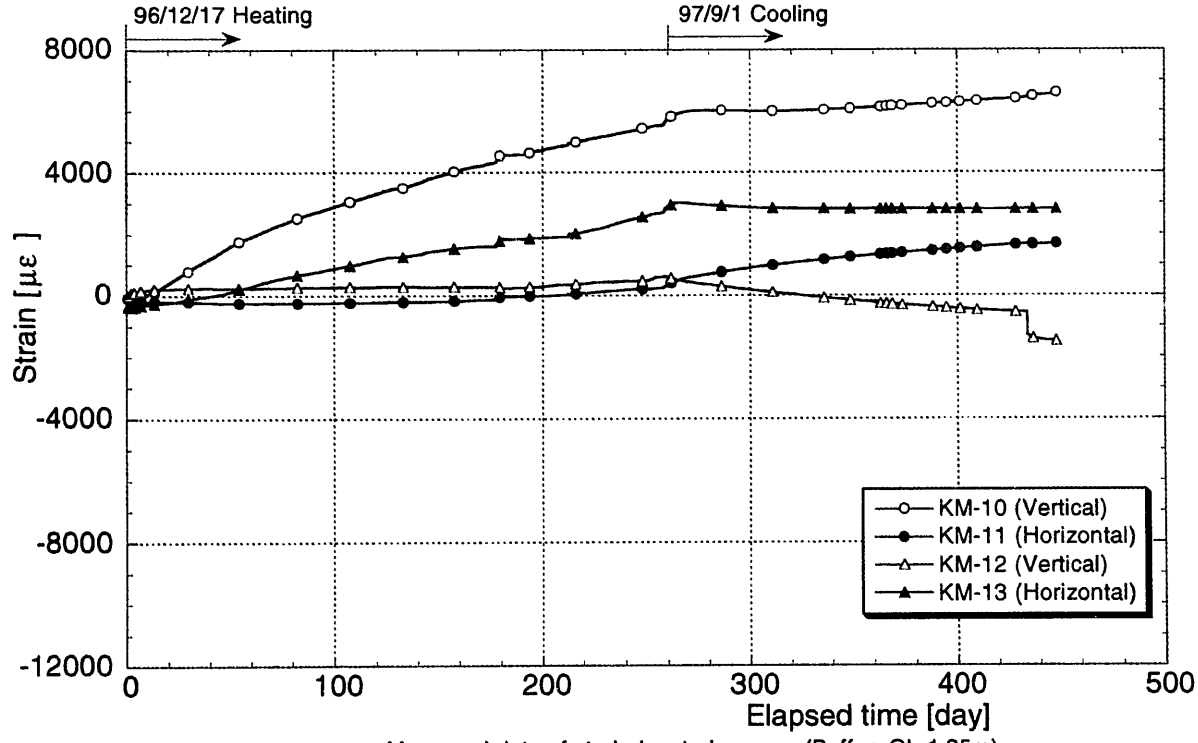

Measured data of strain by starin gauge (Buffer, GL-1.25m)
(1996/12/17-1998/3/10)

Figure 5-40 Time history of the strain in the buffer (GL-1.25m)

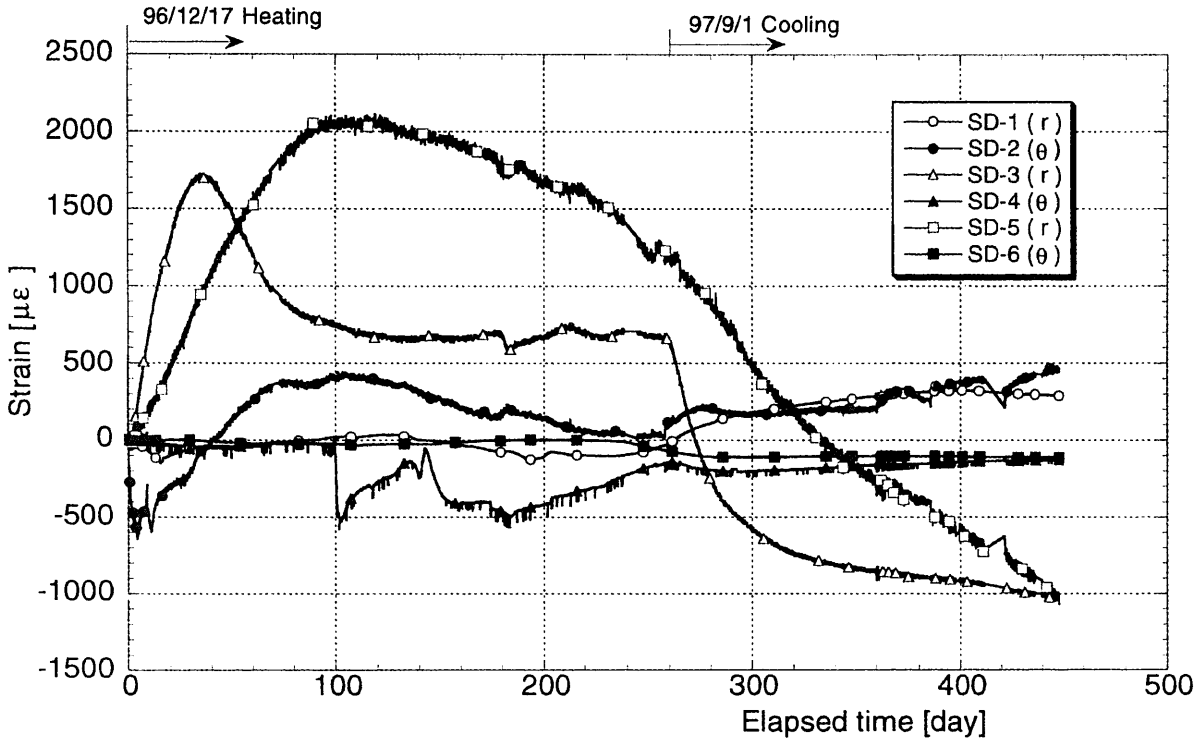

Measured data of strain by Strain gauge (Rock, KBM1)
(1996/12/17-1998/3/10)

Figure 5-41 Time history of the strain in the rock (KBM1)

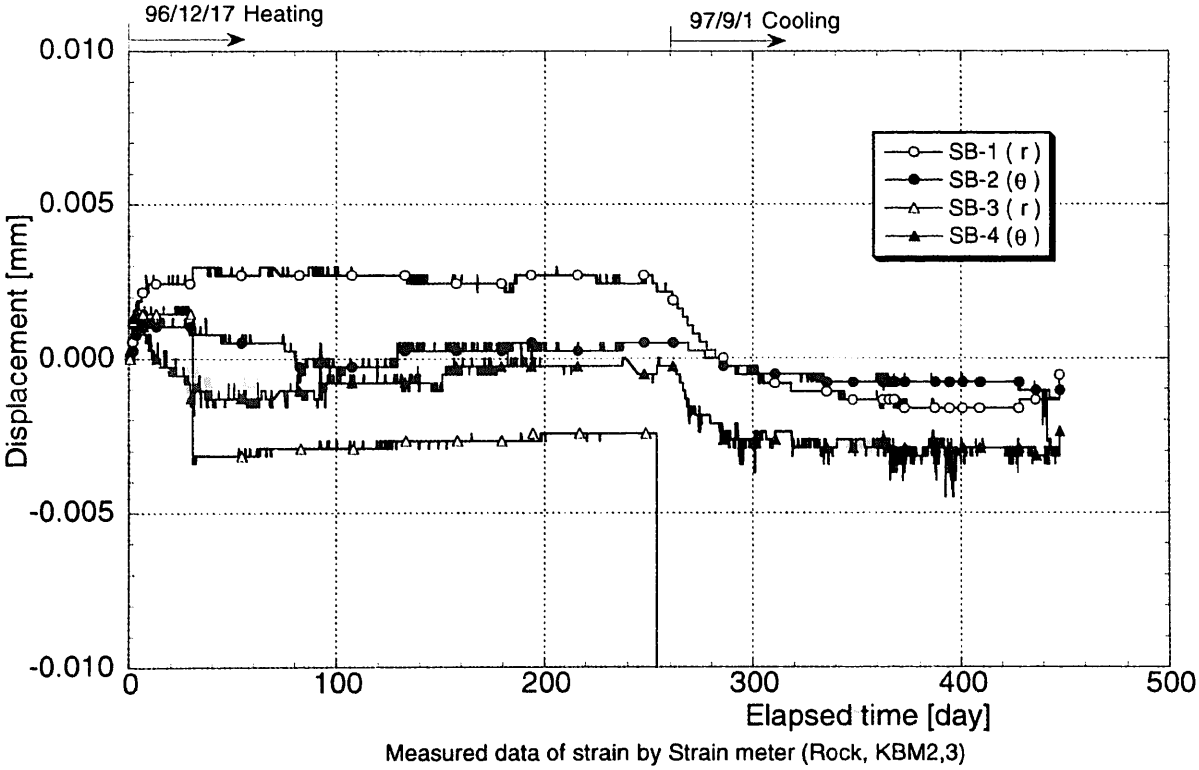

Measured data of strain by Strain meter (Rock, KBM2,3)
(1996/12/17-1998/3/10)

Figure 5-42 Time history of the strain in the rock (KBM2,3)

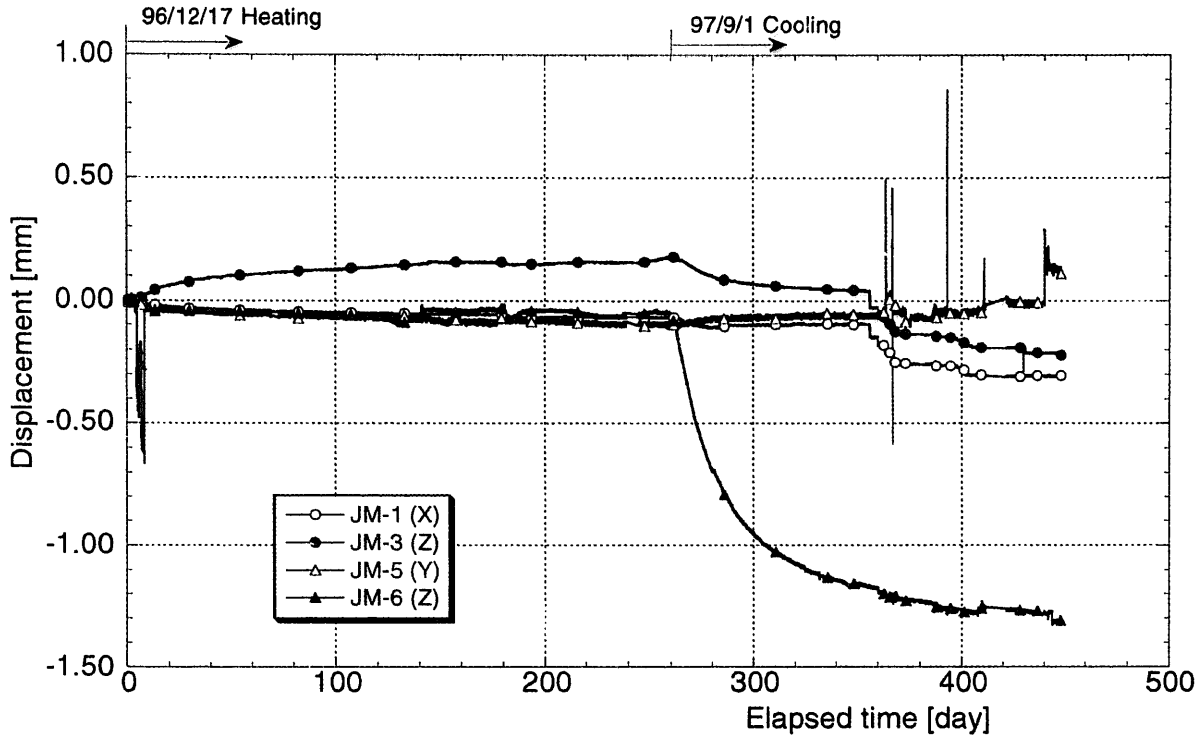

Measured data of displacement by Joint deformeter (Rock, KBM6,7)
(1996/12/17-1998/3/10)

Figure 5-43 Time history of the strain in the rock (KBM6,7)

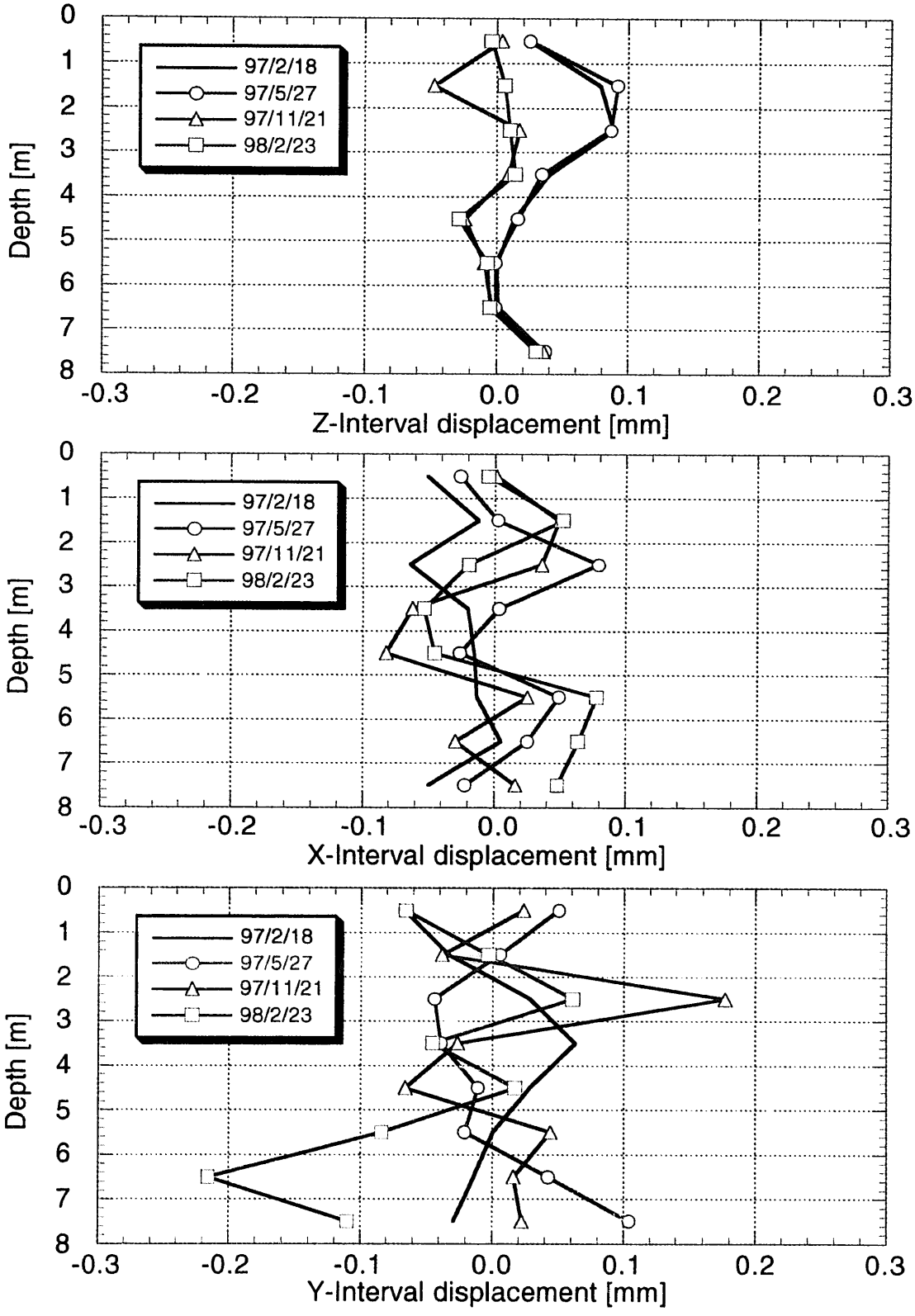

Figure 5-44 Displacement distribution in the rock (KBM4)

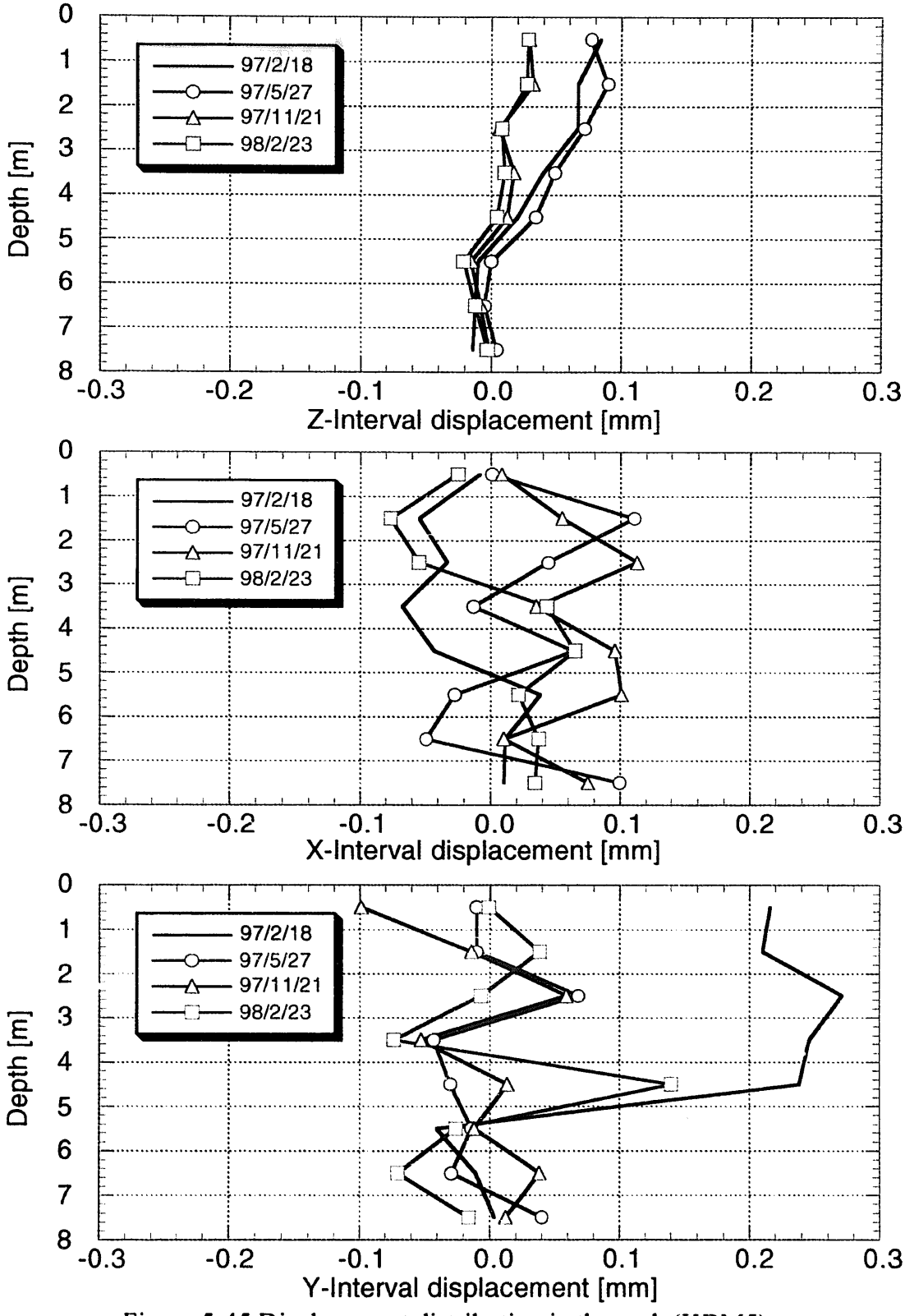

Figure 5-45 Displacement distribution in the rock (KBM5)

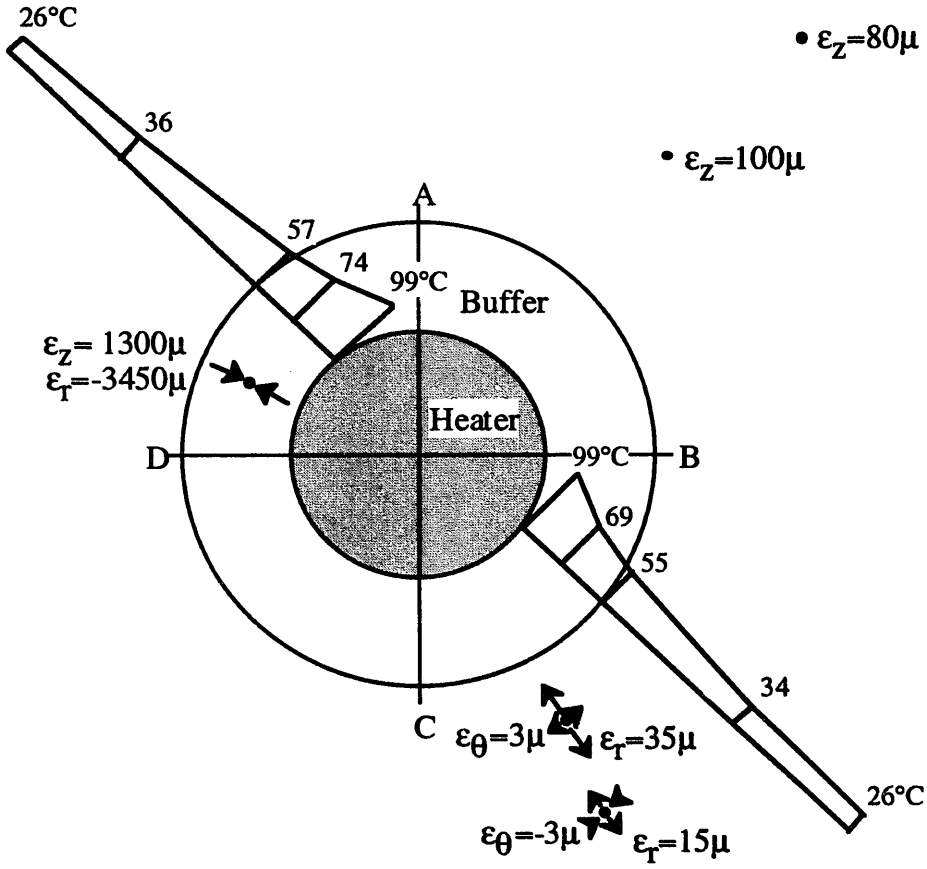

161 days after heater on
5/27 1997
GL -3.0m

Figure 5-46 Distribution of temperature and strain in rock and buffer
(Heater center level, After 161days from the start of heating)

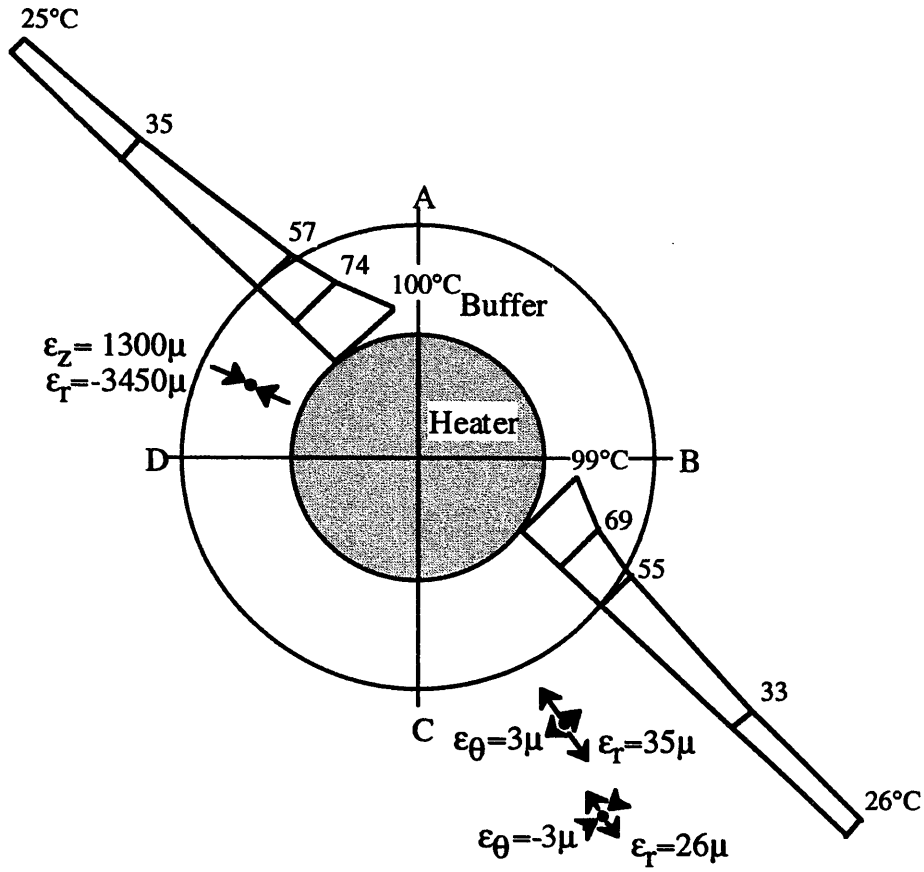

255 days after heater on
8/19 1997
GL -3.0m

Figure 5-47 Distribution of temperature and strain in rock and buffer
(Heater center level, After 255days from the start of heating)

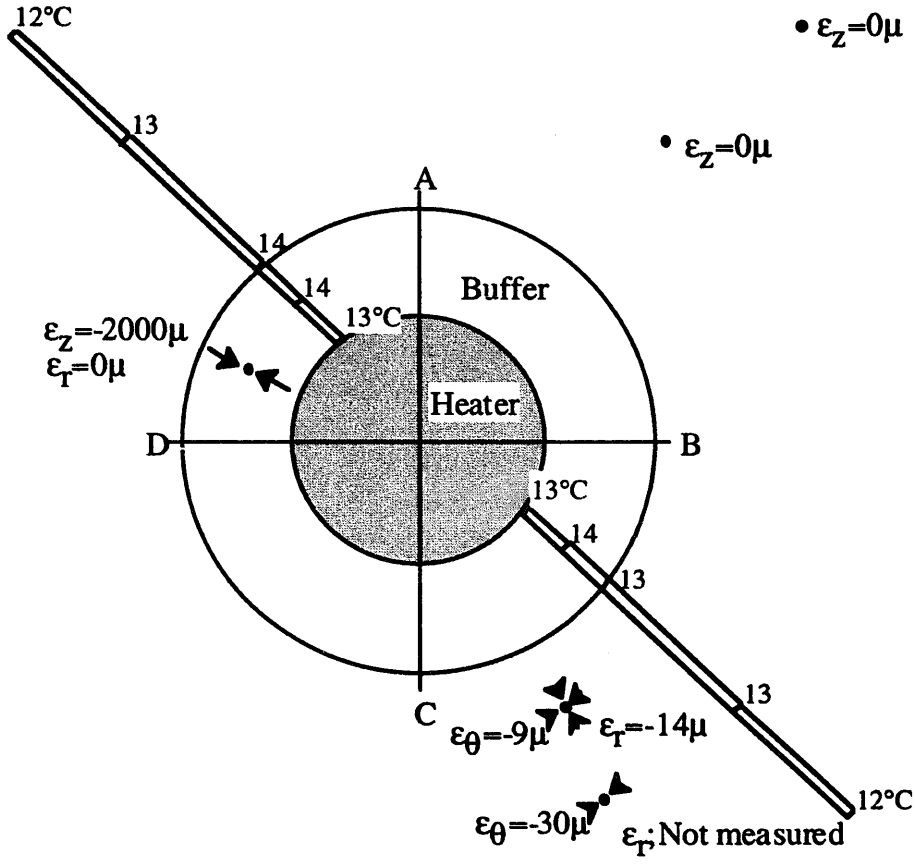

180 days after heater on
2/27 1998
GL -3.0m

Figure 5-47 Distribution of temperature and strain in rock and buffer
(Heater center level, After 180days from the stop of heating)

5.4 Summary of coupled test

In this section, we discuss the T-H-M phenomena measured during the heating and cooling phase and align the phenomena that occurred in buffer and rock. Table 5-2 shows the remarkable phenomena measured during the heating and cooling phase. Because the experiment was performed by the temperature control, heat flux was large at first, and then it decreased and constant at 50days past. Therefore, we divide the heating phase into two steps. We define the test phase from start to 50days past as "first step of heating phase" and test phase from 50days past to the end of heating phase as "second step of heating phase". In the second step, temperature in the buffer is almost constant but that in the rock mass increases gradually, though the increasing speed is lower than that of the first step. In the cooling phase, heater was turned off, however heat flux was generated due to the heat capacity of the heater and it became zero after 10days from the start of cooling phase. The temperature of buffer and rock decreased gradually and after six months became almost the same as the initial value.

The phenomena that were occurred at heater center level in each phase are as follows.

(1) First step of heating phase

- Water in the buffer moved from the inside (Heater side) to the outside (Rock side). This phenomenon was shown from the measurement result that the buffer at the middle part was wetting at first. As a result, the buffer near heater was drying and the buffer near rock was wetting. In this test, the driving force due to the thermal gradient is stronger than that due to the inflow from the rock. This reason may be that the pore pressure in the rock is low.
- The change of pore pressure in rock was low, while pore pressure at the interface between rock and buffer became negative temporarily at the start of experiment.
- Total pressure near the heater went up from the start of experiment and it became constant immediately. The buffer was compressive along the radial direction temporarily, and then it became tension.
- The rock was tensile both along the radial direction and vertical direction. It is because of the thermal expansion. The rock was tensile along the tangential direction at first, and then it became compressive. The value of tensile strain along the vertical direction was larger than that along the radial direction. This reason is that the restriction along the vertical direction is little.
- The strain in the buffer along the radial direction shows the compression and that along the vertical direction shows the tension.
- The fracture aperture became little. It was impossible to understand the three dimensional movement of fracture, however, it was confirmed that fracture was closed due to the thermal expansion of rock mass.

In the first step of heating phase, increasing in temperature and water movement in buffer predominated, while strain and stress were transitive and showed the complex behavior. The reason may be that this complex behavior is affected by the thermal expansion of heater and rock, the drying shrinkage of buffer, swelling of buffer, and so forth.

(2) Second step of heating phase

- Water movement in the buffer from the inside (Heater side) to the outside (Rock side) continued. As a result, the buffer at the middle part was drying.
- The pore pressure at the interface between the buffer and rock mass increased and that in

the rock mass also increased slightly. The pore pressure was raised at some points suddenly, and value moved near to the hydrostatic pressure. It is conceivable that groundwater infiltrated to the measuring point of borehole because of the fracture aperture change due to the heating.

- The ascent speed of total pressure became slow. The strain in the buffer became little both along the radial and vertical directions.
- The strain in the rock became constant. The displacement of fracture also became constant.

In the second step of heating phase, continuous water movement due to the thermal effect, increasing of pore pressure at the interface between buffer and rock, sudden ascent of pore pressure in the rock were observed. The ascent speed of total pressure became slow and strain became almost constant.

(3) Cooling phase

- Water in the buffer moved from the outside (Rock side) to the inside (Heater side). However, the buffer near rock maintained the saturation
- The pore pressure at the interface between the buffer and rock mass decreased when the heater was turned off, and then pore pressure became constant. The pore pressure in the rock decreased slightly.
- The total pressure decreased and became constant.
- The strain in buffer shows the opposite phenomena with the heating phase, that is, the strain along the radial direction shows the tension and that along the vertical direction shows the compression.
- The strain in rock shows the compression. The fracture was opened.

In the cooling phase, the opposite phenomena with heating phase were observed due to the recovery of temperature. These phenomena include the decreasing of pore pressure, decreasing of total pressure, recovery of strain, and so forth. In respect to the water movement in the buffer, infiltration into the drying part was not observed enough because test period was not enough. However, water content increased continuously and did not constant at the end of experiment.

At last, we show the reciprocal action of coupled thermo-hydro-mechanical phenomena that was known by this experiment as shown in Table 5-3. These phenomena were measured at the center level of the heater.

Table 5-2 characteristics of T-H-M data during heating and cooling phases

		Water content	Pore pressure			Total pressure	Strain		Joint deformation
		Buffer (B)	(B)	Buffer-Rock (B)-(R)	Rock (R)	Buffer (R)	Buffer (B)	Rock (R) (Heater level)	
Heating phase	First step	**Heater level** Inside: Drying Middle: Wetting Outside:Wetting	Not measured	**Heater level:** −(very early)→Const. **Others:** Const.	Not Const. (varying)	σ_r: **Inside(Heater level):** + **Outside:** + or − σ_z: **GL-5.0m:** Const. **GL-0.5m:** Const. or +	ε_r: **Heater level:** +→− **Others:** −or Const. ε_z: **Heater level:** Const.→+ **Others:** +	ε_r: +or +→− ε_θ: +→− ε_z: +	**Δz:** (Direction is referred to Figure 2-3) Fracture1: − Fracture2: Const.
	Second step	**Heater level** Inside: Const. Middle: Drying Outside: Const.		**Heater level:** + **Others:** Const.	Const. or Slightly + (sudden 'increasing' was observed at fracture area)	σ_r: **Inside(Heater level):** + **Outside:**+ or − σ_z: **GL-5.0m:** − **GL-0.5m:** Const.	ε_r: **Heater level:** Const. **Others:** −, Const. or+ ε_z: **Heater level:** Const. **Others:** Const.→−,+ or Const.	ε_r: Const. ε_θ: Const. ε_z: Const.	**Δz:** Fracture1: Const. Fracture2: Const.
Cooling phase		**Heater level** Inside: Wetting Middle: Wetting Outside: Const.		**Heater level:** −(very early)→Const. **Others:** Slightly−→Const. or Const.	Slightly −	σ_r: **Inside(Heater level):** −(very early)→ Const. **Outside:** Const. or Slightly + σ_z: **GL-5.0m:** Slightly + **GL-0.5m:** Const. or−→+	ε_r: **Heater level:** + **Others:** + ε_z: **Heater level:** − **Others:** −	ε_r: − ε_θ: − ε_z: −	**Δz:** Fracture1: + Fracture2: +
				−: Decreasing +: Increasing			−: Compression +: Expansion		−: Closing +: Opening

* "Heater level" means that these phenomena were measured at the center level of the heater.

Table 5-3 Reciprocal action of coupled thermo-hydro-mechanical phenomena measured in the Kamaishi in-situ experiment
(At the center level of the heater)

	Thermal phenomena	Hydraulic phenomena	Mechanical phenomena
Thermal phenomena		**Hydraulic→Thermal** ・[Heat transfer due to the hot water movement in the buffer during the heating phase]. ・Decreasing of the temperature at the several borehole sections in the rock mass due to the inflow of the groundwater.	**Mechanical→Thermal** ・Not measured
Hydraulic phenomena	**Thermal effect→Hydraulic effect** ・Water movement in the buffer due to the effect of thermal gradient ・Pore pressure increasing at the interface between rock mass and buffer due to the water movement in the buffer and water inflow from the rock mass ・Pore pressure increasing at the interface between rock mass and buffer due to the effect of the heating ・Sudden pore pressure increasing at the several borehole sections in the rock mass where the some fractures exit during the heating phase ・water content increasing due to the water inflow from the rock mass during the cooling phase		**Mechanical→Hydraulic** ・ Recovery of the pore pressure in the rock mass to the hydrostatic pressure [due to the change of fracture aperture]
Mechanical phenomena	**Thermal effect→Mechanical effect** ・Increasing of the total pressure at the surface of the heater during the heating phase, and decreasing of the total pressure during the cooling phase ・Compression of the buffer along the radial direction and expansion of the buffer along the vertical direction due to the effect of the heating ・[Thermal expansion of the heater and the resulting compression of the buffer] ・Thermal expansion of the rock mass. Thermal expansion is restricted at the horizontal direction, but that is free at the vertical direction. ・[Occurrence of the thermal stress at the radial and the tangential directions.]. ・Change of the fracture aperture (closing and opening) due to the effect of heating and cooling.	**Hydraulic→Mechanical** ・Increasing of the total pressure due to the swelling of the buffer	

[ ]: These phenomena were not measured directly, but these were presumed from other data

6. Sampling of the buffer material

During heating and cooling phase, water content was monitored with hygrometers and psychrometers. During heating phase, monitoring data showed the change of the distribution of water potential in the buffer material of the test pit. Water content was calculated from the water potential using equations determined from the results of the laboratory tests.

Sampling of the buffer material was conducted at the end of heating and cooling phase to evaluate the equation. Sampling schedule was as follows.

Heating phase
- Heater on -December 17, 1996 to September 1, 1997
- Sampling -August 20 to 29, 1997

Cooling phase
- Heater off -September 1, 1997
- Sampling -February 24 to March 2, 1998

6.1 Water content of the buffer material

6.1.1 Sampling points

Sampling of the buffer material was conducted in the sampling lines. Sampling line 1 and 2 were adjacent to the monitoring line O-BBC and O-CD (see Figure 6-1). A concrete lid was fixed on the top of the test pit to restrain the swelling pressure of the buffer material. It was unable to remove the lid to obtain the samples. Therefore, the lid had some guide-pipes for sampling in Figure 6-2. The guide-pipe had a window that was bolted during T-H-M experiment. In sampling, the window, 72 mm in diameter, was unbolted.

Figure 6-3 shows the sampling points in heating and cooling phase. In sampling borehole of a, b and c, there had 3 points in level, 70 to 100 cm, 120 to 150 cm, 170 to 200 cm. In sampling borehole of d, e and f, there had 6 points in addition, 220 to 250 cm, 270 to 300 cm, 320 to 350 cm, 370 to 400 cm, 420 to 450 cm, 470 to 500 cm. In sampling borehole of d and f, the samples for microbial analysis (Stoes-Gascoyne et al., 1996) were obtained, too.

6.1.2 Sampling method

Samples were obtained as core samples by the standard penetration test (JIS A 1219-1995). Pre sampling was conducted to the same buffer material at Big-Ben in Tokai Works in JNC. The methods of in-situ sampling reflected the results of it. The test procedure is as follows (see Figure 6-4). Sampler (see Figure 6-5) is sounded by a weight that weighs 63.5 kg. The weight falls 75 cm to the hammer. The number of times of the sampler penetrating into the buffer material up to 30 cm is counted. This number defines the hardness and the degree of compaction of the soil. One sampling length was 50 cm. 20 cm of the upper part was drilled by boring machine. The borehole of 66 mm in diameter was opened. The sampler was penetrated from 20 to 50 cm. Obtained sample measured weight was bottled. Water content was calculated by equation (6.1)

$$\omega = 100\ (Ww / Ws)\ (\%) \qquad (6.1)$$

Here, ω is the water content. Ww is the weight of the water in the sample. Ws is the weight of

oven-dried sample.

Figure 6-6 shows the sampling points. When the buffer material was too hard to penetrate the sampler, the sample was divided to the obtained size. Much dust happened during the drilling of sampling borehole, because dry type boring was selected to obtain the sample. Figure 6-7 shows the dust collector.

6.1.3 Countermeasure for deviation of borehole

Trial of sampling was conducted at Big-Ben prior to the in-situ sampling. Some troubles were occurred in the trial. When the adjacent boreholes were drilled, after drilling of first borehole, second borehole deviated to the first one in some level. The deviation of borehole was considered to cause the cross each other in addition. Figure 6-8 shows the considerable situations of drilling. Therefore, the countermeasure against these situations was to put a vinyl chloride pipe in the borehole after sampling. A hollow pipe was considered to become flat by the swelling pressure of the buffer material. The installed pipe was full filled with the mortar. The end of the pipe was coated with the silicone rubber to prevent the direct contact between bentonite and the mortar.

During heating phase, T-H-M experiment continued. The unfilled sampling borehole was considered to cause the local decrease of density to the buffer material around the borehole. The installed pipe into the drilling borehole filled about 58 % of the open space. After installation of the pipe, total open space was only about 0.2 % to the area of the test pit. It was considered that this space was negligible to decrease of density of the buffer material.

6.2 Distribution of the water content

6.2.1 Results of sampling

Tables 6-1 to 6-6 show the obtained value of water content at the end of heating phase. Tables 6-7 to 6-12 show the obtained value of water content at the end of cooling phase. The level of the table shows the points of the obtained sample. The blank of the level shows the section of boring. Samples were the black rectangular marks of Figure 6-3. The coordinates of the sampling point show the center of the divided piece of a sample. A number of the sample means a number of the bottle. The number of penetration of the sampler, as N value, is described in the table.

N value is defined the number of the penetration of the sampler up to 30 cm into the specimen. In sand, the number over 51 indicates the well consolidation. In soil, the number over 31 indicates the solidification. In this sampling, the penetration length was not the same. The number of the penetration length as equivalent to 30 cm was indicated to the N value.

At the end of heating phase, the points around heater annulus, bottom of the sampling borehole a, b and c and the level of 200 to 400 of the sampling borehole d, indicated the low water content of 4 percent or less. Initial water content of the buffer was 15 %. Water content decreased about 11 % during heating. The sample of the water content of 4 % was very dry and too hard to release it from the sampler. Therefore, the obtained sample was observed directly after splitting the sampler without release.

The point of the highest water content was 18.2 % in the level of 280 of the sampling borehole f. The gradient between sampling borehole d and e was 0.49 %/cm and between the borehole e and f was 0.86 %/cm in this level. There was the steep gradient near the rock mass.

Water content as 4 % around the heater at the end of heating phase increased up to 7 % at the end of cooling phase. All samples were released from the sampler. The point of the highest water content was 24.8 % in the level of 295 of the sampling borehole f. The points of the highest water content of both in heating and cooling phase were almost the same coordination. Therefore, it was considered that the distribution of water content was uniform in each level. The gradient between sampling borehole d and e was 0.37 %/cm and between the borehole e and f was 1.21 %/cm in the level about 290. There was the steep gradient adjacent to the rock mass as at the end of heating phase.

From the comparison of the shape of gradient of water content at the end of heating and cooling phase, the more steep gradient around heater at the end of heating phase and the more steep gradient near rock mass at the end of cooling phase. It was considered that movement of water in buffer was subject to the thermal effect of the heater in the end of heating phase and to the infiltration of water from the rock mass at the end of cooling phase.

Figure 6-9 shows the relationship between N value and water content. There were some points of the N value over 1000 times. The vertical axis was on both a log and a linear scale. The N values in the end of heating phase were bigger than that at the end of cooling phase. The sample of water content over 21 % had the same N value as 14 at the end of cooling phase. The points of the almost same water content were the almost same N value in both phases. Temperature of buffer didn't affect the relations between N value and water content. N value showed the minus correlation with the water content. That was the same tendency between Young's modulus and the water content (Fujita et al., 1992). It was considered that N value was the indicator of the hardness of the buffer.

Figure 6-10 shows the distribution of N value in the test pit. There were some points of N value over 100 times around the heater at the end of heating phase. The buffer around the heater hardened. It was considered that the gradient of temperature affected to the movement of water, especially around the heater, at the end of heating phase. N value of almost points decreased in cooling phase. However, the upper part of the heater remained high N value.

Figure 6-11 shows the distribution of water content of each sampling borehole. Distribution of water content of the upper and lower part of the heater was almost the same. Thermal effect by the heater influenced the water content around the heater. Water content increased from the sampling borehole d to f. In the borehole d, water content of all points were 5 % or less around the heater. In the borehole e, water content of all points was 10 % or less around the heater. In the borehole f near rock mass, water content of all points were 15 %, as initial water content, or less around the heater. This tendency shows the decrease of water content around the heater. Just upper part of the heater as coordination of the level of 170 to 200, the gradient of water content of borehole a, b and c was large. Water content decreased sharply around the heater. This gradient showed in good agreement with the correlation in Figure 6-10.

Water content of all points in cooling phase increased. Water content of the points of the borehole d around heater was about 10 %. The points of the borehole f showed the highest water content at each level, and it was considered to be the influence of the infiltration of water from the rock mass.

Figures 6-12 and 6-13 show the contour of the distribution of temperature and water content in heating and cooling phase. The distribution of temperature was described with the monitoring data. The distribution of water content was described with the sampling.

Water content as 10 % or less was distributed around the heater in heating phase. In the sampling section, the distribution of water content was symmetrically. The distribution of temperature was symmetrically, too. Temperature was about 100 around the heater. It was considered that thermal effect affected the decrease of water content around heater.

Bound of 10 and 15 % of water content approached to the heater and one of 20 % appeared near rock mass in cooling phase. Temperature of the test pit was around 12 °C. It was considered that the infiltration of water from rock mass accelerated.

6.2.2 Comparison between monitoring data and sampling data

One of the objectives of sampling was to check the adequacy of the equations determined from the results of laboratory tests. The equation was used to calculate water content from the monitoring data. In-situ experiment has many uncertain elements than laboratory tests. The adequacy of the equation in-situ was essential problem.

Figures 6-14 and 6-15 show the comparison of the data between monitoring and sampling. In Figure 6-14, left side was the points of monitoring and sampling, right side was the plots of the obtained data. Figure 6-15 was the same. Regarding the monitoring points in the left side figure, only the points that had monitoring data were described.

As shown in Figure 6-1, the sampling line 1 was adjacent to the monitoring line O-BBC, the sampling line 2 was adjacent to the monitoring line O-CD. Therefore, it was considered that the values of the point, which was the same distance from the center of the test pit, were approximately the same in each line.

As shown in Figure 6-14, both monitoring data and sampling results were plot at the end of heating phase. Both of them were in good agreement. It was considered that the equation to calculate the water content was adequate. On the boundary between rock and bentonite, water content was almost 25 %. In this water content, OT-9607 was fully saturated at dry density of 1.65 g/cm^3. Figure 6-15 shows the results at the end of cooling phase. Both monitoring data and sampling results were in good agreement. Therefore, the equation was adequate in both heating and cooling phases.

However, the only some points had both monitoring data and sample. It is necessary to consider the arrangement of monitoring points and the number of monitoring sensors, i.e. installation of some monitoring sensors in the same monitoring points.

Table 6-1 Water content of sampling of borehole a

Level [cm]	Coordinate (r, z)	Impacting valie	N value	Sample No.	Water content [%]
73-110	20, 80	51	41	6	15.3
	20, 90			7	16.9
	20,100			8	18.0
120-160	20,130	62	47	9	15.7
	20,140			10	17.0
	20,150			11	15.6
170-200	20,180	43	43	12	12.9
	20,190			13	10.4
	20,200			14	6.3

Table 6-2 Water content of sampling of borehole b

Level [cm]	Coordinate (r, z)	Impacting valie	N value	Sample No.	Water content [%]
70-100	32.5, 80	91	91	22	16.2
	32.5, 90			23	15.7
120-150	32.5, 130	61	61	24	14.7
	32.5, 140			25	16.2
170-200	32.5, 180	72	72	26	12.3
	32.5, 190			27	9.0

Table 6-3 Water content of sampling of borehole c

Level [cm]	Coordinate (r, z)	Impacting valie	N value	Sample No.	Water content [%]
74-104	45, 80	54	54	28	16.6
	45, 90			29	15.9
120-150	45,130	52	52	31	16.3
	45,140			32	16.0
170-200	45,180	72	72	33	13.8
	45,190			34	11.4

Table 6-4 Water content of sampling of borehole d

Level [cm]	Coordinate (r, z)	Impacting valie	N value	Sample No.	Water content [%]
70-88	55, 80	50	83	15	16.9
88-100	55, 90	34	85	16	15.7
120-150	55,130	65	65	17	15.9
	55,140			18	17.0
170-188	55,180	60	100	19	13.1
	55,185			20	9.3
188-193	55,190	200	1200	21	4.5
221-251	55,230	195	195	81	3.5
	55,240			79	3.8
268-298	55,280	102	102	77	4.7
	55,290			80	3.4
320-350	55,330	103	103	75	4.7
	55,340			76	4.1
369-399	55,380	148	148	74	4.2
	55,390			78	4.4
420-450	55,430	52	52	71	11.6
	55,440			72	13.7
470-500	55,480	56	56	70	16.6
	55,490			73	15.7

Table 6-5 Water content of sampling of borehole e

Level [cm]	Coordinate (r, z)	Impacting valie	N value	Sample No.	Water content [%]
72-102	65, 80	88	88	35	16.6
	65, 90			36	15.5
120-150	65,130	43	43	37	15.7
	65,140			38	15.8
170-200	65,180	53	53	39	16.3
	65,190			40	15.0
222-252	65,230	100	100	30	9.2
	65,240			41	9.5
267-297	65,280	112	112	42	9.6
	65,290			43	9.4
320-350	65,330	73	73	44	8.2
	65,340			45	8.0
368-398	65,380	109	109	46	7.4
	65,390			47	8.3
420-450	65,430	41	41	48	13.1
	65,440			49	14.3
468-498	65,480	43	43	50	15.4
	65,490			51	15.6

Table 6-6 Water content of sampling of borehole f

Level [cm]	Coordinate (r, z)	Impacting valie	N value	Sample No.	Water content [%]
70-100	75, 80	59	59	52	17.4
	75, 90			53	16.0
118-148	75,130	32	32	54	16.4
	75,140			55	17.2
172-202	75,180	29	29	56	16.7
	75,190			57	16.8
222-252	75,230	27	27	58	14.7
	75,240			59	16.6
269-299	75,280	25	25	60	18.2
	75,290			61	15.7
318-348	75,330	28	28	62	15.1
	75,340			63	13.1
369-399	75,380	43	43	64	11.5
	75,390			65	12.0
418-448	75,430	31	31	66	14.4
	75,440			67	16.1
471-501	75,480	57	57	68	16.1
	75,490			69	16.1

Table 6-7 Water content of sampling of borehole a

Level [cm]	Coordinate (r, z)	Impacting valie	N value	Sample No.	Water content [%]
70-100	20, 80	34	34	100	16.7
	20, 90			93	14.7
120-150	20,130	32	32	96	14.7
	20,140			97	16.2
170-200	20,180	64	64	94	8.2
	20,190			99	7.0

Table 6-8 Water content of sampling of borehole b

Level [cm]	Coordinate (r, z)	Impacting valie	N value	Sample No.	Water content [%]
70-100	32.5, 80	40	40	91	16.8
	32.5, 90			95	15.3
120-150	32.5, 130	48	48	98	14.8
	32.5, 140			92	16.8
170-200	32.5, 180	74	74	86	14.0
	32.5, 190			87	10.1

Table 6-9 Water content of sampling of borehole c

Level [cm]	Coordinate (r, z)	Impacting valie	N value	Sample No.	Water content [%]
70-100	45, 75	39	39	71	16.6
	45, 85			72	16.6
	45, 95			73	16.3
120-150	45,125	48	48	74	14.4
	45,135			75	15.0
	45,145			76	15.7
170-200	45,175	83	83	77	13.2
	45,185			78	12.3
	45,195			79	7.1

Table 6-10 Water content of sampling of borehole d

Level [cm]	Coordinate (r, z)	Impacting valie	N value	Sample No.	Water content [%]
70-100	55, 75	40	40	62	17.0
	55, 85			d-1	16.7
	55, 95			51	16.0
120-150	55,125	31	31	47	15.0
	55,135			d-2	16.0
	55,145			41	16.0
170-200	55,175	56	56	49	15.0
	55,185			d-3	14.0
	55,195			40	12.0
220-250	55,225	76	76	48	7.0
	55,235			d-4	6.8
	55,245			36	7.0
270-300	55,275	62	62	26	8.0
	55,285			d-5	8.8
	55,295			31	9.0
320-350	55,325	70	70	22	8.0
	55,335			d-6	9.4
	55,345			25	8.0
370-400	55,375	94	94	35	8.0
	55,385			d-7	7.1
	55,395			34	8.0
420-450	55,425	34	34	30	13.0
	55,435			d-8	14.1
	55,445			24	15.0
470-500	55,475	30	30	28	17.0
	55,485			d-9	16.0
	55,495			29	19.0

Table 6-11 Water content of sampling of borehole e

Level [cm]	Coordinate (r, z)	Impacting valie	N value	Sample No.	Water content [%]
70-100	65, 80	27	27	32	17.7
	65, 90			33	17.0
120-150	65,130	40	40	27	15.4
	65,140			21	16.0
170-200	65,180	26	26	17	16.3
	65,190			12	16.2
220-250	65,230	38	38	6	11.5
	65,240			7	11.8
270-300	65,280	33	33	11	12.9
	65,290			16	12.7
320-350	65,330	35	35	8	12.3
	65,340			9	11.7
370-400	65,380	28	28	10	11.2
	65,390			13	12.1
420-450	65,430	20	20	14	15.3
	65,440			15	17.0
470-500	65,480	19	19	18	17.1
	65,490			19	17.7

Table 6-12 Water content of sampling of borehole f

Level [cm]	Coordinate (r, z)	Impacting valie	N value	Sample No.	Water content [%]
70-100	75, 75	18	18	84	19.7
	75, 85			82	19.0
	75, 95			83	18.5
120-150	75,125	21	21	89	17.5
	75,135			85	17.2
	75,145			88	17.1
170-200	75,175	19	19	90	18.0
	75,185				19.7
	75,195			63	20.3
220-250	75,225	14	14	64	18.7
	75,235				20.6
	75,245			65	-
270-300	75,275	14	14	66	22.1
	75,285				23.0
	75,295			50	24.8
320-350	75,325	14	14	39	21.8
	75,335				23.5
	75,345			38	20.2
370-400	75,375	18	18	43	17.2
	75,385				17.7
	75,395			44	18.2
420-450	75,425	19	19	42	19.1
	75,435				20.4
	75,445			37	18.8
470-500	75,475	20	20	67	18.2
	75,485				18.8
	75,495			46	18.0

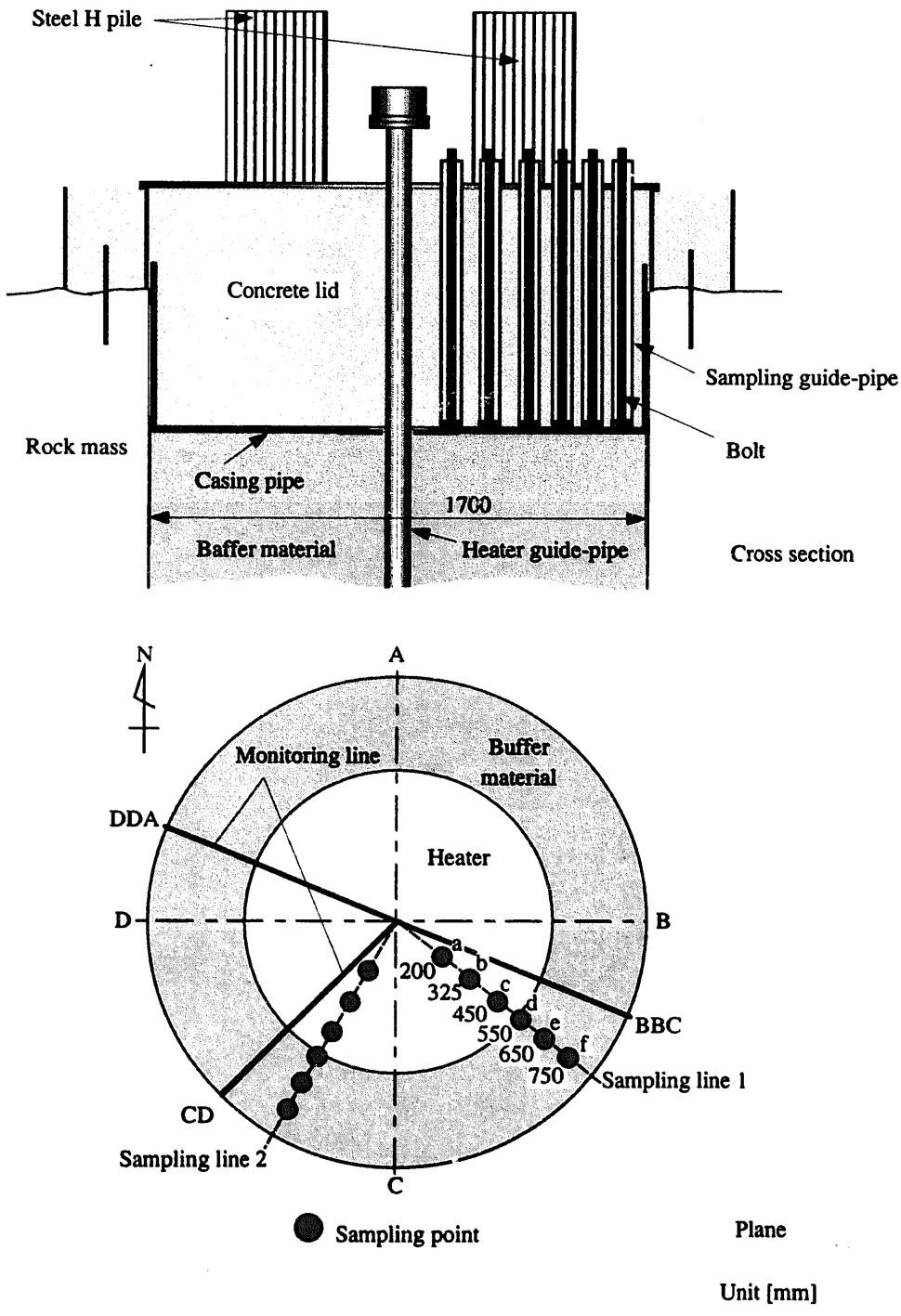

Figure 6-1 Points of the sampling borehole
(Upper; Cross section, Lower; Plane)

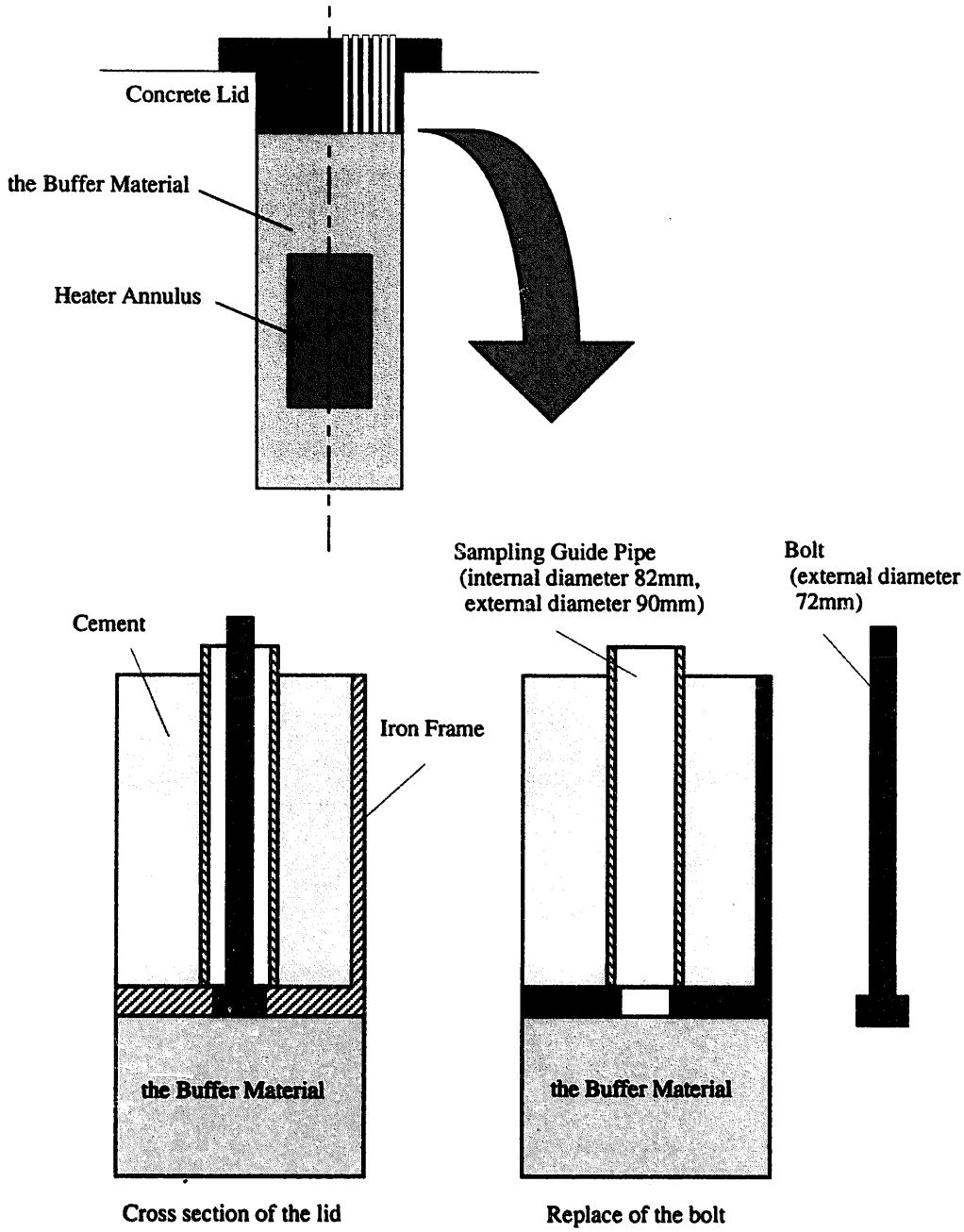

Figure 6-2 Device of the sampling guide pipe

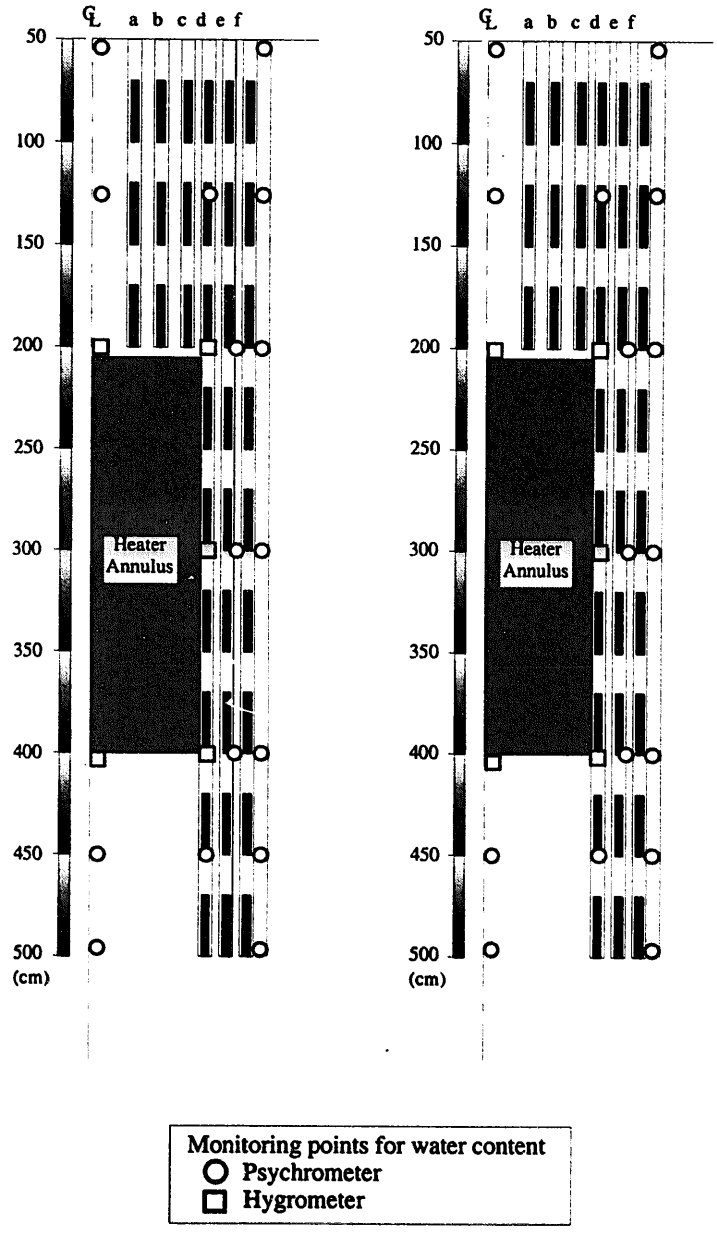

Figure 6-3 Sampling points
(Left; End of the heating phase, Right; End of the cooling phase)

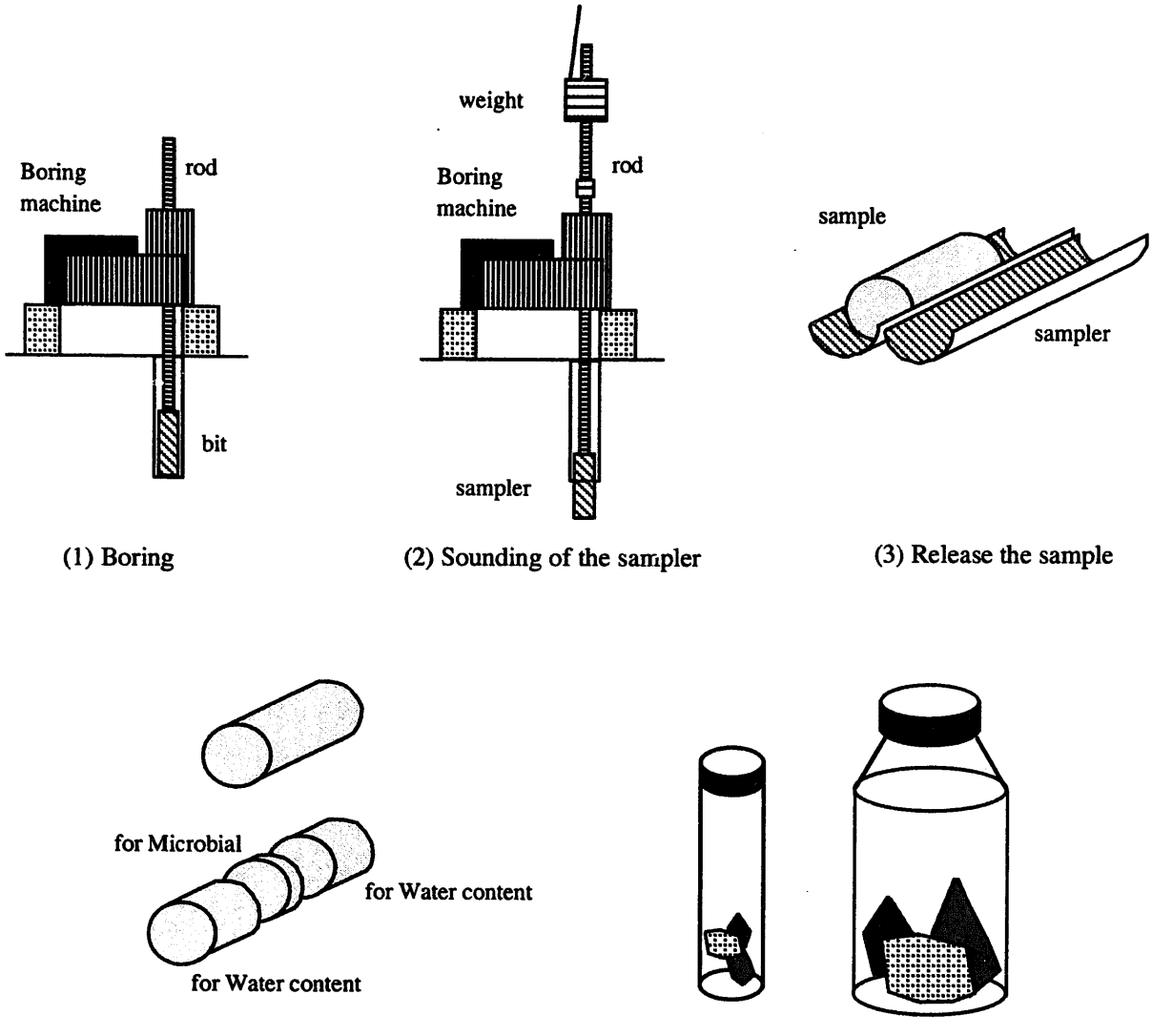

(1) Boring

(2) Sounding of the sampler

(3) Release the sample

(4) Cut the sample in three pieses

(5) Bottling the sample

Figure 6-4 The procedure of sampling of the buffer material during heating and cooling phase

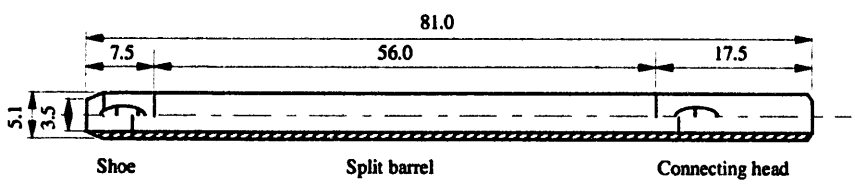

Parts	size [cm]
Length of Sampler	81.5
Length of Shoe	7.5
Length of Split barrel	56.0
Length of Connecting head	17.5
External diameter	5.1
Internal diameter	3.5
Angle of the Shoe	19°47'

Figure 6-5 Sampler for Standard penetration test (JIS A 1219-1995)

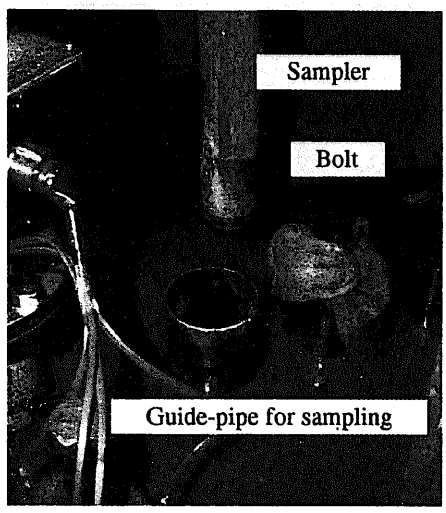

Figure 6-6 Sampling Points

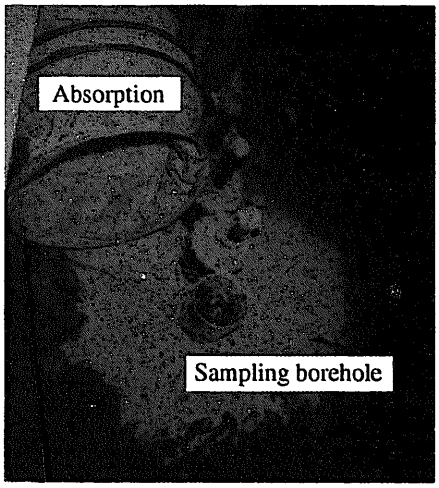

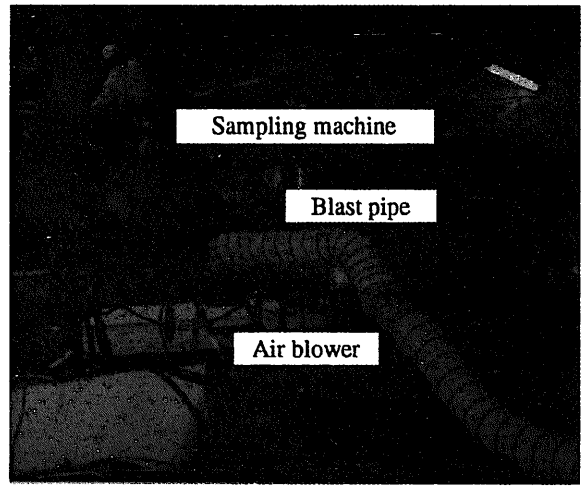

Absorption of debris of sampling

Air blower and blast pipe for debris of sampling

Figure 6-7 Dust collector system for Sampling
(in the end of cooling phase)

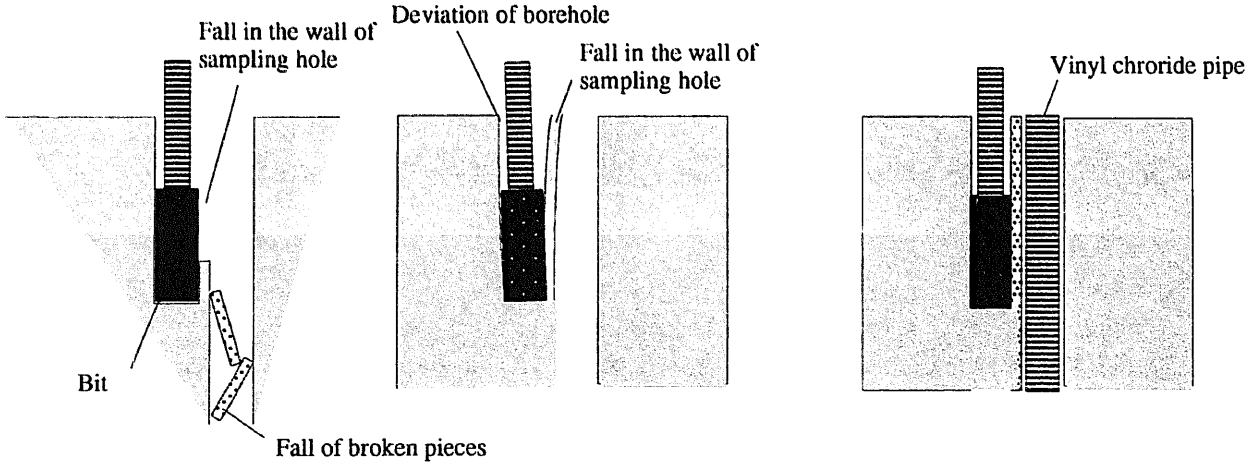

Figure 6-8 Treatment against the fall of
the wall of a sampling hole

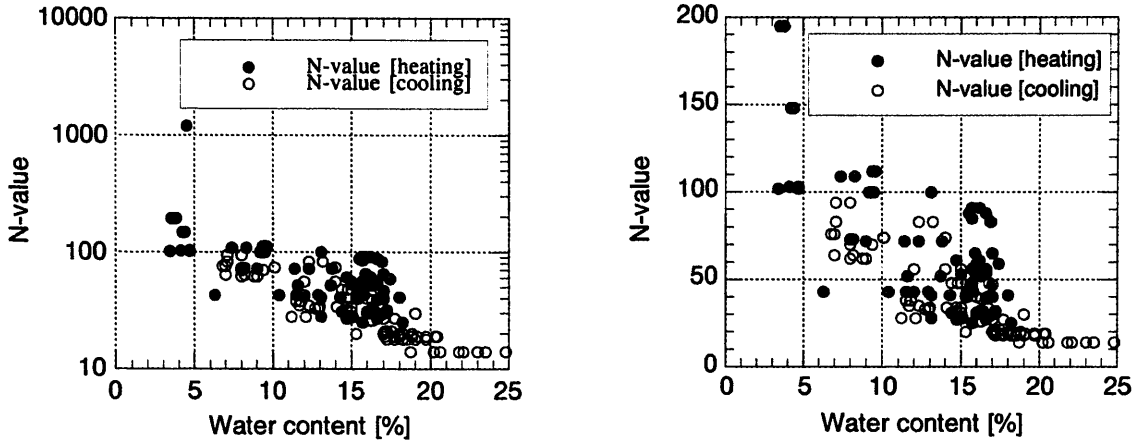

Figure 6-9 Relationship between N value and water content
(Left; Logarithmic scale, Right; Linear scale)

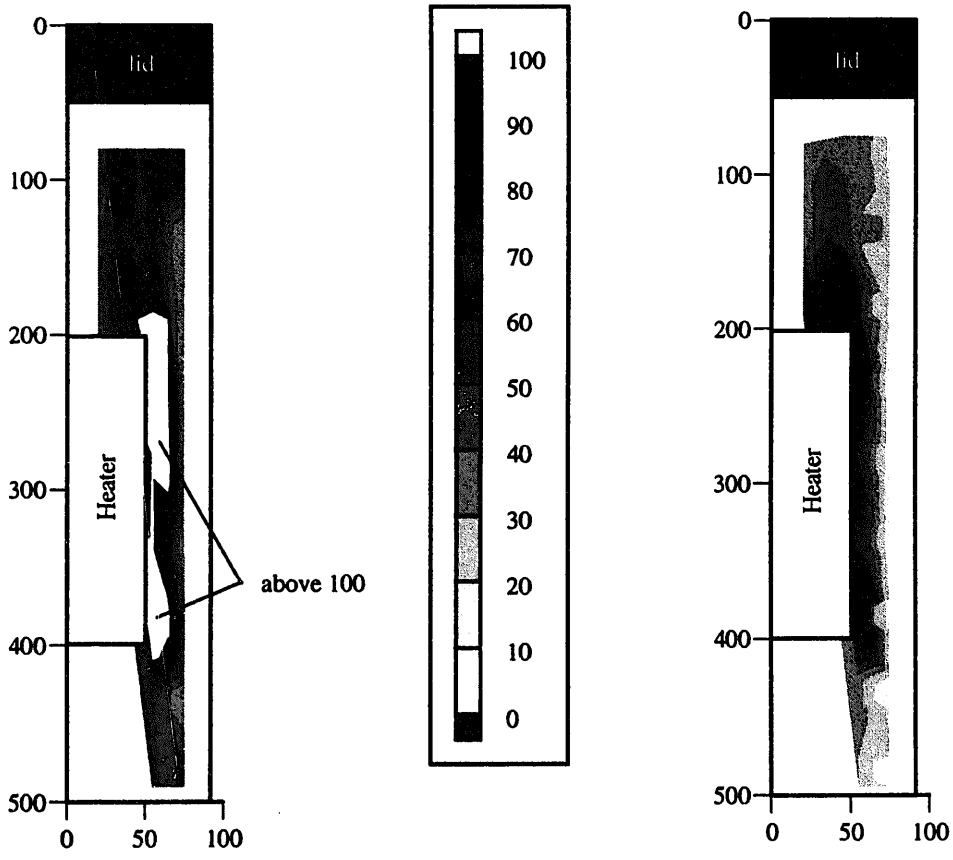

Figure 6-10 Distribution of N value
(Left; at the end of heating phase, Right; at the end of cooling phase)

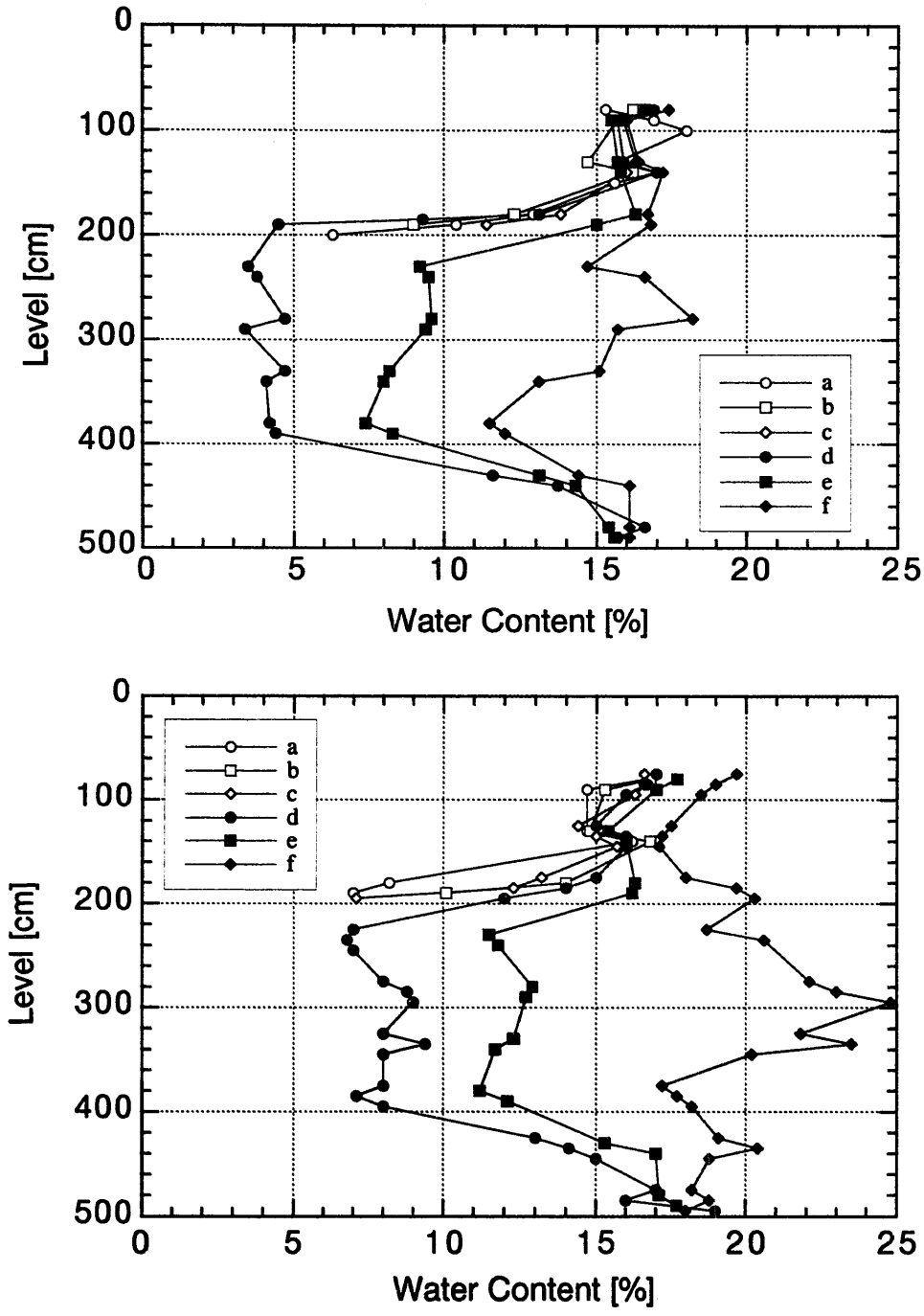

Figure 6-11 Distribution of water content in the buffer material
(Upper; at the end of heating phase, Lower; at the end of cooling phase)

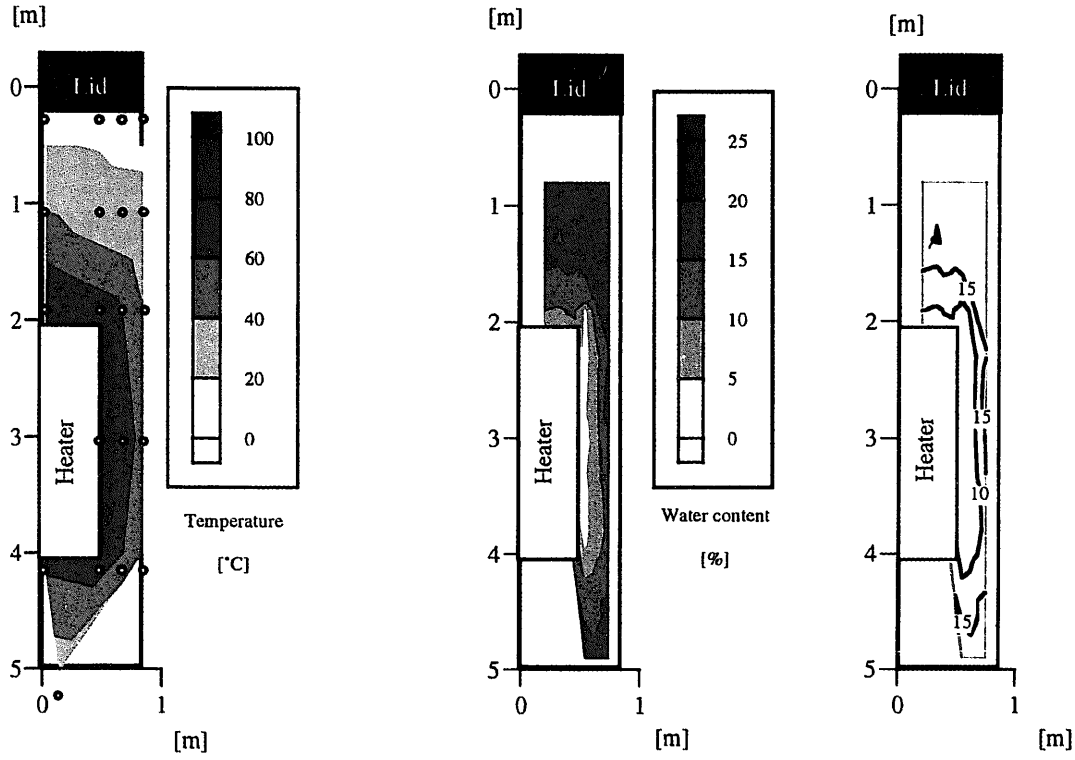

Figure 6-12 Distribution of temperature and water content at the end of heating phase

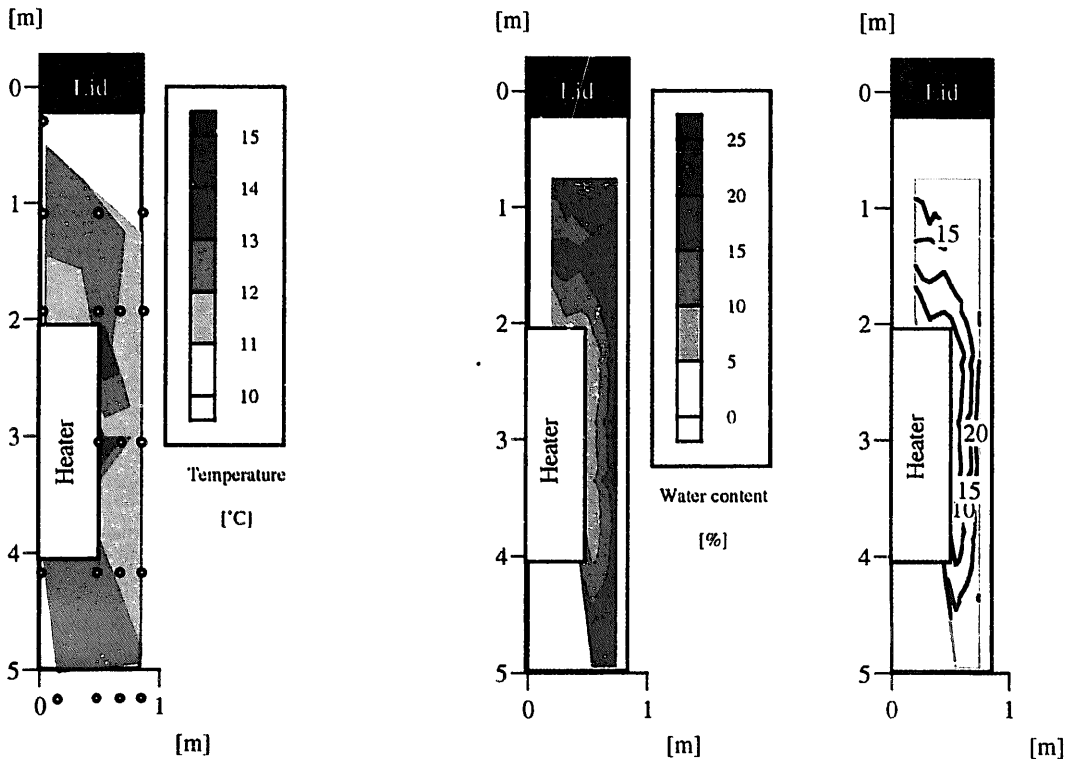

Figure 6-13 Distribution of temperature and water content at the end of cooting phase

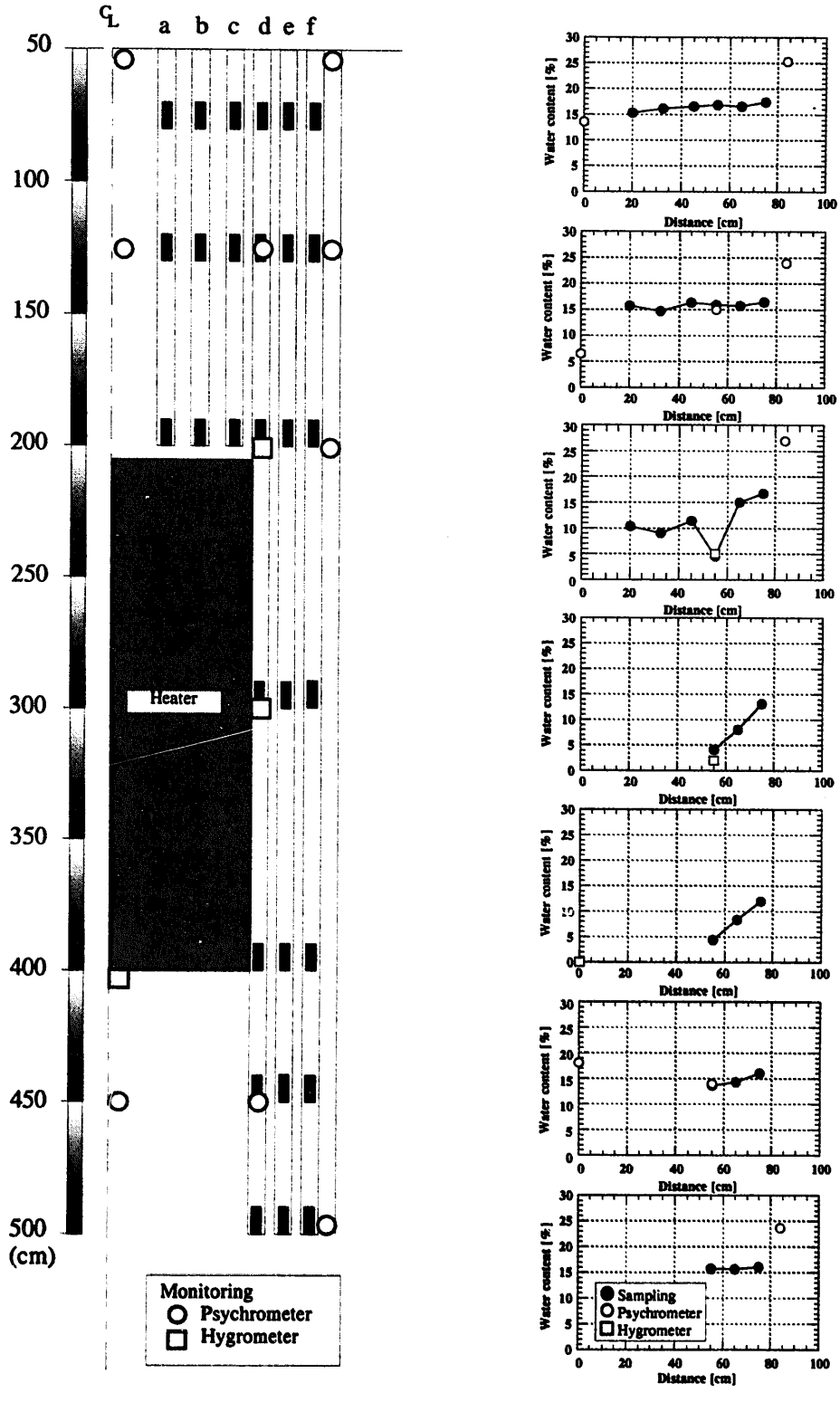

Figure 6-14 Comparison between monitoring data and sampling
[In heating phase, 250days after heater on]

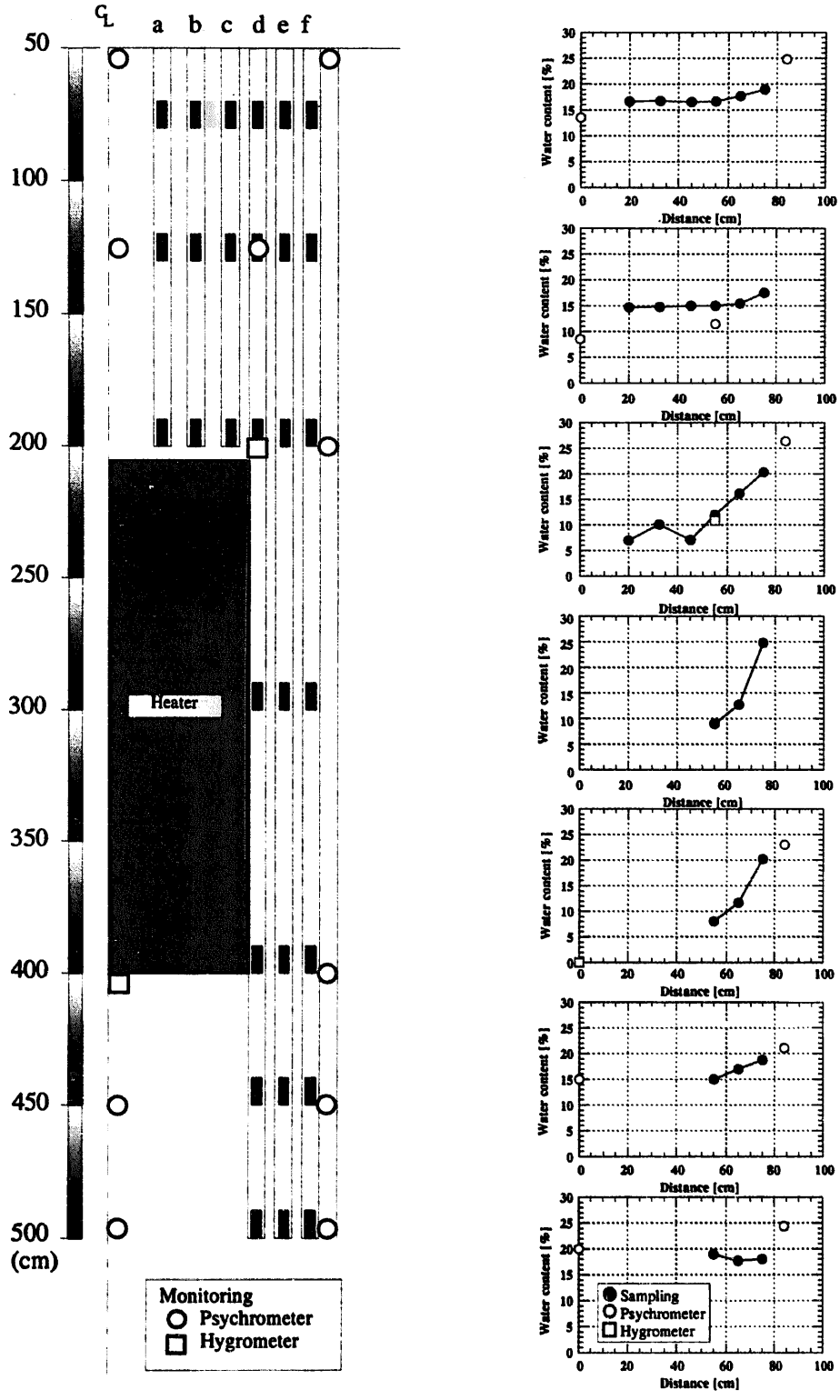

Figure 6-15 Comparison between monitoring data and sampling
[In cooling phase, 180days after heater off]

6.3 Microbial analysis

The disposal tunnel and pit would not be a sterile environment and the presence and activity of a microbial population would be expected. Therefore, the potential effects of microbial activity in the tunnel and the pit on the performance of the engineered barrier system have been assessed (Stroes-Gascoyne and West, 1994). In this experiment, some samples were taken to determine the survived bacteria in the buffer material during the heating and cooling phase. Total number of bacteria and heterotrophic bacteria were observed. Heterotrophic bacteria are one of the most important microorganisms that seem to affect the corrosion of the overpack, for example. Samples were obtained from the sampling borehole d and f at the end of heating and cooling phase. Each obtained sample was divided three pieces. Middle one was for the microbial analysis (see Figure 6-4). The surface of the sample was quickly burned and packed into the sterile plastic tube. The tube was kept in the cold storage till the analysis.

The pre-processed samples were cultured in the organic culture. Table 6-13 shows the composition of the culture. The samples were cultured at 20 °C or 50 °C for 5 days. Figures 6-16 to 6-19 show the total aerobic heterotrophic bacteria. As shown in Figure 6-16, no bacteria cells were counted in the samples that were cultured at 20°C. However, a few bacteria were detected in the samples cultured at 50°C at the point of the level 435 cm. It was considered that these bacteria were thermophilic bacteria. Around the heater, there were no bacteria during heating. In Figure 6-17, no bacteria cells were counted in the samples in cooling phase that were cultured at 50°C. This result was in good agreement with the empirical fact that thermophilic bacteria was unable to survive in the room temperature. Some bacteria were detected in the samples cultured at 20 °C in upper and lower sides of the heater. It was considered that some bacteria got into the buffer material with the infiltration of the underground water.As shown in Figure 6-18, no bacteria cells were counted around the heater. A few bacteria were detected in the samples cultured at 50 °C at the point of the level 85 cm. There were no bacteria in the samples cultured at 50 °C in cooling phase in Figure 6-19. This result also was in good agreement with the empirical fact regarding thermophilic bacteria. Some bacteria were detected in the samples cultured at 20 °C including the sample in the same level of the heater. This distribution of the bacteria was considered to depend on the infiltration of the underground water.

The total number of bacteria was unable to be detected in this analysis. The difficulty of the analysis of the total number of bacteria in bentonite was indicated by Stroes-Gascoyne and West (Stroes-Gascoyne and West, 1994).

Table 6-13 Composition of the organic culture for heterotrophic bacteria
(Reasoner, D. J. and Geldereich, E. E., 1985)

Component	Concentration (g/l)
Difco Bacto Peptone	0.50
Casamino Acids	0.50
Yeast Extract	0.50
Glucose	0.50
Soluble Starch	0.50
K_2HPO_4	0.30
$MgSO_4$ $7H_2O$	0.05
Sodium Pyruvate	0.30
Agar	15.0

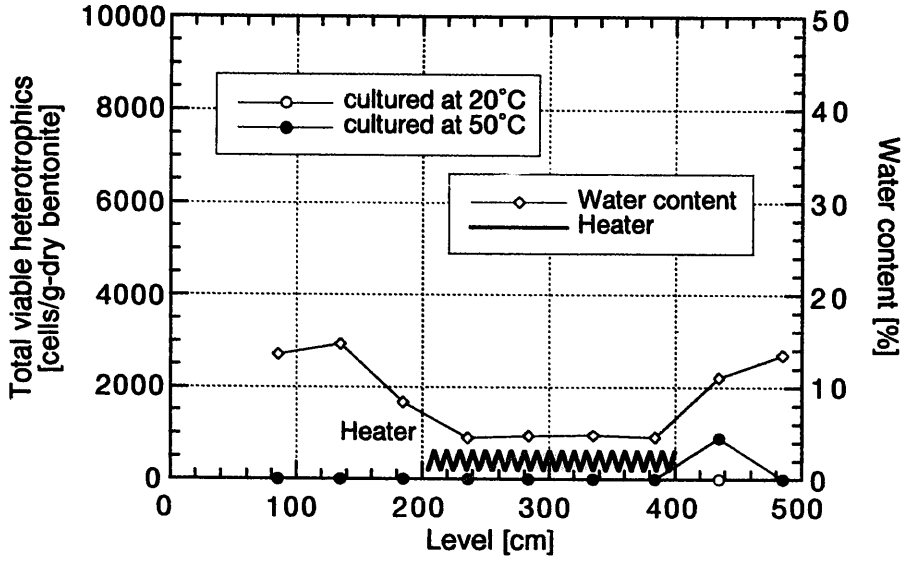

Figure 6-16 Relationship between total viable heterotrophics and water content in sampling borehole d in heating phase

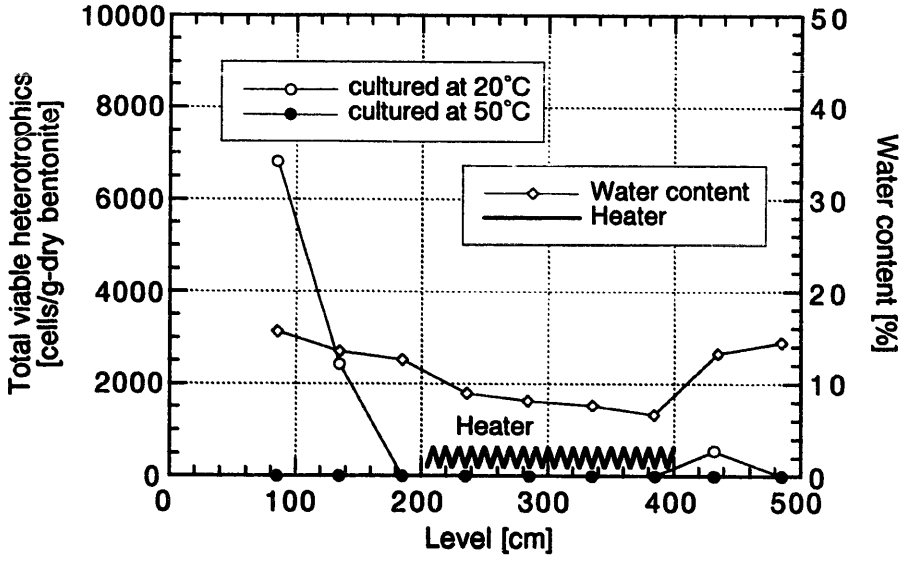

Figure 6-17 Relationship between total viable heterotrophics and water content in sampling borehole d in cooling phase

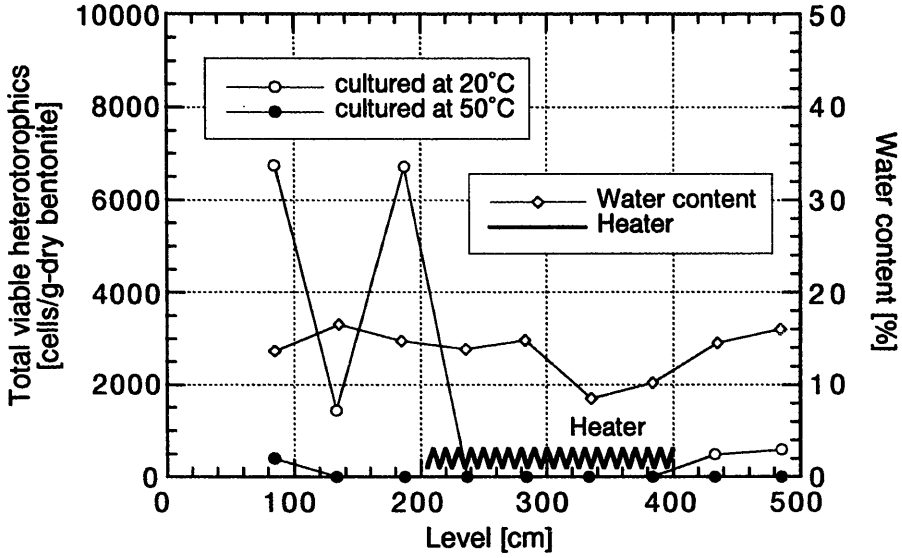

Figure 6-18 Relationship between total viable heterotrophics and water content in sampling borehole f in heating phase

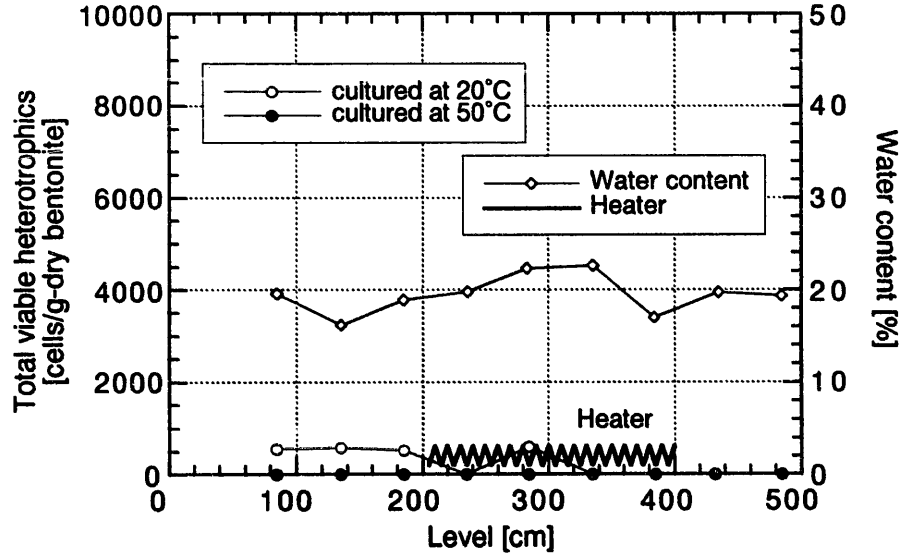

Figure 6-19 Relationship between total viable heterotrophics and water content in sampling borehole f in cooling phase

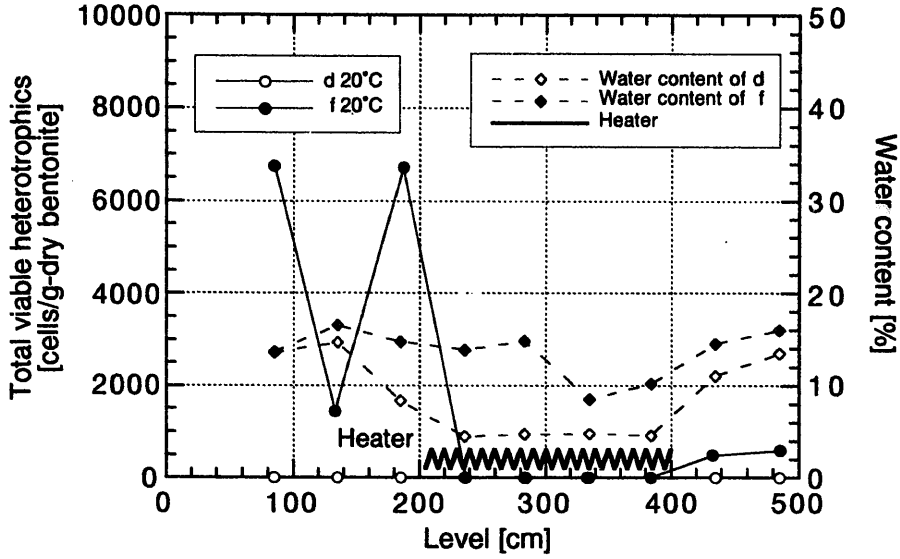

Figure 6-20 Total viable heterotrophs in heating phase samples cultured at 20 °C

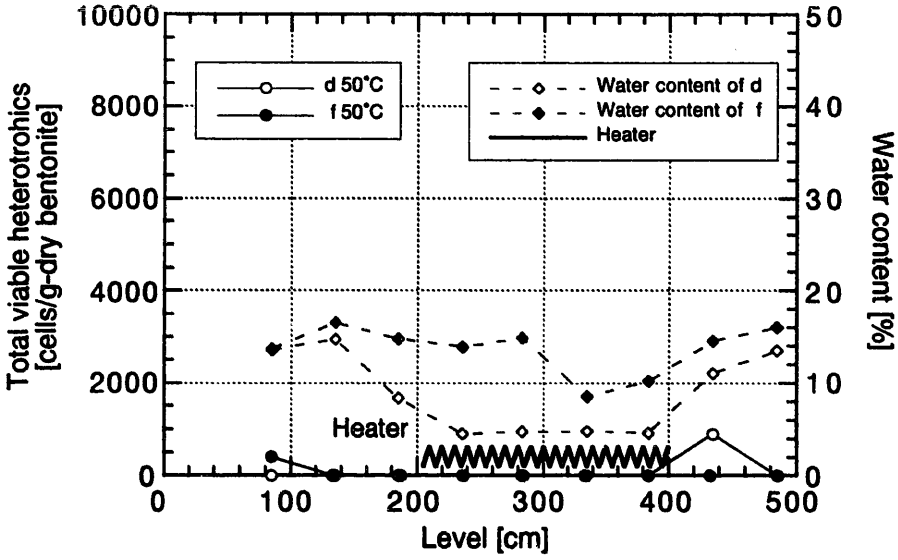

Figure 6-21 Total viable heterotrophs in heating phase samples cultured at 50 °C

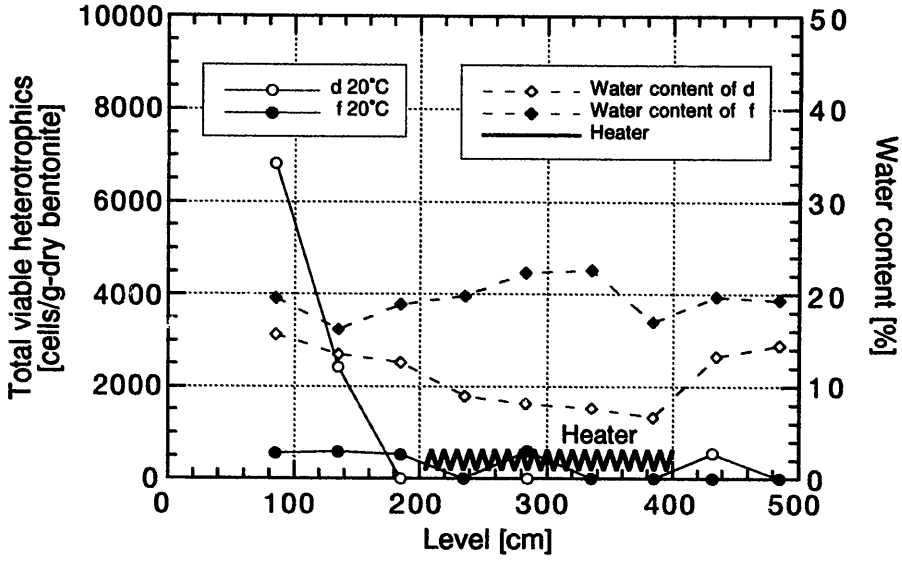

Figure 6-22 Total viable heterotrophs in cooling phase samples cultured at 20 °C

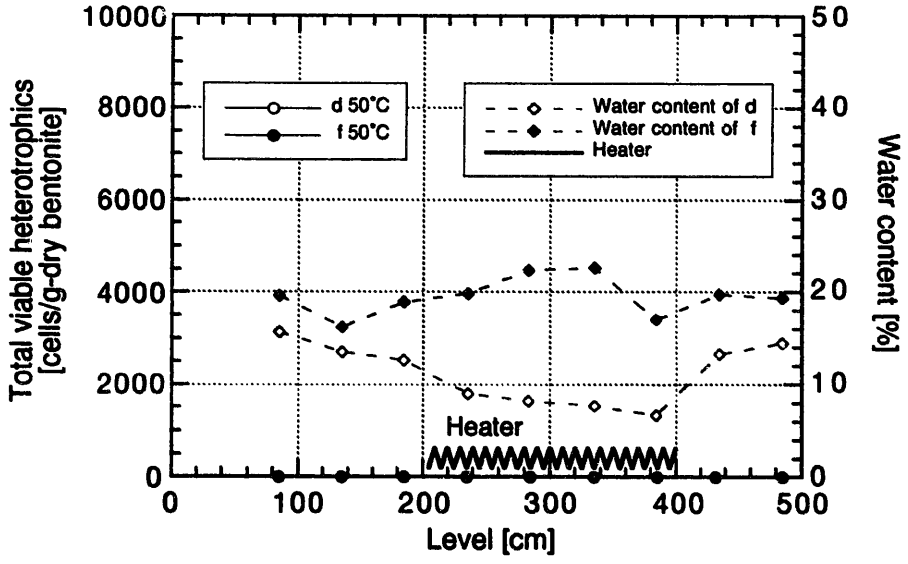

Figure 6-23 Total viable heterotrophs in cooling phase samples cultured at 50 °C

7. Decommissioning of the test pit

Decommissioning of the test pit was performed to observe the distribution of water content of the whole buffer material in the pit and the environmental conditions of the buffer material around heater. Sampling schedule was as follows.

Decommissioning phase
Sampling -May 8 to June 30, 1998

7.1 Distribution of water content and density of the buffer material

Figure 7-1 shows the sampling points in decommissioning phase. Water content was measured in the sections of a, b, c, d, e, f, g, h, i and j. Dry density was measured on the sections of I, II and III. Decommissioning of the buffer material in the test pit conducted from the top to the bottom. Section a, b and c had 2 sampling lines and there were 33 measurement points. Section d, e, f and g had 2 sampling lines and there were 16 points. Section h, I and j had 16 sampling lines and there were 165 points. Section I had 2 sampling lines and there were 12 points. Section II had 2 sampling lines and there were 8 points. Section III had 2 sampling lines and there were 13 points.

Figure 7-2 shows the contour map of water content on each vertical section, O-AB, O-CD, O-BBC, O-DDA. In all sections, distribution of water content was almost same. Water content nearby rock mass was around 25 % as saturated water content. Around heater, water content was below 10 %.

Figure 7-3, 7-4 and 7-5 show the contour maps of water content on the horizontal section. Distribution of water content was approximately concentric circle. Nearby point A and D, water content was little high. In this direction, monitoring sensor cables were led to the top of the test pit. It was considered that emplacement of the buffer material around those points were not completely in setting up it.

Figure 7-6 shows the sampling points of the detail sampling section for the distribution of water content in one layer. This Figure shows the plane and the cross section of the sampling points. Sampling points were the top of each layer and the inside of the layer. Figure 7-7 shows the distribution of water content of each section in one layer. The distribution of water content in each layer was approximately uniform in vertical direction.

Density of the buffer material was measured using core cutter. Figure 7-8 shows the distribution of wet density of the buffer material. Wet density was around 1.90-2.10 g/cm^3. Figure 7-9 shows the distribution of dry density of it. Dry density was around 150-1.80 g/cm^3. The points adjoined to the rock mass had low density. It was considered that the complete emplacement of the buffer material in those areas was difficult.

7.2 Dehydrated cracks

All heater frames were removed, when decommissioning of the buffer material was on the level 400. Some cracks were observed on the interface between surface of heater frame and the buffer material. Figure 7-10 shows the crack map of the buffer material. It was considered that the thermal effect of the heater caused dehydration of the buffer material. Cracks were

distributed at random and there was no tendency. Some cracks had above 10 cm in depth. Next layer on level 410 had also some cracks.

7.3 Environmental conditions of the buffer material

The environmental conditions, which are related to metal corrosion in the buffer material, were measured around heater frame. Measurement items were resistivity, polarization resistance, corrosion potential, heater to soil potential, corrosion rate by measuring polarization resistance on test prove, oxidation-reduction potential, and pH.

Figure 7-11 shows the measured points for the conditions. The measurements were carried out at levels of 185, 205, 260, 310, 360 and 390 cm. Oxidation-reduction potential (Eh) and pH were measured at the points of 59, 69 and 79 cm on measuring line BC away from the center of the heater. Other parameters were measured basically in measuring lines BC, C and DAA. Additional measuring line was ABB-B on level 390 cm. There were 2 points as 65 and 80 cm away from the center of the heater. There was only one point in each measuring line on level 185 cm. Additional measuring points were located between point 65 and 80 in all measuring lines on level 310 cm.

Figure 7-12 shows the measurement method of the environmental conditions. Measurement holes were drilled 10cm in depth. Measurement prove was hammered into the buffer material. Resistivity, polarization resistance, corrosion potential, heater to soil potential, corrosion rate by measuring polarization resistance on test prove were measured.

Table 7-1 shows the results of resistivity, polarization resistance, corrosion potential, heater to soil potential, corrosion rate by measuring polarization resistance on test prove. The values of resistivity range from 312 to 3330 ohm cm. The values of polarization resistance range from 44 to 1620 ohm. All data of corrosion potential were around –750 mV. Heater to soil potential range from –576 to –242 mV. The values of corrosion rate by measuring polarization resistance on test probe range from 0.018 to 0.613 mm/y.

Table 7-2 shows the results of oxidation-reduction potential (Eh) and pH. Eh was measured by a portable Eh meter and pH was measured by a portable pH meter. The values of Eh range from 292 to 467 mV vs SHE, and the walues of pH range from 6.6 to 8.2.

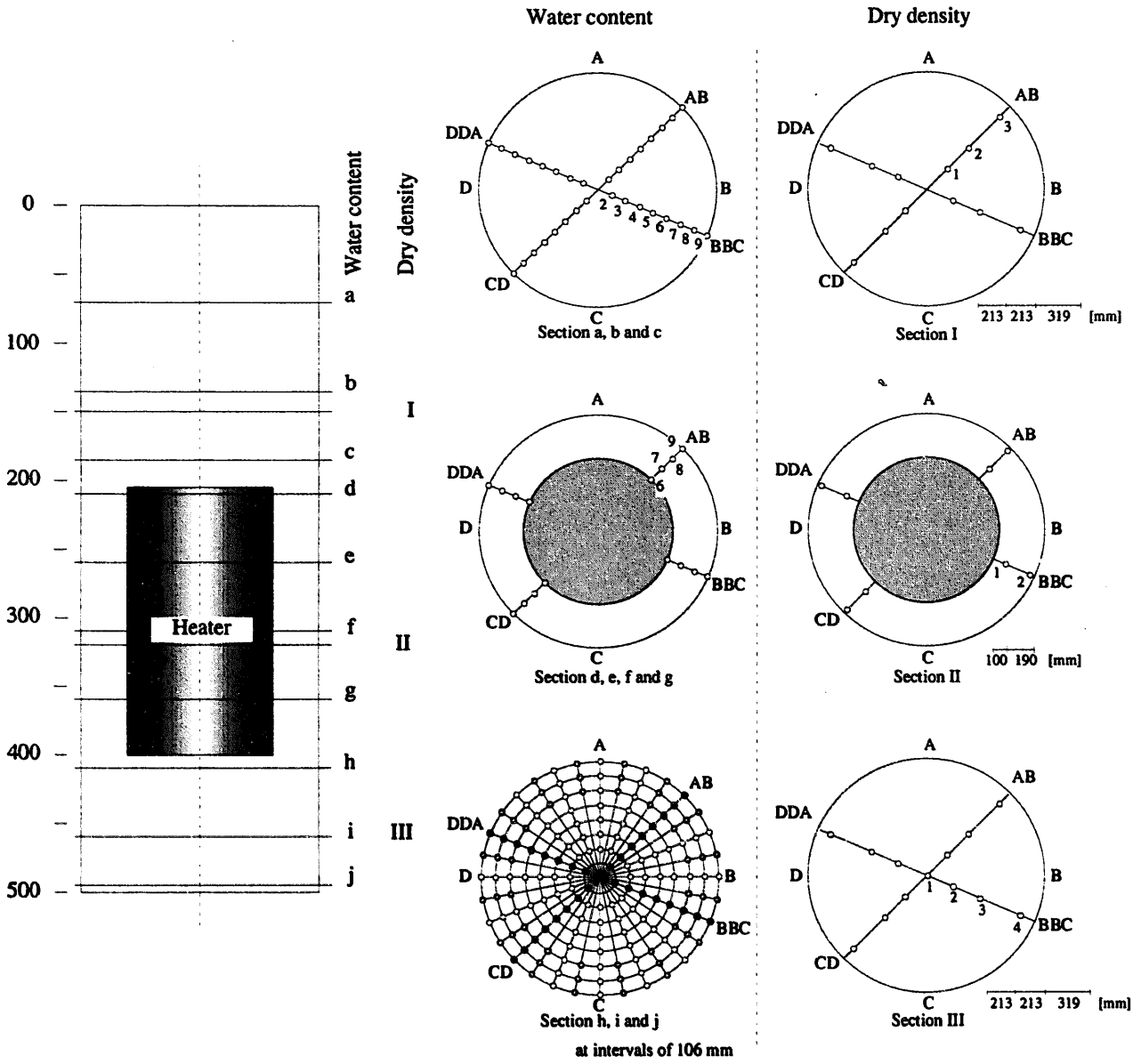

Figure 7-1 Sampling points
(in decommision phase)

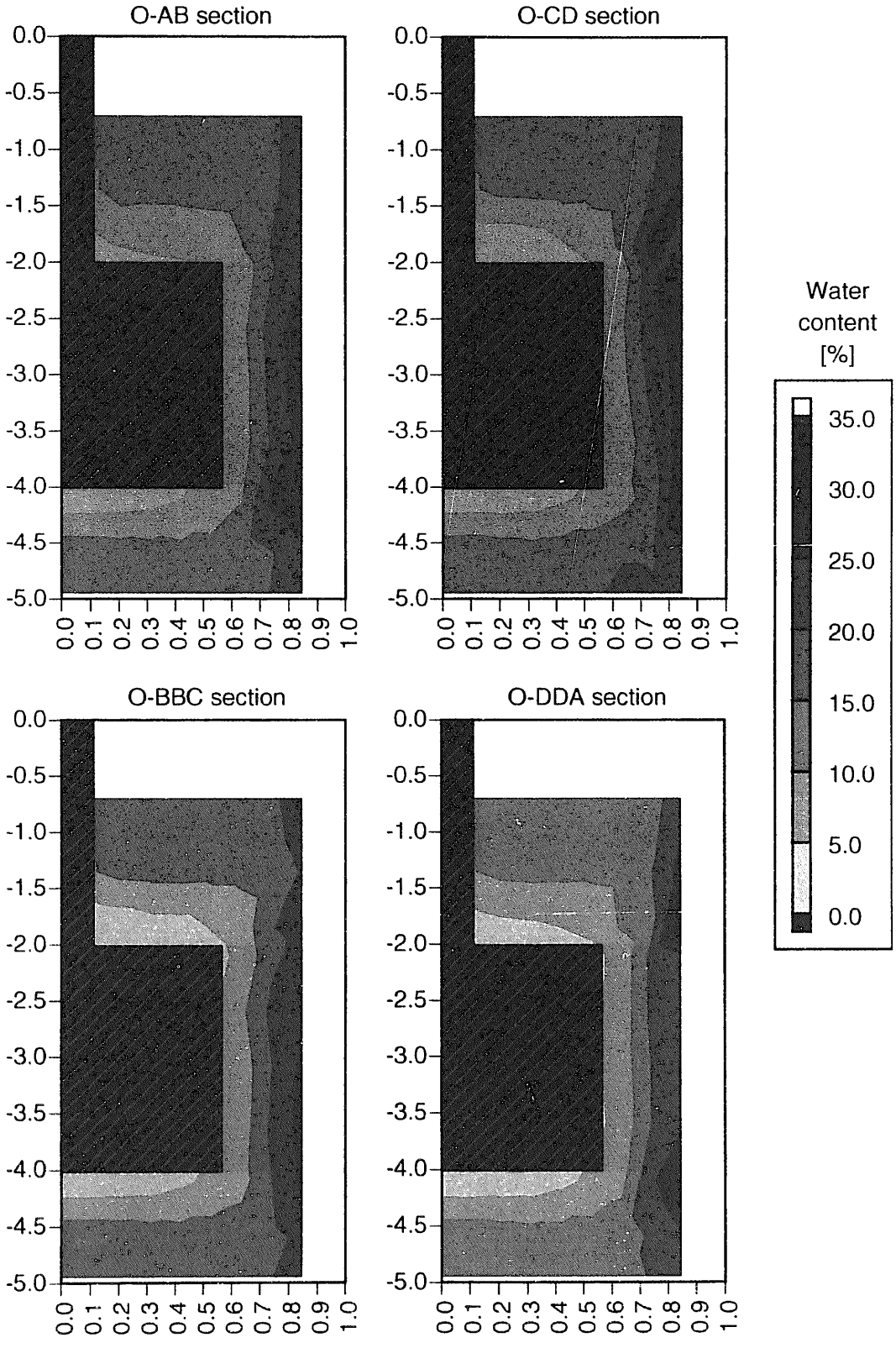

Figure 7-2 Contour map of the test pit on vertical section

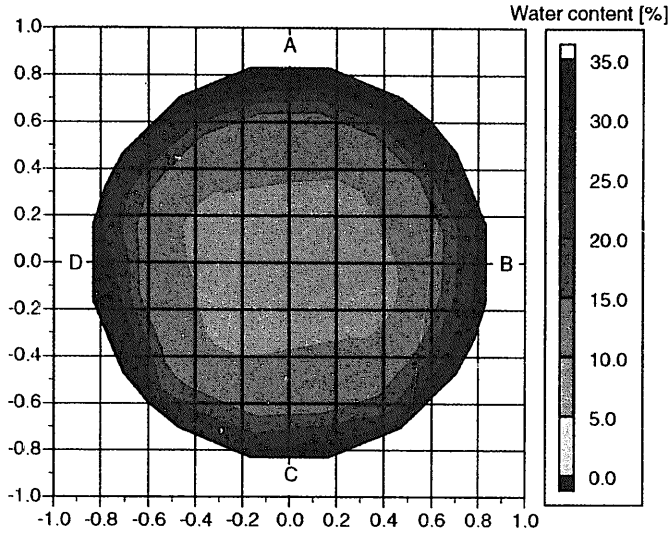

Figure 7-3 Contour map of the horizontal section h (410 level)

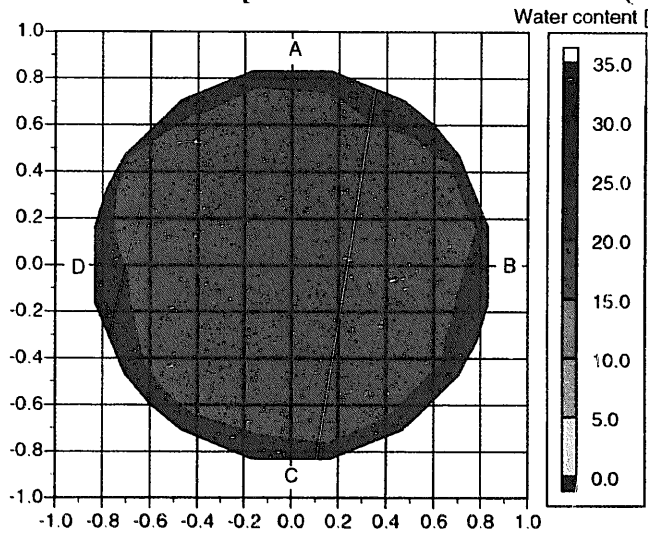

Figure 7-4 Contour map of the horizontal section i (460 level)

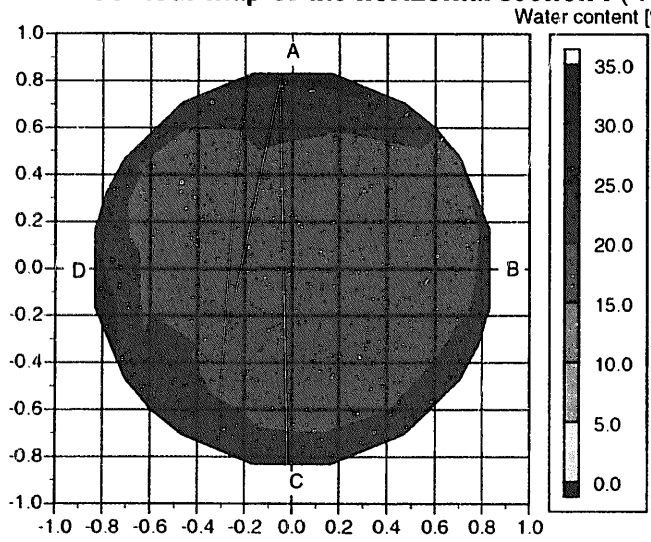

Figure 7-5 Contour map of the horizontal section j (490 level)

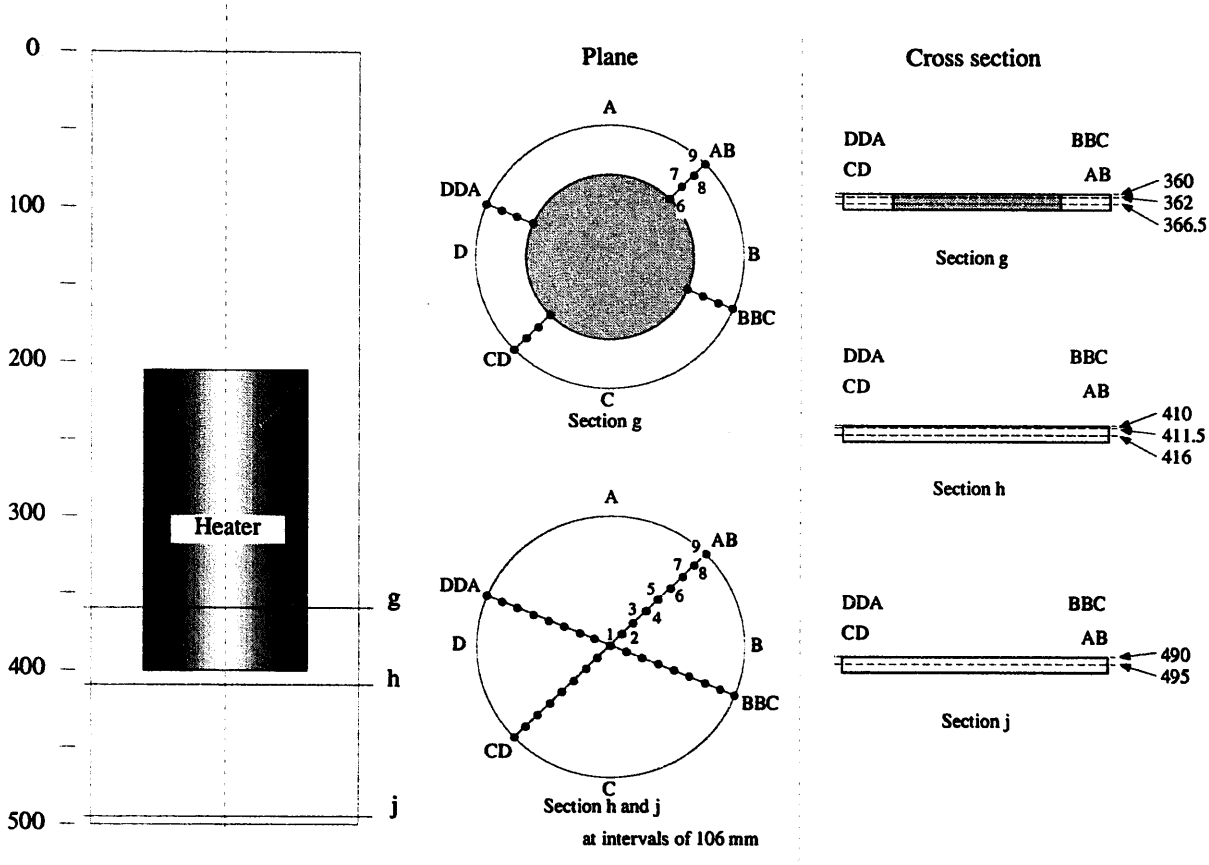

Figure 7-6 Sampling points
(in one layer)

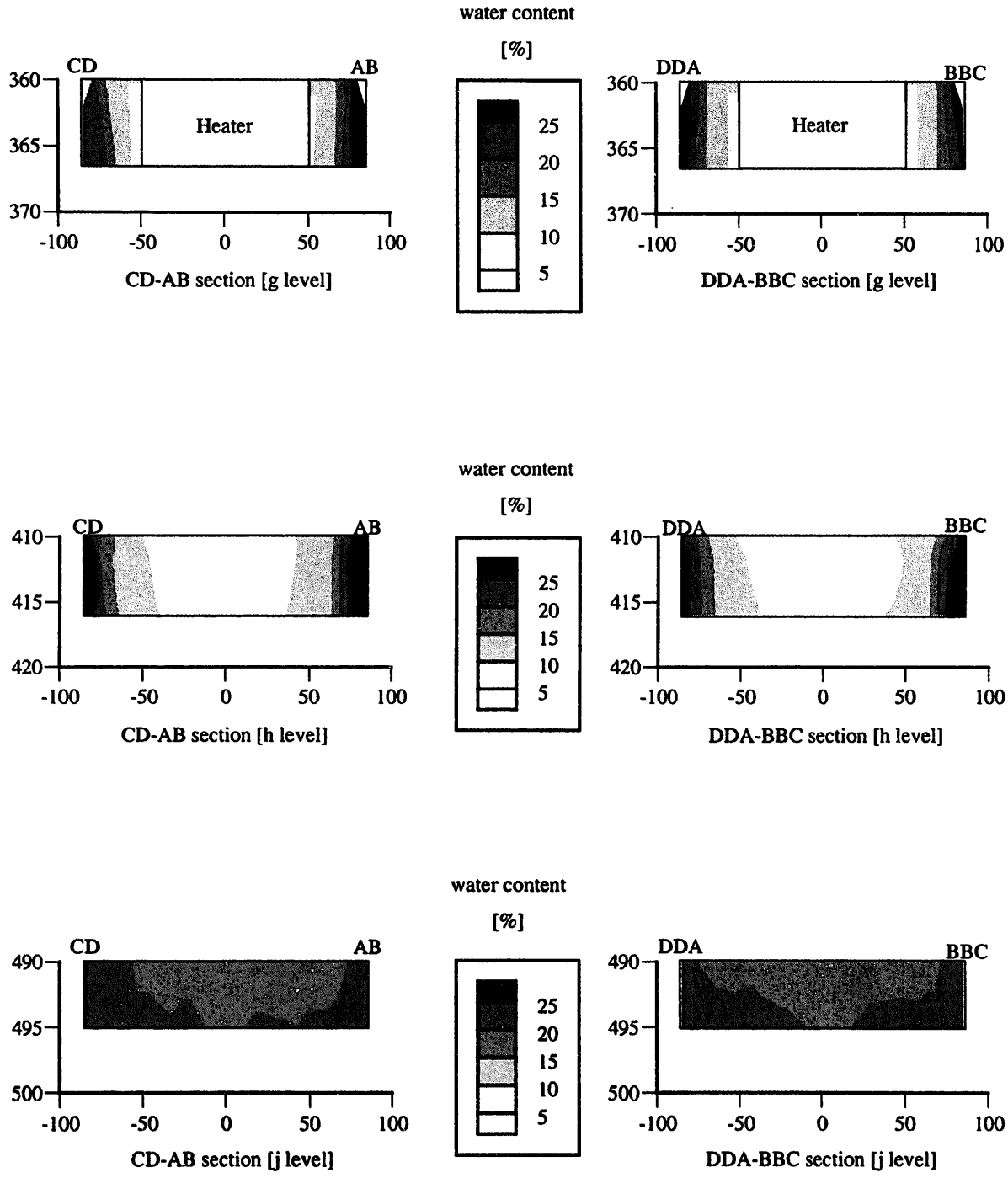

Figure 7-7 Distribution of water content
in vertical sections on g, h and j levels

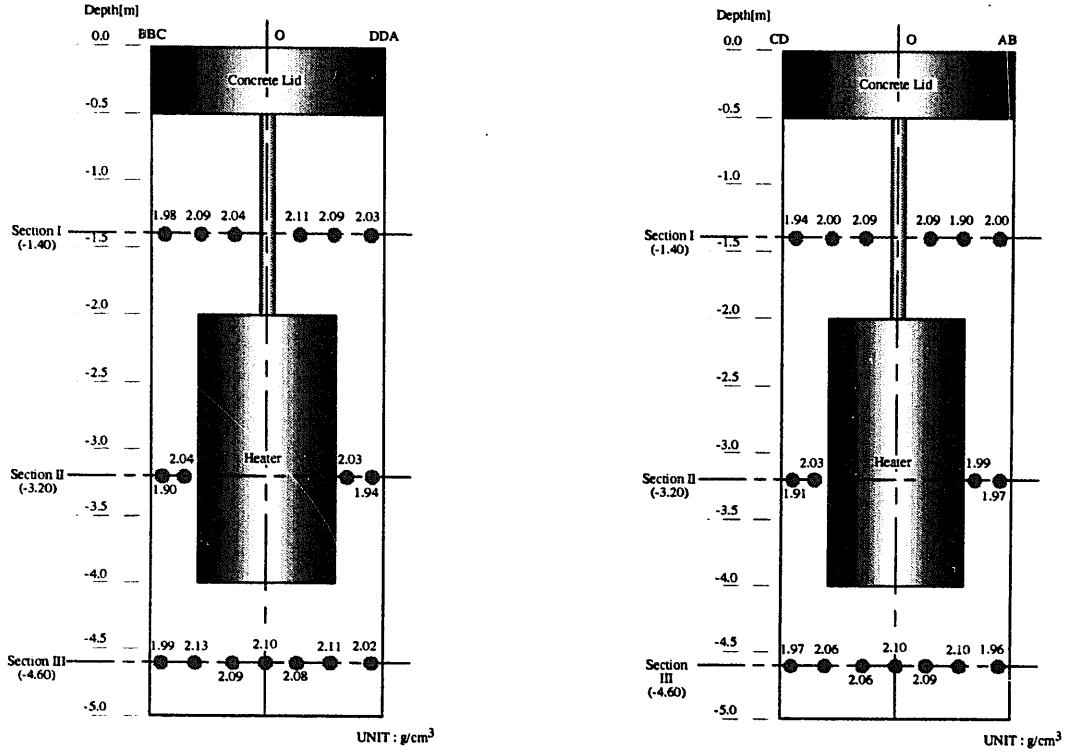

Figure 7-8 Distribution of wet density of the baffer material
(Left; section BBC-O-DDA, Right; section CD-O-AB)

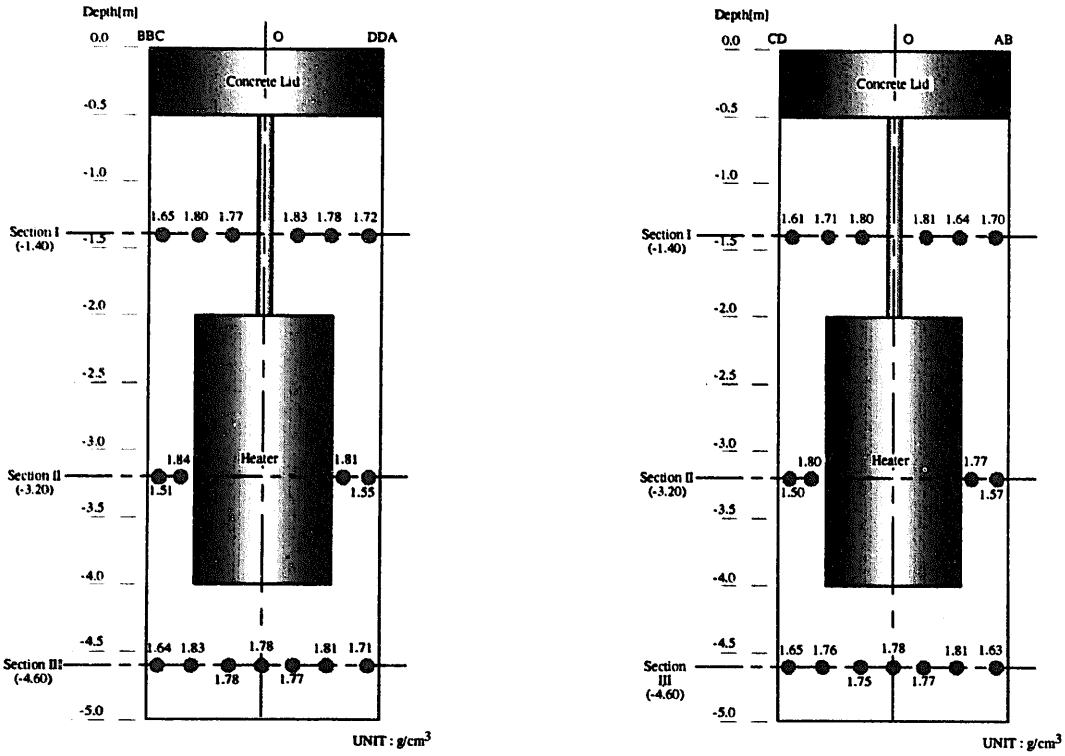

Figure 7-9 Distribution of dry density of the baffer material
(Left; section BBC-O-DDA, Right; section CD-O-AB)

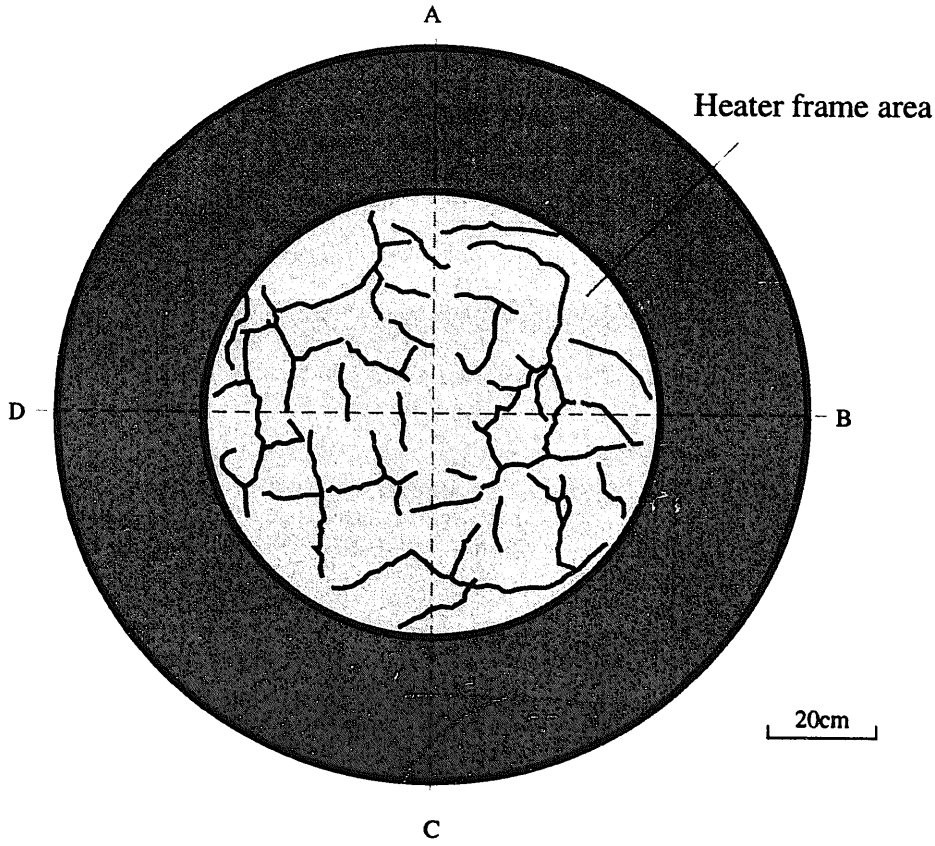

Figure 7-10 Crack map of the buffer material touched
the surface of the heater (400 level)

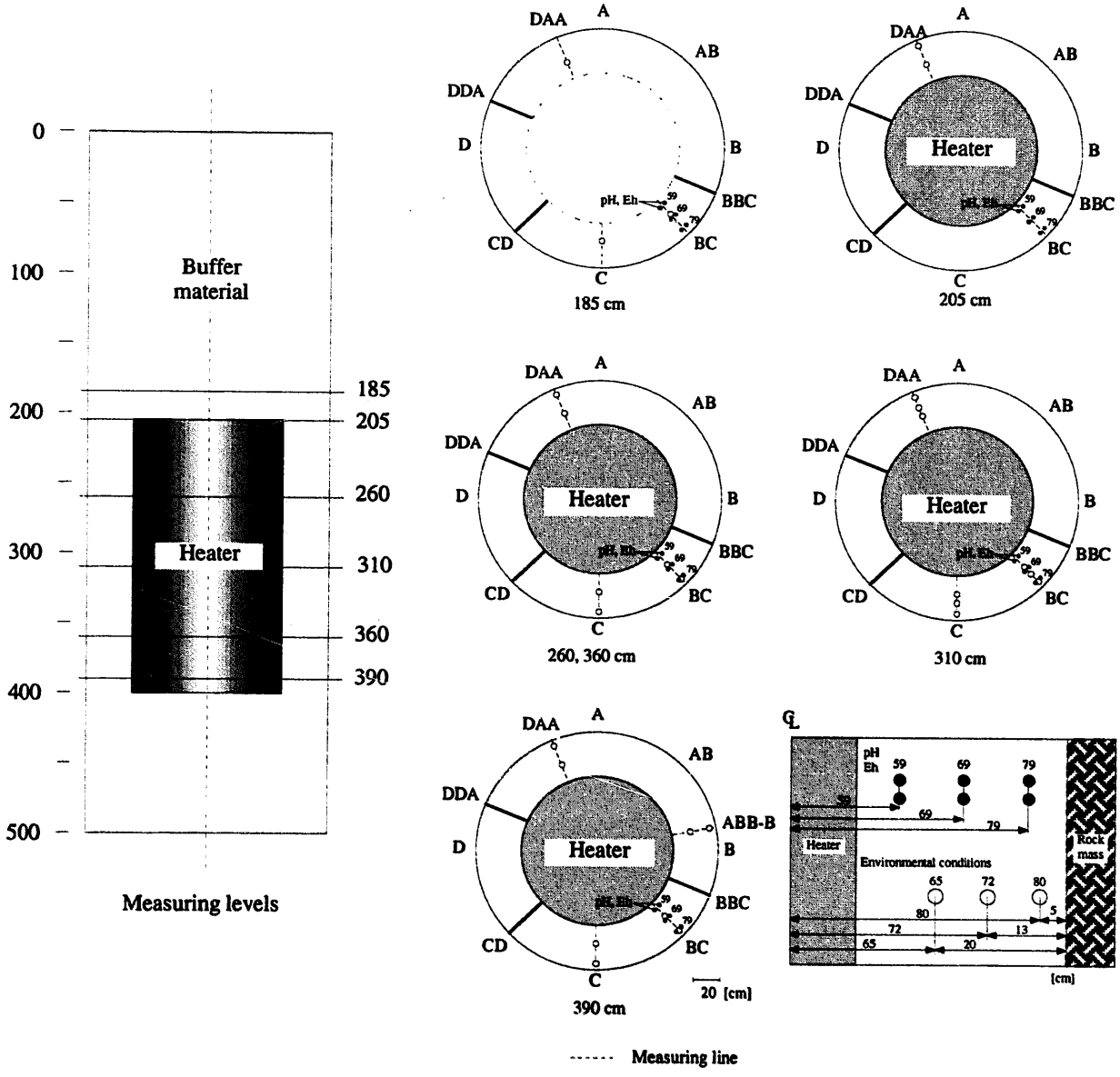

Figure 7-11 Measuring points for the environment of the buffer material

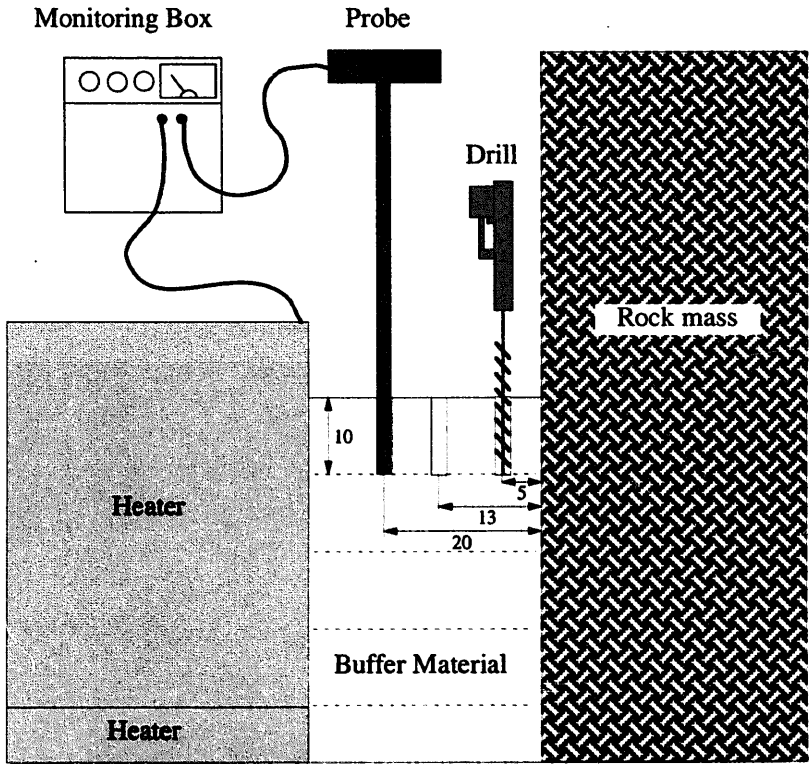

Figure 7-12 Measurement of the environmental conditions of the buffer material

Table 7-1 Environmental conditions of the buffer material

Dicommissioning Level [cm]	Measuring Level [cm]	Resistivity [ohm cm]										
		BC			C			DAA			ABB-B	
		65	72	80	65	72	80	65	72	80	65	80
185	195	550			319			3330				
205	215							752		340		
260	270	952		354	632		332	883		365		
310	320	1445	362	344	642	375	350	857	425	340		
360	370	3215		548	2280		344	1430		378	2165	405
360	375	806		354	1030		340	1050		376	1685	351
390	400	797		341	572		338	941		345	999	367
390	405	574		363	550		312	803		323	731	338

Dicommissioning Level [cm]	Measuring Level [cm]	Polarization resistance [ohm]										
		BC			C			DAA			ABB-B	
		65	72	80	65	72	80	65	72	80	65	80
185	195	256			116			1620				
205	215							139		159		
260	270	82		85	67		69	89		56		
310	320	103	65	71	80	74	78	57	44	48		
360	370	545		103	328		101	263		52	407	81
360	375	85		73	167		108	130		64	371	87
390	400	117		103	92		103	78		58	112	88
390	405	109		126	106		112	97		65	89	89

Dicommissioning Level [cm]	Measuring Level [cm]	Corrosion potential [mV]										
		BC			C			DAA			ABB-B	
		65	72	80	65	72	80	65	72	80	65	80
185	195	-810			-743			-752				
205	215							-736		-770		
260	270	-755		-801	-745		-785	-734		-759		
310	320	-733	-792	-792	-757	-801	-808	-719	-756	-779		
360	370	-722		-786	-735		-808	-643		-771	-697	-789
360	375	-747		-798	-723		-819	-747		-788	-722	-806
390	400	-782		-832	-773		-815	-702		-795	-734	-821
390	405	-808		-832	-791		-827	-710		-812	-752	-825

Dicommissioning Level [cm]	Measuring Level [cm]	Heater to soil potential [mV]										
		BC			C			DAA			ABB-B	
		65	72	80	65	72	80	65	72	80	65	80
185	195	-365			-345			-319				
205	215							-564		-576		
260	270	-248		-250	-242		-244	-246		-244		
310	320	-260	-257	-262	-269	-274	-277	-255	-257	-256		
360	370	-280		-274	-301		-305	-250		-256	-297	-300
360	375	-277		-275	-302		-307	-254		-259	-297	-302
390	400	-293		-306	-297		-298	-293		-256	-304	-305
390	405	-296		-310	-293		-303	-293		-308	-304	-304

Dicommissioning Level [cm]	Measuring Level [cm]	Corrosion rate by measuring polarization resistance on test probe [mm/y]										
		BC			C			DAA			ABB-B	
		65	72	80	65	72	80	65	72	80	65	80
185	195	0.257			0.110			0.018				
205	215							0.246		0.182		
260	270	0.344		0.329	0.421		0.402	0.301		0.496		
310	320	0.276	0.434	0.399	0.343	0.385	0.357	0.523	0.613	0.608		
360	370	0.052		0.272	0.082		0.281	0.105		0.536	0.073	0.342
360	375	0.336		0.377	0.189		0.263	0.221		0.427	0.081	0.311
390	400	0.243		0.228	0.311		0.270	0.368		0.474	0.256	0.316
390	405	0.287		0.229	0.277		0.245	0.307		0.423	0.320	0.307

Table 7-2 Oxidation-reduction potential and pH of the buffer marterial

Dicommissioning Level [cm]	Measuring Level [cm]	Oxidation-reduction potential [mV vs SHE]								
		BC 59		Ave.	BC 69		Ave.	BC 79		Ave.
185	195	417	389	403	432	406	419	291	293	292
205	215	442	362	402	412	397	405	377	367	372
260	270	370	311	341	326	335	331	288	317	303
310	320	453	320	387	451	414	433	469	428	449
360	370	498	344	421	507	427	467	475	459	467
390	400	508	351	430	492	430	461	443	439	441

Dicommissioning Level [cm]	Measuring Level [cm]	pH								
		BC 59		Ave.	BC 69		Ave.	BC 79		Ave.
185	195	7.1	7.2	7.2	6.6	7.2	6.9	7.1	7.6	7.3
205	215	7.0	8.1	7.5	6.5	7.6	7.0	7.7	7.9	7.8
260	270	6.7	9.1	7.9	7.0	7.8	7.4	8.1	8.4	8.2
310	320	6.5	8.8	7.7	8.2	8.2	8.2	7.5	7.6	7.6
360	370	5.8	7.4	6.6	6.2	7.9	7.0	7.3	8.9	8.1
390	400	6.8	7.9	7.3	6.5	8.0	7.2	8.0	8.3	8.2

8. Summary

For the safety assessment of the high-level radioactive waste, it is necessary to evaluate the coupled thermal, hydraulic and mechanical phenomena that will be occurred in the rock mass and engineered barrier due to the effect of heat generation of waste, groundwater inflow and stress in the geoenvironment. These phenomena will be elucidated through the study by the laboratory tests, mock-up tests and in-situ tests. "Coupled Thermo-Hydro-Mechanical Experiment at Kamaishi Mine" was performed as a part of in-situ experiment.

The feature of this experiment is that this experiment has been adopted as a test case of international project "DECOVALEX" and "VALUCLAY". Therefore, this experiment reflects many opinions and comments from the researchers in the world. As a result, we were able to carry out the experiment efficiently.

Studies subject of the in-situ experiment includes the measurement of the coupled phenomena, understanding of the coupled phenomena and the evaluation by the analysis model, and so on. We summarize the important factor about the measurement method and analysis approach that was obtained by this experiment.

①Measurement method

It is important to observe the phenomena that will be occurred in the near field for a long term after the radioactive waste is disposed in order to contribute to the safety assessment of the geological disposal. However, it was difficult to continue the experiment by the limit of the site in the case of Kamaishi mine. In this experiment, the duration of heating phase was only 8 months, and it means that we only obtained the data in a short time as compared with actual disposal period. However, this data is very valuable because the period of this in-situ experiment corresponds to a transitional period just after the radioactive waste is disposed. One of the major problems in the in-situ experiment is applicability evaluation of the measurement technique. In fact, high-precision measurement will be required under the rigorous conditions like high temperature, high stress and high pore pressure in the case of actual geological disposal site. The situation of this in-situ experiment is more or less similar to the actual condition of the geological disposal site, therefore, it will be able to evaluate the applicability of the measurement method from the obtained data.

(1) Thermal effect

The temperature in the buffer and the rock mass was measured by several kind of the sensors. The different sensors at the same point showed almost the same value and the proper temperature distribution was obtained in this experiment.

The heat flux changed rapidly just after the heater was turned on. This means that the heat flux meter can measure the heat flow in the engineered barrier prior to the increasing of the temperature in the buffer and the rock, that is, the sensitivity of the sensors are confirmed.

(2) Hydraulic effect

The movement of the water in the buffer was measured by the thermocouple psychrometer and the hygrometer with accuracy. As a results, the quick movement of water in the buffer from the heater side to the rock side due to the thermal gradient was observed. Furthermore, after the heater was turned off, the water movement taking a relatively long time in the buffer from the outside to the heater side was also observed.

However, some sensors were broken down and measurement value exceeds the limitation during the test period. Therefore, these are important subjects to investigate the cause of failure, to develop the durable sensor and to make efforts on the improvement of the measurement range of the sensor.

(3) Mechanical effect

The total pressure in the buffer was measured by the small-scale pressure cell. The measurement data that was measured by the sensor on the rock surface indicate wide variation as shown in Chapter 5. The reason may be that rock surface is not smooth enough for the pressure cell that was used in this experiment.

②Analysis approach

The disposal environment is complex as mentioned above. Therefore, the unpredicted phenomena may occur. In practice, interesting phenomena was observed in Kamaishi experiment, e.g., diameter change of the test pit, inflow rate distribution into the test pit, infiltration distribution into the buffer from the rock mass and occurrence of the swelling pressure, and so on. Consequently, it is important to evaluate these phenomena by the numerical model and to predict the long-term phenomena. Here, we must try to explain these phenomena by using the existing numerical model and the information that will need for the numerical analysis, e.g., rock property, boundary condition and initial condition. When it is difficult to explain these measured phenomena as the result of above approach, it is important to clarify the cause of this discrepancy. These studies will contribute to the development of the analysis approach to evaluate the near-field phenomena for the geological disposal of the high-level radioactive waste management.

We summarize the Kamaishi T-H-M experiment from the standpoint of analysis approach and show the subjects in the future.

(1) Thermal effect

Temperature of the heater (waste package) is important as the inner boundary condition. In this experiment, output power of the heater was controlled by the temperature at the bottom of heater. As a result, temperature of the heater at this control point became almost constant at the steady state. However, there is difference in temperature at the heater surface. Consequently, it is a subject in the future to clarify the cause of this phenomenon.

(2) Hydraulic effect

Pore pressure distribution in the rock mass is important just as the permeability distribution in order to evaluate the hydraulic effect in the near field. In this experiment, the flooding pool on the floor of the test drift was set to establish the hydraulic boundary condition.

The water movement from the heater side to the rock side during the heating phase and the water movement from the rock side to the heater side during the cooling phase show the validity of the assumption that water movement

existing fracture and occurrence of the new fracture, and so on. However, in this experiment, thermal energy was only due to one heater and heating period was only eight months, that is, thermal energy was small and heating period was short as compared with actual condition of the geological disposal of the high-level radioactive waste. As a result, it is conceivable that the obvious change of the strain both in the buffer and the rock was not measured. The causes of stress generation in the engineered barrier are considered due to the swelling pressure in the buffer by the infiltration of the groundwater from the rock and the thermal expansion of the engineered barrier and rock, and the change of the pore pressure, and so on. These correlations are complex, resulting in occurrence of the complex stress field.

References

Campbell, G.S. and Gardner, W.H. (1971): Psychrometric measurement of soil water potential: Temperature and bulk density effects, Soil Sci. Soc. Am. Proc., 35, 8-12.

Chijimatsu,M., Fujita,T. , Sugita,Y. and Ishikawa,H. (1996a): Coupled thermo-hydro-mechanical experiment at Kamaishi mine, Technical Note 03-95-03, Initial data around T-H-M experiment area, PNC TN8410 96-057, Power Reactor and Nuclear Fuel Development Corporation (PNC)

Chijimatsu,M. , Fujita,T. , Sugita,Y. and Ishikawa,H. (1996b): Coupled thermo-hydro-mechanical experiment at Kamaishi mine, Technical Note 05-95-05, Laboratory rock property tests, PNC TN8410 96-060, Power Reactor and Nuclear Fuel Development Corporation (PNC)

Chijimatsu,M. , Fujita,T. , Sugita,Y. , Ishikawa,H. and Kobayashi,A. (1996c): Coupled thermo-hydro-mechanical experiment at Kamaishi mine, Technical Note 07-95-07, Hydraulic tests, PNC TN8410 96-058, Power Reactor and Nuclear Fuel Development Corporation (PNC)

Chijimatsu,M., Fujita,T., Sugita,Y. and Ishikawa,H. (1996d): Coupled thermo-hydro-mechanikal experiment at Kamaishi mine, Technical Note 02-95-02, instrumentation, PNC TN8410 96-056, Power Reactor and Nuclear Fuel Development Corporation (PNC)

ENRESA (1998): FEBEX, Full-Scale Engineered Barriers Experiment in Crystalline Host Rock, Pre-Operational Stage Summary Report.

Fujita,T., Saotome,A. and Hara,K. (1992): Mechanical property of the buffer material, PNC TN8410 92-170, Power Reactor and Nuclear Fuel Development Corporation (PNC).

Fujita,T., Moro,Y., Hara,K. and Amemiya,K. (1993): Full-Scale Test on Thermo- Hydro-Mechnical Process in Engineered Barrier System, '93 Joint CSCE-ASCE National Conference.

Fujita,T., Chijimatsu,M., Ishikawa,H. Suzuki,H. and Matsumoto,K. (1994): Coupled thermo-hydro-mechanical experiment at Kamaishi mine, Technical Note 01-95-01, Plan, PNC TN8020 94-005, Power Reactor and Nuclear Fuel Development Corporation (PNC)

Fujita,T., Sugita,Y., Chijimatsu,M. and Ishikawa,H. (1996a): Coupled thermo-hydro-mechanical experiment at Kamaishi mine, Technical Note 04-95-04, Fracture characteristics, PNC TN8410 96-061, Power Reactor and Nuclear Fuel Development Corporation (PNC)

Fujita,T., Sugita,Y., Chijimatsu,M. and Ishikawa,H. (1996b): Coupled thermo-hydro-mechanical experiment at Kamaishi mine, Technical Note 06-95-06, Mechanical properties of fracture, PNC TN8410 96-059, Power Reactor and Nuclear Fuel Development Corporation (PNC)

Fujita,T., Chijimatsu,M., Ishikawa,H. Suzuki,H. and Matsumoto,K. (1997): Coupled thermo-hydro-mechanical experiment at Kamaishi mine, Technical Note 11-96-04,

Fundermental properties of Bentonite OT-9607, PNC TN8410 97-071, Power Reactor and Nuclear Fuel Development Corporation (PNC).

Japanese Geotechnical Society (1995): Investigation and experiment on rock (in Japanese).

Japanese Geotechnical Society (1996): Method and explanation of soil test (in Japanese).

Kjartanson,B.H., Chandler,N.A., Wan,A.W.L., Radhakrishna,H.S. and Lau,K-C. (1993): In Situ Assessment of Bentonite/Sand Buffer Material, Joint CSCE-ASCE National Conference on Enviromental Engineering, pp. 747-755.

Kawakami, F. (1983): Soil mechanics, Ver. 5, *Morikita Shuppan* (in Japanese).

Neerdael,B., Meynendonckx,P. and Voet,M. (1992): The Bacchus backfill experiment at the Hades underground reserch facilityy at Mol, Belgium, Final Report, EUR 14155.

Pusch,R. and Börgesson,L. (1985): Final report of the buffer mass test - volume II, SKB Technical report 85-12.

Reasoner, D.J. and Geldereich, E.E. (1985): A new medium for the enumeration and subculture of bacteria from potable water, Appl. Environ. Microbiol. 1, pp.1-7.

Shiozawa, S. (1991): Soil water potential measurement using psychrometers, *Dojo no butsurisei*, No. 62, pp.53-61 (in Japanese).

Stroes-Gascoyne, S. and West, J.M. (1994): Microbial issues pertaining to the Canadian concept for the disposal of nuclear fuel waste, Atomic Energy of Canada Limited Report, AECL –10808, COG-93-54.

Sugita,Y., Chijimatsu,M., Fujita,T. and Ishikawa,H. (1997): Coupled thermo-hydro-mechanical experiment at Kamaishi mine, Technical Note 12-96-05, Instrumentation in buffer, PNC TN8410 97-072, Power Reactor and Nuclear Fuel Development Corporation (PNC).

Sugita,Y., Chijimatsu,M., Fujita,A. and Oanh,T.D.P (1998): Coupled thermo-hydro-mechanical experiment at Kamaishi mine, Technical Note 14-99-01, Verification of the buffer material emplacement technique, JNC TN8410 99-***, Japan Nuclear Cycle Development Institute (JNC).

Appendix A Inspection of the sensor

T-H-M test was run continuously for 450days, then, some sensors those were installed in the rock mass and the buffer would be wrong or broken during the test phase. Therefore, we carried out the inspection of the sensors those could be taken out from the in-situ site and made compensation for the measured data. The inspected sensors are shown in Table A-1.

Table A-1 Inspected sensors

Location	Sensor	Number
Buffer	Pressure cell	30
	Pore pressure transducer	15
Rock	Pore pressure transducer	29

A-1 Inspection method

A-1.1 Pressure cell

Compensation equation for the pressure cell is obtained by the relationship between the known supplementary pressure to the pressure cell and the measured value by the pressure cell. The schematics of the inspection for the pressure cell are shown in Figures A-1 and A-2. The known supplementary pressure is added by the screw jack as shown in figures. The schematic of the pressure addition at the vertical direction is shown in Figure A-1 and that at the horizontal direction is shown in Figure A-2. The known supplementary pressure is measured by the load cell as shown in figures.

The inspection is carried out in two cases. First one is the case that pressure increase step by step, and the other is the case that pressure decrease step by step. The maximum supplementary pressure is set at 2.0MPa and each step is set at 100kPa. Compensation equation is obtained by using all inspection data.

A-1.2 Pore pressure transducer installed in the buffer

Compensation equation for the pore pressure transducer in the buffer is obtained by the relationship between the known supplementary water pressure to the pore pressure transducer and the measured value by the pore pressure transducer. The schematic of the inspection for the pore pressure transducer is shown in Figures A-3. The water pressure is added by the compressed air as shown in Figure A-3. The known supplementary water pressure is measured by the high-precision Bourdon gauge as shown in Figure A-3.

The inspection is carried out in two cases. First one is the case that pressure increase step by step, and the other is the case that pressure decrease step by step. The maximum supplementary water pressure is set at 500kPa and each step is set at 100kPa. Compensation equation is obtained by using all inspection data.

A-1.3 Pore pressure transducer installed in the rock

Compensation equation for the pore pressure transducer in the rock is obtained by the relationship between the known supplementary water pressure to the pore pressure transducer and the measured value by the pore pressure transducer. The schematic of the inspection for the pore pressure transducer is shown in Figures A-4. The water pressure is added by the compressed air as shown in Figure A-4. The known supplementary water pressure is measured by the high-precision Bourdon gauge as shown in Figure A-3.

The inspection is carried out in two cases. First one is the case that pressure increase step by step, and the other is the case that pressure decrease step by step. The maximum supplementary water pressure is set at 200kPa and each step is set at 50kPa. Compensation equation is obtained by using all inspection data.

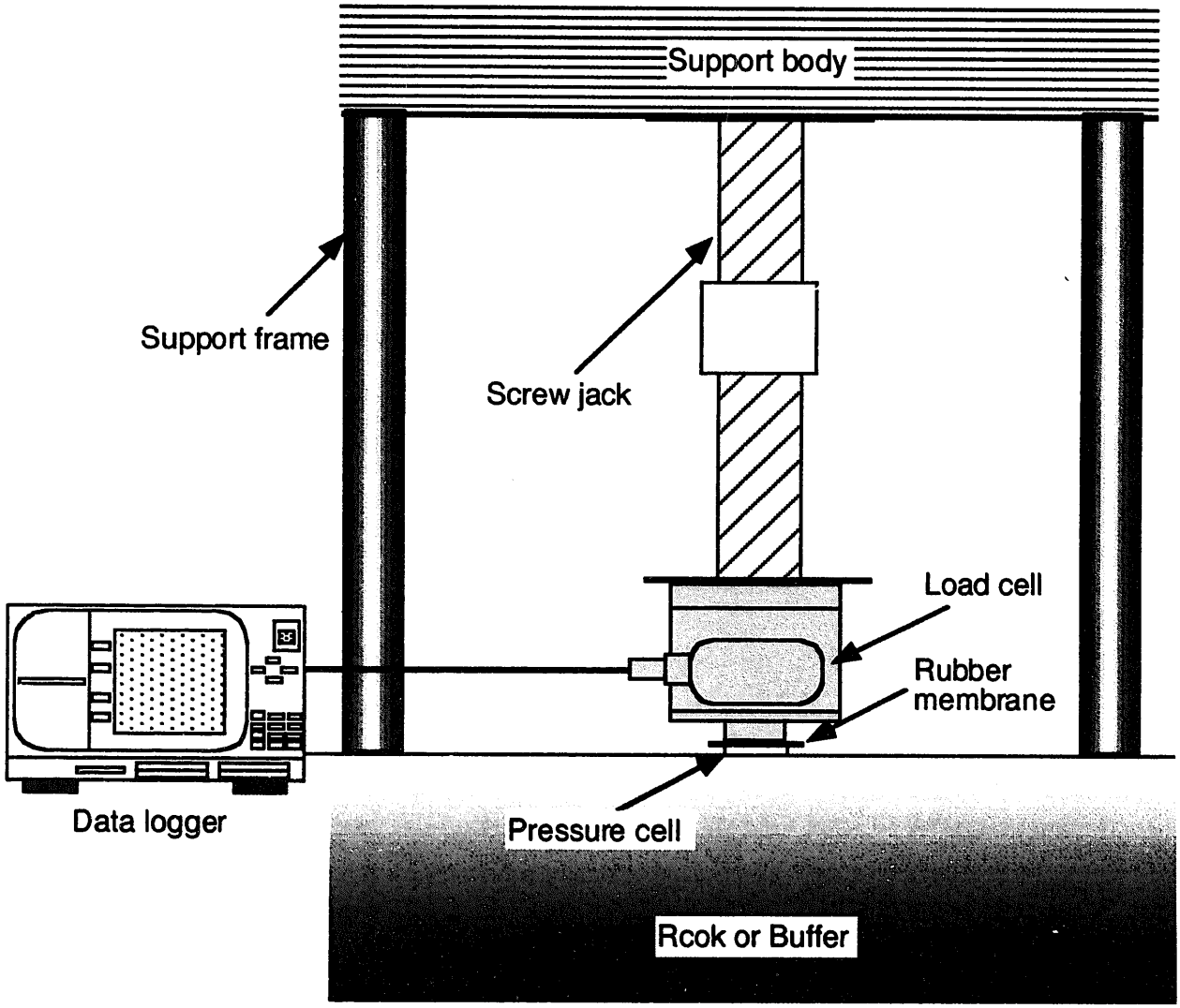

Figure A-1 Inspection of the pressure cell
(Vertical direction)

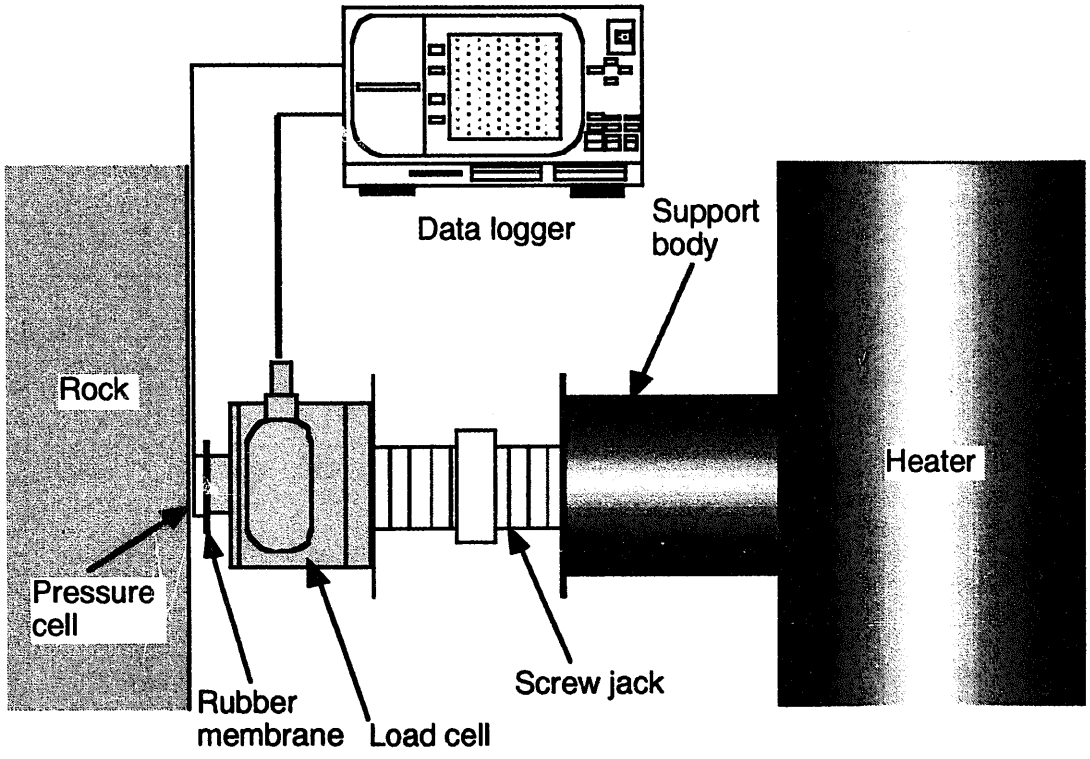

(a) Side view

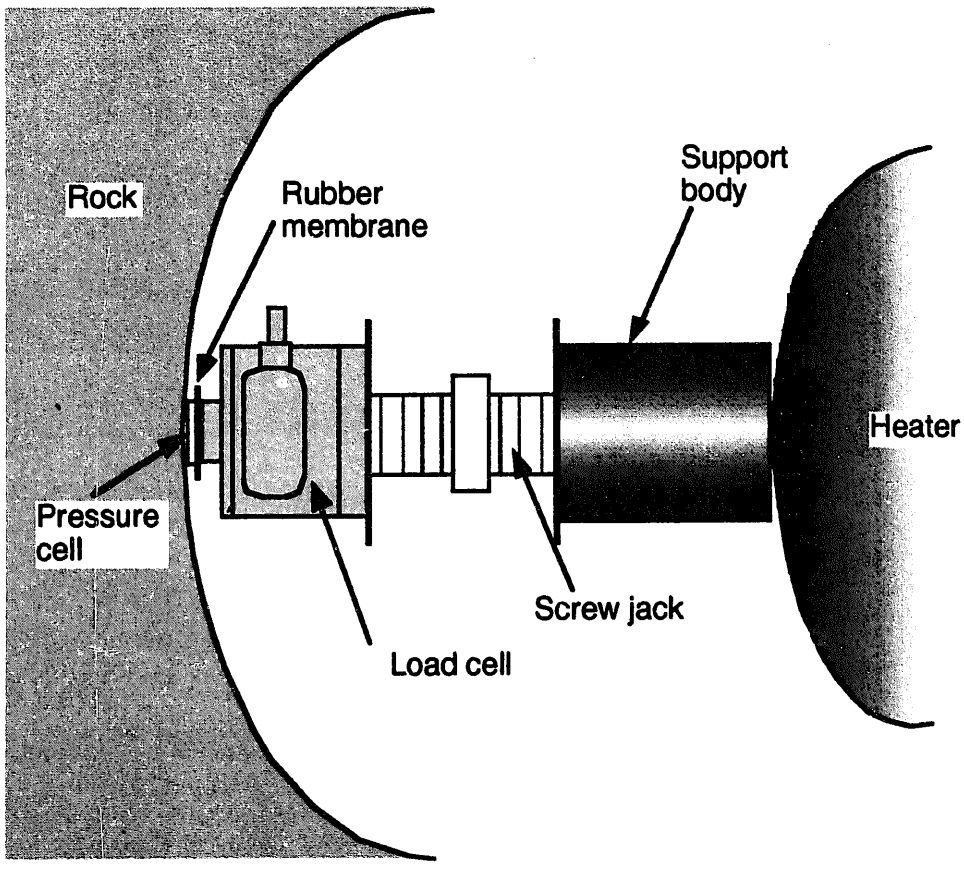

(b)Upper view

Figure A-2 Inspection of the pressure cell (Horizontal direction)

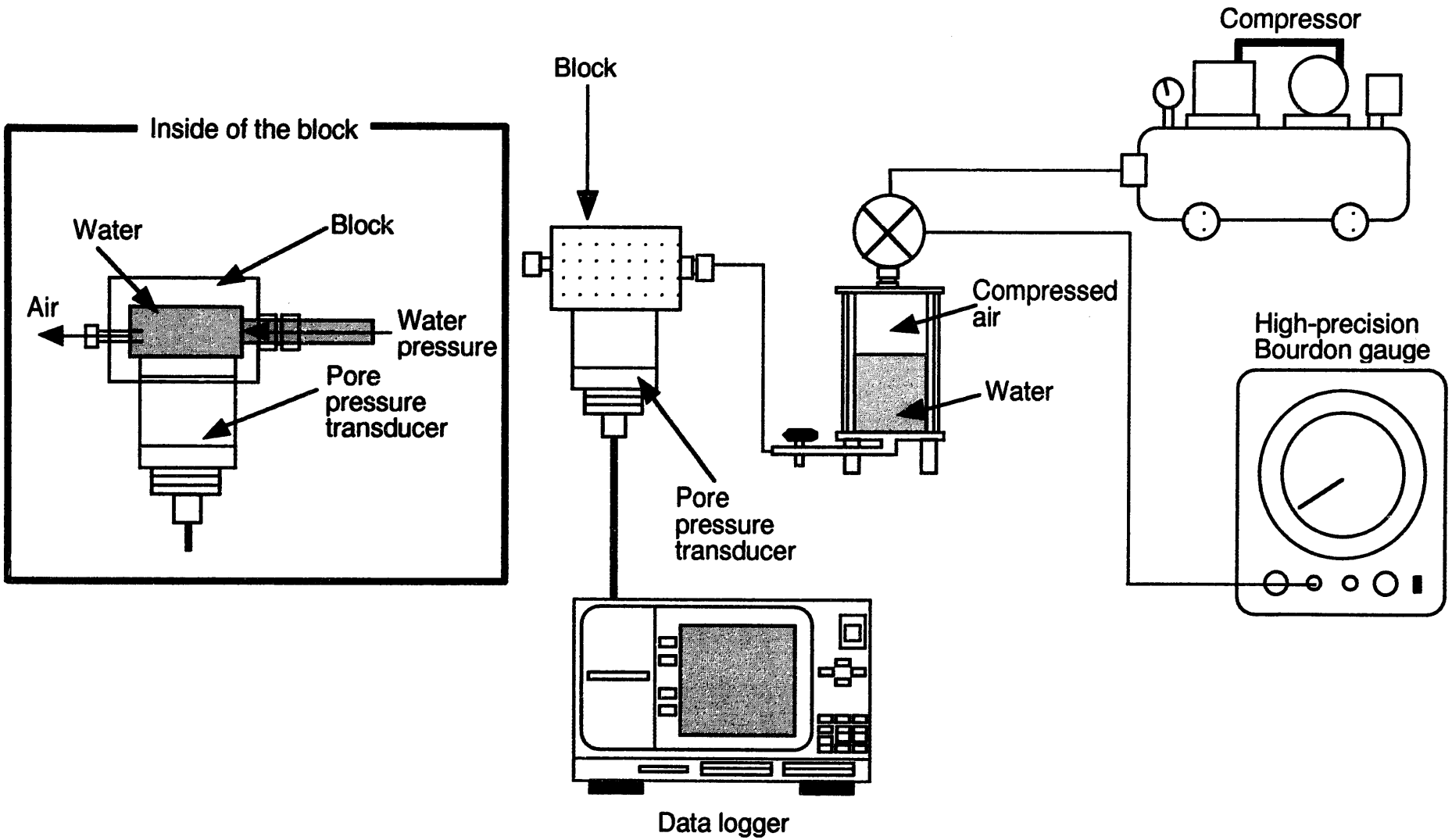

Figure A-3 Inspection of the pore pressure transducer installed in the buffer

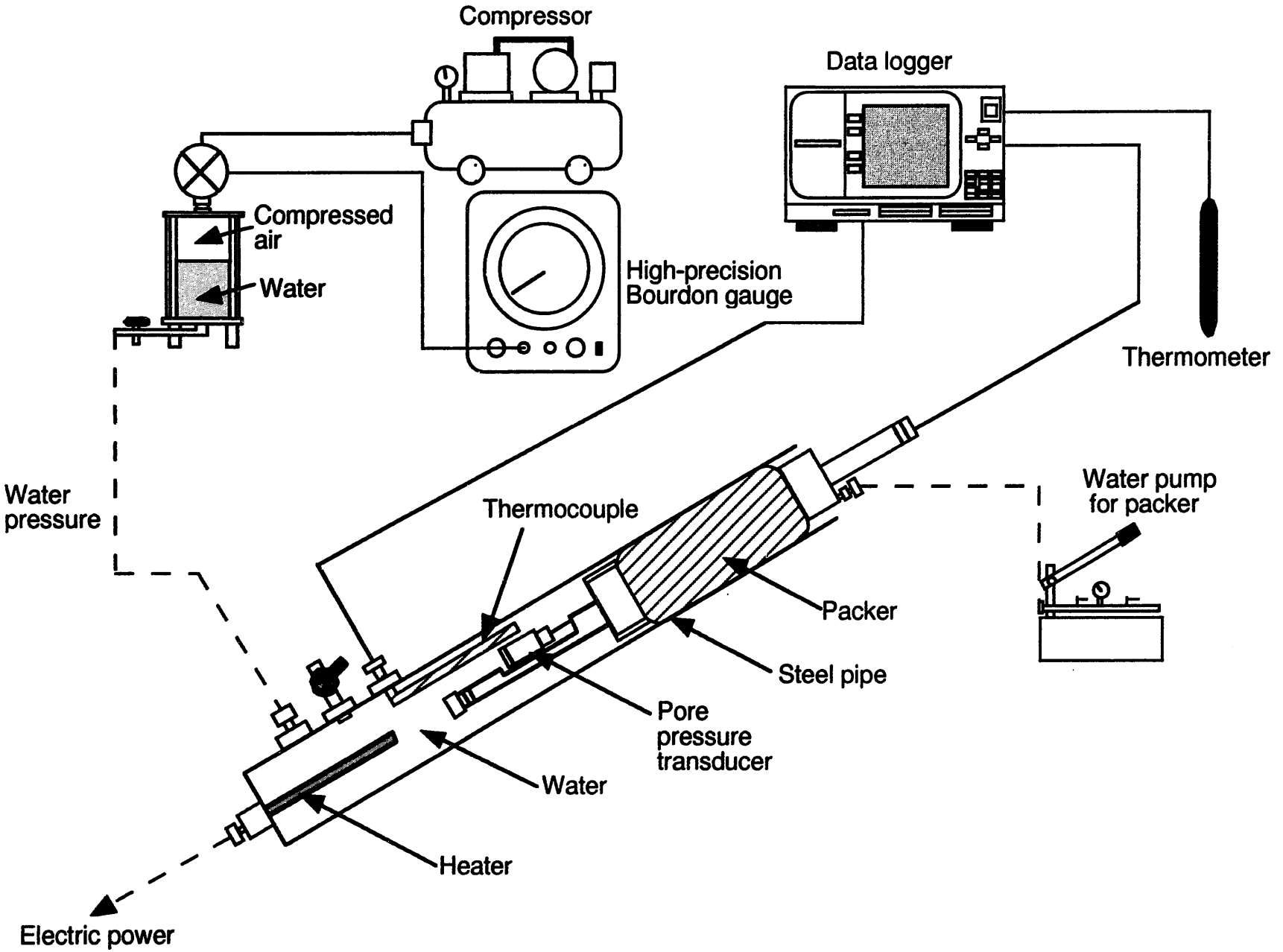

Figure A-4 Inspection of the pore pressure transducer installed in the rock

A-2 Compensation results

A-2.1 Pressure cell

Compensation for the pressure cell was carried out as follows.

(1) Correction of the proofreading coefficient

We found the mistake of the proofreading coefficient in the data logger during the experiment. Therefore, we proofread the measurement data before the compensation by inspection results. Proofreading was performed with following equation by using the correct value that was shown in Table A-2. The proofreading coefficient α is the inputted value in the data logger and the proofreading coefficient β is the correct value.

(Real value) = (measured value)
$\times$((proofreading coefficient β)$/$(proofreading coefficient α))

(2) Compensation by inspection results

Inspection results for the pressure cell are shown in Table A-3. Compensation was carried out by using following equation.

(Compensation value)=(Coefficient A)+(Coefficient B)$\times$(Real value)

(3)Compensation of initial value

We set the value at the start of heating as zero.

The results that are obtained by above-mentioned compensation are shown in Chapter 5.

The results that are obtained by compensation of (1) and (2) are shown in Figures A-5 to A-13. These figures set the value as zero when the pressure cell was installed in the buffer.

Table A-2 Proofreading coefficient of pressure cell

Sensor Number	Serial Number	Proofreading coefficient α	Rated capacity [kPa]	Strain [$\times 10^{-6}$]	Proofreading coefficient β	β/α
PS-1	69047	1.02410	4905	10440	0.46983	0.45877
PS-2	69036	1.02020	4905	10400	0.47163	0.46230
PS-3	69037	1.03390	4905	10540	0.46537	0.45011
PS-4	69038	0.99669	4905	10160	0.48278	0.48438
PS-5	69044	0.95745	4905	9760	0.50256	0.52490
PS-6	69045	0.96138	4905	9800	0.50051	0.52062
PS-7	69041	1.00650	4905	10260	0.47807	0.47498
PS-8	69040	0.97707	4905	9960	0.49247	0.50403
PS-9	69042	1.02410	4905	10440	0.46983	0.45877
PS-10	69043	0.95745	4905	9760	0.50256	0.52490
PS-11	69030	1.03000	4905	10500	0.46714	0.45354
PS-12	69031	0.98100	4905	10000	0.49050	0.50000
PS-13	69032	0.97119	4905	9900	0.49545	0.51015
PS-14	69033	1.00450	4905	10240	0.47900	0.47686
PS-15	69034	0.98492	4905	10040	0.48855	0.49603
PS-16	69035	0.95745	4905	9760	0.50256	0.52490
PS-17	69049	0.95549	4905	9740	0.50359	0.52705
PS-18	69050	0.99669	4905	10160	0.48278	0.48438
PS-19	69051	0.96726	4905	9860	0.49746	0.51430
PS-20	69052	0.96138	4905	9800	0.50051	0.52062
PS-21	69053	0.96138	4905	9800	0.50051	0.52062
PS-22	69054	0.97707	4905	9960	0.49247	0.50403
PS-23	69055	1.01430	4905	10340	0.47434	0.46768
PS-24	69028	0.95540	4905	9740	0.50359	0.52710
PS-25	69046	0.96720	4905	9860	0.49746	0.51433
PS-26	69048	0.99470	4905	10140	0.48373	0.48631
PS-27	69026	1.01630	4905	10360	0.47346	0.46586
PS-28	69027	1.01430	4905	10340	0.47437	0.46768
PS-29	69029	1.02610	4905	10460	0.46893	0.45700
PS-30	69039	0.98492	4905	10040	0.48855	0.49603

Table A-3 Inspection results of the pressure cell

Sensor	Depth [m]	Sensor Number	Pressurization		Decompression		Compensation	
			coefficient A [kPa]	coefficient B	coefficient A [kPa]	coefficient B	coefficient A [kPa]	coefficient B
Pressure cell	-5.00	PS-1	-493	-0.673	-590	-0.688	-514	-0.671
	-4.50	PS-2	-756	-0.685	-673	-0.665	-718	-0.676
		PS-3	-1361	-0.794	-1336	-0.784	-1343	-0.787
		PS-4	1598	-0.729	1788	-0.667	1658	-0.670
	-4.00	PS-5	-404	-1.137	-310	-1.137	-350	-1.132
		PS-6	317	-0.979	214	-1.020	268	-1.000
		PS-7	-1217	-0.970	-1235	-0.982	-1227	-0.977
		PS-8	506	-1.060	603	-1.023	558	-1.034
		PS-9	283	-0.730	443	-0.659	361	-0.695
		PS-10	-26	-0.652	27	-0.629	-4	-0.643
	-3.00	PS-11	-150	-0.632	-79	-0.616	-112	-0.623
		PS-12	1454	-0.786	1636	-0.619	1503	-0.632
		PS-13	-159	-0.669	-159	-0.665	-160	-0.668
		PS-14	993	-0.975	1043	-0.950	1018	-0.960
		PS-15	-284	-0.698	-301	-0.702	-291	-0.699
		PS-16	165	-0.937	245	-0.923	209	-0.924
	-2.05	PS-17	116	-0.660	150	-0.652	139	-0.653
		PS-18	-1147	-0.882	-962	-0.835	-1033	-0.852
		PS-19	-	-	-	-	-	-
		PS-20	-862	-0.847	-649	-0.785	-735	-0.807
		PS-21	319	-0.692	270	-0.695	294	-0.696
		PS-22	2074	-0.739	2145	-0.678	2103	-0.699
		PS-23	308	-0.652	392	-0.692	357	-0.632
	-1.25	PS-24	452	-0.597	473	-0.599	463	-0.598
		PS-25	18	-0.590	121	-0.576	80	-0.579
		PS-26	-172	-0.625	-183	-0.617	-175	-0.619
	-0.50	PS-27	158	-1.010	-89	-1.093	94	-1.016
		PS-28	271	-0.797	-18	-0.866	193	-0.800
		PS-29	-505	-0.947	-721	-0.973	-563	-0.950
		PS-30	-82	-0.771	-476	-0.872	-213	-0.801

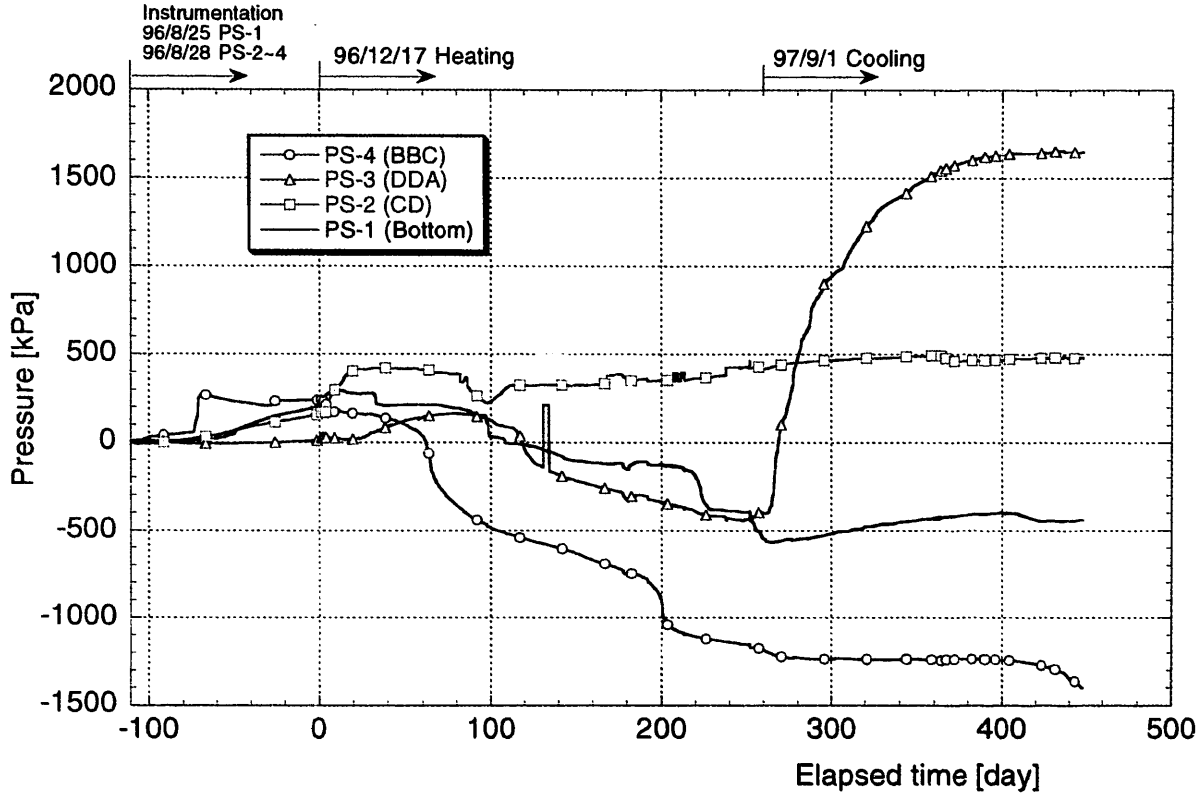

Figure A-5 Measurement result after the installation of pressure cell (GL-4.5m: Outside, GL-5.0m;Bottom)

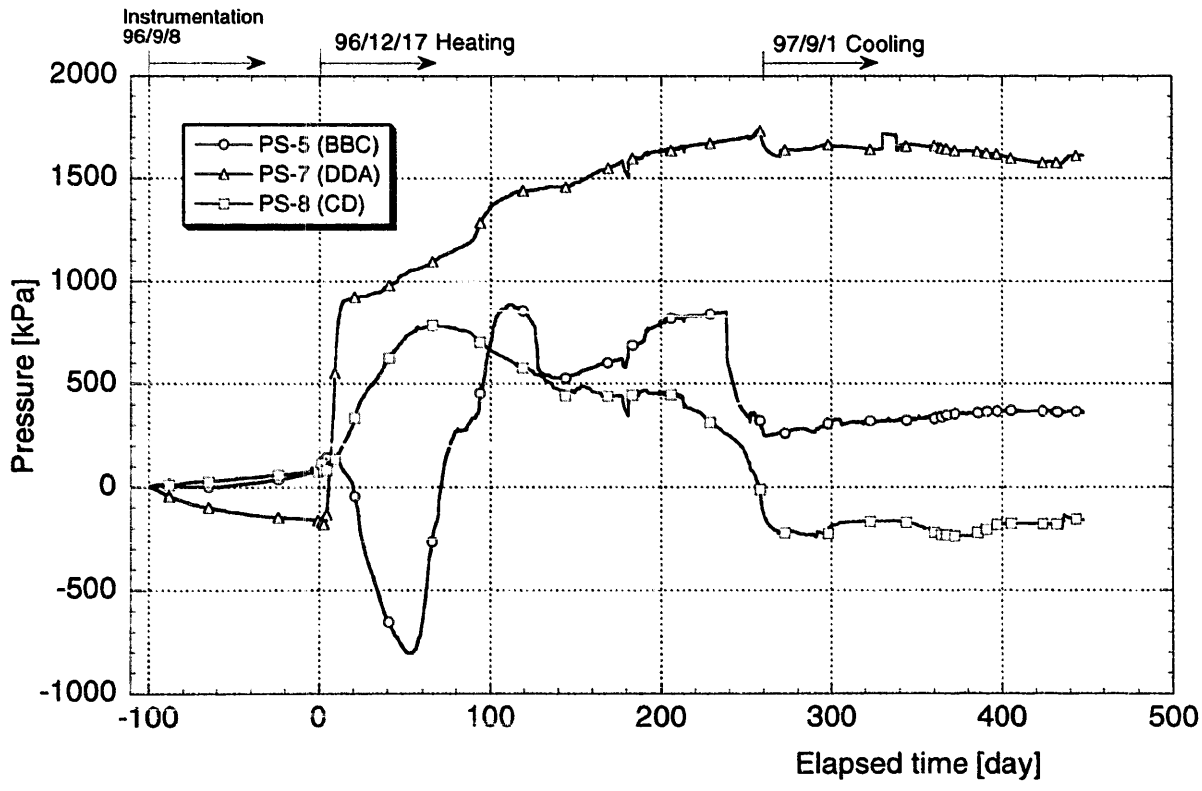

Figure A-6 Measurement result after the installation of pressure cell (GL-4.0m: Outside)

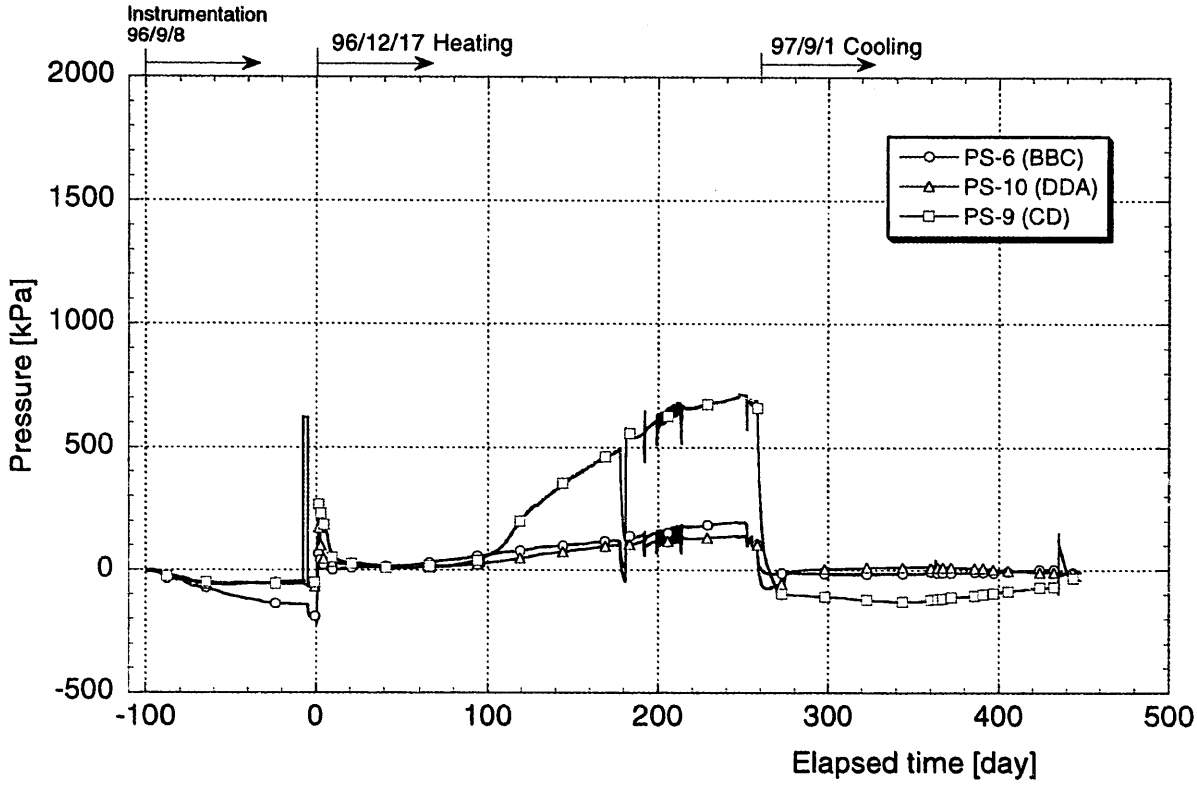

Figure A-7 Measurement result after the installation of pressure cell (GL-4.0m: Inside)

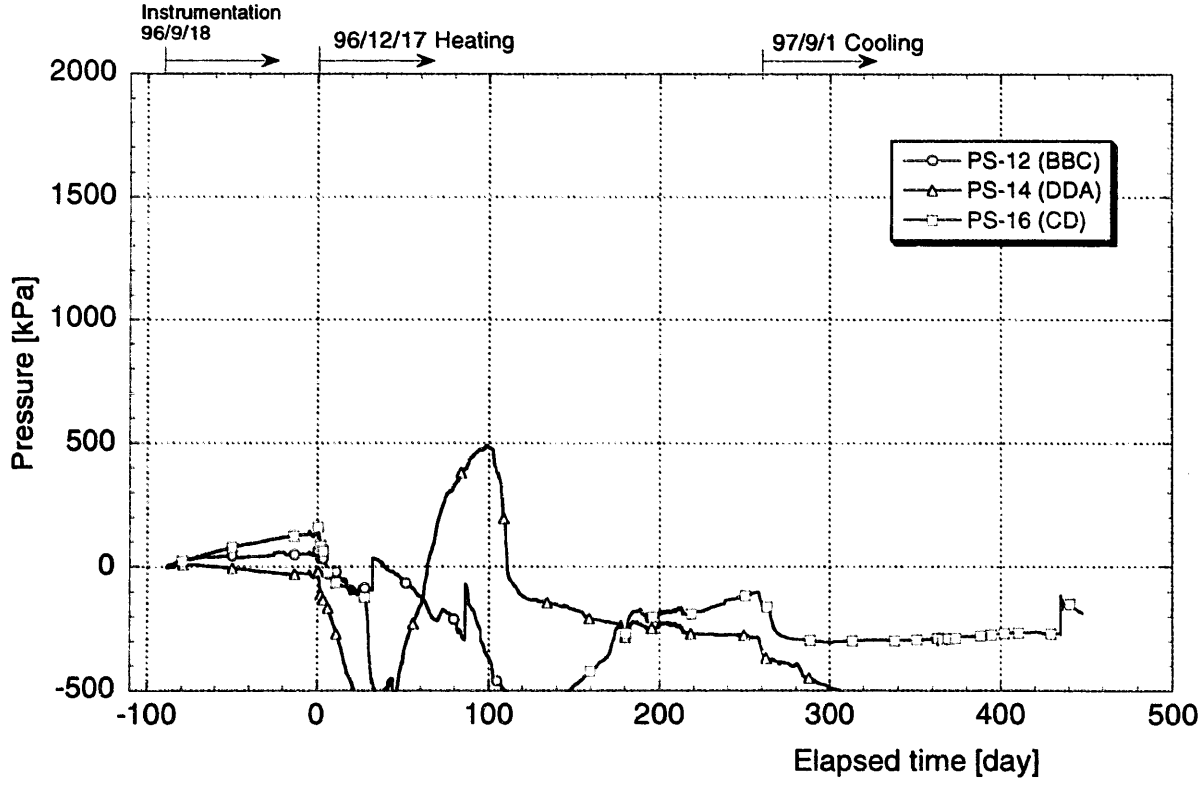

Figure A-8 Measurement result after the installation of pressure cell (GL-3.0m: Outside)

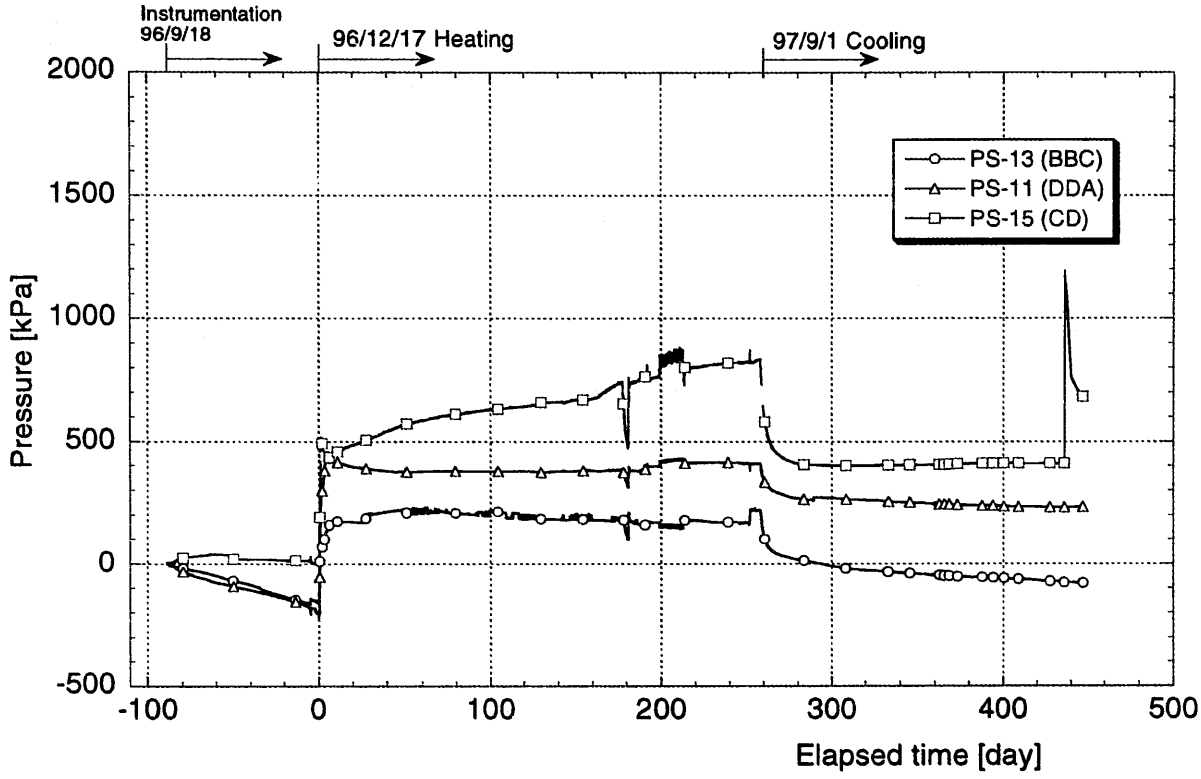

Figure A-9 Measurement result after the installation of pressure cell (GL-3.0m: Inside)

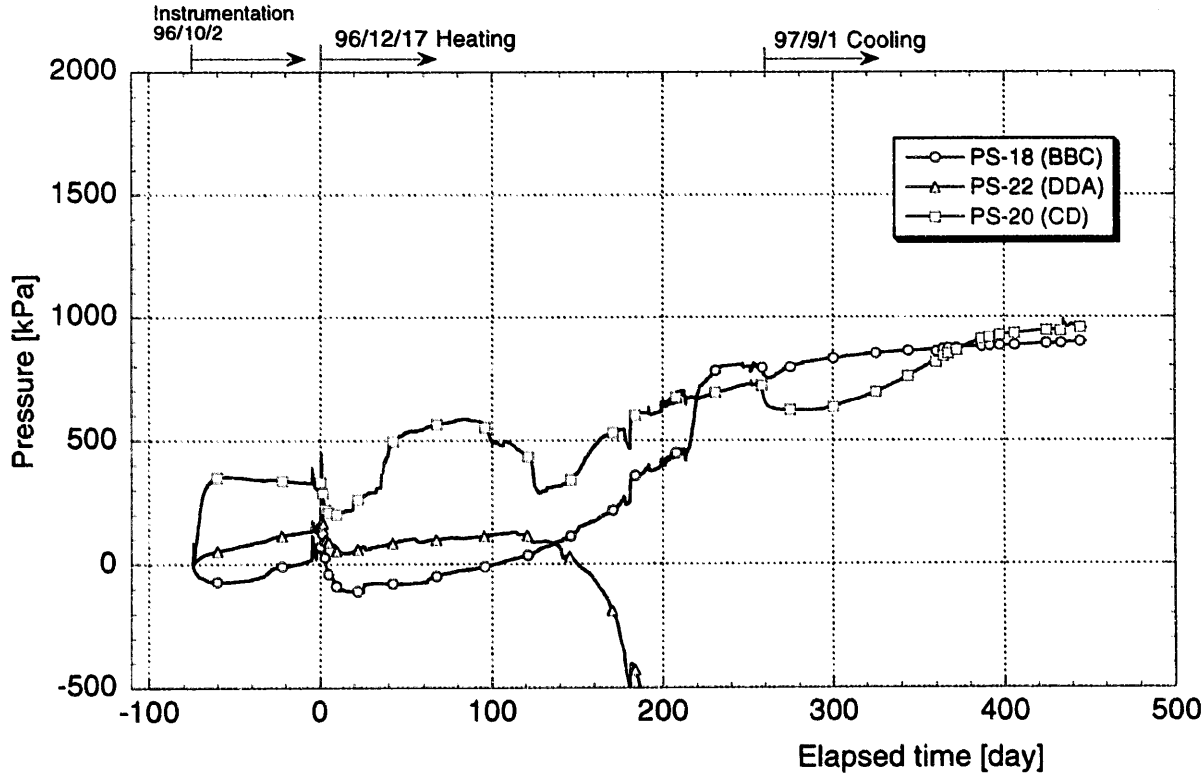

Figure A-10 Measurement result after the installation of pressure cell (GL-2.0m: Outside)

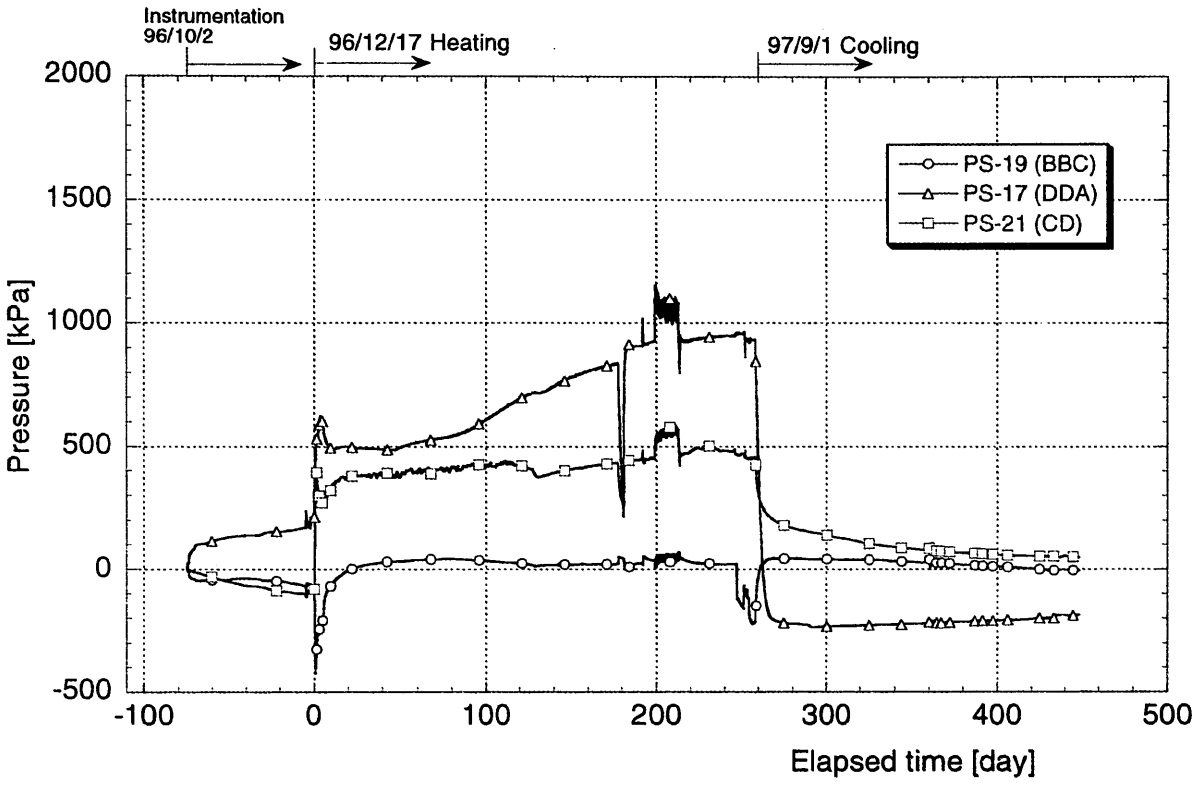

Figure A-11 Measurement result after the installation of pressure cell (GL-2.0m: Inside)

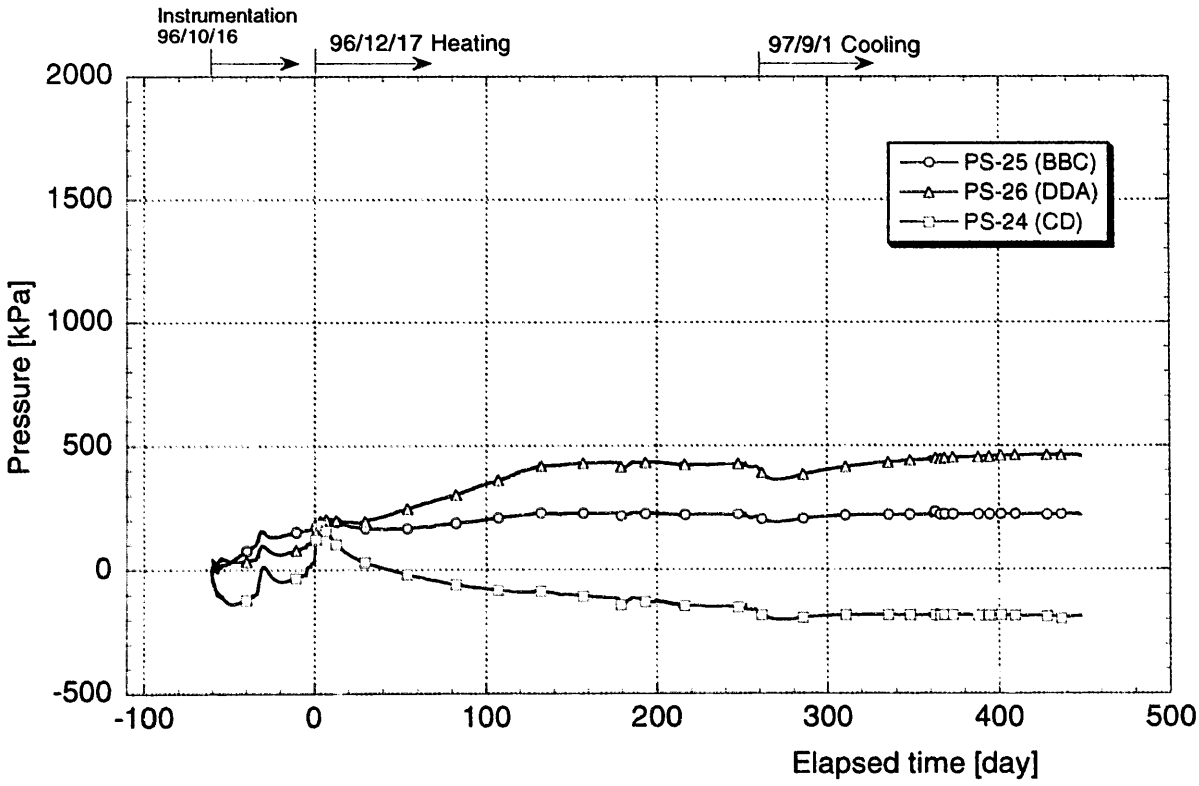

Figure A-12 Measurement result after the installation of pressure cell (GL-1.25m: Outside)

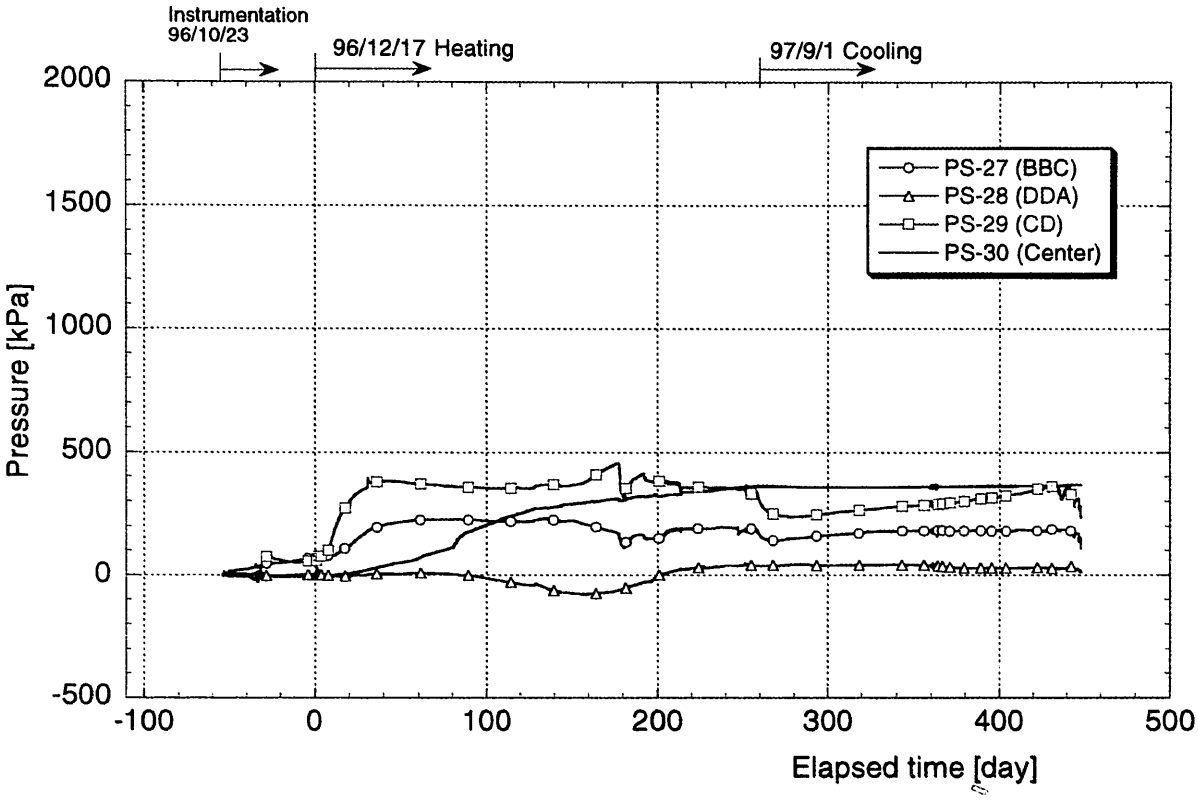

Figure A-13 Measurement result after the installation of pressure cell (GL-0.5m: Upper)

A-2.2 Pore pressure transducer

Tables A-4 and A-5 show the inspection results of the pore pressure transducer. Compensation was performed with following equation by using the coefficient A and B as shown in tables.

(Compensation value Y)＝((Measured value X)—(coefficient A))／(coefficient B)

Here, we could not obtain the compensation values about the sensor number PT-4H, PT-11H, PT-15H, PT-21H, PT-24H, PT-26H that were installed in the rock mass

Table A-4 Inspection results of the pore pressure transducer installed in the buffer

Sensor	Depth [m]	Sensor Number	Pressurization		Decompression		Compensation	
			coefficient A [kPa]	coefficient B	coefficient A [kPa]	coefficient B	coefficient A [kPa]	coefficient B
Pore Pressure transducer	-5.00	PC-1H	-10.500	1.003	-9.895	1.004	-10.198	1.003
		PC-2H	-17.765	0.987	-18.067	0.986	-17.916	0.987
		PC-3H	-16.946	0.996	-16.585	0.996	-16.765	0.996
		PC-4H	-14.102	1.004	-13.997	1.004	-14.049	1.004
		PC-5H	-16.263	0.986	-16.831	0.987	-16.547	0.986
		PC-6H	-13.850	0.998	-13.278	0.995	-13.564	0.996
		PC-7H	-19.108	0.990	-19.194	0.989	-19.151	0.989
	-4.00	PC-8H	-10.278	0.996	-9.248	0.994	-9.763	0.995
	-3.00	PC-9H	-33.265	1.035	-32.743	1.035	-32.995	1.035
		PC-10H	-10.488	0.986	-12.249	0.988	-11.368	0.987
		PC-11H	-22.220	0.987	-21.989	0.988	-22.104	0.987
	-2.05	PC-12H	-17.964	1.010	-19.158	1.007	-18.561	1.009
	-1.25	PC-13H	-20.366	1.061	-19.057	1.057	-19.479	1.058
		PC-14H	-33.386	1.058	-32.363	1.055	-32.875	1.056
		PC-15H	3.469	1.048	4.050	1.048	3.759	1.048

Table A-5 Inspection results of the pore pressure transducer installed in the rock

Sensor	Location	Sensor Number	Pressurization		Decompression		Compensation	
			coefficient A [kPa]	coefficient B	coefficient A [kPa]	coefficient B	coefficient A [kPa]	coefficient B
Pore pressure transducer	KBH1-1	PT-1H	-6.846	0.992	-5.536	0.987	-6.212	0.990
	KBH1-2	PT-2H	-5.513	0.979	-6.067	0.991	-5.823	0.986
	KBH1-3	PT-3H	-1.216	0.986	0.575	0.974	-0.480	0.983
	KBH1-4	PT-4H	-	-	-	-	-	-
	KBH1-5	PT-5H	-1.694	0.977	-1.803	0.974	-1.890	0.978
	KBH2-1	PT-6H	0.043	0.981	-1.187	0.988	-0.576	0.985
	KBH2-2	PT-7H	1.637	0.975	1.427	0.979	1.460	0.978
	KBH2-3	PT-8H	2.421	0.958	-2.818	0.992	-0.167	0.975
	KBH2-4	PT-9H	1.333	0.987	1.466	0.984	1.415	0.985
	KBH3-1	PT-10H	-0.758	0.995	-0.390	0.988	-0.782	0.996
	KBH3-2	PT-11H	-	-	-	-	-	-
	KBH3-3	PT-12H	3.554	0.983	3.554	0.982	3.428	0.985
	KBH3-4	PT-13H	173.450	0.872	175.500	0.860	174.110	0.873
	KBH3-5	PT-14H	177.490	0.894	176.340	0.903	176.470	0.907
	KBH4-1	PT-15H	-	-	-	-	-	-
	KBH4-2	PT-16H	0.189	0.985	-0.609	0.984	-0.276	0.986
	KBH4-3	PT-17H	22.896	0.986	22.420	0.993	22.609	0.990
	KBH4-4	PT-18H	-2.697	0.978	-1.048	0.972	-1.891	0.975
	KBH4-5	PT-19H	28.225	0.985	31.156	0.965	29.444	0.980
	KBH5-1	PT-20H	-0.241	0.996	-1.880	1.019	0.779	0.989
	KBH5-2	PT-21H	-	-	-	-	-	-
	KBH5-3	PT-22H	0.747	0.986	-0.249	0.987	0.249	0.986
	KBH5-4	PT-23H	9.965	0.989	11.411	0.980	10.668	0.985
	KBH5-5	PT-24H	-	-	-28.251	1.294	-	-
	KBH6-1	PT-25H	-0.343	1.003	-0.943	1.009	-0.674	1.006
	KBH6-2	PT-26H	-	-	-	-	-	-
	KBH6-3	PT-27H	-0.123	0.985	-0.842	0.991	-0.484	0.988
	KBH6-4	PT-28H	14.784	0.982	13.920	0.989	14.299	0.987
	KBH6-5	PT-29H	2.221	0.983	3.130	0.975	2.747	0.978

Appendix B Sampling results at decommission

Figures B-1 to B-6 show the location of the sampling points at decommission. Figure B-1 shows the height of the sampling section. Figure B-2 shows the location of the sampling points at sections a, b and c. Figure B-3 shows the location of the sampling points at sections d, e, f and g. Figures B-4 to B-6 show the location of the sampling points at sections h, I and j. Table B-1 show the digital data of the water content at decommission

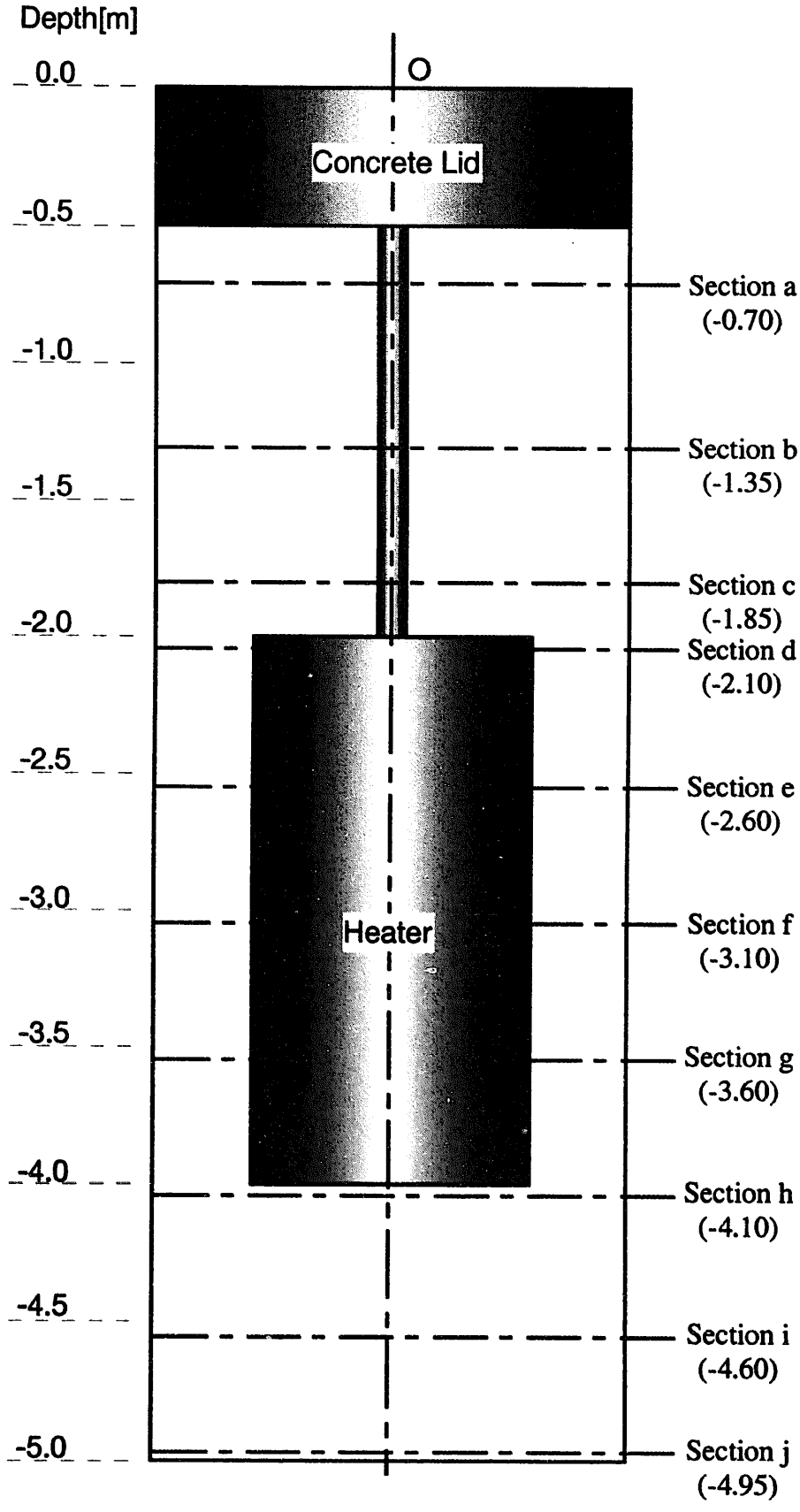

Figure A-1 Height of the sampling section

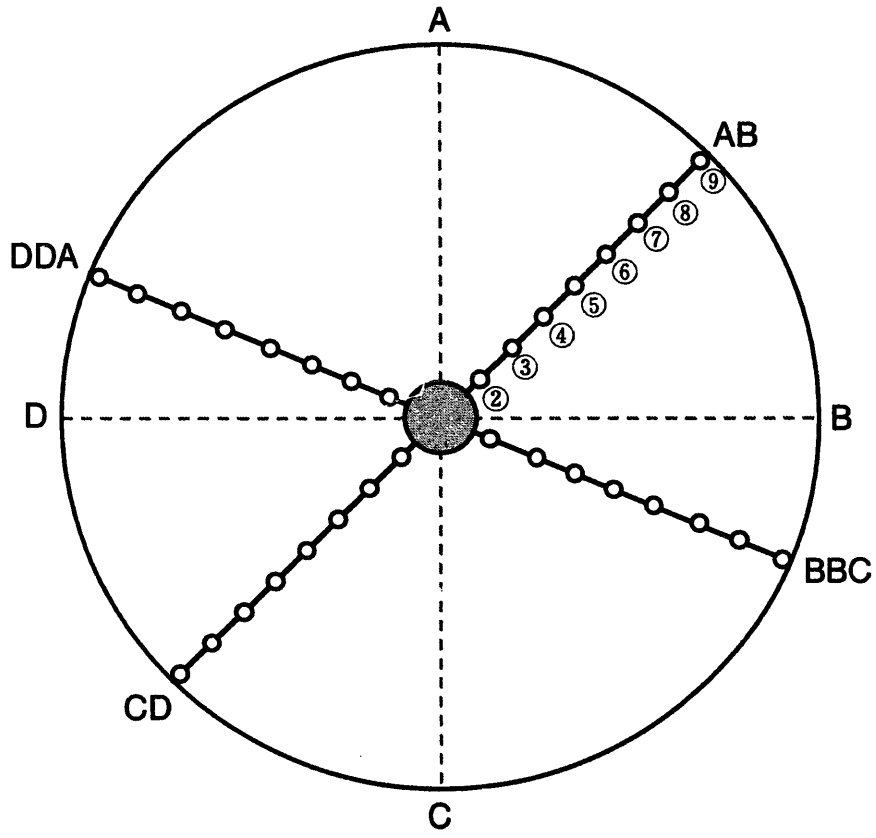

Figure A-2 Location of the sampling points (Section a, b, c)

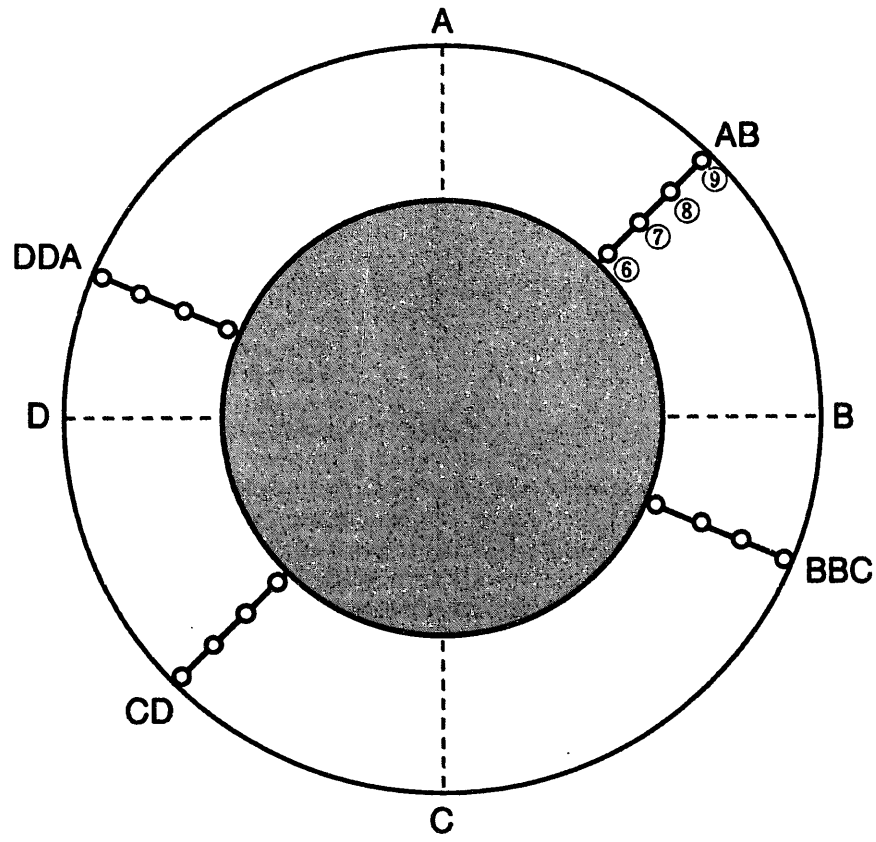

Figure A-3 Location of the sampling points (Section d, e, f, g)

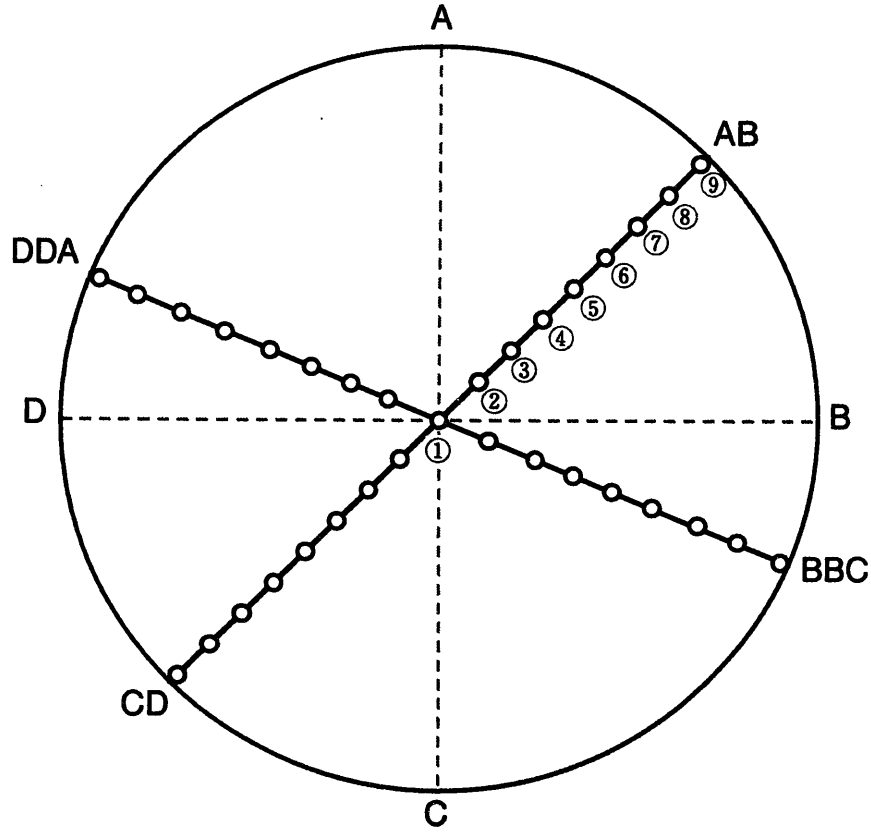

Figure A-4 Location of the sampling points (Section h, i, j) (No.1)

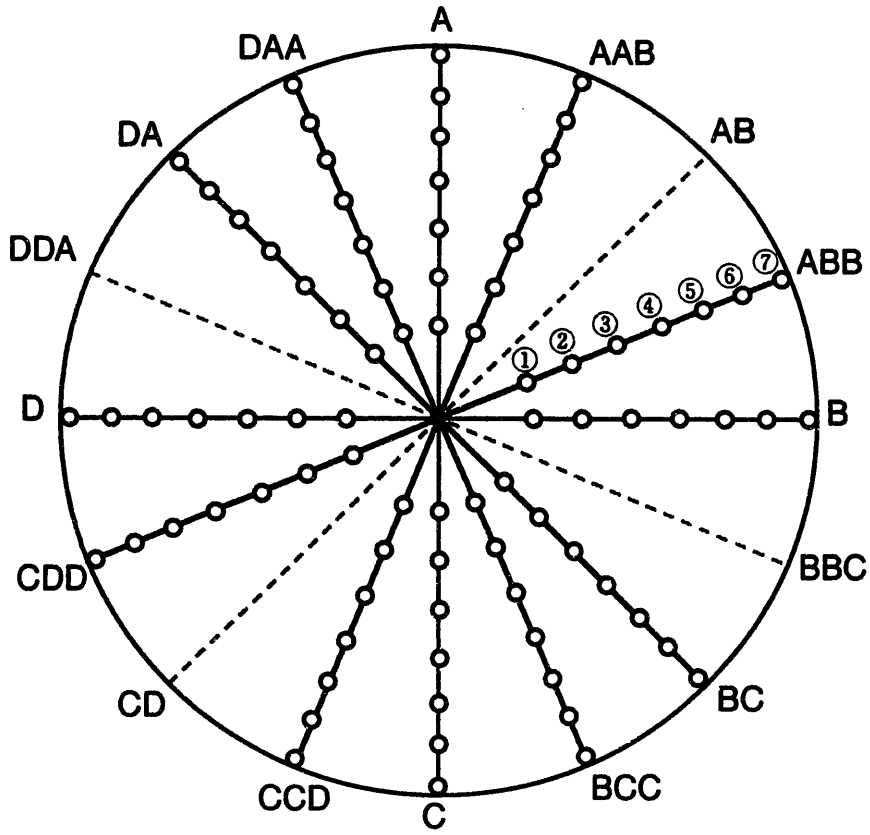

Figure A-5 Location of the sampling points (Section h, i, j) (No.2)

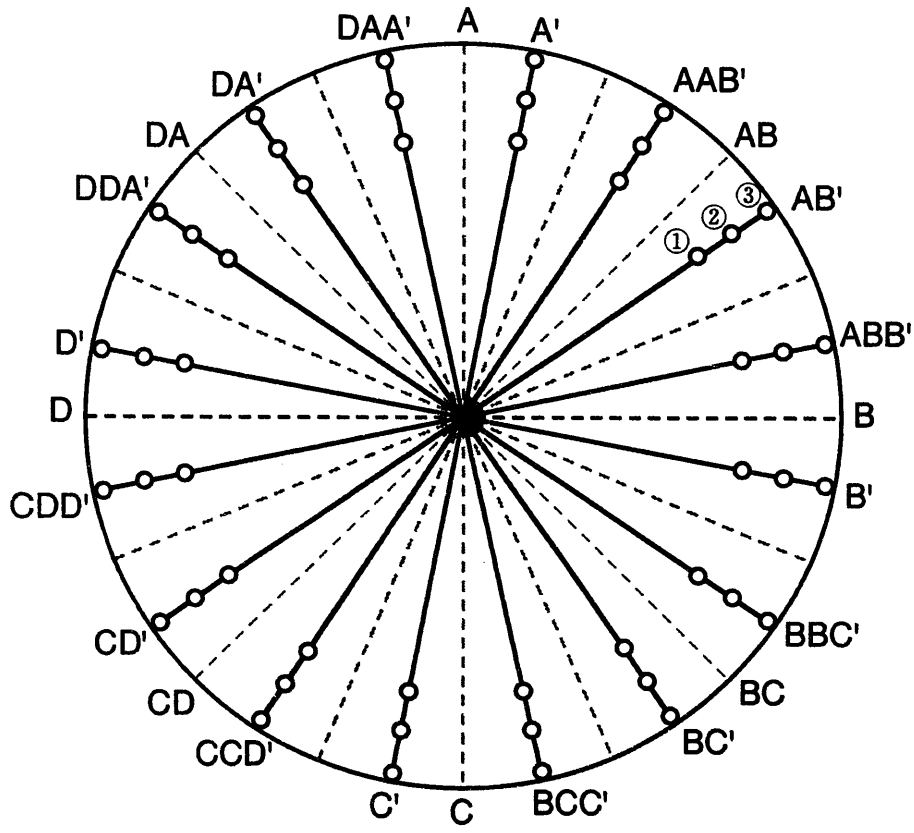

Figure A-6 Location of the sampling points (Section h, i, j) (No.3)

Table B-1 Measured water content at decommission

Section	Line	Location	[%]				[%]				[%]				[%]
a	AB	②	16.8	b	AB	②	14.3	c	AB	②	8.4	d	AB	②	
		③	16.9			③	17.0			③	10.7			③	
		④	17.1			④	16.5			④	11.1			④	
		⑤	17.1			⑤	16.5			⑤	11.8			⑤	
		⑥	17.1			⑥	16.7			⑥	12.2			⑥	8.9
		⑦	17.3			⑦	16.9			⑦	14.8			⑦	11.6
		⑧	18.6			⑧	18.6			⑧	20.2			⑧	19.6
		⑨	23.1			⑨	23.7			⑨	22.5			⑨	24.8
	CD	②	16.7		CD	②	14.5		CD	②	6.1		CD	②	
		③	16.8			③	16.5			③	5.8			③	
		④	17.0			④	16.7			④	6.8			④	
		⑤	17.6			⑤	16.9			⑤	9.6			⑤	
		⑥	17.1			⑥	16.6			⑥	12.1			⑥	9.1
		⑦	17.3			⑦	16.9			⑦	16.0			⑦	12.4
		⑧	18.7			⑧	20.0			⑧	27.8			⑧	24.1
		⑨	22.7			⑨	26.2			⑨	22.3			⑨	30.2
	DDA	②	16.7		DDA	②	14.7		DDA	②	5.8		DDA	②	
		③	16.8			③	16.5			③	6.3			③	
		④	16.8			④	16.8			④	7.9			④	
		⑤	17.0			⑤	16.9			⑤	8.0			⑤	
		⑥	16.8			⑥	16.5			⑥	10.3			⑥	8.4
		⑦	17.2			⑦	16.5			⑦	12.0			⑦	11.1
		⑧	18.8			⑧	17.6			⑧	19.8			⑧	18.6
		⑨	23.1			⑨	20.3			⑨	21.3			⑨	22.7
	BBC	②	16.5		BBC	②	14.8		BBC	②	7.6		BBC	②	
		③	16.6			③	16.3			③	8.7			③	
		④	16.5			④	16.6			④	9.2			④	
		⑤	16.7			⑤	16.3			⑤	10.1			⑤	
		⑥	16.7			⑥	16.1			⑥	11.5			⑥	8.5
		⑦	17.3			⑦	16.4			⑦	15.5			⑦	11.8
		⑧	18.6			⑧	19.7			⑧	18.6			⑧	21.2
		⑨	22.0			⑨	26.9			⑨	33.4			⑨	24.6

Table B-1 Measured water content at decommission

Section	Line	Location	[%]				[%]				[%]
e	AB	②		f	AB	②		g	AB	②	
		③				③				③	
		④				④				④	
		⑤				⑤				⑤	
		⑥	10.1			⑥	10.2			⑥	9.6
		⑦	13.5			⑦	12.4			⑦	12.6
		⑧	22.5			⑧	21.5			⑧	20.7
		⑨	28.7			⑨	28.7			⑨	27.2
	CD	②			CD	②			CD	②	
		③				③				③	
		④				④				④	
		⑤				⑤				⑤	
		⑥	9.8			⑥	9.9			⑥	8.9
		⑦	14.6			⑦	13.5			⑦	11.7
		⑧	23.7			⑧	21.8			⑧	19.2
		⑨	27.4			⑨	27.7			⑨	28.4
	DDA	②			DDA	②			DDA	②	
		③				③				③	
		④				④				④	
		⑤				⑤				⑤	
		⑥	9.7			⑥	9.5			⑥	9.1
		⑦	13.9			⑦	12.2			⑦	12.5
		⑧	21.2			⑧	19.8			⑧	21.0
		⑨	24.8			⑨	26.2			⑨	26.9
	BBC	②			BBC	②			BBC	②	
		③				③				③	
		④				④				④	
		⑤				⑤				⑤	
		⑥	8.9			⑥	9.5			⑥	8.6
		⑦	12.0			⑦	12.2			⑦	11.7
		⑧	21.1			⑧	20.0			⑧	20.0
		⑨	24.0			⑨	25.3			⑨	24.3

Table B-1 Measured water content at decommission

Section	Line	Location	[%]	Section	Line	Location	[%]	Section	Line	Location	[%]
h	AB	①	6.59	i	AB	①	18.99	j	AB	①	16.41
		②	6.77			②	18.69			②	17.38
		③	7.02			③	18.00			③	17.55
		④	8.11			④	17.47			④	17.83
		⑤	9.93			⑤	16.61			⑤	17.62
		⑥	12.42			⑥	16.61			⑥	17.57
		⑦	14.72			⑦	17.39			⑦	17.99
		⑧	26.18			⑧	19.61			⑧	20.20
		⑨	30.23			⑨	23.60			⑨	20.27
	CD	②	6.90		CD	②	19.18		CD	②	16.92
		③	6.79			③	18.16			③	18.13
		④	7.56			④	17.35			④	18.11
		⑤	9.15			⑤	17.77			⑤	18.36
		⑥	11.54			⑥	17.61			⑥	18.99
		⑦	13.23			⑦	19.52			⑦	21.52
		⑧	17.23			⑧	19.51			⑧	20.58
		⑨	31.11			⑨	22.44			⑨	25.25
	DDA	②	6.61		DDA	②	19.05		DDA	②	16.75
		③	6.81			③	18.76			③	17.80
		④	7.29			④	17.86			④	17.83
		⑤	8.96			⑤	17.30			⑤	18.35
		⑥	11.26			⑥	17.25			⑥	18.11
		⑦	13.12			⑦	18.01			⑦	18.56
		⑧	19.89			⑧	18.82			⑧	19.83
		⑨	26.03			⑨	21.03			⑨	23.23
	BBC	②	6.51		BBC	②	19.06		BBC	②	16.79
		③	6.79			③	18.16			③	17.89
		④	7.12			④	17.42			④	18.22
		⑤	8.72			⑤	17.31			⑤	18.27
		⑥	11.21			⑥	17.17			⑥	17.85
		⑦	13.79			⑦	17.62			⑦	18.82
		⑧	24.22			⑧	20.79			⑧	20.28
		⑨	29.41			⑨	24.52			⑨	21.20
	A	①	6.75		A	①	14.51		A	①	18.06
		②	7.76			②	16.86			②	18.15
		③	9.72			③	16.96			③	19.02
		④	11.94			④	16.43			④	19.81
		⑤	15.53			⑤	16.86			⑤	20.58
		⑥	28.07			⑥	18.28			⑥	25.72
		⑦	33.33			⑦	20.57			⑦	32.17

Table B-1 Measured water content at decommission

Section	Line	Location	[%]	Section	Line	Location	[%]	Section	Line	Location	[%]
h	AAB	①	6.85	i	AAB	①	17.57	j	AAB	①	17.40
		②	7.90			②	17.13			②	18.22
		③	9.66			③	16.17			③	18.52
		④	12.22			④	16.45			④	20.10
		⑤	14.02			⑤	16.95			⑤	20.75
		⑥	24.72			⑥	19.31			⑥	24.36
		⑦	26.20			⑦	24.01			⑦	24.13
	ABB	①	6.60		ABB	①	17.89		ABB	①	17.56
		②	7.73			②	17.49			②	18.04
		③	9.21			③	17.22			③	18.11
		④	11.43			④	17.50			④	18.02
		⑤	13.66			⑤	17.62			⑤	18.00
		⑥	23.23			⑥	18.67			⑥	19.04
		⑦	26.45			⑦	21.24			⑦	21.66
	B	①	6.48		B	①	18.19		B	①	19.57
		②	7.26			②	17.41			②	18.28
		③	9.21			③	17.07			③	18.48
		④	11.44			④	16.97			④	18.43
		⑤	13.39			⑤	17.38			⑤	18.42
		⑥	22.49			⑥	18.59			⑥	19.84
		⑦	26.52			⑦	22.02			⑦	20.58
	BC	①	6.60		BC	①	18.32		BC	①	17.62
		②	6.96			②	17.43			②	17.82
		③	8.20			③	17.02			③	18.15
		④	10.24			④	17.04			④	17.82
		⑤	12.70			⑤	17.72			⑤	20.00
		⑥	23.96			⑥	19.80			⑥	20.44
		⑦	30.67			⑦	22.68			⑦	21.67
	BCC	①	6.28		BCC	①	18.10		BCC	①	17.37
		②	6.59			②	17.58			②	17.43
		③	7.96			③	17.16			③	17.30
		④	10.02			④	17.06			④	17.58
		⑤	13.01			⑤	17.94			⑤	18.16
		⑥	20.56			⑥	19.54			⑥	20.07
		⑦	29.01			⑦	20.71			⑦	22.52
	C	①	6.42		C	①	17.87		C	①	17.47
		②	6.95			②	18.24			②	17.62
		③	8.42			③	17.72			③	18.43
		④	10.78			④	17.52			④	18.38
		⑤	13.01			⑤	19.05			⑤	19.03
		⑥	20.84			⑥	20.49			⑥	20.72
		⑦	28.36			⑦	24.48			⑦	23.17

Table B-1 Measured water content at decommission

Section	Line	Location	[%]	Section	Line	Location	[%]	Section	Line	Location	[%]
h	CCD	①	7.13	i	CCD	①	20.21	j	CCD	①	17.46
		②	7.51			②	17.88			②	17.53
		③	9.11			③	17.67			③	17.82
		④	11.08			④	17.36			④	18.45
		⑤	13.17			⑤	17.83			⑤	19.70
		⑥	19.79			⑥	19.02			⑥	21.72
		⑦	26.18			⑦	22.72			⑦	26.04
	CDD	①	6.75		CDD	①	18.49		CDD	①	17.84
		②	7.97			②	17.81			②	17.56
		③	9.29			③	17.23			③	17.93
		④	11.69			④	17.20			④	18.00
		⑤	14.38			⑤	17.91			⑤	19.55
		⑥	26.64			⑥	20.80			⑥	25.43
		⑦	32.21			⑦	25.89			⑦	38.91
	D	①	6.91		D	①	18.37		D	①	17.44
		②	7.22			②	17.75			②	17.44
		③	9.37			③	17.70			③	17.37
		④	11.44			④	17.21			④	18.05
		⑤	13.53			⑤	17.94			⑤	19.25
		⑥	24.87			⑥	20.40			⑥	21.13
		⑦	29.11			⑦	23.54			⑦	23.47
	DA	①	7.09		DA	①	18.54		DA	①	17.73
		②	7.82			②	17.90			②	17.89
		③	9.12			③	17.52			③	17.95
		④	11.32			④	17.43			④	18.25
		⑤	13.56			⑤	17.49			⑤	18.76
		⑥	22.85			⑥	18.85			⑥	18.85
		⑦	26.17			⑦	20.74			⑦	21.28
	DAA	①	7.19		DAA	①	17.55		DAA	①	17.37
		②	7.75			②	18.04			②	18.22
		③	9.40			③	17.03			③	18.46
		④	11.46			④	17.18			④	19.13
		⑤	14.81			⑤	17.34			⑤	19.77
		⑥	26.29			⑥	18.96			⑥	21.53
		⑦	28.60			⑦	22.77			⑦	22.55

Table B-1 Measured water content at decommission

Section	Line	Location	[%]	Section	Line	Location	[%]	Section	Line	Location	[%]
h	A'	①	13.85	i	A'	①	17.26	j	A'	①	20.36
		②	24.16			②	19.57			②	22.88
		③	30.73			③	25.21			③	29.14
	AAB'	①	13.91		AAB'	①	17.48		AAB'	①	19.66
		②	23.96			②	21.28			②	21.18
		③	29.17			③	24.26			③	22.95
	AB'	①	13.65		AB'	①	17.21		AB'	①	17.89
		②	22.81			②	18.90			②	18.68
		③	28.08			③	21.03			③	19.98
	ABB'	①	13.19		ABB'	①	17.22		ABB'	①	18.14
		②	21.35			②	18.68			②	19.34
		③	26.65			③	21.54			③	20.56
	B'	①	13.69		B'	①	17.79		B'	①	18.52
		②	22.51			②	21.14			②	19.52
		③	28.57			③	22.97			③	21.45
	BBC'	①	13.89		BBC'	①	17.28		BBC'	①	18.10
		②	23.28			②	19.63			②	20.65
		③	29.33			③	22.33			③	22.45
	BC'	①	13.04		BC'	①	17.95		BC'	①	17.92
		②	18.36			②	19.10			②	20.28
		③	28.94			③	25.02			③	22.80
	BCC'	①	13.72		BCC'	①	18.05		BCC'	①	18.67
		②	23.05			②	19.13			②	20.60
		③	30.36			③	22.07			③	21.97
	C'	①	13.05		C'	①	17.31		C'	①	18.86
		②	20.35			②	20.21			②	21.04
		③	27.02			③	23.12			③	23.95
	CCD'	①	13.41		CCD'	①	18.07		CCD'	①	20.11
		②	19.68			②	19.48			②	23.61
		③	25.69			③	22.52			③	23.31
	CD'	①	13.44		CD'	①	17.66		CD'	①	22.06
		②	24.77			②	19.78			②	20.79
		③	32.70			③	22.70			③	23.33
	CDD'	①	13.72		CDD'	①	18.08		CDD'	①	19.13
		②	26.64			②	21.57			②	24.46
		③	30.88			③	27.46			③	28.68
	D'	①	13.25		D'	①	17.63		D'	①	18.88
		②	21.92			②	19.48			②	20.70
		③	27.28			③	23.36			③	23.88
	DDA'	①	13.81		DDA'	①	17.63		DDA'	①	18.28
		②	21.15			②	18.21			②	19.58
		③	25.42			③	20.47			③	20.66
	DA'	①	13.54		DA'	①	17.30		DA'	①	19.11
		②	23.19			②	19.43			②	19.92
		③	26.96			③	22.13			③	21.90
	DAA'	①	14.25		DAA'	①	17.23		DAA'	①	20.62
		②	25.46			②	18.60			②	23.13
		③	34.07			③	24.02			③	27.44